IDENTIFICATION OF VARIABILITY IN SUB-ARCTIC SEA ICE CONDITIONS DURING THE YOUNGER DRYAS AND HOLOCENE

by

Patricia Cabedo Sanz

A thesis submitted to Plymouth University in partial fulfilment for the degree of:

DOCTOR OF PHILOSOPHY

Petroleum and Environmental Geochemistry Group

School of Geography, Earth and Environmental Sciences

Plymouth University

September 2013

Dedicated to all my family.

Thanks!

"Nuestra gloria más grande no consiste en no haberse caído nunca, sino en haberse levantado después de cada caída" (Confucio)

Identification of variability in sub-Arctic sea ice conditions during the Younger Dryas and Holocene

by
Patricia Cabedo Sanz

ABSTRACT

The presence of the sea ice diatom biomarker IP_{25} in Arctic marine sediments has been used in previous studies as a proxy for past spring sea ice occurrence and as an indicator of wider palaeoenvironmental conditions for different regions of the Arctic over various timescales.

The current study describes a number of analytical and palaeoceanographic developments of the IP_{25} sea ice biomarker. First, IP_{25} was extracted and purified from Arctic marine sediments. This enabled the structure of IP_{25} to be confirmed and enabled instrumental (GC-MS) calibrations to be carried out so that quantitative measurements could be performed with greater accuracy.

Second, palaeo sea ice reconstructions based on IP_{25} and other biomarkers were carried out for a suite of sub-Arctic areas within the Greenland, Norwegian and Barents Seas, each of which represent contrasting oceanographic and environmental settings. Further, an evaluation of some combined biomarker approaches (e.g. the PIP_{25} and DIP_{25} indices) for quantifying and/or refining definitions of sea ice conditions was carried out. Temporally, particular emphasis was placed on the characterisation of sea ice conditions during the Younger Dryas and the Holocene. Some comparisons with other proxies (e.g. foraminifera, IRD) were also made.

A study of a sediment core from Andfjorden (69.16˚N, 16.25˚E), northern Norway, provided unequivocal evidence for the occurrence of seasonal sea ice conditions during the Younger Dryas. The onset (ca. 12.9 cal. kyr BP) and end (ca. 11.5 cal. kyr BP) of this stadial were especially clear in this location, while in a study from the Kveithola Trough (74.52˚N, 16.29˚E), western Barents Sea, these transitions were less apparent. This was attributed to the presence of colder surface waters and the occurrence of seasonal sea ice both before and after this stadial at higher latitudes. Some regional differences regarding the severity of the sea ice conditions were also observed, although an overall general picture was proposed, with more severe sea ice conditions during the early-mid Younger Dryas and less sea ice observed during the late Younger Dryas.

A shift in the climate towards ice-free conditions was recorded in northern Norway during the early Holocene (ca. 11.5 – 7.2 cal. kyr BP). Milder conditions were also observed during the Holocene in the western Barents Sea, with three main climate periods observed. During the early Holocene (ca. 11.7 – 9.5 cal. kyr BP), the position of the spring ice edge was close to the study area which resulted in high productivity during summers. During the mid-late Holocene (ca. 9.5 – 1.6 cal. kyr BP), sea ice was mainly absent due to an increased influence of Atlantic waters and northward movement of the Polar Front. During the last ca. 1.6 cal. kyr BP, sea ice conditions were similar to those of the present day.

In addition to the outcomes obtained from the Norwegian-Barents Sea region, comparison of biomarker and other proxy data from 3 short cores from Kangerdlugssuaq Trough (Denmark Strait/SE Greenland) with historical climate observations allowed the development of a model of sea ice conditions which was then tested for longer time-scales. It is suggested that the IP_{25} in sediments from this region is likely derived from drift ice carried from the Arctic Ocean via the East Greenland Current and that two main sea surface scenarios have existed over the last ca. 150 yr. From ca. AD 1850 – 1910, near perennial sea ice conditions resulted in very low primary productivity, while from ca. AD 1910 – 1986, local sea ice conditions were less severe with increased drift ice and enhanced primary productivity. This two-component model was subsequently developed to accommodate different sea surface conditions that existed during the retreat of the Greenland Ice Sheet during the deglaciation (ca. 16.3 – 10.9 cal. kyr BP).

Table of Contents

LIST OF FIGURES

LIST OF TABLES

ACKNOWLEDGEMENTS

First and foremost I would like to say my most sincere and deepest thanks to my two supervisors, Prof. Simon Belt and Dr. Thomas Brown, who gave me the opportunity of undertaking this PhD in the first place and who have supported me throughout these three years, and during my writing-up stage. I could not have done it without your help and your immense patience; I have learnt so many things from you.

I am also grateful to Prof. Paul Worsfold and Prof. Maeve Lohan for their support and encouragement since I first arrived in England and unable to speak any English! Your enthusiasm made me realise how wonderful research is.

I would also like to thank Prof. John Andrews and Dr. Anne Jennings (University of Colorado), for sharing their samples, information and knowledge, which has greatly contributed to this study.

Thanks to Dr. Jochen Knies (NGU, Trondheim) for contributing to my work, and thanks to Dr. Katrine Husum (University of Tromsø) for sharing samples.

Thanks to my colleagues from the CASE network, with whom I had the opportunity to share knowledge and travel to amazing places.

I would also like to thank the technical staff of the School of Environmental Sciences (Plymouth University), Andrew, Andy, Claire and Ian for their expertise and assistance and to Dr. Paul Sutton for his constant technical support.

On a more personal note, I would like to thank everyone in the BGC group and in Plymouth who have accompanied and supported me during my PhD. Thanks for your friendship and for making this a great experience! My deepest thanks to Estela & Sebas and Sara for your great support and for all the great moments we have shared and also to Alba: la Antonia, with whom I have shared so many experiences and fun times. A special thanks also to Mike, Kate, Dave, Holly, Adil, Wiebke, Charlotte, Balbina: la croquetilla sentimental, Bravo-cente and my old friend Matt, for their invaluable friendship in good times and support in bad times, especially during this last year. Thanks for making me get my smile back!

También me gustaría agradecer a mis amigos en España: Asahi, Laura, Patty, Amelia, Angela, Sonia y PANA! Siempre me habéis apoyado desde la distancia y animado siempre que lo he necesitado.

Finalmente, no tengo palabras para expresar lo agradecida que estoy a toda mi familia, que aunque pequeña, es la mejor familia que una podría desear. Gracias a todos por el apoyo incondicional que siempre me habéis brindado, durante los buenos y malos momentos.

AUTHOR'S DECLARATION

At no time during the registration for the degree of Doctor of Philosophy has the author been registered for any other University award without prior agreement of the Graduate Committee.

Work submitted for this research degree at the Plymouth University has not formed part of any other degree either at Plymouth University or at another establishment.

This study was financed with the aid of a research studentship from the European Community's 7th Framework Programme FP7 2007/2013, Marie-Curie Actions, under Grant Agreement No.238111.

A programme of advanced study was undertaken, with relevant scientific seminars and conferences attended, at which work was often presented.

Word count of main body of thesis: 47551

Signed . . . . . .

Patricia Cabedo Sanz

Date: September 2013

PUBLICATIONS

Aagaard-Sørensen, S., Husum, K., **Cabedo-Sanz, P**., Belt, S.T., Forwick, M., Andreassen, K., Hald, M. (*In prep*). Paleoceanographic reconstruction at the western Barents Sea Margin during the last deglaciation. (Chapter 5, Last deglaciation).

Belt, S.T., Brown, T.A., Ampel, L., **Cabedo-Sanz, P**., Fahl, K., Kocis, J., Massé, G., Navarro-Rodriguez, A., Ruan, J., Xu, Y. (2013). An inter-laboratory investigation of the Arctic sea ice biomarker proxy IP_{25} in marine sediments: Key outcomes and recommendations. Climate of the Past 9, 5263-5298.

Berben. S.M.P., Husum, K., **Cabedo-Sanz, P.** and Belt, S.T. (2013). Holocene sub centennial evolution of Atlantic water inflow and sea ice distribution in the western Barents Sea. Climate of the Past 9, 4893-4938. (Chapter 5, Holocene).

Belt, S.T., Brown, T.A., Ringrose, A.E., **Cabedo-Sanz, P**., Mundy, C.J., Gosselin, M., Poulin, M. (2013). Quantitative measurement of the sea ice diatom biomarker IP_{25} and sterols in Arctic sea ice and underlying sediments: Further considerations for palaeo sea ice reconstrucion. Organic Geochemistry 62, 33-45.

Alonso-Garcia, M., Andrews, J.T., **Cabedo-Sanz, P**., Darby, D.A., Jaeger, J. (2013). A comparison between multi-proxy and historical data (AD 1990-1840) of drift-ice conditions on the East Greenland shelf (~66°N). The Holocene 23, doi: 10.1177/0959683613505343. (Chapter 6, Part A)

Cabedo-Sanz, P., Belt, S.T., Knies, J., Husum, K. (2013). Identification of contrasting seasonal sea ice conditions during the Younger Dryas. Quaternary Science Reviews 79, 74-86. (Chapter 4)

Belt, S.T., Brown T.A., **Cabedo-Sanz, P.** and Navarro Rodriguez, A. (2012) Structural confirmation of the sea ice biomarker IP_{25} found in Arctic marine sediments. Environmental Chemistry Letters 10, 189-192. (Chapter 3)

Belt, S.T., Brown, T.A., Navarro Rodriguez, A., **Cabedo-Sanz, P.**, Tonkin, A. and Ingle, R. (2012) A reproducible method for the extraction, identification and quantification of the Arctic sea ice proxy IP_{25} from marine sediments. Analytical Methods 4, 705-713.

PRESENTATIONS AND CONFERENCES ATTENDED

Advanced Climate Dynamics Course (ACDC) summer school, Nyksund, **Norway**, 21st August 2013. Oral presentation: "IP_{25}: Background and Applications".

25rd Annual Meeting of the British Organic Geochemical Society, Plymouth, **U.K**, 10th – 11th July 2013. Oral presentation: "Sub-Arctic sea ice conditions during the Younger Dryas and Holocene".

Changing Arctic and Subarctic Environment (CASE) Synthesis Workshop, Helmholtz Centre for Ocean Research (GEOMAR), Kiel, **Germany**, 29th – 30th April 2013. Oral presentation: "Identification of variable seasonal sea ice conditions during the Younger Dryas".

4th Annual Biogeochemistry Centre Conference. University of Plymouth, Plymouth, **U.K**, 17th December 2012. Oral presentation: "Proxy-based sea ice reconstructions for two Arctic locations with similar latitudes yet highly contrasting oceanographic and environmental settings".

American Geophysical Union Fall Meeting 2012, San Francisco, **U.S.A**, 3rd – 7th December 2012. Oral presentation: "Identification of variable seasonal sea ice conditions during the Younger Dryas".

European Geosciences Union General Assembly 2012, Vienna, **Austria**, 23rd – 27th April 2012. Poster presentation: "Calibration and Application of a Novel Biomarker for Arctic Sea-Ice Reconstructions".

Mid-term progress meeting of the Changing Arctic and Subarctic Environment (CASE) project, University of Amsterdam, **Netherlands**, 26th – 27th January 2012. Oral presentation: "Calibration and Application of a Novel Biomarker for Arctic Sea-Ice Reconstructions".

3rd Annual Biogeochemistry Centre Conference, University of Plymouth, Plymouth, **U.K**, 9th December 2011. Oral presentation: "Calibration and Application of a Novel Biomarker for Arctic Sea-Ice Reconstructions".

UK Arctic Science Conference, University of Leeds, **U.K**, 14th – 16th September 2011. Poster presentation: "Application of the IP_{25} Biomarker for Arctic Sea-Ice Reconstructions". Awarded poster presentation prize.

1st Changing Arctic and Subarctic Environment (CASE) project progress meeting, Geological Survey of Norway (NGU), Trondheim, **Norway**, 27th – 28th April 2011. Oral presentation: "Calibration and application of a novel biomarker for Arctic sea-ice reconstruction".

2nd Annual Biogeochemistry Centre Conference, University of Plymouth, Plymouth, **U.K**, 17th December 2010. Oral presentation: "Calibration and Application of a Novel Biomarker for Arctic Sea-Ice Reconstructions".

LIST OF COMMON ABBREVIATIONS

AIW – Atlantic Intermediate Water
AMS – Accelerator mass spectrometry
AO – Arctic Oscillation
BG – Beaufort gyre
CASE – Changing Arctic and sub-Arctic environment
DCM – Dichloromethane
DIP_{25} – Ratio between diene II and IP_{25}
EGC – East Greenland Current
GC – Gas chromatography
GC-MS – Gas chromatography – mass spectrometry
GIS – Greenland Ice Sheet
HBI – Highly branched isoprenoid
HPLC – High performance liquid chromatography
HSG – Hematite stained grains
IC – Irminger Current
IP_{25} – C_{25} highly branched isoprenoid monoene
IRD – Ice rafted debris
NAC – North Atlantic Current
NAO – North Atlantic Oscillation
NCC – Norwegian Coastal Current
NMR – Nuclear magnetic resonance
MAT – Mean annual temperature
PIP_{25} – Ratio between IP_{25} and a phytoplankton biomarker
RF – Response factor
SIM – Selective ion monitoring
SST – Sea surface temperature
THE – Total hexane extract
TIC – Total ion current
TOC – Total organic carbon
TOE – Total organic extract
TPD – Trans-Polar Drift
WSC – West Spitsbergen Current
7-HND – 7-hexylnonadecane
9-OHD – 9-octyl-8-heptadecene

CHAPTER ONE

1 Introduction

1.1 The Arctic Ocean

The Arctic Ocean is an intricate system and plays an important role in controlling the Earth's climate, largely due to extensive seasonal and year round ice cover (e.g. Comiso and Parkinson, 2004; Serreze et al., 2007; Polyak et al., 2010). Sea ice has a major influence on the Earth's climate system by controlling fluxes of heat and moisture across the ocean-atmosphere interface. The melting of sea ice and the associated release of low-salinity water influences deep water formation and the thermohaline circulation, further enhancing the significance of the Arctic on global climate. Further, the ice-albedo (amount of solar radiation reflected by a surface) and snow-albedo feedbacks associated with the high reflectivity of ice and snow also influence the Earth's climate (Dieckmann and Hellmer, 2010; Miller et al., 2010). As such, during warm periods, there are fewer snow-covered areas and, therefore, less reflection of solar radiation, which results in a decrease of the albedo effect (Stein, 2008). As a consequence, major changes in energy balances and oceanic and atmospheric circulation of the Arctic Ocean can be observed (e.g. Schubert and Stein, 1996; Comiso and Parkinson, 2004; Miller et al., 2010). Ice cover, which expands and retreats seasonally, is the most defining feature of the surface of the Arctic Ocean (e.g. Polyak et al., 2010). Two main ice types characterise the Arctic Ocean: first-year ice, which represents a single year's growth and multi-year or perennial ice which has survived at least one melt season. Changes in the extent and thickness of the ice, both on short and long time scales, affect the ocean and the atmosphere in northern latitudes (e.g. Perovich and Richter-Menge, 2009;

Miller et al., 2010; Polyak et al., 2010; Kinnard et al., 2011). In recent decades, Arctic sea ice (especially perennial sea ice) has undergone dramatic changes, with significant thinning and reduction of total area, such as the minimum recorded during the summer of 2012 (Figure 1.1) when compared with the 34-year satellite record (Schiermeier, 2012).

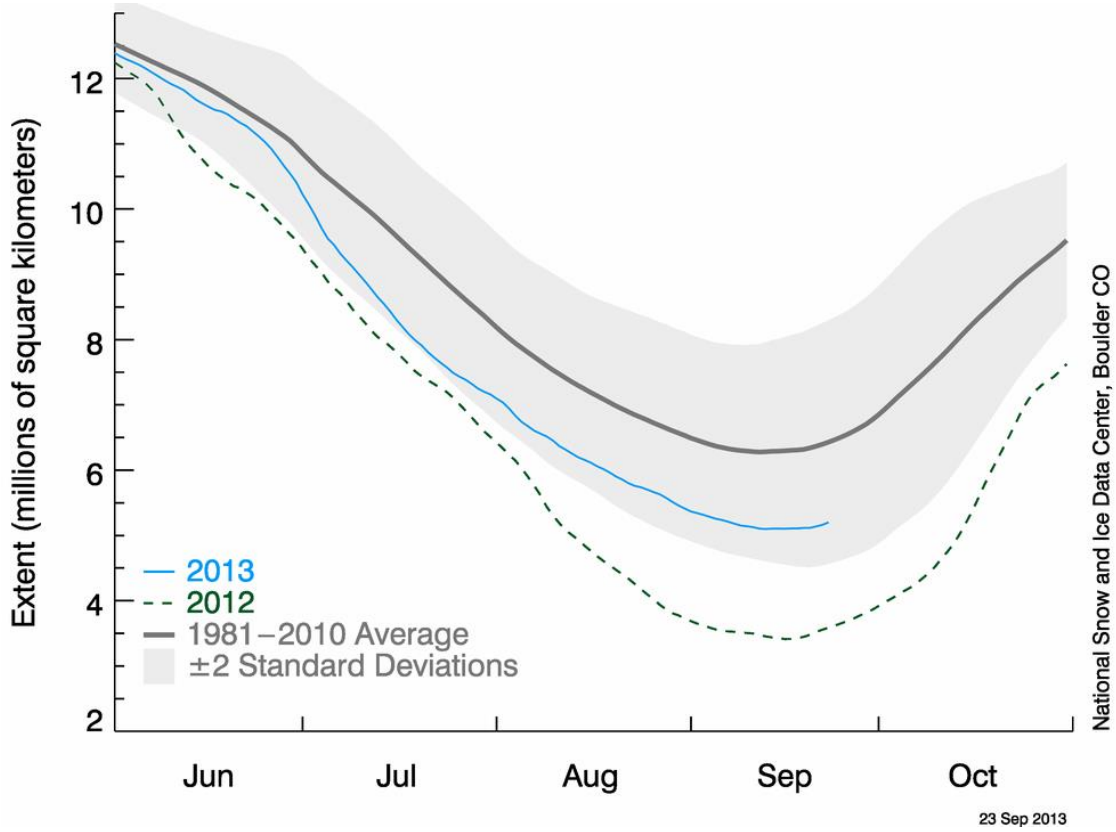

Figure 1.1: Arctic sea ice extent (area of ocean with at least 15% sea ice cover). The grey line represents average extent between 1981 and 2010. The green dotted line represents Arctic sea ice extent during 2012.

Further, it has been suggested that the decreasing trend of ice extent over the last two decades cannot be entirely explained by natural internal climate-system variability, but likely involves external factors such as forcing due to anthropogenic greenhouse gasses (e.g. Moritz et al., 2002; Johannessen et al., 2004; Kinnard et al., 2011). In addition, the loss in Arctic sea ice will pose social, economic, political and ecological challenges (Perovich and Richter-Menge, 2009).

Thus, reconstruction of Arctic sea ice variations is necessary to understand if recent sea ice loss is induced by natural cycles on Earth, or whether this is an accelerated phenomenon caused by external forcing (e.g. Moritz et al., 2002; Miller et al., 2010). In addition, reconstruction of past sea ice datasets will help improve the accuracy of model-based estimates of future changes in climate.

1.2 Marine proxies for palaeoenvironmental reconstructions in the Arctic Ocean

The need to reconstruct past climate conditions in the Arctic has led to extensive research in this area over many years. The majority of these have been based on the application of a wide range of environmental proxies (a recent review is given by Polyak et al., 2010). In this section, a general overview of the most common geological proxies used for reconstruction of ancient and modern environmental conditions in the Arctic Ocean is presented.

1.2.1 Micropalaeontological proxies

1.2.1.1 Foraminifers

Foraminifera (typically < 1 mm length but can reach up to ca. 20 cm) are single-celled protists with shells made of calcium carbonate ($CaCO_3$) or agglutinated sediment particles, that are found in a wide range of marine environments and may be planktonic or benthic in their mode of life (Murray, 2002; Gooday, 2003). For example, benthic foraminifera are commonly used as indicators of primary production (Wollenburg and Kuhnt, 2000) and are also used to calculate sea level, bottom water temperatures and

salinity (e.g. Jennings et al., 2004; Sejrup et al., 2004; Leorri et al., 2013). Planktonic foraminifera have been used as proxies for primary production (Carstens et al., 1997), as well as tools for reconstructing sea surface temperatures through the application of transfer functions (e.g. Pflaumann et al., 1996; Pflaumann et al., 2003; Sarnthein et al., 2003c; Kucera et al., 2005). Planktonic and benthic foraminifera are also important in correlating and dating sediment cores (Stein, 2008 and references therein). However, Husum and Hald (2012) recently raised concerns regarding reconstructions of sea surface and subsurface temperatures based on planktonic foraminifera, such as the use of datasets based on surface sediment samples that probably cover thousands of years instead of modern conditions. In addition, the reduced geographical coverage from the region under study results in a poor coverage of all representative environmental conditions. Further, Husum and Hald (2012) developed an Arctic training set (using the > 100 μm size fraction) from which more robust reconstructions of subsurface temperatures were obtained for summer temperatures at 100 m water depth. A further limitation regarding the use of foraminifera lies in the dissolution of aragonite/carbonate material as a result of increased organic carbon input and its subsequent degradation in sediments (e.g. Archer and Maier-Reimer, 1994; Wollenburg and Kuhnt, 2000). As such, it is important to quantify the state of preservation in foraminiferal assemblages (e.g. Broecker and Clark, 2001; Beer et al., 2010). Despite these limitations, oxygen ($^{18}O/^{16}O$) and carbon ($^{13}C/^{12}C$) stable isotopes of foraminiferal carbonate shells have been used in numerous studies to estimate palaeoenvironmental parameters such as temperature, to quantify global changes in sea level and deep-sea circulation (Cooke and Rohling, 2001; Ravelo and Hillaire-Marcel, 2007; Ishimura et al., 2012 and references therein).

Regarding their use for palaeo sea ice reconstructions, benthic foraminifera have been used as a palaeo sea ice indicator (e.g. Jennings et al., 2002b; Scott et al., 2009) and,

although they give information on sea ice cover variation, they are not considered direct proxies for sea ice and their response to changing sea ice conditions is not well understood (Seidenkrantz, 2013). In addition, studies based on planktonic foraminifera have also been used to reconstruct sea ice cover in the Arctic (Sarnthein et al., 2003a).

1.2.1.2 Calcareous nannofossils

Nannofossils are derived from coccolithophores, single-celled algae, protists and phytoplankton belonging to the division of haptophytes. They are formed by special calcium carbonate plates called coccoliths (typically < 20 μm length) and cannot live under permanent sea ice cover.

The abundant presence of nannofossils has been interpreted in terms of the occurrence of open water conditions in the Arctic Ocean (Gard, 1993) and such a measure has been used as a qualitative proxy for circulation changes in the northern North Atlantic (e.g. Samtleben and Schröder, 1992; Baumann et al., 2000; Andrews and Giraudeau, 2003; Giraudeau et al., 2010). In addition, the abundance ratio between two species of coccoliths (*Emiliania huxleyi* and *Coccolithus pelagicus*) in fossil assemblages from the central Nordic Seas has been suggested as a proxy measure for the location of the Arctic Front (Baumann et al., 2000) and has been recently tested in the eastern Nordic Seas over the last 3000 yr (Dylmer et al., 2013).

1.2.1.3 Ostracodes

Ostracodes (typically 1 mm in length) are small bivalved crustaceans that commonly occur in Quaternary Arctic sediments (Taldenkova et al., 2005). Many species of ostracodes are ecologically susceptible to specific oceanic conditions (Jones et al.,

1999) and their assemblages have been used in numerous studies to reconstruct Arctic palaeoceanography (e.g. Cronin et al., 1994; Jones et al., 1999; Taldenkova et al., 2005; Poirier et al., 2012) and sea ice history (e.g. Cronin et al., 2010; Cronin et al., 2013).

1.2.1.4 Diatoms

Diatoms are unicellular (primarily photosynthetic) microalgae (1 – 1000 μm) with a cell wall made of silica (Crosta and Koç, 2007). Diatoms have adapted to a wide range of planktonic and benthic marine habitats and represent an essential source of primary production in the Arctic ecosystem (e.g. Falk-Petersen et al., 2009; Brown, 2011). Freshwater diatoms, which are often part of the particulate organic matter transported by rivers onto shelves, have been used to reconstruct surface-water conditions in the Greenland, Iceland and Norwegian seas through the last 14 kyr BP (Karpuz and Jansen, 1992; Koç et al., 1993). Furthermore, marine diatoms are indicators of primary production (Koç et al., 2002), and the presence of sea ice diatoms in marine sediments can be used to infer past sea ice coverage (e.g. Stein et al., 2004; Justwan et al., 2008). Diatom assemblages can also be used to identify different organic carbon sources (i.e. terrestrial/freshwater *versus* marine) in shelf sediments (Stein, 2008 and references therein). In addition, the relationship between diatom assemblages and summer surface water salinity can be used to reconstruct palaeosalinity and sea ice (e.g. Polyakova and Stein, 2004).

1.2.1.5 Palynomorphs

Palynomorphs are an additional microfossil group used in palaeoenvironmental reconstructions as well as stratigraphic markers in Arctic Ocean sediments (Stein,

2008). The main group of marine palynomorphs used for palaeoenvironmental and palaeoclimate reconstructions are dinoflagellates (flagellate protists) and their remaining cysts (dinocysts; typically 10 – 150 μm in length), which are characterised by an organic resistant walled material that results in a high degree of preservation.

De Vernal et al. (2001) raised a number of limitations when reconstructing quantitative palaeoceanographic conditions using dinocysts. These included morphological variation within taxa, sparse hydrological data and large inter-annual variations of temperature and salinity in surface Arctic waters. In addition, a new technique based on the best-analogue method for quantitative reconstruction of sea surface conditions for the northernmost Atlantic and Arctic regions was proposed (de Vernal et al., 2001). Using transfer functions based on dinoflagellate cyst assemblages, Solignac et al. (2006) reconstructed sea surface parameters such as temperature, salinity and sea ice cover extent (as months yr^{-1}) during the Holocene on the East Greenland shelf. However, some inconsistencies regarding the environmental conditions (i.e. sea ice cover extent) during the Holocene in a study in the same area were found by Jennings et al. (2011) and these were attributed to the lack of sufficient data points for calibration of the dinoflagellate database from this area. A recent synthesis of dinocyst-based palaeoenvironmental reconstructions for Arctic and sub-Arctic areas during the Holocene is given by de Vernal et al. (2013b).

A further (common) limitation of microfossil-based proxies (e.g. foraminifera, coccolith, ostracode, diatom and dinoflagellate) is the high degree of expertise required regarding species identification, together with ensuring consistency between laboratories and adoption of common methodologies. In addition, the interpretation of such proxies relies on biological, chemical and physical factors (e.g. temperature,

salinity, nutrients, grazing) that influence the distributions of microorganisms in the water column before sinking and reaching underlying sediments (e.g. Polyak et al., 2010; Belt et al., 2012b; de Vernal et al., 2013a).

1.2.2 Ice Rafted Debris (IRD)

Ice Rafted Debris (IRD) are sediments that have been transported by icebergs and/or sea ice. Although many studies use the coarse sediment fraction, the sand-size within studies ranges from > 63 μm to > 2mm (e.g. Nam et al., 1995; Andrews et al., 1997; Andrews, 2000; Spielhagen et al., 2004). It has also been shown that sediment > 63 μm or higher is indicative of iceberg deposition in the Arctic Ocean, while lower numbers can be indicative of both iceberg and sea ice origin (Spielhagen et al., 2004; Polyak et al., 2010).

A large number of studies in the North Atlantic and Nordic Seas have used IRD as a proxy for reconstructing palaeoclimate conditions (e.g. Bond et al., 2001; Sarnthein et al., 2003b; Moros et al., 2004; Moros et al., 2006). Further, anomalously thick layers of IRD, known as Heinrich events (Heinrich, 1988), were thought to be derived from ice sheet/ice shelf collapse and massive release of icebergs (Bond and Lotti, 1995; Dowdeswell et al., 1995). In addition, proxies for sediment transport in drift ice include hematite-stained quartz sand grains (Bond et al., 2001), sand-size quartz (Eiríksson et al., 2000; Moros et al., 2006), coal fragments (Bischof and Darby, 2000) as well as the presence of calcite and dolomite (Andrews et al., 2010) and quartz wt% (< 2 mm) measured by Quantitative X-ray diffraction (e.g. Moros et al., 2006; Andrews and Eberl, 2007; Andrews, 2011; Andrews and Jennings, 2013). Sediment source identifications

have been developed based on the chemical fingerprinting of entrained Fe oxide mineral grains in Arctic Ocean sea ice (Darby, 2003; Darby et al., 2012).

1.2.3 Organic geochemical proxies

Palaeoenvironmental studies and organic carbon source identification (marine and terrigenous) can be conducted through the analysis of different organic geochemical proxies such as bulk parameters and individual biomarker distributions.

The most common organic geochemical bulk parameters are total organic carbon (TOC) and organic carbon/organic nitrogen ratios, used to make a distinction in marine sediments between marine (algal) and terrigenous (higher plant) organic matter (Schubert and Stein, 1996). Carbon/sulphur ratios are used to obtain information about the oxygenation of bottom waters (Leventhal, 1987, 1995), while the stable carbon isotope ($^{13}C/\ ^{12}C$) ratio of the organic fraction in marine sediments has been used to elucidate the marine or terrigenous provenance of the organic fraction (e.g. Mueller-Lupp et al., 2000; Goñi et al., 2013).

Biomarkers are molecular fossils that indicate the existence, past or present, of living organisms (Eglinton and Calvin, 1967). During the last few decades, a large number of biomarker-based studies for palaeoclimate reconstructions have been carried out (a review is given by Eglinton and Eglinton, 2008). The methodologies employed for the production of such molecular proxy datasets are usually based on organic solvent extractions to recover all the organic material from the sediments, followed by fractionation, purification and quantification by analytical instrumentation such as gas chromatography-mass spectrometry (GC-MS) or high performance liquid chromatography (HPLC) (e.g. Eglinton and Eglinton, 2008; Stein, 2008).

Example of biomarkers are long-chain alkanes, which are typically used to characterise terrigenous organic carbon (Schubert and Stein, 1996). Further, a widespread technique used for estimating past sea surface temperatures (SST), is based on the alkenone composition of coccolithophorids found in marine sediments and commonly used to derive the alkenone unsaturation index, U_{37}^{K} (Brassell et al., 1986). However, the optimum use of the U_{37}^{K} index for reconstruction of palaeotemperatures is between 10°C and 25°C, which limits its use in the Arctic, where temperatures are normally below 5°C and coccoliths are rare or absent. Therefore, the reconstructions based on alkenones are largely restricted to sub-Arctic areas (e.g. Rosell-Melé, 2001). A further approach for reconstructing SST is via the so-called TEX_{86} index (tetraether index of compounds with 86 carbon atoms) (e.g. Kim et al., 2010). The TEX_{86} index is based on the strong relationship between SST and the distribution of crenarchaeotal isoprenoid glycerol dibiphytanyl glycerol tetraethers (GDGTs) which are membrane lipids biosynthesised mainly by Crenarchaeota (prokaryotes organisms).

Of the other biomarkers found commonly in marine sediments, sterols have been used as indicators of different algal communities, reflecting contrasting oceanographic conditions, including the occurrence of sea ice. For example, 24-methylenecholesterol was previously reported as the main sterol in sea ice diatom communities during the spring bloom in McMurdo, Antarctica (Nichols et al., 1993) and was suggested as a potential proxy for Arctic sea ice by Knies (2005). In contrast, a structurally related sterol, brassicasterol, is produced by a large number of phytoplankton and has been used as a geochemical indicator of open water (ice-free) conditions (Müller et al., 2009). However, the specificity of such biomarkers is probably limited as they are formed in a large variety of environments and are not especially source-specific. For example, sterols can be derived from diverse sources within the marine environment (Volkman, 1986).

In summary, several biomarkers have been used for palaeo temperature reconstructions (i.e. alkenones, GDGTs) but these have focussed mainly on sea surface temperature determinations. In contrast, reconstruction of sea ice occurrence has generally been made by extrapolation of proxy-based climate measurements such as SST and therefore there has long been a need to develop a more specific proxy for the past occurrence of sea ice.

1.2.4 Highly branched isoprenoid alkenes and the IP_{25} sea ice biomarker

C_{25} and C_{30} highly branched isoprenoid (HBI) alkenes are secondary metabolites derived from certain diatom genera and species found in a large variety of marine environments (e.g. Robson and Rowland, 1986; Rowland and Robson, 1990; Belt et al., 2000a). Gearing et al. (1976) first reported the occurrence of C_{25} HBIs in sediments. Later, Robson and Rowland (1986) determined the parent carbon skeleton of C_{25} HBIs by synthesis (Figure 1.2).

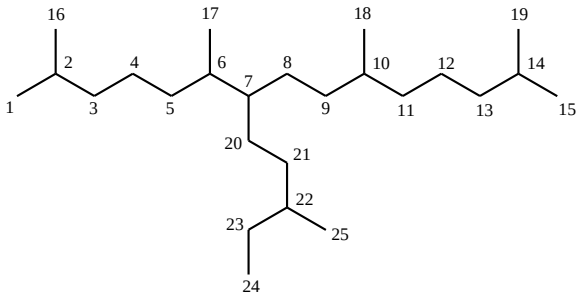

Figure 1.2: Molecular structure of a HBI with 25 carbon atoms.

Volkman et al. (1994) identified marine diatoms as the biological sources of at least some HBI alkenes and some freshwater diatoms were later identified as sources by Belt et al. (2001c). The molecular structures of a number of individual HBI alkenes were identified after culturing of *Haslea ostrearia*, *Rhizosolenia setigera* and some other

diatoms (Wraige et al., 1997; Sinninghe-Damsté et al., 1999a; Sinninghe-Damsté et al., 1999b; Allard et al., 2001; Belt et al., 2001a; Belt et al., 2001c, b; Belt et al., 2006). Studies regarding the position and stereochemistry of double bonds were performed (Belt et al., 2000a; Belt et al., 2000b), and the biosynthesis of HBI alkenes by diatoms was also investigated (Massé et al., 2004).

In addition to structural determination studies, other investigations focused on the environmental variables that influence the growth of diatoms and distributions of HBIs, such as salinity, light and temperature (Wraige et al., 1997; Wraige et al., 1998; Rowland et al., 2001). In *H. ostrearia*, for instance, the extent of unsaturation in the alkenes was shown to vary with culture temperature. Thus, at 25 ˚C and 15 ˚C the major isomers found were tetra- and tri-unsaturated alkenes respectively, while at 5 ˚C, di-unsaturated alkenes were the most abundant (Rowland et al., 2001) (Figure 1.3).

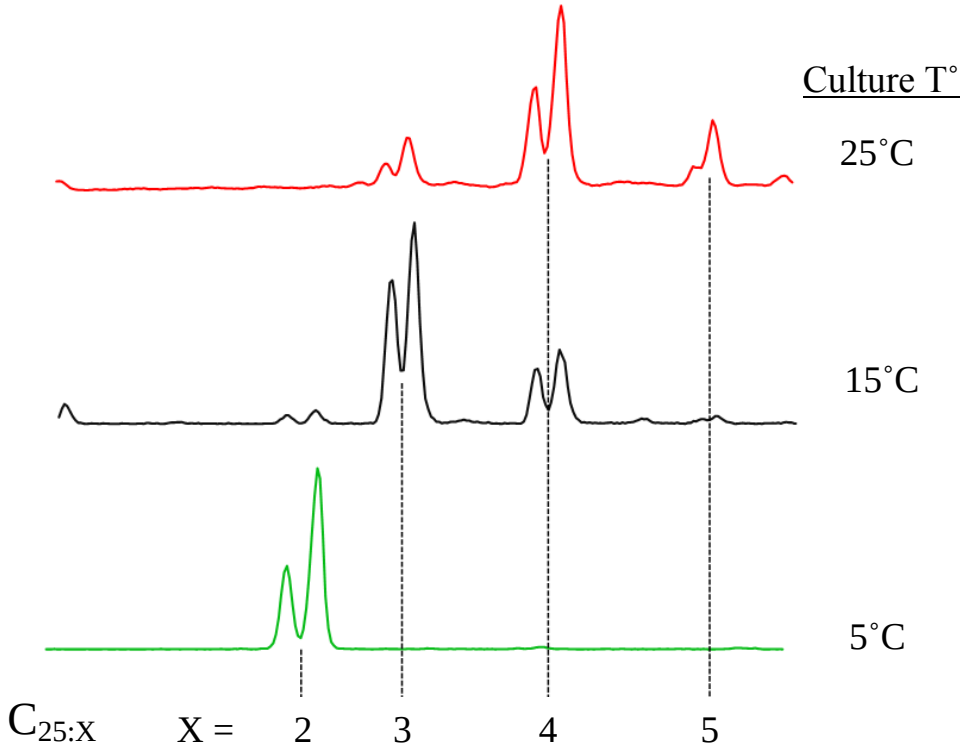

Figure 1.3: Partial gas chromatograms illustrating the distributions of alkenes in *H. ostrearia* cultures grown at different temperatures, where the X indicates the degree of unsaturation in the HBIs (modified from Rowland et al., 2001).

Based on these outcomes, it was hypothesised that, in Arctic sea ice, where the temperature is below 5 ˚C, production of mono-unsaturated HBI alkenes by certain *Haslea* spp., might be possible. In addition, it was suggested that such compounds might be better preserved in sediments than the more unsaturated HBIs and, therefore, might be useful as palaeo sea ice indicators (Belt et al., 2007).

Indeed, an initial investigation by Belt et al. (2007) found that a mono-unsaturated HBI alkene was detected in sea ice samples from the Canadian Arctic and sub-Arctic. In addition, the same mono-unsaturated HBI, subsequently termed IP_{25} (Ice Proxy with 25 carbon atoms; Figure 1.4), was later identified in sediments from the Canadian Arctic and from different Arctic regions (e.g. Belt et al., 2008; Müller et al., 2009; Vare et al., 2010). Diatoms belonging to the *Haslea* genus were suggested as a possible source of IP_{25} (Belt et al., 2007).

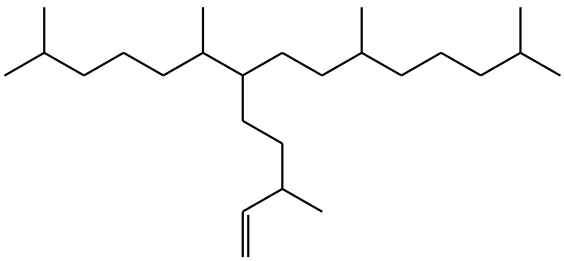

Figure 1.4: Molecular structure of the C_{25} mono-unsaturated HBI alkene termed IP_{25} (Unsaturation point at position 23/24).

Since its discovery by Belt et al. (2007), the presence and relative abundances of IP_{25} have been used in a number of palaeo sea ice reconstructions, representing different Arctic regions over a range of timescales (a recent review is given by Belt and Müller, 2013). Briefly, these studies include the Barents Sea (last 300 yr) (Vare et al., 2010), north Iceland (last 2000 yr) (Massé et al., 2008; Andrews et al., 2009), the Canadian Arctic Archipelago (last 10000 yr) (Belt et al., 2010), northern Fram Strait (last 30000 yr) (Müller et al., 2009), the northern Barents Sea continental margin (last 150000 yr

BP) (Stein et al., 2012) and Fram Strait (last ca. 2.2 Ma) (Stein and Fahl, 2013). More recent investigations have aimed to establish the relationship between IP_{25} abundances from surface sediments in different Arctic locations and known recent sea ice conditions derived from satellite data (Müller et al., 2011; Navarro-Rodriguez et al., 2013; Stoynova et al., 2013; Xiao et al., 2013). A further approach, has been to combine abundances of IP_{25} with those of an open water indicator (e.g. a phytoplankton biomarker such as a sterol) to generate the so-called PIP_{25} index in an attempt to provide more quantitative measures of palaeo sea ice (Müller et al., 2011). Finally, a number of IP_{25} based sea ice reconstructions have been successfully incorporated into multi-proxy and large-scale climate modelling studies (Antoniades et al., 2011; Axford et al., 2011; Kinnard et al., 2011; Miller et al., 2012).

These previous studies have demonstrated the potential of IP_{25} as a specific (only produced by some sea ice diatoms), sensitive (produced in sufficient quantity to be detected and quantified) and stable (resistant to degradation over thousands of years) biomarker for palaeo-sea-ice reconstructions (Belt et al., 2007). Further work is required, however, to increase the knowledge regarding this sea ice biomarker through investigation of other Arctic and sub-Arctic areas with contrasting environmental conditions.

1.3 The current project – background to 'CASE'

The current research work has been carried out within *The Changing Arctic and Subarctic Environment* (CASE, EU FP7) project. CASE is an interdisciplinary Initial Training Network investigating marine biotic indicators of past climate change. The aim of the overall project was to describe and identify the mechanisms and impacts of recent environmental changes in the Nordic Seas as well as to evaluate the nature and amplitudes of oceanographic and climate changes and their implications on the structure of the marine ecosystem during the present interglacial (the Holocene). CASE investigations have been conducted in three specific regions: (1) The Fram Strait and northern Svalbard continental margin, which represents the main inflow channel of Atlantic waters into the Arctic Ocean; (2) The southern Barents Sea, where the Norwegian Atlantic Current flows into the Barents Sea influencing the seasonal sea-ice melt; (3) The East Greenland and northern Iceland shelves, where southward flowing polar waters are carried to the mid-latitude Atlantic across the Denmark Strait (Figure 1.5).

1.3.1 Specific aims of the current project within the CASE project

The main regions investigated by the research work described here and which contribute to the CASE project are northern Norway & the south-western Barents Sea (Figure 1.5 (2)) and south-east Greenland (Figure 1.5 (3)). Overall, the main aim of this study was targeted towards sea ice reconstruction in particular, and the application of the IP_{25} proxy, from a number of sub-Arctic regions with contrasting oceanographic and environmental settings. In addition to the spatial evaluation of IP_{25}, the timescales have focused on the Younger Dryas and the Holocene (specific aims of each particular study will be introduced in each chapter). For example, northern Norway, which is currently

ice-free all year round, is greatly influenced by warm and saline Atlantic water which contributes to the formation of North Atlantic Deep Water and is a very sensitive area to climatic change (Hald and Hagen, 1998) (Figure 1.5a). The western Barents Sea (Figure 1.5b) is also dominated by Atlantic waters but is also influenced by Arctic waters. As a result, this region experiences some sea ice cover but the inter-annual variability is high. However, during glacial periods, colder conditions than those of today occurred; for instance, during the Last Glacial Maximum (LGM) Norway and the Barents Sea were covered by a vast ice sheet (e.g. Mangerud et al., 1998; Vorren and Plassen, 2002b; Clark et al., 2009). In contrast, the south-east Greenland region (Figure 1.5c) represents a very different oceanographic and environmental setting. This region is a critical region due to the interaction between the Polar and sub-Polar climate systems. Currently, on the Greenland side of Denmark Strait, the oceanographic conditions are severe, with 8 – 10 months sea ice cover during the year, with numerous tidewater glacier margins injecting icebergs into the fjords and adjacent shelf. During colder periods, such as the LGM, a re-advance of the Greenland Ice Sheet (GIS) resulted in more sea ice cover over the East Greenland continental margin (Kellogg et al., 1978; Kellogg, 1980).

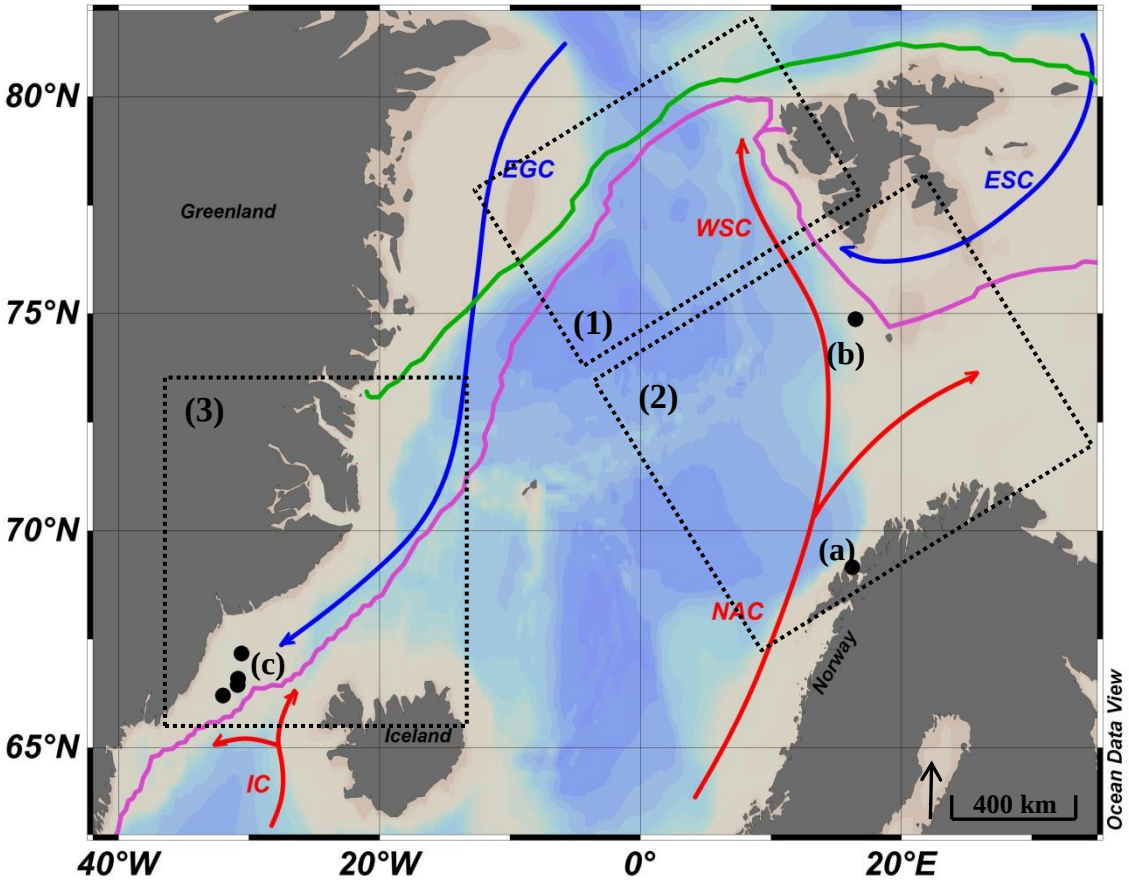

Figure 1.5: Overview map of the study areas showing March (magenta line) and September (green line) median sea ice extent (> 15% monthly mean concentration) for 1981 – 2010 (National Snow and Ice Data Center, Boulder, Colorado). Black dotted squares represent specific areas studied by the CASE project: (1) Fram Strait and northern Svalbard continental margin, (2) Southern Barents Sea and (3) East Greenland and northern Iceland. Black dots represent specific areas investigated within the current study: (a) northern Norway, (b) western Barents Sea and (c) south-east Greenland. Major cold currents are shown by blue arrows: East Greenland Current (EGC) and East Spitsbergen Current (ESC). Main warm currents are shown by red arrows: Irminger Current (IC), North Atlantic Current (NAC) and West Spitsbergen Current (WSC).

In order to achieve these aims, a number of investigations were carried out, which are presented and discussed in the following chapters:

Chapter 2: *General laboratory and analytical methods.* This chapter provides a description of the general laboratory and instrumental analytical procedures used, together with an account of a number of methodological developments that have been necessary to obtain the data used to address the main aims of this research.

Chapter 3: *Quantification of IP_{25} and other HBIs in marine sediments.* This chapter describes the extraction, purification and analytical (GC-MS) calibration of IP_{25} in Arctic marine sediments. The GC-MS calibration of other di- and tri-unsaturated HBIs in Arctic marine sediments is also presented.

Chapter 4: *Results (1): Seasonal sea ice conditions in northern Norway during the Younger Dryas.* This chapter describes the sedimentary analysis of IP_{25} (and other biomarkers) in a sediment core from Andfjorden, northern Norway to characterise sea ice conditions from ca. 13.8 – 7.2 cal. kyr BP and the Younger Dryas, in particular.

Chapter 5: *Results (2): Seasonal sea ice conditions in the western Barents Sea following the last deglaciation.* This chapter describes a biomarker-based reconstruction of the palaeo sea ice conditions in the western Barents Sea margin during the last ca. 15.7 cal. kyr BP. Further, the comparison of biomarker data with other proxy studies (including some from the same core) allowed the overall oceanographic conditions to be identified.

Chapter 6: *Results (3): Environmental and drift ice conditions in south-east Greenland: from recent to ancient sediments.* Part A of this chapter describes a multi-proxy based study of three short gravity cores (last ca. 150 yr) from the outer Kangerdlugssuaq Trough, within Denmark Strait, south-east Greenland. The outcomes were compared to existing historical and instrumental data and a model from which longer term palaeoceanographic reconstructions could be tested was proposed. Part B is based on a multi-proxy analysis of a sediment core located in the same area over a longer timescale (ca. 16.3 – 10.9 cal. kyr BP). The model provided in Part A was tested during this interval, to elucidate the palaeoclimate conditions in the Kangerdlugssuaq Trough. Some modifications to the initial model were also proposed.

Chapter 7: *Conclusions and future work.* This chapter summarises the main outcomes from each of the individual study areas and provides suggestions of future work that might be needed to improve the application of IP_{25} (and related biomarkers) for palaeo sea ice reconstruction in the Arctic.

CHAPTER TWO

2 General laboratory and analytical methods

2.1 Introduction

This chapter describes the general experimental procedures undertaken as part of this research work, including instrumentation and laboratory operating conditions in addition to chemical identification and quantification. Any necessary methodological developments carried out during this research are also described.

2.2 General procedures

2.2.1 Freeze drying

Frozen sediment samples were freeze-dried for 24 – 48 hours in a Thermo Savant Modulyo D freeze dryer at -45ºC and 0.2 mbar. Individual sediment horizons were weighed before and after freeze drying to determine water content by difference.

2.2.2 Internal standards for lipid quantification

Addition of the following internal standards prior to extraction was used to permit quantification of extracted compounds; 9-octyl-8-heptadecene (9-OHD, 10 μL; 10 μg mL^{-1}; Figure 2.4b) and 7-hexylnonadecane (7-HND, 10 μL; 10 μg mL^{-1}; Figure 2.4c) were added for quantification of HBIs (including IP_{25}) and 5α-androstan-3β-ol (10 μL; 10 μg mL^{-1}; Figure 2.6c) was added for quantification of sterols. A detailed description

of the methodological development carried out regarding the internal standards for quantification of HBIs is presented in Section 2.3.1 of this chapter.

2.2.3 Total organic extracts (TOEs)

For each sediment extraction, DCM : MeOH (2:1 *v/v*) was added using a glass pipette (Figure 2.1) in sufficient volume (ca. 3 mL), to cover sediments with an excess of ca. 1 mL above the sediment surface. The vials were then sealed using lined polypropylene screw caps (7 mL, Fisher, UK) and ultrasonicated (Transsonic T420, Camlab; ca. 15 min) to stimulate the disaggregation of the sediment thus permitting more efficient solvent penetration of sediment matrices. The samples were centrifuged (2500 rpm; ca. 30 s) and the supernatant fluid was decanted using a pipette, into a clean pre-labelled 7 mL glass vial. The extraction procedure was repeated twice more (DCM : MeOH, 1: 0.5 *v/v*) yielding the total organic extract (TOE) (Steps 1 to 8 in Figure 2.1).

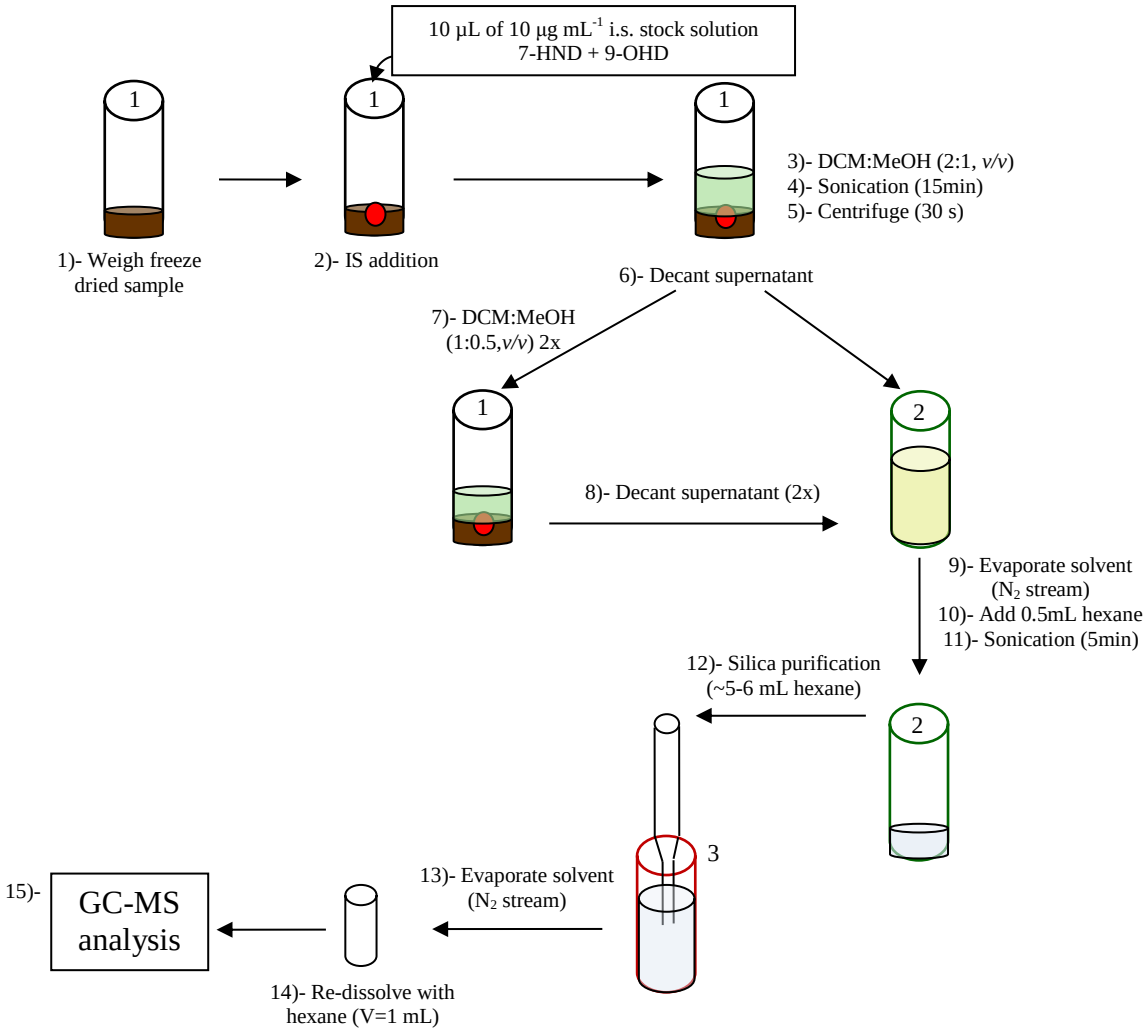

Figure 2.1: Schematic figure showing the steps of the organic extraction and silica purification for HBI analysis.

2.2.4 Partial purification of lipid extracts by silica column chromatography

Following removal of the solvent from the combined extracts using nitrogen (step 9 in Figure 2.1), the resulting dried total organic extracts (TOE) were re-dissolved in hexane (0.5 mL: Rathburn, UK) and ultrasonicated (5 min) before being transferred into a small-scale chromatography column made of a glass pipette, containing a small plug of cotton wool (DCM-extracted) and deactivated chromatography grade silica (ca 0.7 g; 60-200 µm, Fisher, UK). Columns were pre-conditioned by rinsing with hexane (ca. 3

mL) prior to the addition of sediment extracts. Following the addition of the sediment extract using a glass pipette, IP_{25} and other hydrocarbons (hexane; 6 mL) and sterols (20:80 methylacetate/hexane; 6 mL) were collected in pre-labelled 7 mL glass vials as two single fractions prior to evaporation of hexane by N_2 stream (25 ˚C) (Steps 10 to 12 in Figure 2.1).

Identification of IP_{25} in some sediment extracts was made difficult due to low abundance and/or the occurrence of other highly abundant co-eluting organic compounds that prevented further concentration of the extracts. In such cases, additional purification by Ag-Ion chromatography was required. A detailed description of the approach developed for identification of IP_{25} in such cases is given in Section 2.5.

2.2.5 Derivatisation

To increase the volatility of some polar compounds on the apolar GC-MS column (HP-5ms), sterols were derivatised prior to GC-MS analysis using 50 µL of N,O-bis(trimethylsilyl)trifluoroacetamide (BSTFA). Vials were sealed using aluminium lined polypropylene screw caps and parafilm (Fisher, UK) and heated for 1 hour at 70ºC. The silylated extracts were then transferred to a 2 mL vial and diluted with DCM to an appropriate concentration for GC-MS analysis.

2.2.6 Gas chromatography – mass spectrometry

Dried samples were transferred (hexane; 3 x 100 μL) to 2 mL GC vials (Chromacol, UK) and diluted appropriately for analysis by gas chromatography-mass spectrometry (GC-MS) (Steps 13 to 15 in Figure 2.1). An Agilent 7890A GC coupled to a 5975 series mass selective detector fitted with an Agilent HP-5ms (30 m x 0.25 mm x 0.25 μm) column was used, along with 1 μL auto-splitless injection (300˚C) with helium carrier gas (1 mL min^{-1} constant flow). Total ion current (TIC; *m/z* 50 – 500 daltons) and selective ion monitoring (SIM; -0.3 +0.7 *m/z* of interest) techniques were used to determine compounds detected after elution, with an electron voltage of 70 eV. The GC oven was heated from 40 – 300˚C at 10˚C min^{-1} and held at 300˚C for 10 minutes. The retention time and mass spectrum of individual compounds was identified using TIC chromatograms whereas compound quantification was performed from SIM chromatograms due to its high selectivity as well as increased sensitivity. In some cases, and when the samples required further concentration for GC-MS analysis, 300 μL GC vials (Chromacol, UK) were used.

2.2.7 Quantification of HBIs and sterols

2.2.7.1 Quantification of HBIs

Identification of HBIs isolated from marine sediments was established by comparison of the respective mass spectra with those of authentic compounds kept in the laboratory. Specifically, each lipid was identified from the mass spectrum molecular ion, fragmentation pathway (Figure 2.2, Figure 2.3 and Figure 2.4), and retention index (IP_{25}: 2086; diene II: 2085; triene Z: 2045; triene E: 2092; triene 5/6: 2103; triene 6/17:

2107) calculated using Equation 2.1. R*i* denotes retention index and R*t* is retention time on GC-MS (HP-5ms).

Equation 2.1:

$$Ri = \frac{Rt^{HBI} - Rt^{nC_{20}}}{Rt^{nC_{21}} - Rt^{nC_{20}}/_{100}} + 2000$$

An ionization energy of 70 eV was sufficient to fragment HBIs in the mass selective detector (MSD) and provide characteristic mass spectra (Brown, 2011) (Figure 2.2, Figure 2.3 and Figure 2.4).

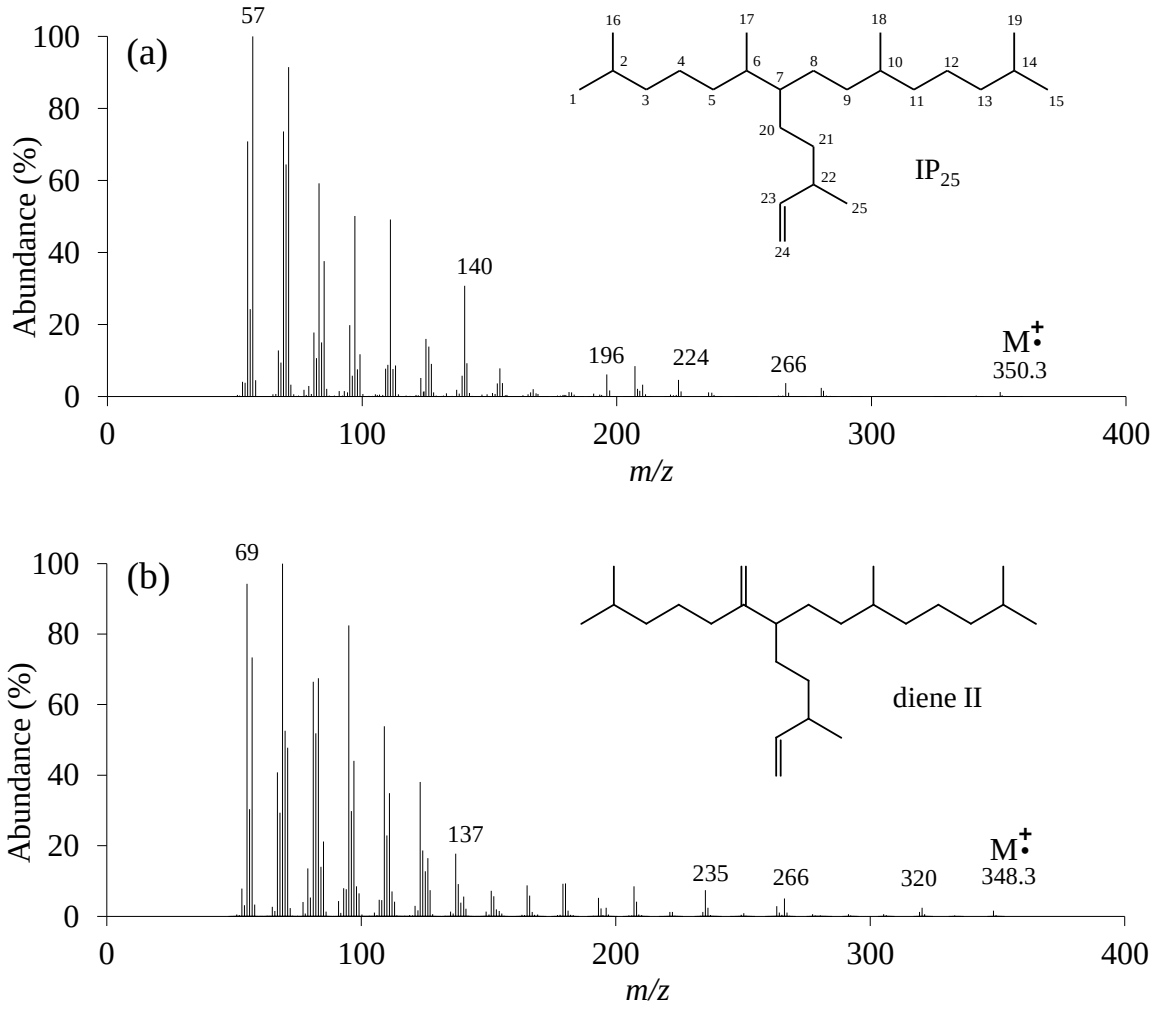

Figure 2.2: Background subtracted mass spectra and structures of: (a) the highly branched isoprenoid alkene IP_{25} (showing HBI numbering system) ($M^{+\bullet}$ = *m/z* 350.3); (b) the HBI alkene diene II ($M^{+\bullet}$ = *m/z* 348.3) described in the current study.

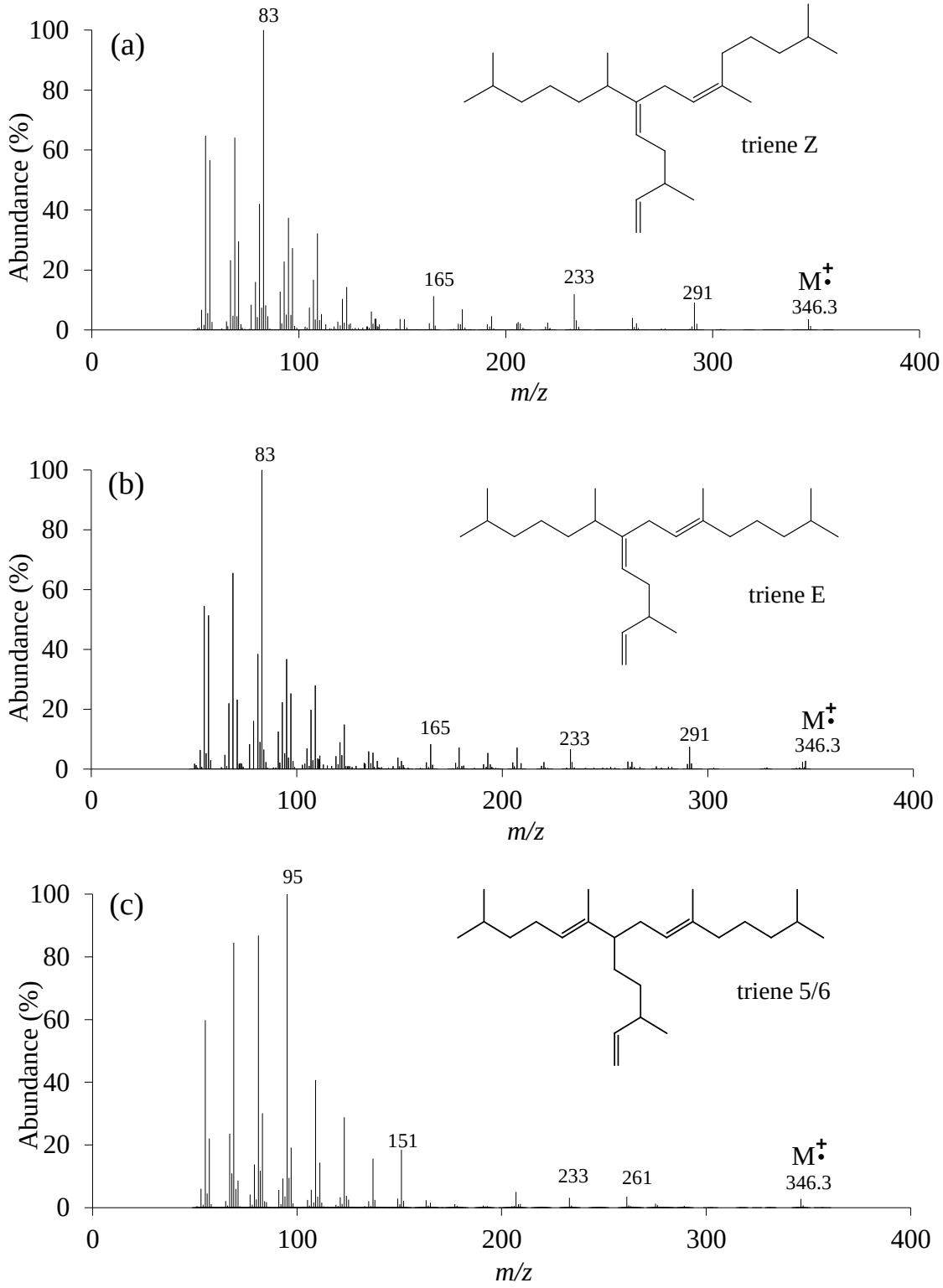

Figure 2.3: Background subtracted mass spectra and structures of highly branched isoprenoid alkenes described in the current study (a) triene Z ($M^{\bullet+}$ = *m/z* 346.3); (b) triene E ($M^{\bullet+}$ = *m/z* 346.3); (c) triene 5/6 ($M^{\bullet+}$ = *m/z* 346.3).

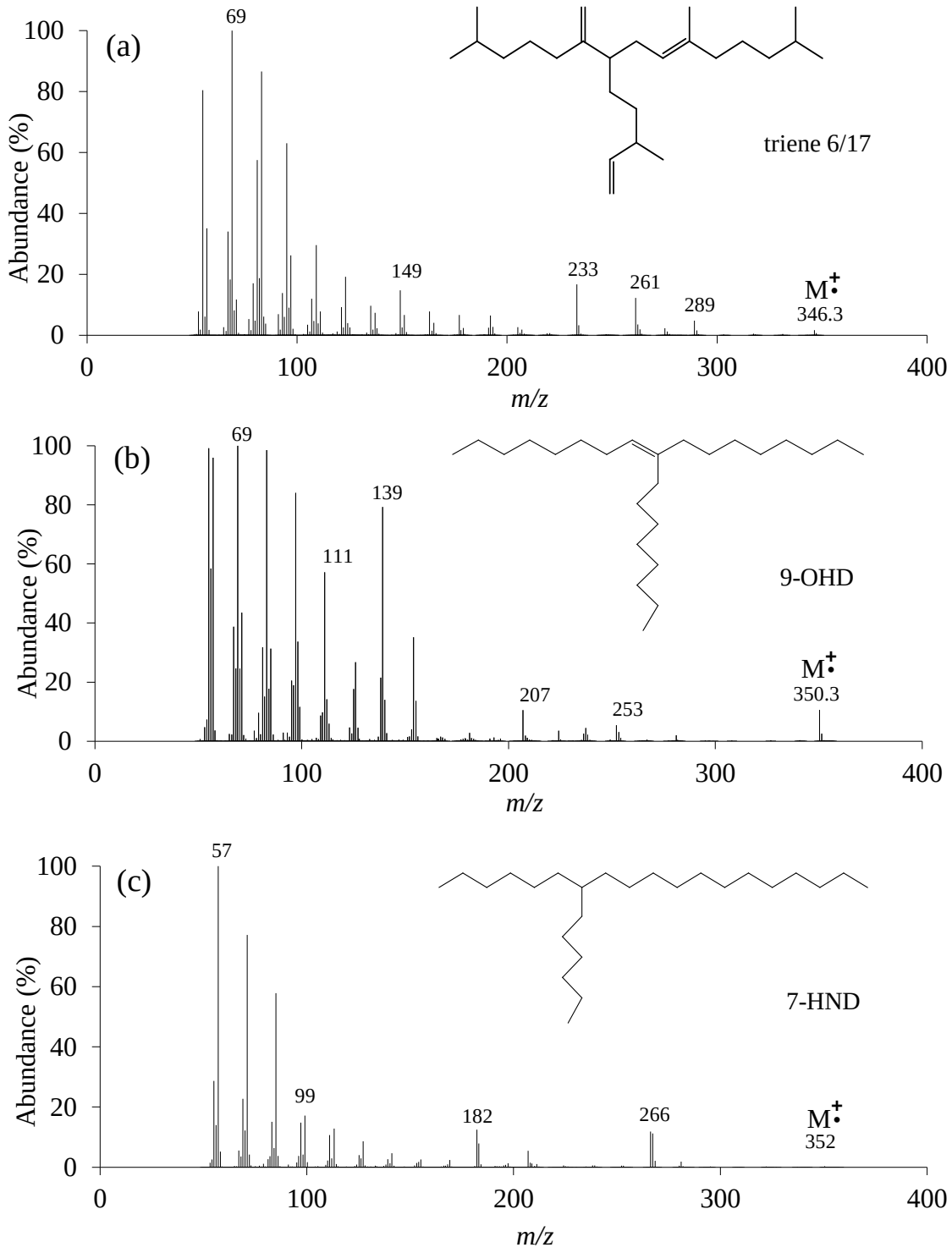

Figure 2.4: Background subtracted mass spectra and structures of highly branched isoprenoid alkenes and internal standards described in the current study (a) triene 6/17 ($M^{+\bullet}$ = *m/z* 346.3); (b) 9-OHD (9-octyl-8-heptadecene; $M^{+\bullet}$ = *m/z* 350.3); (c) 7-HND (7-hexylnonadecane; $M^{+\bullet}$ = *m/z* 352; not visible but indicated).

Quantification of HBIs was achieved by manual integration (Chemstation, version C.03.00 software) of each analyte's molecular ion signal as recorded by GC-MS SIM analysis (IP_{25}: *m/z* 350.3; diene II: *m/z* 348.3; triene Z, triene E, triene 5/6 and triene 6/17: *m/z* 346.3, Figure 2.5). Factors such as extraction efficiency, sediment sample mass and any differences in the relative response factors were accounted for using Equation 2.2.

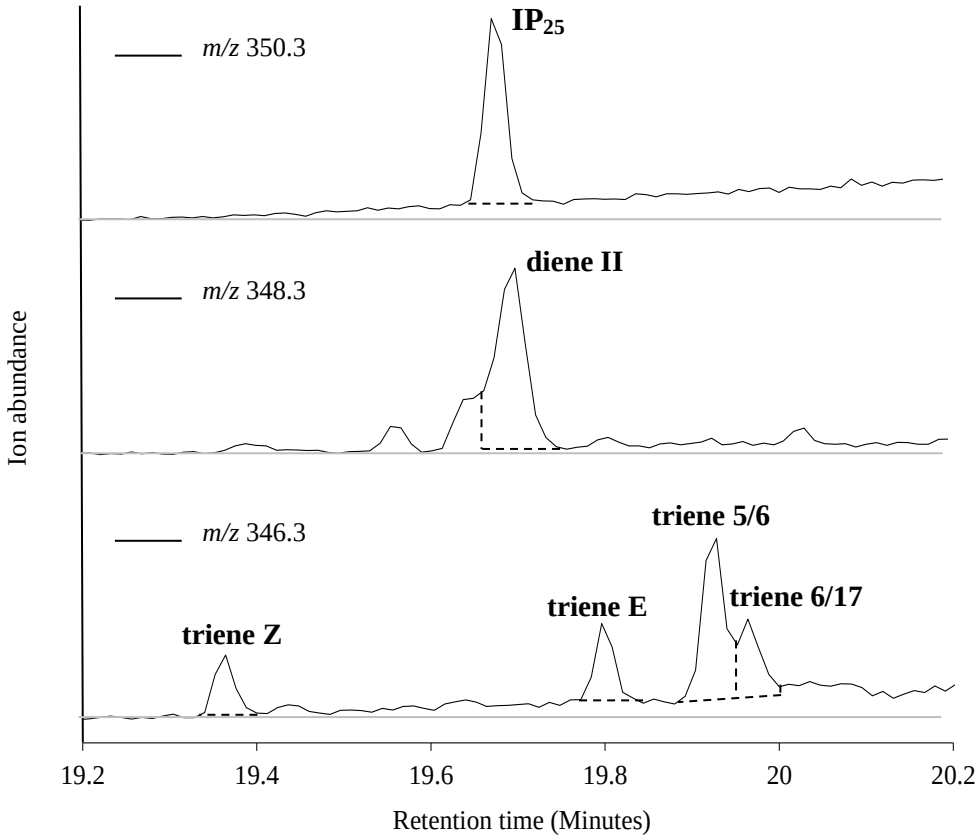

Figure 2.5: Partial GC-MS chromatograms (SIM *m/z* 350.3, 348.3 and 346.3) of silica purified Station 428 sediment extract from the Canadian Arctic Archipelago showing the relative elution order of HBIs and the technique adopted for manual peak integration for later quantification of HBIs (dashed lines).

Equation 2.2:

$$HBI\ (\mu g\ g^{-1} dry\ sediment) = \frac{\frac{P_A HBI}{P_A IS} * RF}{m\ dry\ sediment\ (g)} *\ m\ IS\ (\mu g)$$

Briefly, the ratio between the peak area of a selected HBI (P_AHBI) and the peak area of the internal standard (P_AIS) was multiplied by a GC-MS response factor (RF) to account for different mass spectral responses between the HBI and the internal standards. Then, the modified peak ratios were divided by the mass of sediment extracted (m dry sediment (g)) and finally multiplied by the mass of the internal standard added to the sediment prior to extraction (m IS (μg)), yielding units for HBIs of μg g^{-1} of dry sediment (Equation 2.2; Table 2.1). The approach used for obtaining the response factors between the internal standard (9-OHD) and IP_{25} and di- and tri-unsaturated HBIs can be found in Chapter 3 of this thesis.

Table 2.1: Calculation steps needed to quantify HBI concentration in sediment samples using Equation 2.2. The example shown corresponds to a sediment sample from the Canadian Arctic Archipelago, Station 428. (RF = response factor) (mass dry sediment (g) = 0.64; mass IS (μg) = 0.1) (GC-MS SIM-chromatogram given in Figure 2.5).

HBI	**P_A HBI**	**P_A IS**	**RF**	$\frac{P_A HBI}{P_A IS} * RF$	$\frac{\frac{P_A HBI}{P_A IS} * RF}{m\ dry\ sediment\ (g)}$	$HBI = \frac{\frac{P_A HBI}{P_A IS} * RF}{m\ dry\ sediment\ (g)} * m\ IS\ (\mu g)$
IP_{25}	25228	122372	5.03	1.0369	1.6202	0.1620
diene II	23635	122372	11.29	2.1806	3.4072	0.3407
triene Z	3716	122372	1.82	0.0553	0.0864	0.0086
triene E	4443	122372	1.82	0.0661	0.1033	0.0103

In some cases, due to highly fluctuating downcore total organic carbon (TOC) data, HBI concentrations were normalised relative to TOC (Equation 2.3)

Equation 2.3:

$$HBI\ (\mu g\ g^{-1} OC) = \frac{HBI\ (\mu g\ g^{-1} dry\ sediment)}{TOC\ (\%)} * 100$$

Biomarker concentrations were in some cases expressed as fluxes in order to factor in the temporal changes associated with variable sedimentation rates. The conversion of sedimentary HBI concentrations to annual fluxes (Equation 2.5) was carried out by combining the former with sediment dry bulk densities (DBD) and sedimentation rates

derived from an age model, both of which can be determined experimentally (Belt et al., 2012b). HBI denotes highly branched isoprenoid concentration, DBD is dry bulk density and A_{sed} is the sedimentation rate of a given sediment horizon. The DBD is the intrinsic sediment dry mass per unit volume of the sampled sediment horizon and can be calculated according to Equation 2.4. Dm means dry sediment mass and Wc is Water content.

Equation 2.4:

$$DBD\ (g\ cm^{-3}) = \frac{Dm}{\left(\frac{Wc}{1.025}\right) + \left(\frac{Dm}{2.65}\right)}$$

Equation 2.5:

$$HBI\ (\mu g\ cm^{-2}\ kyr^{-1}) = HBI\ (\mu g\ g^{-1} dry\ sediment) * DBD\ (g\ cm^{-3}) * A_{sed}\ (cm\ kyr^{-1})$$

However, this approach could only be used when a suitable and well-constructed age model for a studied sediment core was available.

Analytical reproducibility during each study was monitored using a standard sediment from the Canadian Arctic Archipelago, with known abundances of biomarkers for every 14 - 16 sediment samples extracted. Overall, the analytical reproducibility during the entire research provided an analytical error value of 10% (n = 42).

2.2.7.2 Quantification of sterols

Identification of sterols was established by comparison of the mass spectra of derivatised (trimethylsilyl, TMS) samples with those of authentic compounds. Sterols studied in this research included 24-methylcholesta-5,22E-dien-3β-ol (hereafter referred to as brassicasterol, Figure 2.6a) and 24-methylcholesta-5,24(28)-dien-3β-ol (hereafter referred to as 24-methylenecholesterol, Figure 2.6b) and the internal standard 5α-androstan-3β-ol (Figure 2.6c).

Quantification of sterols was achieved following the same steps to that of HBIs (Section 2.2.7.1 of this chapter).

The response factor of brassicasterol was obtained by preparation of a calibration curve of a range of brassicasterol concentrations (authentic standard, Sigma-Aldrich; 0.0001 mg mL^{-1}, 0.0002 mg mL^{-1}, 0.0004 mg mL^{-1}, 0.0006 mg mL^{-1}, 0.0008 mg mL^{-1} and 0.001 mg mL^{-1}) against the internal standard (5α-androstan-3β-ol) of equivalent concentration. A GC-MS response factor between the internal standard (5α-androstan-3β-ol) and brassicasterol value of 50 was obtained by dividing the *m/z* response of the 5α-androstan-3β-ol (*m/z* 333.3) by the *m/z* response of brassicasterol (*m/z* 470) in the SIM-chromatogram. This means that the GC-MS response of 5α-androstan-3β-ol at *m/z* 333.3 in the SIM-chromatogram is 50 times larger than that of brassicasterol at *m/z* 470 in the SIM-chromatogram. No authentic 24-methylenecholesterol standard was available for carrying out a calibration curve. However, given that both brassicasterol and 24-methylenecholesterol have the same molecular ion (*m/z* 470) with similar relative abundance values of ca. 12% of the base ion in the mass spectrum (Figure 2.6a and Figure 2.6b), the same response factor of 50 was used for 24-methylenecholesterol quantification.

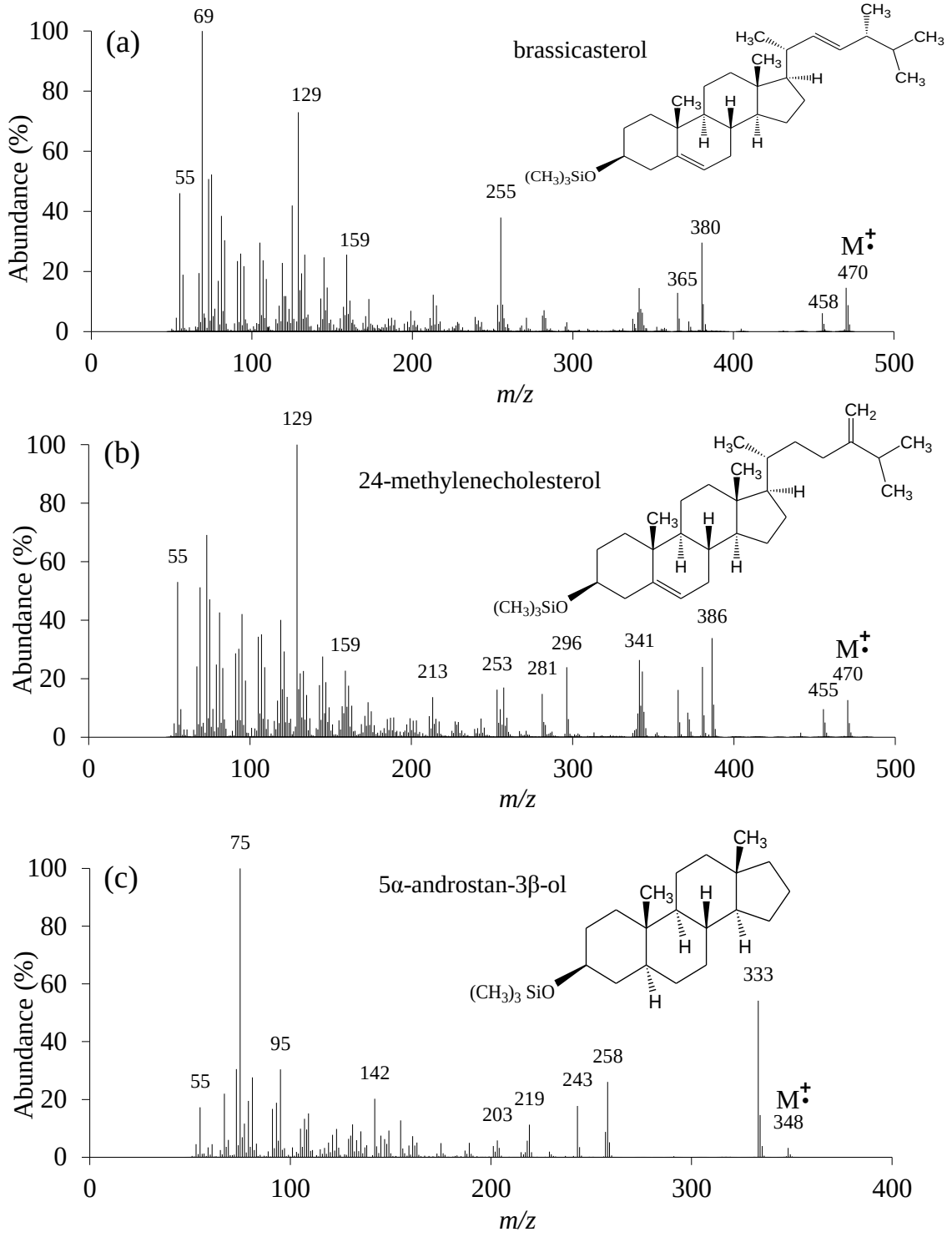

Figure 2.6: Background subtracted mass spectra and structures of C_{28} trimethylsilyl (TMS) sterol ethers described in the current study: (a) 24-Methylcholesta-5,22E-dien-3β-ol (brassicasterol, $M^{+\bullet}$ = *m/z* 470); (b) 24-Methylcholesta-5,24(28)-dien-3β-ol (24-methylenecholesterol, $M^{+\bullet}$ = *m/z* 470); (c) the internal standard 5α-androstan-3β-ol ($M^{+\bullet}$ = *m/z* 348).

2.2.8 Calculation of the PIP_{25} index

Calculation of the PIP_{25} index was achieved by combination of the concentrations of the sea ice biomarker IP_{25} and a biomarker derived from open-water phytoplankton (e.g. brassicasterol) as described previously by Müller et al. (2011). Due to a significant difference between the concentrations of both biomarkers, a balance factor (c), was calculated by dividing the mean IP_{25} concentration by the mean phytoplankton biomarker concentration. The overall PIP_{25} calculation is shown in Equation 2.6.

Equation 2.6:

$$PIP_{25} = \frac{IP_{25}}{(IP_{25} + (Phytoplankton\ biomarker * c\ factor))}$$

2.2.9 Calculation of the DIP_{25} index

In order to examine the concentration relationships between IP_{25} and the co-occurring HBI diene II (hereafter referred to as diene II; Figure 2.2b), relative abundances of IP_{25} and diene II were obtained by integration of the *m/z* 350.3 and 348.3 peaks (molecular ions) from the SIM chromatograms, respectively. The relative magnitudes of these mass spectral responses were used for the analysis, rather than strict concentrations, since calculation of the latter relies on an accurate understanding of the relative GC-MS responses for the two biomarkers (Equation 2.7). P_A denotes the peak area.

Equation 2.7:

$$DIP_{25} = \frac{P_A\ diene\ II}{P_A\ IP_{25}}$$

Although it is also possible to calculate DIP_{25} using concentration in the Plymouth laboratory, this is not necessarily true for other laboratories. Therefore, in terms of

transferability of the approach, the use of single ion ratios possibly represents a more reliable method.

The linear correlation between both biomarkers was also often assessed as a scatter (x-y) representation, where all GC-MS responses for each biomarker (IP_{25} and diene II) were normalised to the maximum value for IP_{25} observed for each core.

2.2.10 Total Organic Carbon

The total organic carbon (TOC %) and nitrogen (TON %) content of sediment were determined using 100 mg ± 5 mg freeze dried sediment which was digested with 10% HCl (1 mL; 18 h) at room temperature to remove inorganic carbonates, after which, the HCl was removed and the sample washed 3 times with milli-Q water. Samples were analysed by Andrew Tonkin (Plymouth University) with a Carlo Erba EA 1110 elemental analyser for carbon, nitrogen and hydrogen.

2.3 Methodological developments

As part of this research, a number of developments regarding laboratory methods were needed. These comprised the validation of a new internal standard for HBI quantification, the development of a Ag-Ion chromatographic technique, the removal of sulphur from sediment extracts and a GC-MS method development to increase sensitivity.

2.3.1 Internal standards for lipid quantification

The addition of internal standards to sediment samples prior to extraction was used to permit quantification of extracted compounds. Moreover, experimental variations such as extraction efficiency, purification and dilution of extracts prior to GC-MS analysis were also considered. Previous IP_{25} studies used 7-hexylnonadecane (7-HND, MW = 352 g mol^{-1}; Figure 2.4c) as an internal standard for quantification. 7-HND has 25 carbon atoms with an alkyl branch similar to that of IP_{25} and was synthesised by Andrew Tonkin (Plymouth University) (Belt et al., 2012b). Indeed, the structural similarities between IP_{25} and 7-HND showed similar extraction and purification efficiencies (Belt et al., 2012b). However, although 7-HND and IP_{25} have similar GC-MS responses in the TIC mode, due to their near identical elemental formula, their responses in SIM mode (*m/z* 99.0 and 350.3 for 7-HND and IP_{25}, respectively), which is used for quantification of analytes, is rather different. In addition, since 7-HND is a saturated hydrocarbon, it is not suitable for use as an internal standard when using the Ag-Ion purification method as it elutes in a different fraction to IP_{25}.

In order to try to overcome these issues, another branched hydrocarbon, 9-octylheptadec-8-ene (9-OHD; Figure 2.4b) was synthesised by Andrew Tonkin (Plymouth University) (Belt et al., 2012b). Unlike 7-HND, 9-OHD contains a single double bond, and has the same molecular weight as IP_{25} (MW = 350.3 g mol^{-1}). The use of 9-OHD as an internal standard therefore had, the potential to show more appropiate behaviour to that of IP_{25} compared to 7-HND, especially regarding extraction, purification and mass spectral responses. A series of experiments were carried out with the purpose of examining the reliability of 9-OHD as an internal standard for quantification of biomarkers, such as IP_{25} and other HBIs.

2.3.2 Volume (mL) of eluent needed for open silica column chromatography

Routine analysis of marine sediments required both extraction and partial purification of total organic extracts (Belt et al., 2012b). In order to establish the volume of eluent (hexane) needed to elute the internal standards as well as desired analytes (e.g. IP_{25}) for open silica column chromatography, two experiments were performed.

Firstly, an experiment that only comprised a sample containing both internal standards was carried out. Silica (0.7 g; 60-200 µm, Fisher, UK) was transferred to a glass pipette, previously plugged with pre-cleaned (DCM) cotton wool. After the silica column was conditioned with hexane (ca. 3 mL), 10 µL of a solution containing both 7-HND and 9-OHD (10 µg mL^{-1} each) was added onto the column. The column was then continuously eluted with hexane, and 0.25 mL fractions collected (4 mL total). Finally, the column was eluted with 4 mL of DCM as a single fraction, to make sure that both internal standards had been completely eluted. After evaporation under a N_2 stream, all fractions were re-suspended in 1 mL of hexane and analysed by GC-MS. Peak areas in the SIM chromatograms were measured at *m/z* 350.3 and 99 for 9-OHD and 7-HND, respectively. The results (Figure 2.7) showed that both internal standards were completely eluted from the silica column using ca. 2.5 mL of hexane. No internal standards were found after 2.5 mL or in the DCM fraction.

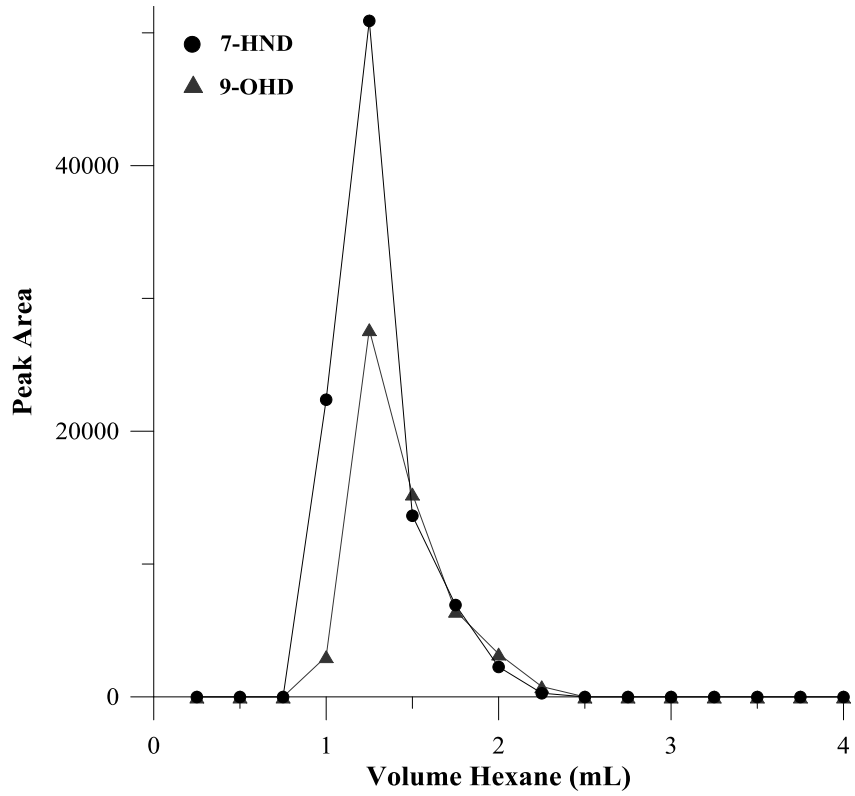

Figure 2.7: Internal standards (7-HND and 9-OHD) peak areas according to volume of hexane (mL) used in open silica chromatography.

In a second experiment, an extract with known IP_{25}, 7-HND and 9-OHD concentrations was added to the silica column. Once again, the results derived from GC-MS analysis showed that both internal standards were completely eluted after ca. 3 mL of hexane (Figure 2.8). IP_{25} was also completely eluted with ca. 2.5 mL of hexane, suggesting that the internal standards 7-HND and 9-OHD showed a similar chromatographic behaviour to that of IP_{25} on the silica column. No internal standards or IP_{25} were detected in the DCM fraction.

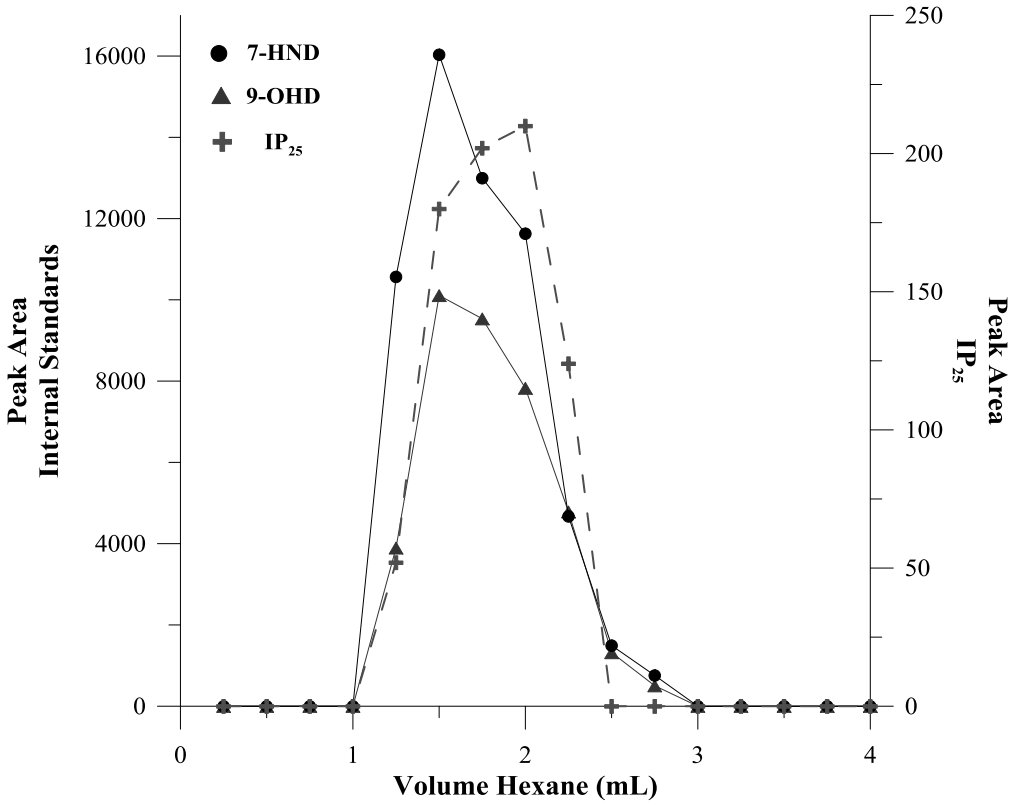

Figure 2.8: Internal standards (7-HND and 9-OHD) and IP_{25} peak areas according to volume of hexane (mL) used in open silica chromatography.

2.3.3 Losses of organic compounds in dried sediment extracts under N_2 stream

An experiment was performed to check the influence of (over) exposure of the N_2 stream on the internal standards. In order to achieve this, a series of 8 vials, each of which contained 10 µL of 7-HND and 9-OHD (10 µg mL^{-1} each) and 1 mL of hexane were prepared. Following complete evaporation of hexane from all vials, one vial was kept as a control (time = 0 min). The remaining vials were kept under continuous N_2 stream and one was removed every 10 min up to 60 min (Figure 2.9). An extra sample was kept for 90 min. Samples were then re-suspended in 1 mL of hexane for analysis by GC-MS.

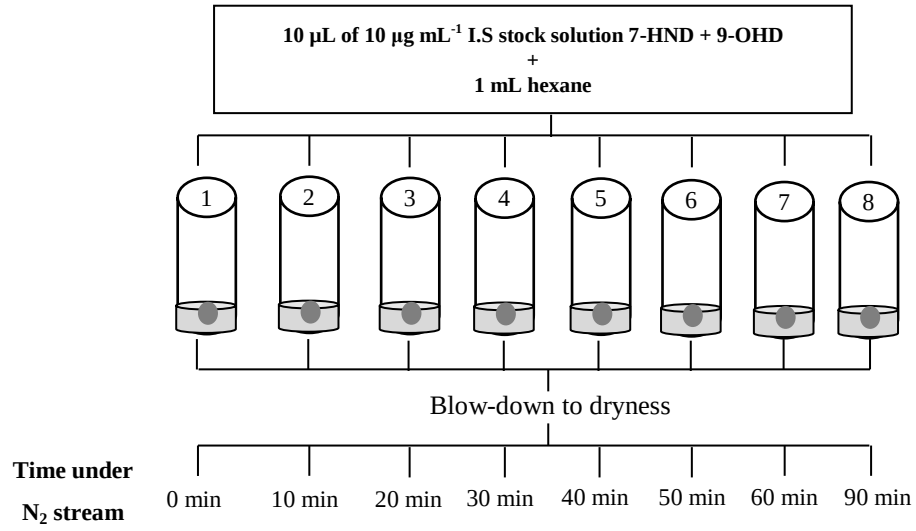

Figure 2.9: Experiment to study the influence of over exposure of the internal standards (7-HND and 9-OHD) under N_2 stream.

Subsequent manual integration of peak areas from SIM chromatograms of each internal standard (m/z 350.3 and 99 for 9-OHD and 7-HND, respectively) of all samples was performed. As shown in Figure 2.10a, decrease in peak areas of both internal standards over time was clear, suggesting that significant losses under extended blow-down under nitrogen were evident. The initial sample (t = 0) was used as the reference from which losses (as percentages) of internal standards for other samples (i.e. 10, 20, 30, 40, 50, 60 and 90 min) were obtained (Figure 2.10b). As seen in Figure 2.10b, a loss of internal standards of ca. 10% after 10 min of exposure under a N_2 stream was observed and losses increased with time. In all of the samples (excluding the 20 min sample), the percentage loss was slightly higher for 9-OHD than 7-HND, indicating that 9-OHD is slightly more volatile than 7-HND. This experiment showed the importance of controlling the samples under N_2 stream as extended blow-down times lead to significant losses of internal standards, and therefore, probably also of IP_{25} and compounds of similar volatilities (Belt et al., 2012b).

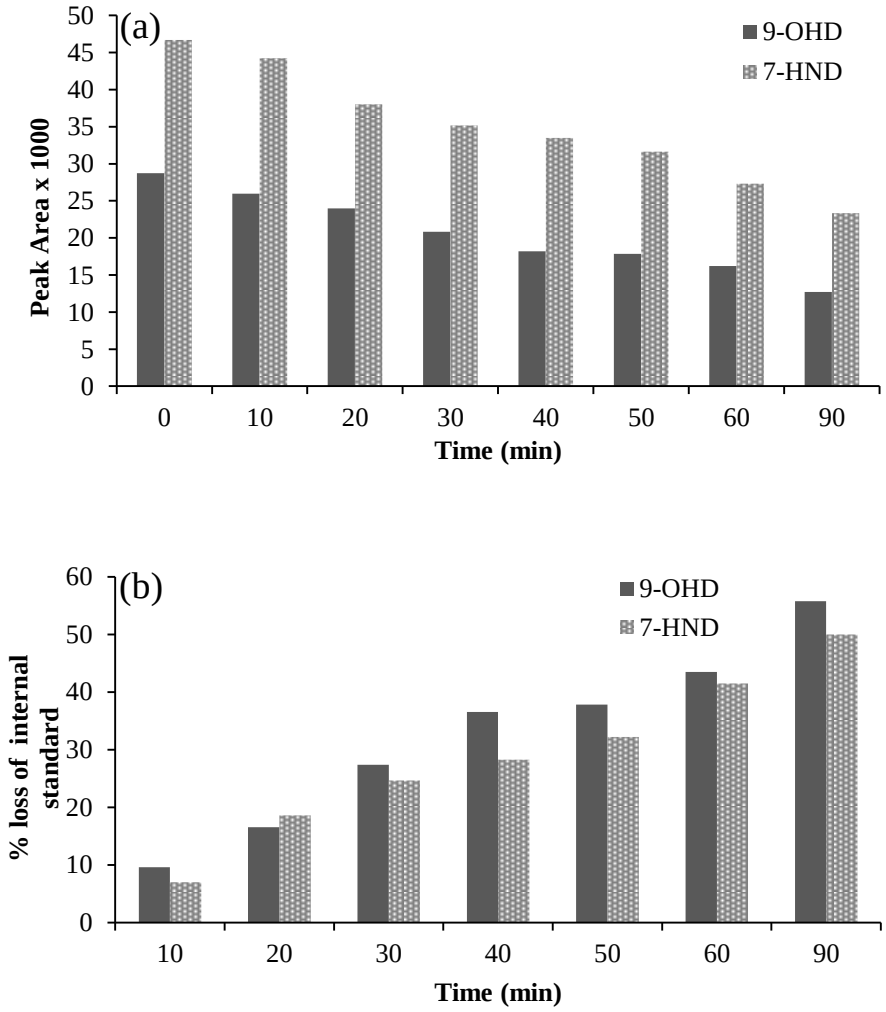

Figure 2.10: (a) Peak area of the internal standards (7-HND and 9-OHD) compared to N_2 stream exposure time; (b) Percentage of internal standards lost over time under N_2 stream.

2.3.4 Study of the contribution of other organic compounds to the Internal Standard and IP_{25} signal in the SIM-chromatogram

Each internal standard used in the extraction process (7-HND and 9-OHD) has a unique retention time when analysed by GC-MS. In order to establish if the peak attributed to the internal standard and IP_{25} had any contribution from co-eluting organic compounds within the sediments, further sediment samples of each of the sediment cores analysed during this research were also analysed without the addition of internal standards. In all the studied sediment cores (except GKC cores as sediment material availability was limited to biomarker analyses) no signal was found at the retention times corresponding to the internal standards (*m/z* 99 for 7-HND and *m/z* 350.3 for 9-OHD) and IP_{25} (*m/z* 350.3).

Although shown not to be a problem here, the existence of analytes that co-elute with the internal standards and IP_{25} could make GC-MS quantification of the analytes of interest less reliable. Therefore, it is suggested that the procedure described here should be adopted regularly when analysing a sediment core in order to make sure that the GC-MS peaks attributed to the internal standards and IP_{25} have no contributions from other compounds.

2.4 Removal of elemental sulphur

In some cases (e.g. JM09-KA11-GC sediment core, Chapter 5) TOEs were found to contain high concentrations of elemental sulphur (S_8, Figure 2.11d) that interfered with the subsequent gas chromatographic analyses. This was removed from the TOEs before further purification based on a rapid, efficient and non-destructive method described previously by Jensen et al. (1977) and based on the following chemical reaction (Equation 2.8). TBA^+ refers to tetrabutylammonium ion.

Equation 2.8:

$$(TBA^+)_2\ SO_3^{2-} + S_{(s)} \rightleftharpoons 2\ TBA^+ + S_2O_3^{2-}$$

A tetrabutylammonium sulphite reagent $(TBA^+)_2SO_3^{2-}$ (TBA reagent) was prepared by adding 3.39 g of tetrabutylammonium hydrogen sulphate, extra pure ($C_{16}H_{37}NO_4S$, Fisher Scientific) in 100 mL of Ultra High Purified (UHP) water saturated with 25 g of sodium sulphite anhydrous (Na_2SO_3, Fisher Scientific). Once the reagent was prepared, hexane (1 mL) was added to the dried TOEs, followed by TBA reagent (1 mL) and 2-propanol (2 mL). This was then shaken by hand (1 min). After addition of Ultra High Purified water (3 mL), the samples were shaken again (1 min) and centrifuged (2500 rpm; 2 min). The hexane layer (containing the lipids of interest) was transferred to a clean vial and the procedure repeated twice more. After evaporation of the solvent by N_2 stream, the TOEs were purified following methods described previously in this chapter (Section 2.2.4).

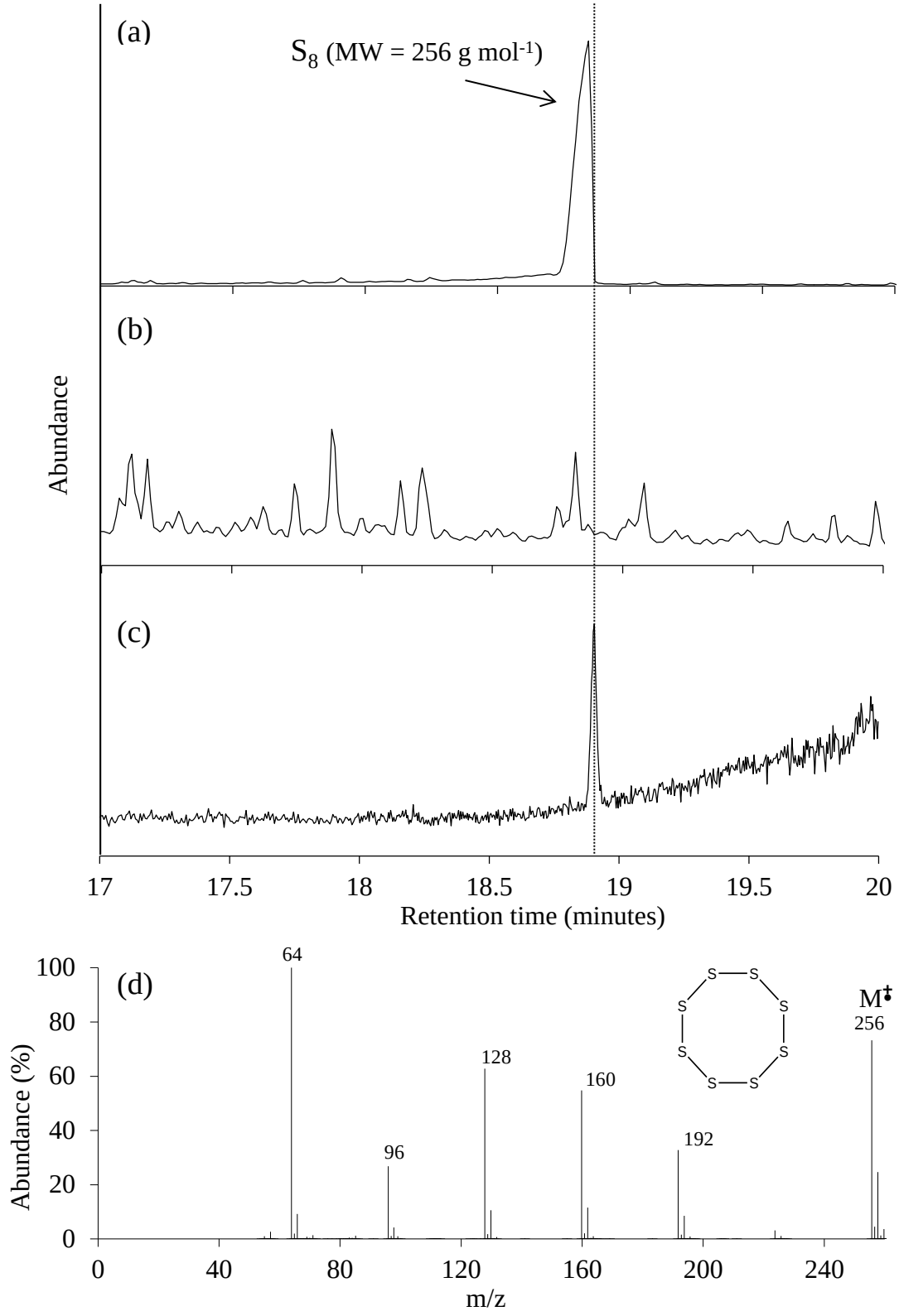

Figure 2.11: (a) TIC GC-MS chromatogram before sulphur removal; (b) TIC GC-MS chromatogram after sulphur removal; (c) SIM GC-MS chromatogram with selected ion *m/z* 350.3 (IP_{25}) after sulphur removal. Dashed line indicates the retention time of IP_{25}; (d) Background subtracted mass spectra and structure of elemental sulphur ($M^{\ddagger}$ = *m/z* 256).

This procedure was tested using a marine sediment. This sediment contained IP_{25}, HBIs and sulphur (Figure 2.11a) (GC-MS). Re-analysis of the same sample after sulphur removal enabled comparison of HBIs concentrations before and after this procedure. As can be seen from Figure 2.11b, the sulphur was successfully removed from the sample using the approach previously described. The IP_{25} biomarker was still present (Figure 2.11c), as well as di- and tri-unsaturated HBIs, with concentrations very similar to those obtained before the sulphur removal (Table 2.2)

Table 2.2: HBIs concentrations (μg g^{-1} dry sed) before and following removal of elemental sulphur from the sediment extract.

HBI	**Concentration (μg g^{-1}dry sed) prior removal of elemental sulphur**	**Concentration (μg g^{-1} dry sed) following removal of elemental sulphur**
IP_{25}	0.0157	0.0142
diene II	0.0982	0.0899
triene Z	0.0379	0.0402
triene E	0.0390	0.0471

2.5 Purification and analysis of IP_{25} and unsaturated HBIs at low concentrations.

2.5.1 Analysis of IP_{25} at low concentrations

In order to detect IP_{25} at very low concentrations, an additional purification step was developed using Ag-Ion chromatography (Supelco discovery® Ag-Ion). With the aim of testing this new methodology, a reference sediment from the Canadian Arctic Archipelago, with a known concentration of IP_{25}, was analysed before and after the Ag-Ion chromatographic purification (Figure 2.13). Once the extracts had been partially purified (SiO_2; hexane), the purified extracts were further fractionated into saturated and unsaturated components using glass pipettes containing Ag-Ion stationary phase

(Supelco discovery® Ag-Ion). Saturated hydrocarbons were eluted first (hexane; 5 mL, then DCM; 5 mL) and unsaturated hydrocarbons (including IP_{25}) were eluted with DCM/acetone (95/5; 10 mL) with further poly-unsaturated hydrocarbons eluted with acetone (5 mL; Figure 2.12).

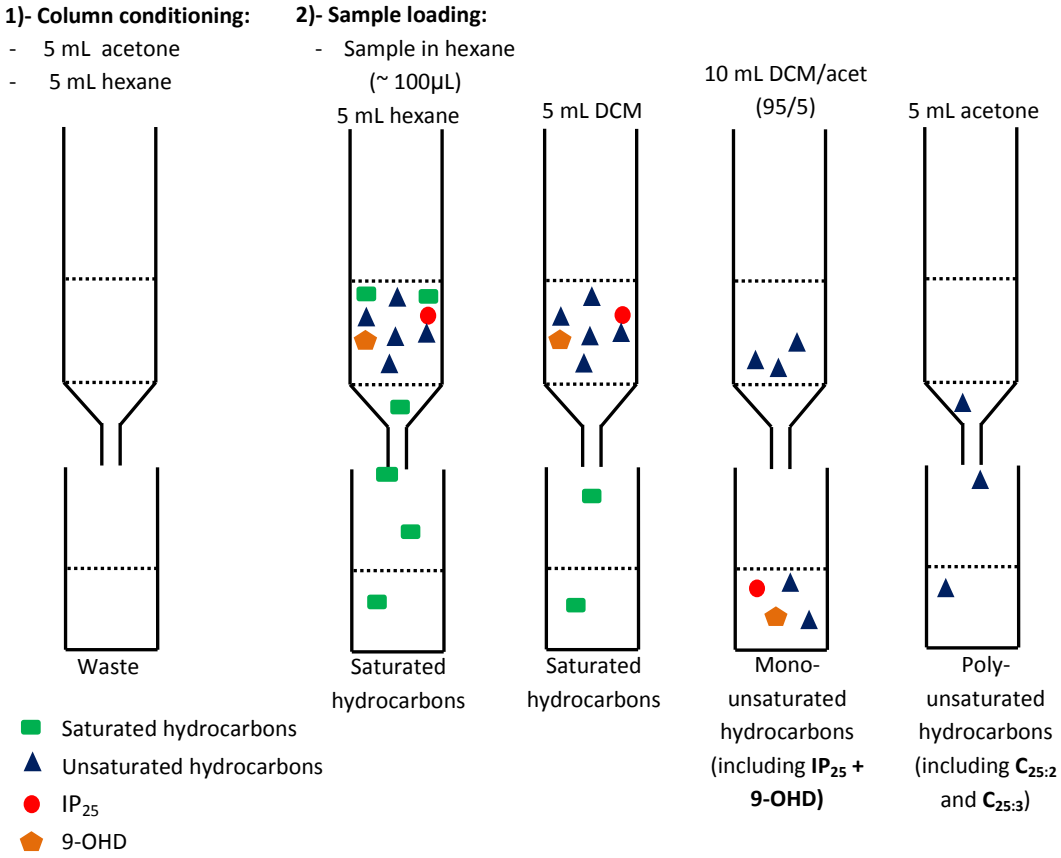

Figure 2.12: Schematic of the Ag-Ion chromatographic procedure for fractionation of saturated and unsaturated hydrocarbons. IP_{25} and the internal standard (9-OHD) used for quantification were eluted together in the DCM/acetone fraction.

Following analysis by GC-MS of the fractions obtained after Ag-Ion chromatography, IP_{25} (Figure 2.13c) and the internal standard (9-OHD) were present in the DCM/acetone (95/5) fraction, and were absent from all other fractions. Other unsaturated hydrocarbons, such as di-unsaturated and tri-unsaturated HBIs, were not recovered in the DCM/acetone (95/5) fraction. SIM GC-MS chromatograms of the sediment sample

before and after Ag-Ion chromatography (DCM/acetone fraction) were consistent, with IP_{25} concentrations of 0.098 and 0.096 μg g^{-1} dry sediment before and after Ag-Ion chromatography respectively (Figure 2.13b and Figure 2.13c), indicating that few if any losses occurred during Ag-Ion purification. The methodology developed was thus considered satisfactory when IP_{25} concentration was relatively high.

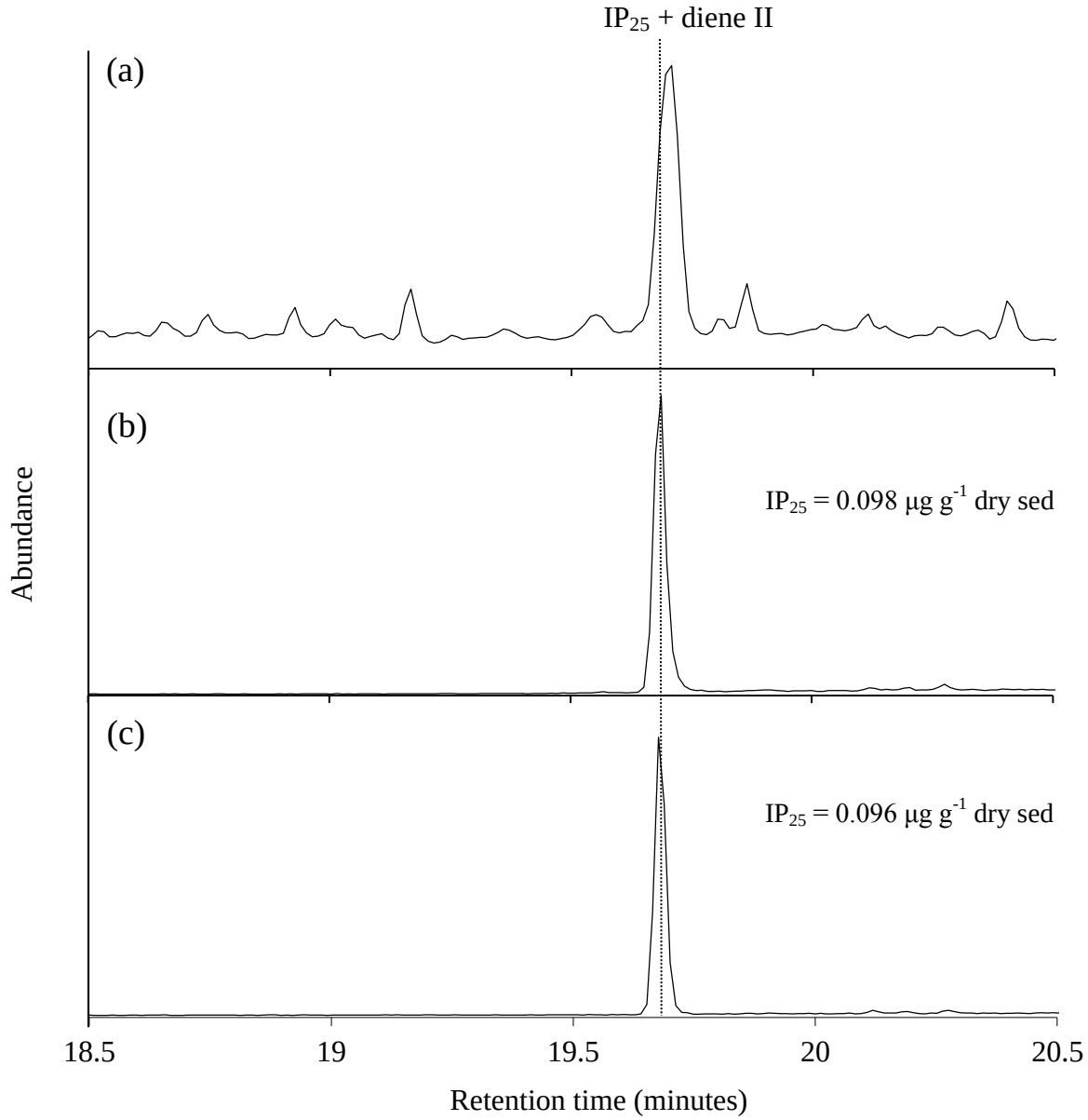

Figure 2.13: (a): TIC GC-MS chromatogram of a reference sediment sample from the Canadian Arctic Archipelago before Ag-Ion chromatography; (b) SIM GC-MS chromatogram with selected ion *m/z* 350.3 before Ag-Ion chromatography; (c) SIM GC-MS chromatogram of the DCM/acetone (95/5) fraction, with selected ion *m/z* 350.3 after Ag-Ion chromatography. Dashed line indicates the retention time of IP_{25}.

Once this methodology had been tested with a sediment sample containing relatively high IP_{25} abundances, a sediment sample from the Denmark Strait area (JM96-1213 core) where IP_{25} appeared absent (or below the limit of detection) using the standard extraction/purification procedure was used for testing. Further purification of the partially purified (SiO_2) TOEs by Ag-Ion chromatography and analysis by GC-MS of the sample containing the DCM/acetone fraction by GC-MS resulted in the successful removal of saturated hydrocarbons that were obscuring the IP_{25} signal. This allowed the detection of IP_{25} at lower detection limits (S/N > 3) (Figure 2.14).

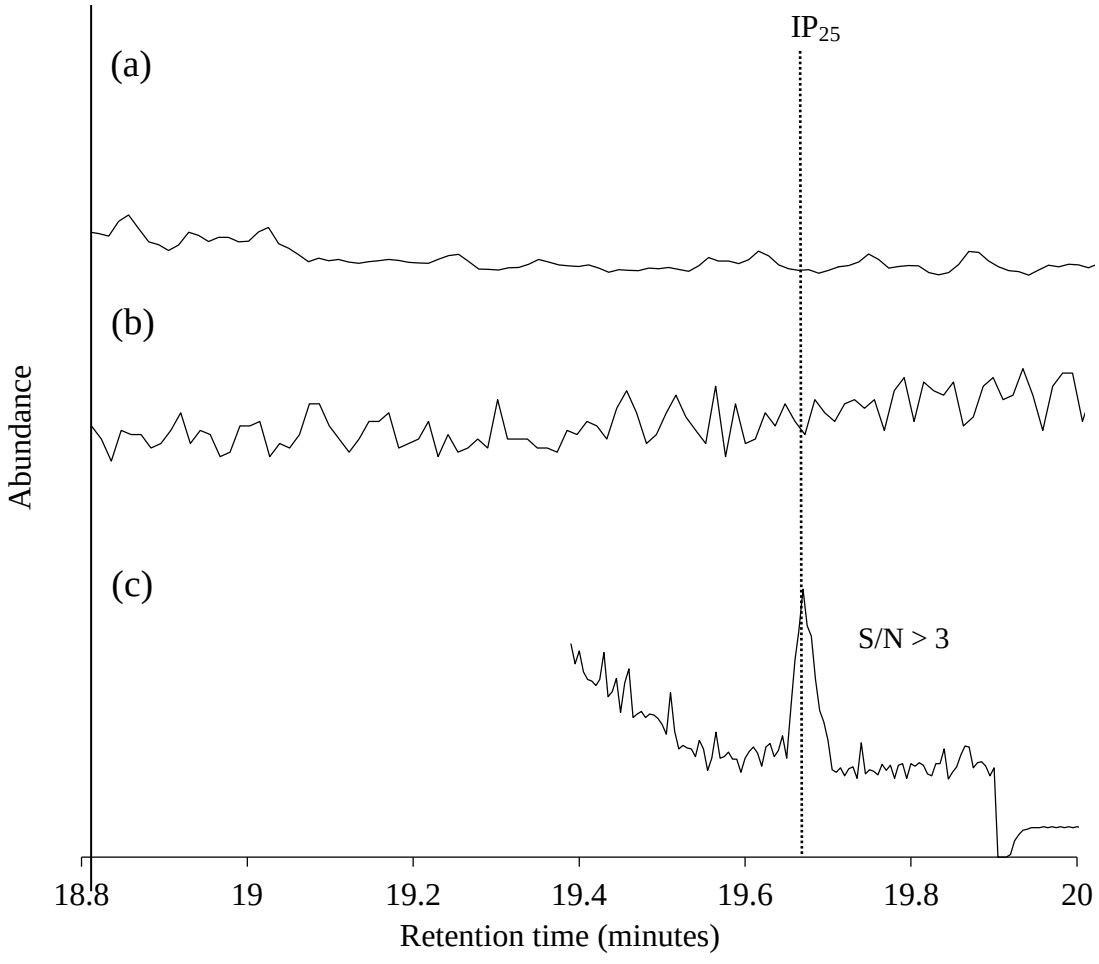

Figure 2.14: (a): TIC GC-MS chromatogram of a sediment sample where IP_{25} was not detectable before Ag-Ion chromatography; (b) SIM GC-MS chromatogram, with selected ion *m/z* 350.3 before Ag-Ion chromatography; (c) SIM GC-MS chromatogram of the DCM/acetone (95/5) fraction, with selected ion *m/z* 350.3 after Ag-Ion chromatography. Dashed line indicates the retention time of IP_{25}.

A number of factors, such as changes in sensitivity of the GC-MS and type of extracted sediment material (i.e. amount and type of organic matter contained in sediments) prevented determination of an exact limit of detection. However, an analytical limit of detection of 10 ng mL^{-1} was estimated from pure IP_{25} using standard GC-MS conditions. In practice the limit of detection will vary based on instrument performance.

2.5.2 Analysis of unsaturated HBIs at low concentrations

When other more unsaturated hydrocarbons (e.g. di- or tri-unsaturated) were needed for analysis (Figure 2.2, Figure 2.3 and Figure 2.4) another procedure similar to the one described previously was used. In this case, the column was first conditioned with 5 mL of acetone and then 5 mL of DCM. The silica purified sample was then diluted in DCM and loaded onto the column. Saturated hydrocarbons were eluted with 5 mL of DCM and unsaturated hydrocarbons (including IP_{25}, 9-OHD and poly-unsaturated HBIs) were eluted with 5 mL of acetone (Figure 2.15).

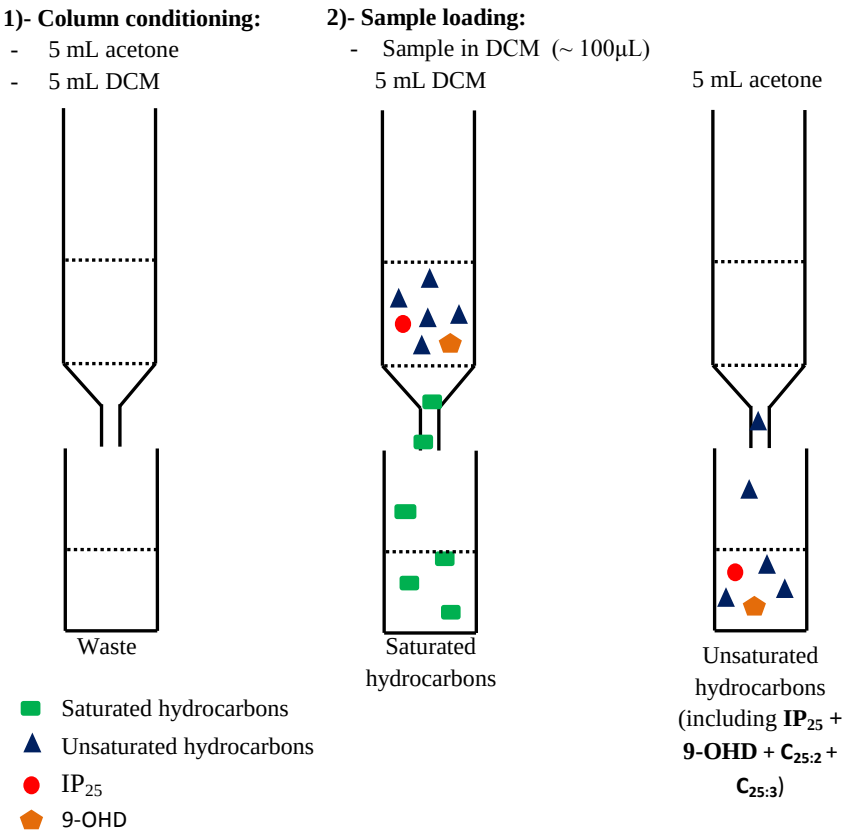

Figure 2.15: Schematic of the Ag-Ion chromatography procedure for fractionation of saturated and unsaturated hydrocarbons.

Next, an attempt was made to reduce the amount of Ag-Ion chromatography material used in each column in order to minimise the amount of solvent used and reduce time and overall cost of the procedure. Previously, Ag-Ion chromatographic purification was carried out with ca. 500 mg of Ag-Ion solid phase. Hexane extracts from a previously analysed sediment were further fractionated into saturated and unsaturated components using glass pipettes containing 100 mg of Ag-Ion chromatography material (Supelco discovery® Ag-Ion). Saturated hydrocarbons were eluted with hexane (1 mL; Figure 2.16) and unsaturated hydrocarbons (including IP_{25}, 9-OHD and the rest of HBIs under study) were eluted with acetone (2 mL) before being dried (N_2).

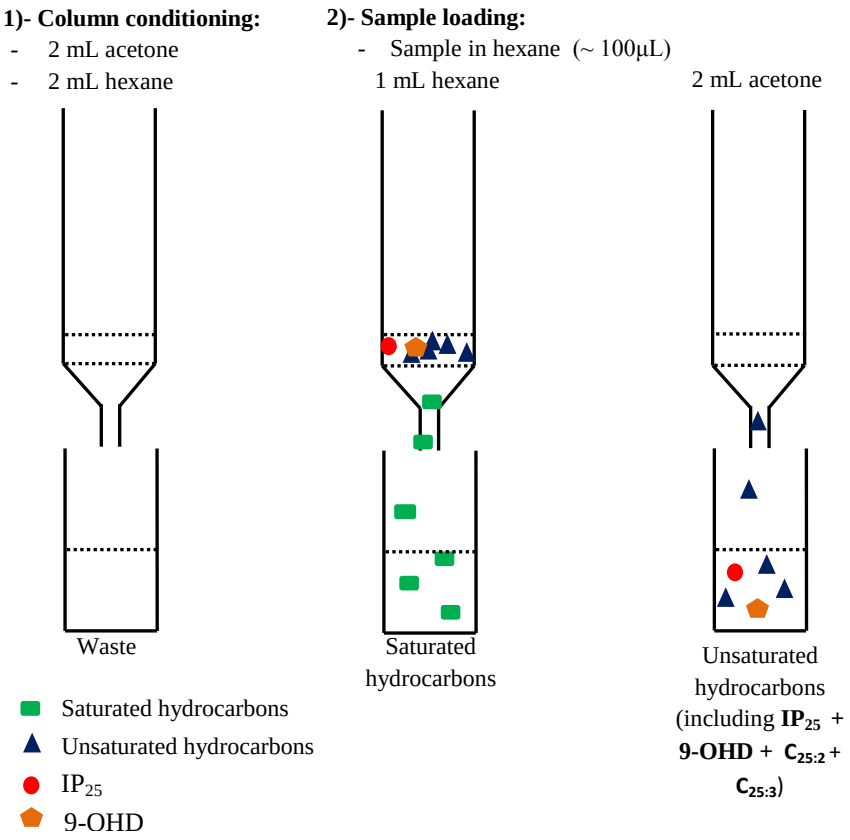

Figure 2.16: Schematic of the Ag-Ion chromatography procedure for fractionation of saturated and unsaturated hydrocarbons using 100 mg of Ag-Ion chromatographic material.

All HBIs were absent from the hexane fraction, which contained mainly saturated hydrocarbons (Figure 2.17b). The acetone fraction (Figure 2.17c) contained all the HBIs of interest, with concentrations that were very similar to those obtained via the standard purification procedure (Table 2.3).

Table 2.3: HBIs concentrations before and after the Ag-Ion chromatography purification procedure.

HBI	**Concentration (µg g^{-1} dry sed) before Ag-Ion**	**Concentration (µg g^{-1} dry sed) following Ag-Ion**
IP_{25}	0.0054	0.0056
diene II	0.0360	0.0360
triene Z	0.0021	0.0020
triene E	0.0024	0.0025

The use of hexane allowed the removal of all saturated hydrocarbons that were present in the sediment extract at relatively high abundances (Figure 2.17b). When comparing relative abundances of the TIC chromatogram of the sediment extract before Ag-Ion chromatography (Figure 2.17a) with that of the acetone fraction (containing the HBIs of interest) after Ag-Ion chromatography (Figure 2.17c), a considerably reduced background signal with lower abundances was observed in the latter. This allowed further concentration of the extract without overloading the MS detector and hence detecting of HBIs at lower concentrations.

This improved approach, therefore, allowed the analysis of all HBIs in the same fraction using less Ag-Ion chromatography material and solvents, thus reducing the time and costs of each chromatographic purification.

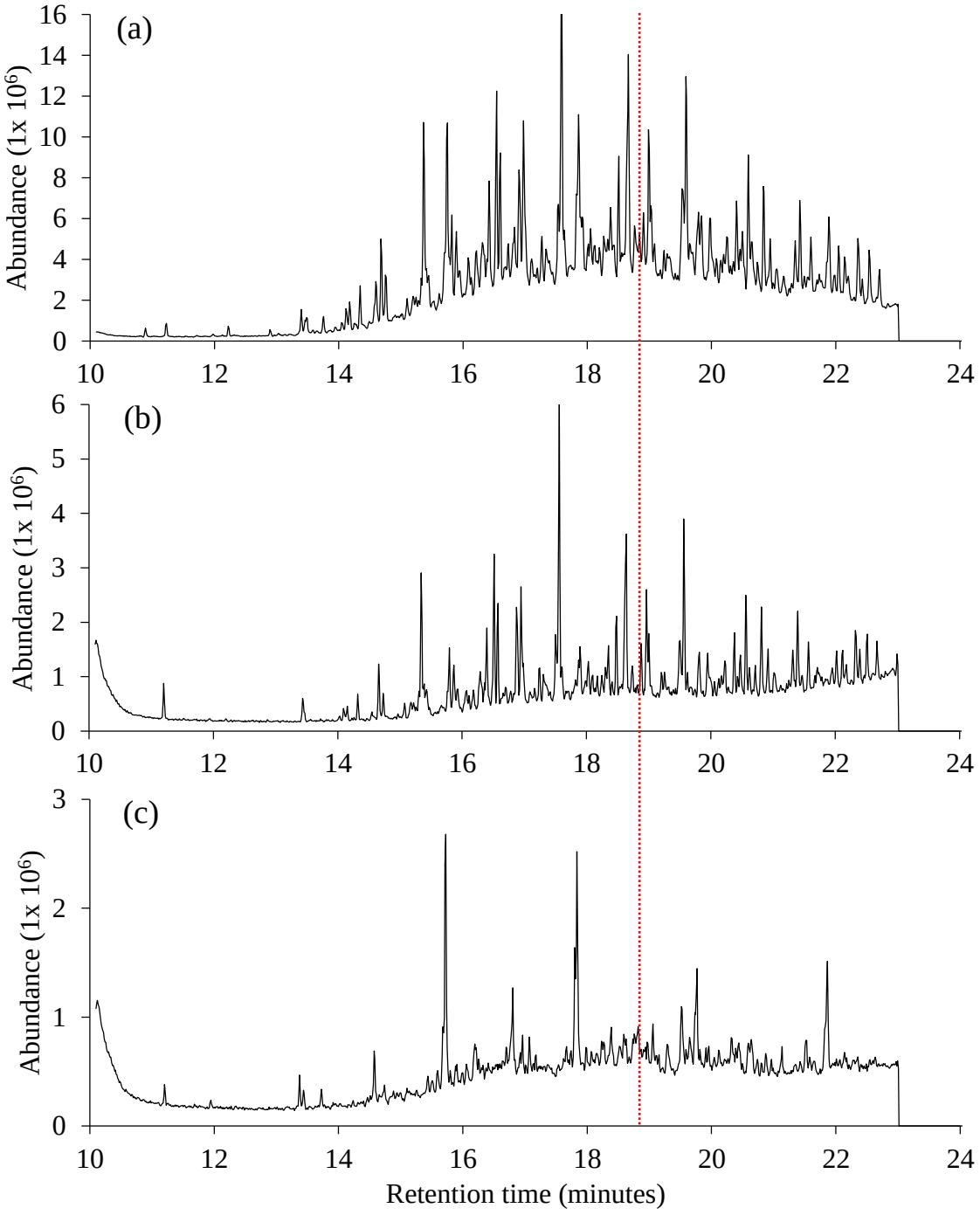

Figure 2.17: (a) TIC GC-MS chromatogram, before Ag-Ion chromatography; (b) TIC GC-MS chromatogram after Ag-Ion chromatography, hexane fraction; (c) TIC GC-MS chromatogram after Ag-Ion chromatography, acetone fraction. Dashed line indicates the retention time of IP_{25}.

2.5.3 GC-MS method development

In order to further improve the instrumental (GC-MS) sensitivity for IP_{25} detection and quantification, a modified method was developed. General features of both methods, the HBI SIM-SCAN regular (so-called 'regular' method) and HBI SIM-SCAN IP_{25} high sensitivity (1) (so-called 'high sensitivity' method(1)) are shown in Table 2.4. A third method (high sensitivity-short detection window (2)) was also developed to allow further concentration of the sample (when possible) without affecting the MS detector, consisting of a shorter detection window focused on the known IP_{25} retention time.

Table 2.4: General features of GC-MS methods developed for regular and high sensitivity analysis of IP_{25}.

Method name	**HBI SIM-SCAN regular**	**HBI SIM-SCAN IP_{25} high sensitivity (1)**	**HBI SIM-SCAN IP_{25} high sensitivity (2)** (short detection window)
Function	Routine HBI detection	Increased sensitivity for IP_{25} only	Increased sensitivity for IP_{25} only
Mass range (*m/z*)	50-500	50-500 (18-20 min = 90-360)	90-360
SIM ions (*m/z*)	350.3, 348.3, 346.3, 99	350.3	350.3
Total run time	36 min	36 min	36 min
GC Temperature profile	$40^{o}C$ - $300^{o}C$ at $10^{o}C\ min^{-1}$ (10 min isothermal)	$40^{o}C$ - $300^{o}C$ at $10^{o}C\ min^{-1}$ (10 min isothermal)	$40^{o}C$ - $300^{o}C$ at $10^{o}C\ min^{-1}$ (10 min isothermal)
Detection time	10-26 min	10-25 min	18.5-19.5 min

Moreover, some changes in the injection method were developed in order to further improve the sensitivity of the analysis. The Agilent 7890A GC coupled to a 5975 series mass selective detector used in this study has a split/splitless injector (Figure 2.18). The injector contains a carrier gas inlet, a septum, septum purge, injector insert, heater block, column connection and a split line or vent. The sample is injected through the septum into the glass liner. The carrier gas (He) enters the chamber and the sample is vaporised to form a mixture of carrier gas, vaporised solvent and vaporised solutes. If

the split vent is closed (Splitless mode), all the analyte sample vaporised in the injector goes onto the column. After the injection (usually 30 – 60 s), the split vent is opened to purge excess solvent (and remaining sample). This technique allows a greater amount of the injected sample to enter onto the column. If the split vent is open (Split mode), then most of the vaporised sample is thrown away to waste via the split vent and only a small portion of the sample is introduced onto the column. In both modes there is a purge flow which prevents septum degradation products from entering in the system and helps keep sample adsorbed on the septum from previous injections from getting into the gas in the injector and creating ghost peaks.

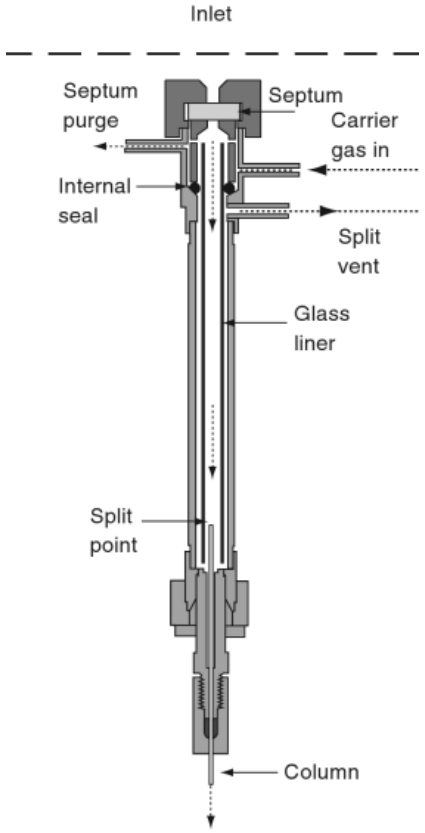

Figure 2.18: Diagram illustrating a split/splitless injector with the split vent open so that only a small portion of the sample injected goes onto the column (Sparkman et al., 2011).

In regular HBI analysis the injector works in splitless mode and therefore all the sample goes onto the column, achieving greater sensitivity than in split mode (Table 2.5). The high sensitivity method used a similar technique, named pulsed splitless where the sample is injected and a pulse pressure of 25 psi is held for 0.35 min. The pulsing effect maximizes sample introduction into the column while narrowing the sample bandwidth. The use of this new method increased the sensitivity up to 22%.

Table 2.5: General features of the split/splitless injector in the regular and high sensitivity GC-MS methods.

Method name	**HBI SIM-SCAN regular**	**HBI SIM-SCAN IP_{25} high sensitivity**
Injection Volume	1 µL	1 µL
Mode	Splitless	Pulsed splitless
Heater	300°C	300°C
Pressure	7.0699 psi	5.7608 psi
Total Flow	104 mL/min	104 mL/min
Septum Purge Flow	3 mL/min	3 mL/min
Gas Saver	20 mL/min after 3min	20 mL/min after 3min
Injection Pulse Pressure	-	25 psi until 0.35 min
Purge Flow to Split Vent	100 mL/min at 0.5 min	100 mL/min at 0.35 min

CHAPTER THREE

3 Quantification of IP_{25} and other HBIs in marine sediments

3.1 Extraction, isolation and GC-MS calibration of IP_{25}

3.1.1 Introduction

3.1.1.1 Isolation and structural characterisation

The structure of what was believed to be IP_{25} was determined previously following synthesis from a closely related C_{25} diene and characterisation using ^{1}H and ^{13}C NMR spectroscopy (Belt et al., 2007). In contrast, the identification of IP_{25} in extracted Arctic marine sediments has, to date, been achieved exclusively by comparison of its gas chromatographic (GC) and mass spectral (MS) responses with those reported for the synthetic (authentic) standard (Belt et al., 2007). The main aim of this chapter was to confirm that the structure of the naturally occurring compound routinely identified in marine sediments as IP_{25} on the basis of its GC and MS characteristics was the same as that of the synthetic standard. In order to achieve this aim, the organic matter from Arctic marine sediments were extracted and purified through several chromatographic techniques to obtain IP_{25} in sufficiently large quantity for analysis by both NMR and GC-MS.

3.1.1.2 Requirement for GC-MS calibration

The accurate quantification of IP_{25} and other HBIs in marine sediments necessitates the use of an internal standard which is added to the sediment material prior to extraction (e.g. Belt et al., 2012b). In the simplest or most ideal cases, the analyte (IP_{25} and other HBIs) and the internal standard would have the same chromatographic and mass spectral characteristics when performing the analysis by GC-MS. However, differences in their chemical structures normally results in different mass spectral responses, especially when quantifying using SIM techniques since not all compounds are ionisable or detectable with similar efficiencies. To accommodate these differences a calibration of the relative GC-MS responses of IP_{25} (and other HBIs) and the internal standard (9-OHD) was carried out to enable accurate quantification of IP_{25} and other HBIs in Arctic marine sediments.

3.1.2 Experimental

3.1.2.1 Sediment material

Marine sediment material was obtained from Barrow Strait, Victoria Strait and Dease Strait in the Canadian Arctic Archipelago in 2005 as part of the ArcticNet cruise as described previously (Belt et al., 2007). Individual (1cm) freeze-dried horizons covering the entire core lengths (0 – 4, 0 – 6 m) were combined into batches of 50 – 3,000 g and extracted using a combination of Soxhlet and suspension/stirring methods.

3.1.3 Extraction procedure

A summary of the laboratory techniques used to obtain IP_{25} from marine sediments is shown in Figure 3.1.

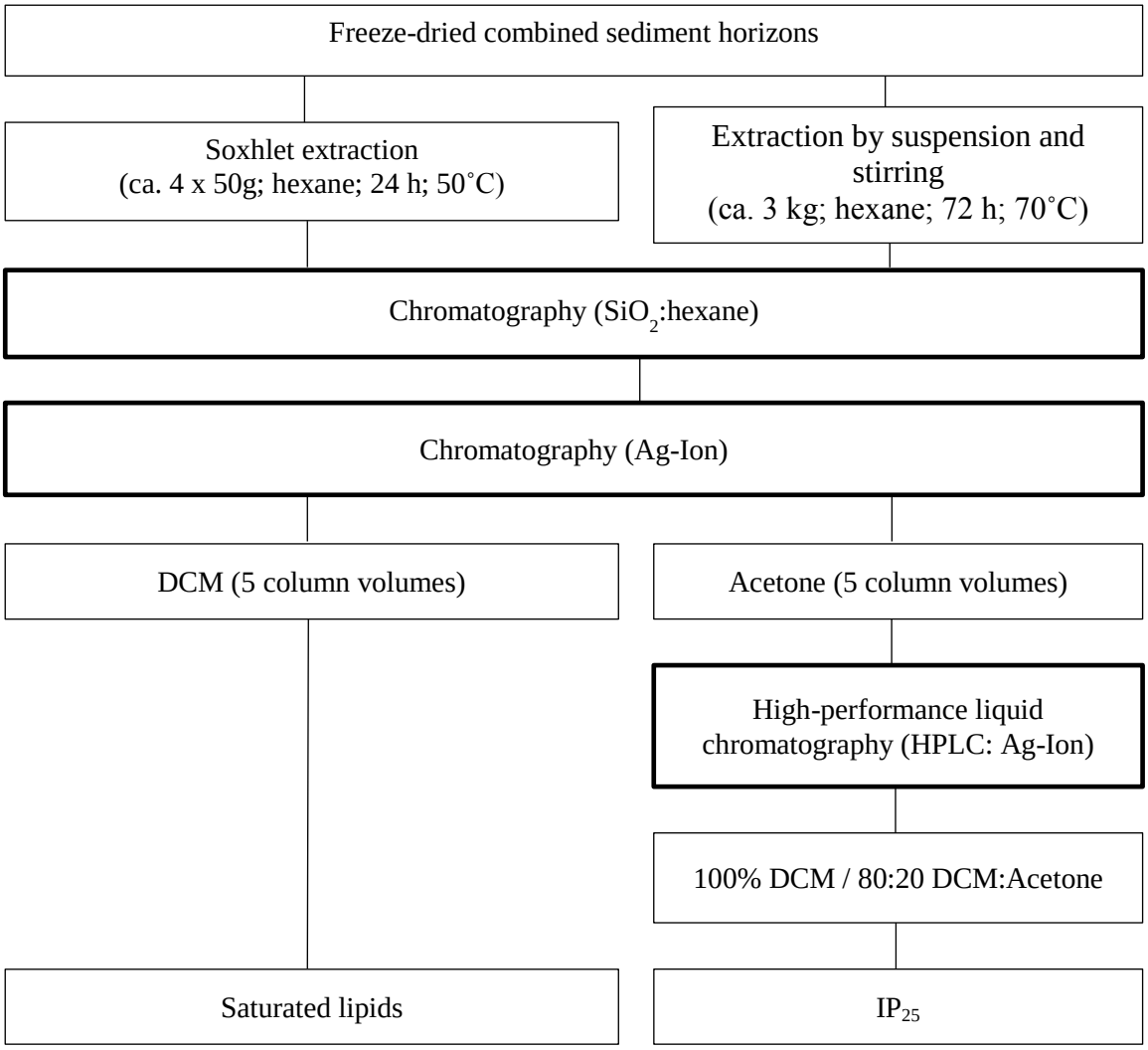

Figure 3.1: Sample extraction and purificaion flow diagram for obtaining IP_{25} from marine sediments.

3.1.3.1.1 Pilot study

The pilot study was a first attempt to make sure that the extraction, identification and quantification of IP_{25} from marine sediments was feasible. Combined horizons from each sampling location were extracted by Soxhlet extraction (Figure 3.2).

Figure 3.2: Series of four soxhlet extraction apparatus.

Approximately 50 g of sediment were added into cellulose extraction thimbles (Fisher, UK) and closed with a pre-cleaned (DCM/MeOH) cotton wool plug. Filled Soxhlet thimbles (x 4) were then refluxed (50˚C, 24 h) using hexane. The Soxhlet assembly was covered with foil to avoid possible photodegradation of HBIs under the influence of light and to provide thermal insulation to improve Soxhlet efficiency.

Following Soxhlet extraction, total hexane extracts (THE) were first partially evaporated by rotary evaporator to a small volume (R-215, Büchi, 25˚C) and then to dryness (N_2 stream; 25˚C) prior to purification.

3.1.3.1.2 Large-scale organic extraction

Since the pilot study (Soxhlet) was found to be effective, but time-consuming (only small amounts of sediment fit in each Soxhlet thimble), a larger-scale organic extraction was carried out to increase the amount of marine sediments extracted.

The extraction principle was largely the same as that used for the Soxhlet method but, in this case, the extraction was executed in a 10 L round bottom flask (Figure 3.3a), using a large stirrer powered by a motor to ensure the thorough mixing of the sediment and the solvent throughout.

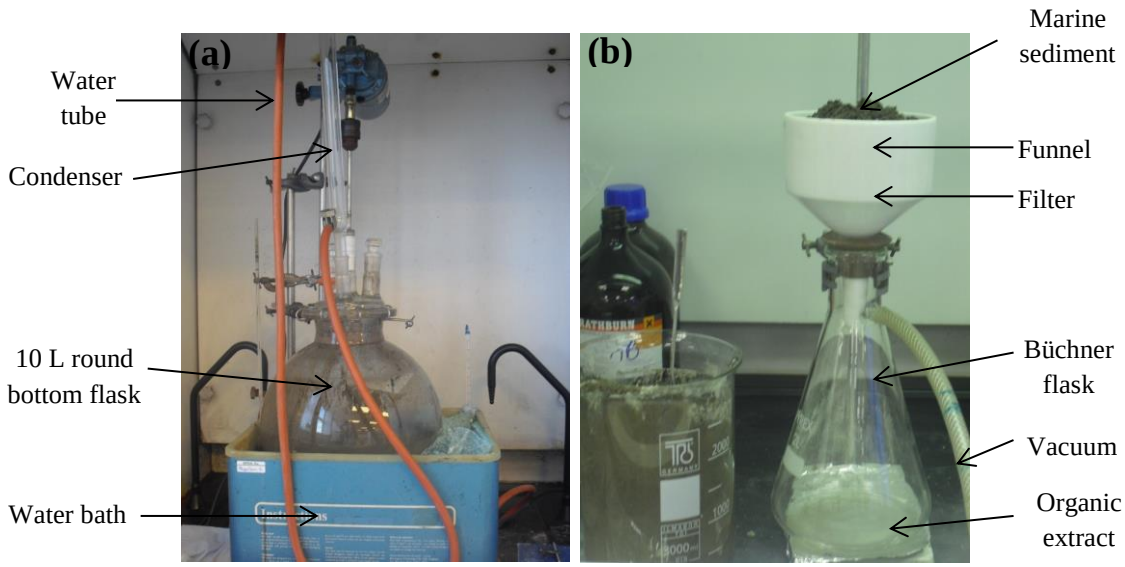

Figure 3.3: (a) Large-scale extraction manifold; (b) Büchner filtration manifold.

Firstly, while stirring, about 5 L of hexane were added into the flask using a glass funnel, followed by ca. 3 kg of the Arctic marine sediment (enabling a total of 16.5 kg being extracted by repeating this procedure). A condenser was inserted to avoid evaporation of the solvent and the manifold was secured. Following extraction of sediments (70˚C, 72h) the resulting suspension was filtered using Büchner filtration (Figure 3.3b), using qualitative filter paper (Whatman 1, 185 mm Ø, 11 μm pore size) and rinsed with further hexane to yield a THE which was then partially evaporated (R-

215, Büchi, 25˚C) and then to dryness (N_2 stream; 25˚C) prior to purification. This procedure greatly improved the amount of sediments extracted each time, thus reducing the overall time of the extraction process.

3.1.3.2 Purification

The purification of THEs was carried out in the same way for both the small scale pilot study and the large-scale organic extraction procedure. Hence, all references to specific information refer to the latter large-scale organic extraction.

Following extraction of marine sediments, purification of THEs was carried out in several steps, starting with open column chromatography (SiO_2) and followed by Ag-Ion solid phase extraction (SPE) and finally Ag-Ion HPLC purification.

3.1.3.2.1 Open-column chromatography

The high content of sulphur, as well as the presence of small amounts of marine sediment particles contained in the flask together with the THEs, prevented accurate determination of yield at this stage. THEs were initially partially purified by repeated small-scale open-column chromatography made of a glass pipette (150 mm, 3 mL capacity) plugged with DCM-extracted cotton wool (ca. 5 mm) and filled with ca. 0.7 g deactivated (non-dried, ambient moisture content) chromatography grade silica (60 – 200 μm, Fisher, UK). Non-polar hydrocarbon fractions, including IP_{25}, were eluted with hexane (3 column volumes), before being evaporated by N_2 stream (25˚C).

3.1.3.2.2 Ag-Ion Solid-Phase Extraction (SPE) purification

Non-polar THEs were further fractionated into saturated and unsaturated components using Ag-Ion SPE cartridges (Supelco Discovery ® Ag-Ion, 750 mg). SPE cartridges were conditioned in the first instance with 5 column volumes of acetone and 5 column volumes of DCM. Following the addition of non-polar THE (1 mg per column) fractions in DCM, saturated and unsaturated (including IP_{25}) hydrocarbons were eluted with 5 column volumes of DCM and 5 column volumes of acetone respectively, before being evaporated by N_2 stream (25˚C).

3.1.3.2.3 High-Performance Liquid Chromatography (HPLC)

Final purification of unsaturated, non-polar THEs was achieved using an Agilent 1100 series HPLC system fitted with a Varian ChromSpher 5 Lipids (250 × 4.6 mm ID) Ag-Ion column using a mobile phase gradient (DCM/acetone) at 1 mL min^{-1} (Figure 3.4). Specific HPLC gradient conditions were as follows: 100% DCM (0 – 5 min), 100% DCM to 100% acetone (5 – 10 min) and 100% acetone (10 – 15 min). Individual fractions (ca. 1 min) were collected manually, and subsequent analysis by GC-MS revealed that IP_{25} eluted between 100% DCM and 80:20 DCM/acetone.

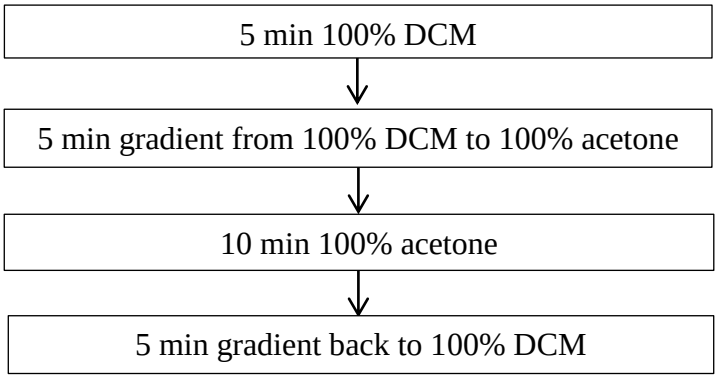

Figure 3.4: High performance liquid chromatography mobile phase gradient of increasing polarity.

3.1.4 Analytical methods

Analysis of extracts was carried out at each stage of purification using GC-MS. Operating conditions were as described in Chapter 2, Section 2.2.6. Following the 3 stage purification, the purity of IP_{25} was determined by GC-MS and NMR spectroscopy and ranged from 50 – 90% depending on the original sediment extracted. ^{1}H and ^{13}C NMR spectra were recorded using a JEOL ECP-400 NMR spectrometer and chemical shifts were measured relative to those of the solvent ($CDCl_3$; ^{1}H: 7.24 ppm; ^{13}C: 77.0 ppm; Table 3.1). NMR analysis and interpretation was carried out by Prof. Simon T. Belt.

3.1.5 Results and Discussion

From each of the three sampling locations, sufficient quantities of the purified IP_{25} biomarker were obtained from the extraction and purification procedure to permit full characterisation by ^{1}H and ^{13}C NMR spectroscopy. The individual recoveries of IP_{25} were 0.5 – 1.0 mg from several kilograms (ca. 16.5 kg) of sediment, consistent with approximate sedimentary concentrations from these locations (Belt et al., 2007). Previously, NMR data for IP_{25} had been reported for a synthetic standard derived from a closely related C_{25} HBI diene, although the complete spectroscopic assignments were not presented and the standard was probably a mixture of diastereoisomers as a consequence of the synthetic procedure (Belt et al., 2007). For each of the purified samples described here, both ^{1}H and ^{13}C NMR spectra demonstrated that IP_{25} was present in Arctic marine sediments as a single stereoisomer, as evidenced by the absence of any doubling (or more) of individual ^{1}H and ^{13}C resonances (detailed information about ^{1}H and ^{13}C assignments is given by Belt et al., 2012a). In addition,

the ^{1}H and ^{13}C spectra were identical for samples of IP_{25} obtained from each of the three core locations. Since IP_{25} was obtained following extraction from combined sediment horizons covering the entire core lengths corresponding to the last ca. 7 – 10 kyr BP (Vare et al., 2009; Belt et al., 2010), the observation of a single diastereomeric form of IP_{25} suggests that any biosynthetic control over its stereochemistry is not altered post-deposition through any diagenetic processes such as epimerisation.

All ^{13}C and ^{1}H NMR spectroscopic assignments for IP_{25} can be found in Table 3.1 (Belt et al., 2012a). In addition to the NMR analysis, the GC-MS characteristics of purified IP_{25} from each sampling location were identical to those reported previously for this biomarker following synthesis as well as extraction from a range of marine sediments (Belt et al., 2007) (Figure 3.5).

Table 3.1: ^{1}H and ^{13}C NMR spectral data for IP_{25} isolated from Canadian Arctic marine sediments. ([a, b] Resonances may be interchanged). (From Belt et al., 2012a).

Carbon number	**Carbon shift (δ/ppm)**	**Proton number**	**Proton shift (δ/ppm)**
1 (16)[a]	22.71, 22.78	1, 15, 16, 19	0.85 (12H, d, J = 7.3 Hz)
2[b]	28.03, 28.06	17	0.74 (3H, d, J = 6.9 Hz)
3	39.44	18	0.82 (3H, d, J = 6.9 Hz)
4	25.61	23	5.67 (1H, ddd, J = 17.6, 10.3, 7.7 Hz)
5	35.48	24	4.91 (2H, m)
6	34.36	25	0.96 (3H, d, J = 6.9 Hz)
7	42.70		
8	29.76		
9	34.96		
10	33.22		
11	37.47		
12	24.80		
13	39.44		
14[b]	28.03, 28.06		
15 (19)[a]	22.71, 22.78		
17	15.52		
18	19.83		
20	29.76		
21	34.44		
22	38.22		
23	145.11		
24	112.32		
25	20.45		

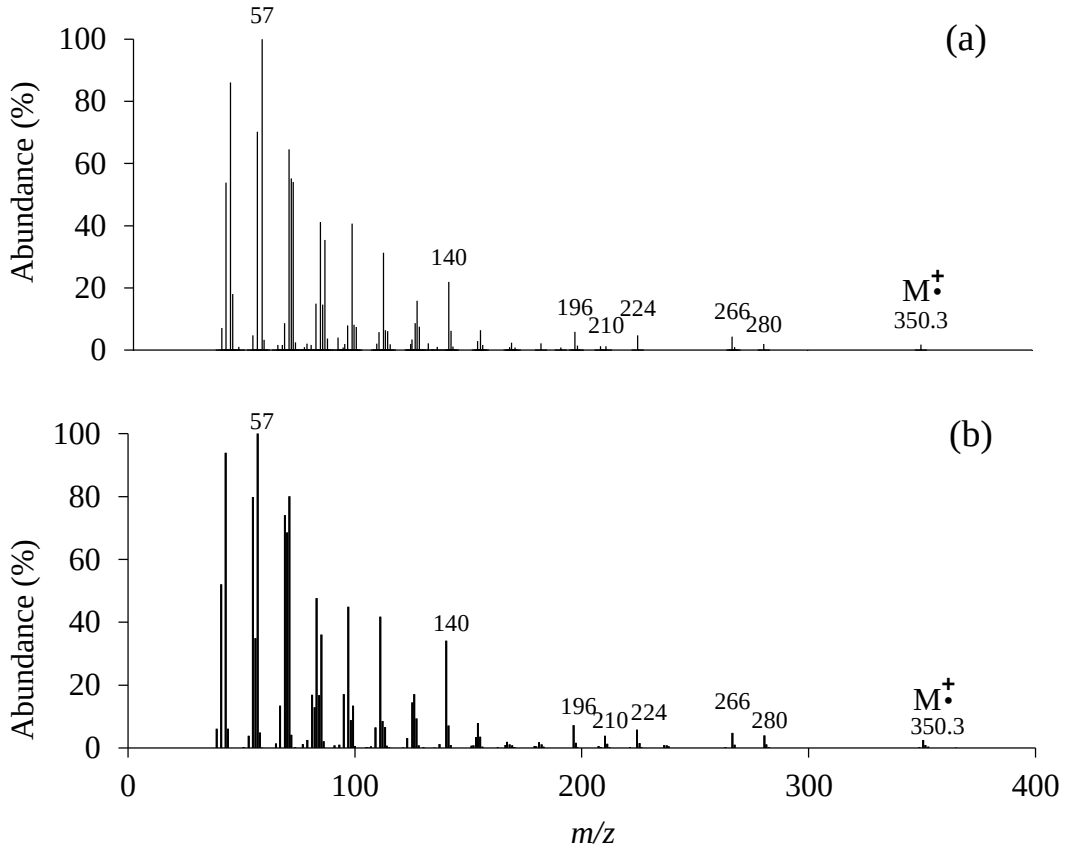

Figure 3.5: Mass spectra of the sea ice diatom biomarker IP_{25}: (a**)** following extraction and purification from Canadian Arctic marine sediments; (b) obtained by synthesis. GC retention indices for both ($RI_{HP\text{-}1}$ = 2090; $RI_{HP\text{-}5ms}$ = 2086).

3.2 GC-MS response calibration

3.2.1 GC-MS response calibration of IP_{25}

As discussed here previously, a GC-MS response factor (RF) needed to be established to account for the differences in mass spectral responses of IP_{25} and the internal standards for the respective *m/z* values used during SIM analysis (*m/z* 350.3 for IP_{25} and 9-OHD). The RF was obtained experimentally by measuring the ratio of the integrated peak areas of the selected ion for IP_{25} and the internal standard (9-OHD) using samples of known concentration within the typical working range for GC-MS analysis of Arctic sediments. Thus, once the purified IP_{25} had been structurally characterised and

quantified by NMR spectroscopy, a stock solution (0.01 mg mL^{-1} each) of both IP_{25} and the internal standard (9-OHD) was prepared by Dr. Thomas Brown (Plymouth University). Further solutions of different concentrations were also prepared from this stock solution as shown in Figure 3.6.

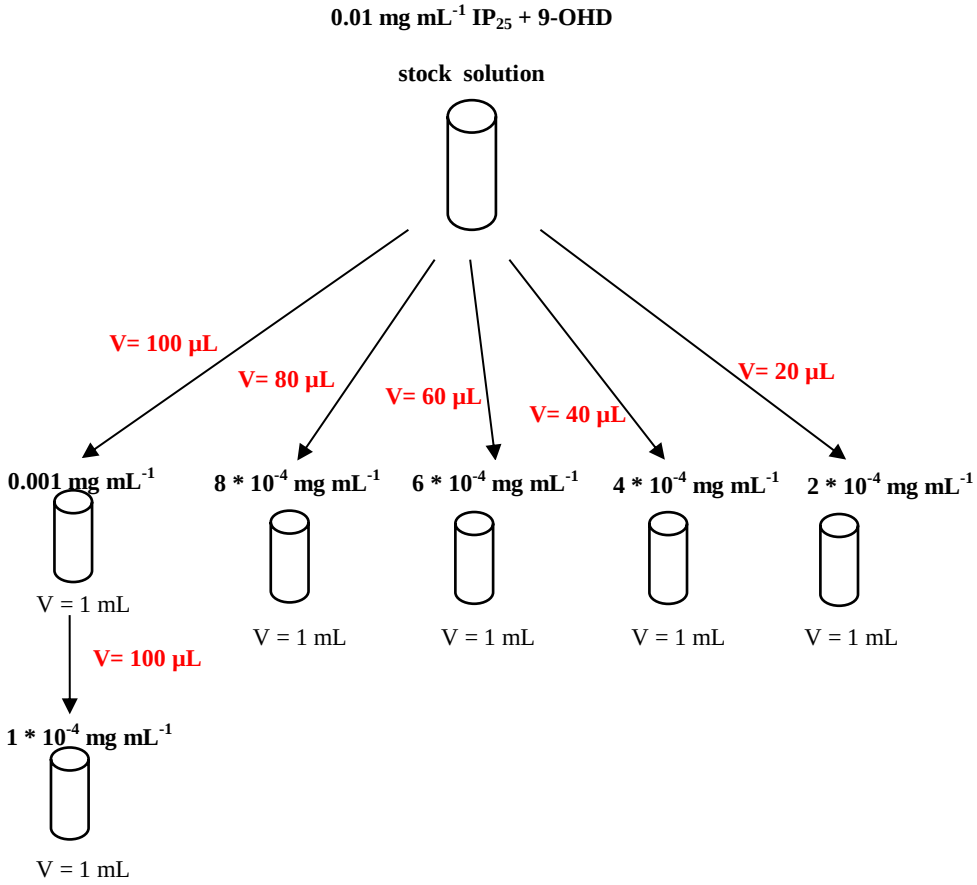

Figure 3.6: Preparation of IP_{25} and 9-OHD standard solutions with hexane.

Standard solutions were then analysed by GC-MS using the standard GC-MS method for analysis of HBIs described previously by Belt et al. (2012b) (Chapter 2) and the RF for each of the standard solutions prepared was obtained by measurement of their individual GC-MS responses (*m/z* = 350.3 for both IP_{25} and 9-OHD) from the SIM-chromatograms. The final RF was obtained by dividing the response of the internal standard (9-OHD) by the response of IP_{25} (Figure 3.7a) for each of the standard

solutions prepared and these ratios were averaged (Oct'11 in Table 3.2). The RF value for the most dilute standard solution (0.0001 mg mL^{-1}, near limit of detection) was higher than the others and this value was not taken into account when calculating the average RF value.

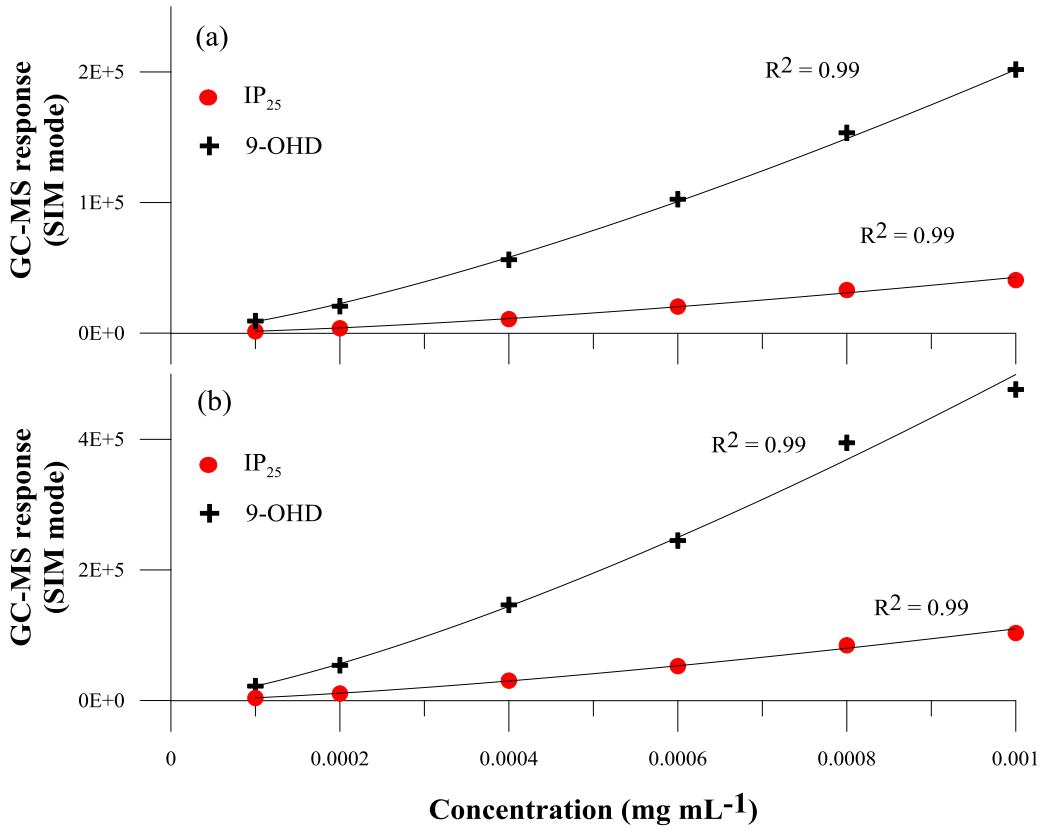

Figure 3.7: Calibration curves of IP_{25} and the internal standard (9-OHD) in SIM mode (*m/z* = 350.3 for both compounds): (a) standard GC-MS method; (b) high-sensitivity GC-MS method.

The mean RF value of 5.03 ± 0.28 between the 9-OHD and IP_{25} obtained (Table 3.2), indicated that the GC-MS response of the 9-OHD at *m/z* 350.3 in the SIM-chromatogram was ca. 5 times larger than that of IP_{25} (*m/z* 350.3). The non-linearity in the curves (Figure 3.7a) made clear that extrapolation of data points based on a linear curve was not reliable. The reasons for the non-linearity of the curves are not yet clear. However, it is known that GC-MS systems achieve very low limit of detections and that at this point, nonlinear areas are described (Hübschmann, 2009).

Table 3.2: Response factor between the internal standard (9-OHD) and IP_{25} for each standard solution and average RF over a range of concentrations. * Individual RF value excluded from calculation of average RF (n = 5); nd no data.

Date	Oct'11	Jan'13	July'13	Dec'11	Jan'13	July'13
GC-MS method	Standard	Standard	Standard	High-sensitivity	High-sensitivity	High-sensitivity
Concentration (mg mL^{-1})	**RF**	**RF**	**RF**	**RF**	**RF**	**RF**
0.001	4.96	6.54	5.07	4.60	5.48	5.7
0.0008	4.63	6.73	5.16	4.65	5.42	5.55
0.0006	5.01	6.65	4.99	4.63	4.96	5.32
0.0004	5.19	6.97	5.65	4.78	5.34	6.05
0.0002	5.38	7.23	5.26	4.94	5.15	5.57
0.0001	6.26*	7.47*	nd	5.35*	nd	nd
Average	**5.03**	**6.82**	**5.22**	**4.72**	**5.27**	**5.64**
SD	0.28	0.28	0.26	0.14	0.21	0.27
RSD (%)	5.54	4.10	4.89	2.94	3.99	4.76

3.2.2 Re-calibration of the GC-MS response factor for a new GC-MS method

The use of an enhanced GC-MS method for increased sensitivity (Chapter 2, Section 2.5.3) necessitated re-calibration of the GC-MS derived RF in order to get a suitable RF between the internal standard (9-OHD) and IP_{25} whilst using the new conditions. This was achieved by measurement of the same standard solutions prepared previously (Figure 3.6) by GC-MS using the new enhanced method. Data in Table 3.2 and Figure 3.7b, both show that the regular and the high-sensitivity methods had a similar response factor between the internal standard (9-OHD) and the IP_{25}, although it was slightly higher in the regular method.

3.2.3 Di- and tri-unsaturated HBIs calibration

Previous calibrations of pure standards of di- and tri-unsaturated HBIs obtained from bulk diatom culture and chromatographic purification from bulk sediment extracts against the internal standard 7-HND have been done in the past (Brown, 2011). The need for periodic calibrations, possibly due to changes in the sensitivity of the GC-MS over time as well as the regular use of a different internal standard for quantification purposes (9-OHD instead of 7-HND) led to the need of GC-MS re-calibration of these compounds against the internal standard. A similar calibration procedure to that described previously for IP_{25} was carried out for a di-unsaturated and four tri-unsaturated HBIs.

Authentic samples of di-unsaturated (diene II; Chapter 2, Figure 2.2b)) and tri-unsaturated (triene E; triene Z; triene 5/6; triene 6/17; Chapter 2, Figures 2.3 and 2.4) HBIs were available from Plymouth University. Initially, a simple purification of each compound by silica column chromatography was performed to remove possible

impurities. Individual HBIs were dissolved in 0.5 mL of hexane and loaded onto a small-scale silica column (after pre-conditioning of the column with hexane) and eluted with ca. 6 mL of hexane. Eluted HBIs were evaporated (N_2 stream) and weighed so that concentrations could be determined for calibration purposes.

Separate stock solutions were prepared as described previously for IP_{25} (Figure 3.6), each one containing the individual HBI and the internal standard (9-OHD) (triene Z and E were contained in the same solution). A GC-MS RF between the internal standard (9-OHD) and each individual HBI was obtained by dividing the *m/z* response of the 9-OHD (*m/z* 350.3) by the *m/z* response of each individual HBI (*m/z* 348.3 for the diene II and *m/z* 346.3 for the trienes) in the SIM-chromatogram (Figure 3.8).

As can be seen from Table 3.3, the RF obtained between the internal standard (9-OHD) and diene II was ca. 2 times higher than that of 9-OHD/IP_{25}. Similarly, the 9-OHD/triene 6/17 RF was very similar to that of 9-OHD/diene II. Both diene II and triene 6/17 have double bonds at positions 6/17 and 23/24 (Figure 2.2b and Figure 2.4a) plus a double bond in position 9/10 in triene 6/17. The similarity in the molecular structure of both compounds probably resulted in similar behaviour during GC-MS analysis and therefore similar RF. In contrast, the RF obtained for 9-OHD/triene 5/6 significantly differed from those of 9-OHD/diene II and 9-OHD/triene 6/17 (ca. 5 times lower, Table 3.3) probably due to a different position of one of the double bonds (position 5/6) (Figure 2.3c), which resulted in a different behaviour by GC-MS.

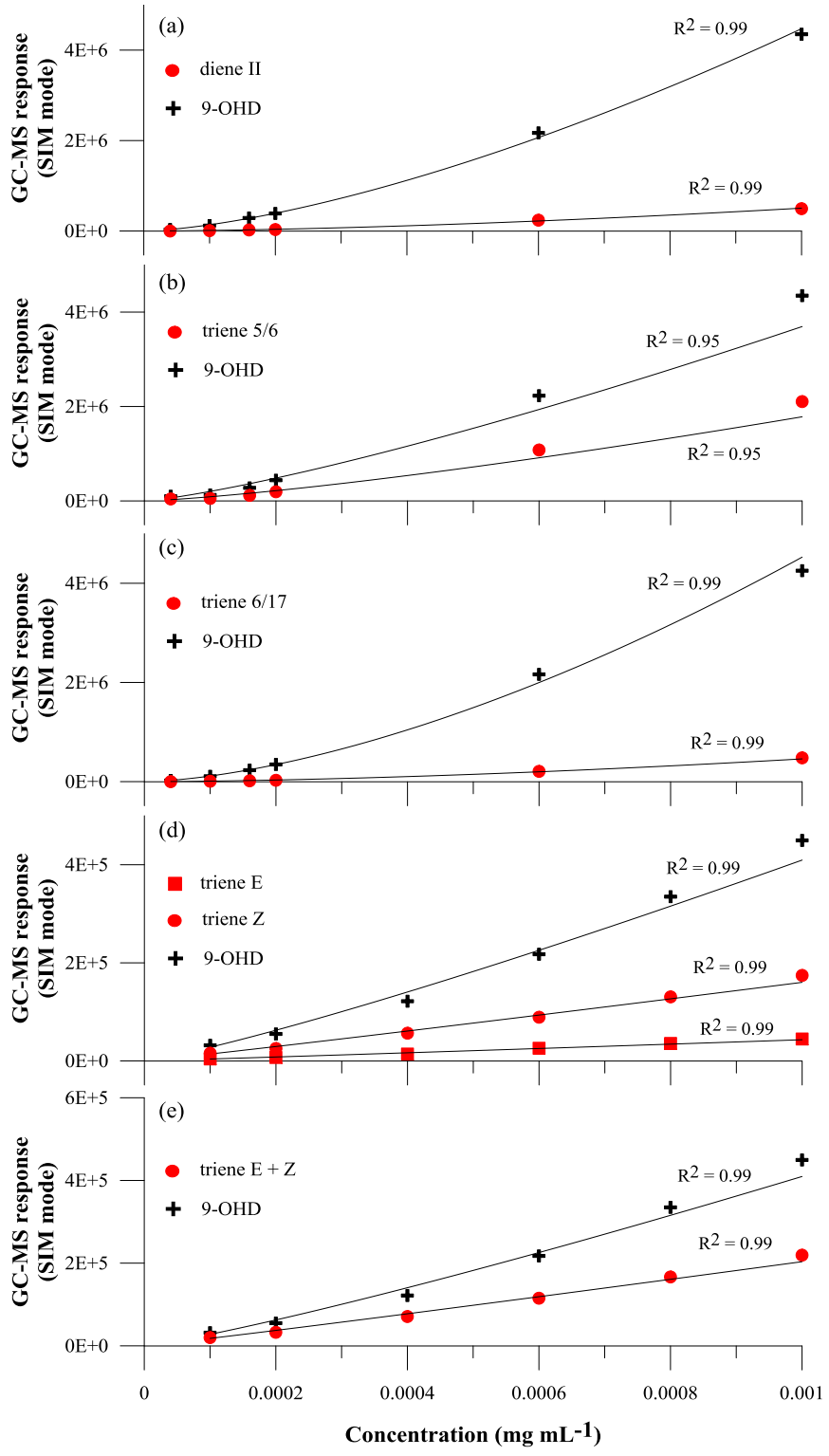

Figure 3.8: (a) Calibration curve of diene II and the internal standard (9-OHD) in SIM mode (*m/z* = 348.3 for diene II and *m/z* = 350.3 for 9-OHD); (b) Calibration curve of triene 5/6 and the internal standard (9-OHD) in SIM mode (*m/z* = 346.3 for triene 5/6 and *m/z* = 350.3 for 9-OHD); (c) Calibration curve of triene 6/17 and the internal standard (9-OHD) in SIM mode (*m/z* = 346.3 for triene 6/17 and *m/z* = 350.3 for 9-OHD); (d) Calibration curves of trienes E and Z and the internal standard (9-OHD) in SIM mode (*m/z* = 346.3 for trienes E and Z and *m/z* = 350.3 for 9-OHD); (e) Calibration curve of triene E+Z and the internal standard (9-OHD) in SIM mode (*m/z* = 346.3 for trienes E+Z and *m/z* = 350.3 for 9-OHD).

Regarding trienes Z and E, both authentic standards were contained in the same solution since the similar chromatographic behaviour of these HBIs prevented further separation. This prevented individual GC-MS calibrations from being made. As such, a series of standard solutions containing both trienes were prepared as previously explained (Figure 3.6). The relative distribution of triene Z and E in all the standard solutions following analysis by GC-MS in both TIC and SIM modes was 79% and 21%, respectively. The absence of changes in the relative distributions of these two isomers (between TIC and SIM) suggests that both HBIs have the same GC-MS RF relative to the internal standard (9-OHD). This is further confirmed on the basis of comparison of the respective mass spectra (Figure 2.3a and Figure 2.3b), where the molecular ion of both triene Z and E comprise ca. 3% of the total mass spectral response. Hence, a GC-MS RF for both HBIs was calculated by dividing the response of the internal standard in the SIM chromatogram by the response of both trienes: 9-OHD/(triene Z+E) (Figure 3.8e).

Table 3.3: Response factors between the HBIs calibrated and the internal standard (9-OHD).

HBI	RF	St. Dev	RSD (%)
diene II	11.37	0.46	4.05
triene 6/17	10.93	0.76	6.95
triene 5/6	2.29	0.05	2.18
triene Z	1.82	0.19	10.47
triene E	1.82	0.19	10.47

3.2.4 Reproducibility/consistency of the GC-MS over time

In order to check the variability of the RF value and therefore the consistency of the GC-MS method (standard) over time, the same IP_{25}/9-OHD calibration standards were re-analysed in triplicate (over a 7 day period), about one year after the first calibration was obtained (in Jan'13). The results obtained from GC-MS analysis of three replicate analyses of the same standard solutions (Figure 3.9a) showed that the variability in the sensitivity of the instrument fell within a maximum analytical error of 8%. Further, as can be seen from Table 3.2, there was a noticeable change in the RF of nearly two units relative to the first calibration, pointing out the need for periodic calibrations to monitor any changes in the instrument and therefore the derived RF value. In addition, the RF varied for standard solutions of different concentration (Figure 3.9b) and the RF value for the most diluted standard solution (0.0001 mg mL^{-1}) was again comparably higher than the rest of RF obtained; therefore, this value was not taken into account when calculating the average RF value.

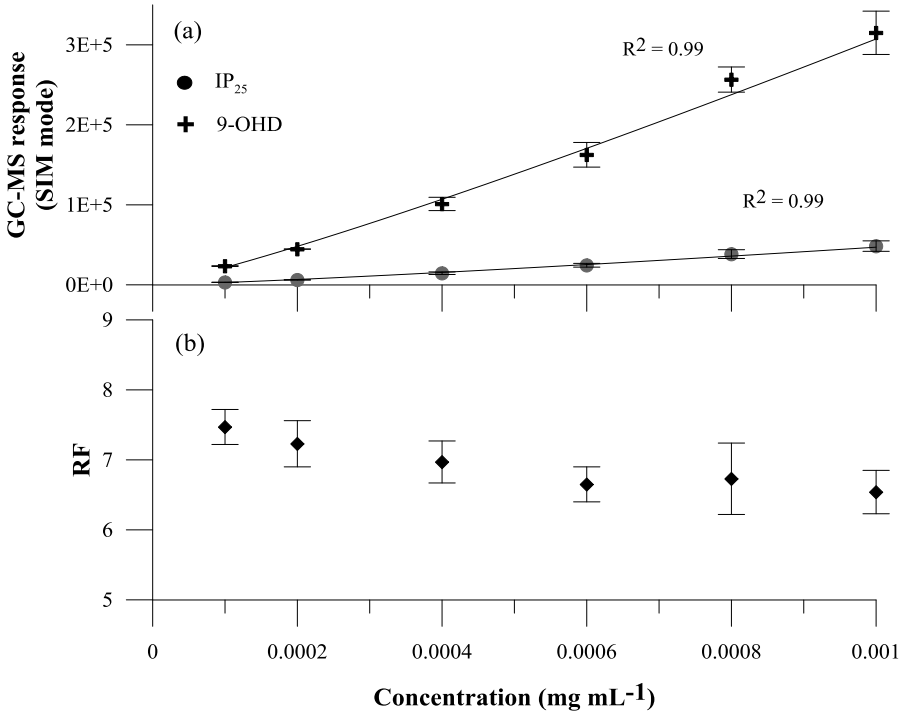

Figure 3.9: (a) Calibration curves for IP_{25} and the internal standard (9-OHD) in SIM mode (*m/z* = 350.3 for both compounds) for 3 replicates; (b) Mean RF value for each standard solution. Error bars are ± 1 s.d.

Overall, individual calibration standards of 9-OHD/IP_{25}, 9-OHD/diene II and 9-OHD/trienes Z-E were analysed by GC-MS both using the standard and high-sensitivity methods in Oct'11, Jan'13 and July'13 (Table 3.2, Table 3.4, Table 3.5 and Figure 3.10).

Table 3.4: Response factor between the internal standard (9-OHD) and diene II for each standard solution and average RF over a range of concentrations; nd no data.

Date	Oct'11	Jan'13	July'13	Dec'11	Jan'13	July'13
GC-MS method	Standard	Standard	Standard	High-sensitivity	High-sensitivity	High-sensitivity
Concentration (mg mL^{-1})	**RF**	**RF**	**RF**	**RF**	**RF**	**RF**
0.001	11.14	14.01	9.70	nd	13.12	8.19
0.0008	11.07	15.46	9.09	nd	13.56	7.86
0.0006	nd	15.33	9.73	nd	13.77	7.84
0.0005	11.05	nd	nd	nd	nd	nd
0.0004	nd	nd	nd	nd	nd	nd
0.0002	11.89	14.28	8.50	nd	15.71	7.66
0.0001	nd	14.49	8.92	nd	15.69	7.24
Average	**11.29**	**14.71**	**9.19**	**nd**	**14.37**	**7.76**
SD	0.40	0.65	0.53	nd	1.15	0.22
RSD (%)	3.57	4.40	5.73	nd	7.98	2.81

Table 3.5: Response factor between the internal standard (9-OHD) and trienes Z and E for each standard solution and average RF over a range of concentrations; nd no data.

Date	Oct'11	Jan'13	July'13	Dec'11	Jan'13	July'13
GC-MS method	Standard	Standard	Standard	High-sensitivity	High-sensitivity	High-sensitivity
Concentration (mg mL^{-1})	**RF**	**RF**	**RF**	**RF**	**RF**	**RF**
0.001	nd	2.05	1.22	nd	1.69	1.06
0.0008	nd	2.01	1.00	nd	1.68	0.95
0.0006	nd	1.89	1.02	nd	1.64	0.93
0.0004	nd	1.71	1.00	nd	1.64	0.88
0.0002	nd	1.68	0.97	nd	1.66	0.94
0.0001	nd	1.58	1.00	nd	1.61	0.96
Average	**nd**	**1.82**	**1.04**	**nd**	**1.65**	**0.95**
SD	nd	0.19	0.09	nd	0.03	0.06
RSD (%)	nd	10.47	8.93	nd	1.71	6.39

The results show that the RF of a GC-MS method (standard or high-sensitivity) varied for a given 9-OHD/HBIs calibration over time (Figure 3.10). Further, these values showed a rather fluctuating pattern (increase/decrease) other than following an increasing or decreasing trend over time. This for instance, could be related to significant GC-MS maintenance procedures that happened during this time frame, as part of routine instrument maintenance schedule, such as MS source clean or GC column changes, which are known to change the ion responses. In general, RF for the high-sensitivity GC-MS method were lower to those of the standard method, apart from the RF between 9-OHD/IP_{25} in July'13 (Figure 3.10).

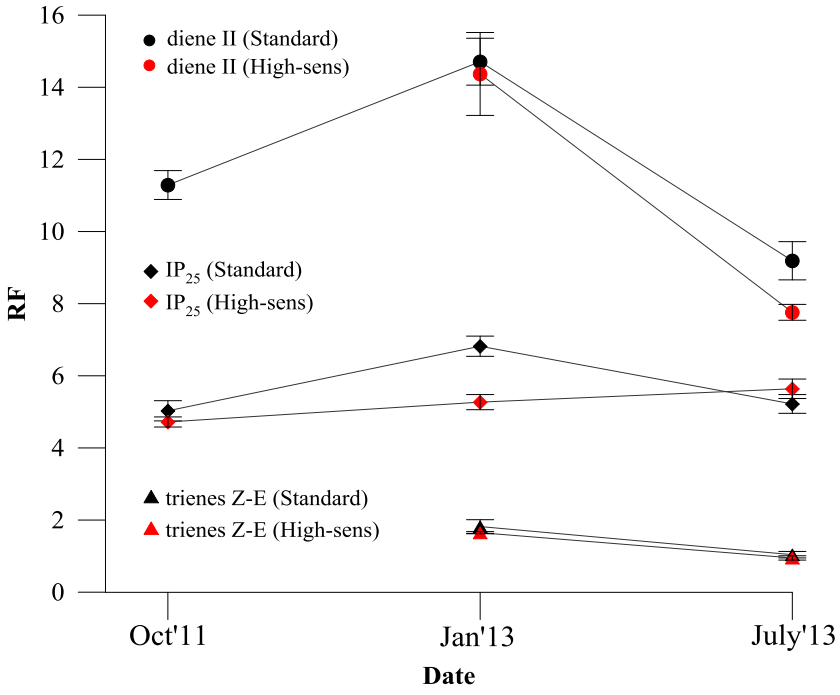

Figure 3.10: Mean RF value of each HBI for the standard and high-sensitivity methods over time.

Altogether, these outcomes suggest that a GC-MS calibration should be carried out regularly for routine HBIs analysis (i.e each day/each week). However, this would be time consuming as well as difficult to achieve due to availability of standards. Another issue of this approach for quantification of HBIs has recently been pointed out by Belt et al. (2013a) regarding the transferability of quantified data between different

laboratories. Belt et al. (2013a) carried out an inter-laboratory calibration between seven different laboratories, and the outcomes suggested that the use of a GC-MS response factor obtained through calibration of standard solutions could be problematic for comparison. More specifically, when a 9-OHD/IP_{25} calibration standard (0.001 mg mL^{-1}) was sent for analysis at another laboratory, then returned to Plymouth for re-analysis, the RF had changed significantly, although the Plymouth GC-MS instrument had not changed. Further, Belt et al. (2013a) suggested that RFs obtained using the distributions of HBIs within sediment material with known concentrations of HBIs could be a better approach as it would also include aspects such as extraction and purification differences between laboratories as well as GC-MS instrumentation.

3.3 Conclusions

The main aim of this chapter was to confirm the structural identification of the Arctic sea ice diatom biomarker IP_{25} when found in marine sediments. This was achieved following large-scale extraction of IP_{25} from three locations in the Canadian Arctic, purification by a combination of chromatographic methods, and analysis by GC-MS and NMR spectroscopy. This work enabled the first accurate confirmation of the structural assignment of the Arctic sea ice diatom biomarker IP_{25} found in marine sediments from more than one location.

Moreover, obtaining authentic IP_{25} from marine sediments facilitated the first ever calibration of the GC-MS response factor between naturally produced IP_{25} and the internal standard (9-OHD), enabling accurate quantification of subsequent samples containing varying amounts of IP_{25} from Arctic marine sediments. Further, calibration of the GC-MS response factor between di- and tri-unsaturated HBIs and the internal standard (9-OHD) were also performed. An assessment of the reproducibility and

consistency of the GC-MS overtime was also carried out. The outcomes suggested that either a periodic calibration of the standards was needed, or the use of a new approach consisting of obtaining the RF using sediment material with known HBI concentrations would need to be considered for routine analysis of HBIs.

CHAPTER FOUR

4 Results (1): Seasonal sea ice conditions in northern Norway during the Younger Dryas

4.1 Introduction

Chapter four describes an investigation of a sediment core from Andfjord, northern Norway (JM99-1200; Figure 4.1) focused on the Allerød – Younger Dryas – Holocene intervals. The current chapter will demonstrate further the potential utility of the IP_{25} biomarker as a palaeo sea-ice proxy, which, when combined with a phytoplankton-derived biomarker, (the so-called PIP_{25} index), has indicated recently to be a useful approach for quantifying spring sea ice conditions (Müller et al., 2011). Moreover, the determination of stability or variability in sea ice conditions will be enhanced here by introducing a new approach consisting of a comparison of IP_{25} concentrations, with those of another similar highly branched isoprenoid (HBI) alkene that is di-unsaturated and thought also to be produced by Arctic sea ice diatoms. This new approach using the ratio between the HBI diene II and IP_{25}, termed "DIP_{25}", will be tested here for the first time.

The Younger Dryas stadial, main focus of this chapter, represents an intriguing and much studied short-term (ca. 1400 yr) event that occurred during the transition from the last glacial to the current interglacial (the Holocene) and was characterised by significant and extended cooling across higher latitude regions of the northern hemisphere. Interest in the Younger Dryas stems, in part, from the predictions of significant economic and ecological impacts that may be induced during abrupt climate

changes (Alley et al., 2003). Numerous studies have investigated the details of the Younger Dryas through Greenland ice records (e.g. Alley et al., 1993; Mayewski et al., 1993; Taylor et al., 1997; Alley, 2000), marine and lake sediment records from Europe (e.g. Isarin et al., 1998; Brauer et al., 2008) and Arctic and sub-Arctic areas (e.g. Gulliksen et al., 1998; Seppä et al., 2002; Vorren and Plassen, 2002a; Ebbesen and Hald, 2004; Bakke et al., 2009; Aagaard-Sørensen et al., 2010), yet the exact triggers that caused this abrupt event are still under debate. One explanation is based around a reduced North Atlantic Meridional Overturning Circulation, which probably resulted from a massive release of melt water into the North Atlantic (e.g. Gildor and Tziperman, 2000; Broecker, 2003; Knutti et al., 2004; McManus et al., 2004; Jennings et al., 2006). A combination of outbursts from Lake Agassiz (North America) and re-routing of continental drainage from the Mississippi river into the North Atlantic Ocean at the onset of the Younger Dryas has generally been considered to be responsible for initiating this abrupt climate change (Clark et al., 2001). More recently, however, it has been shown that the re-routing of Arctic meltwater in a north westerly direction through the Mackenzie Valley made an additional and significant contribution (Teller et al., 2002; Tarasov and Peltier, 2005; Teller et al., 2005; Teller and Boyd, 2006; Murton et al., 2010; Condron and Winsor, 2012). Alternatively, a model involving extensive winter sea ice cover that resulted from more extreme seasonality compared to modern times and would have dramatically altered the heat exchange between the ocean and the atmosphere, has also been proposed (Denton et al., 2005; Lie and Paasche, 2006). Central to the debate, however, remains the occurrence and impact of sea ice to the Younger Dryas stadial. Since reconstructions of sea ice are often made by extrapolation of other proxy-based climate measurements such as sea surface temperature (SST) and sea surface salinity (SSS), there is a clear need to develop proxies that provide more direct evidence for the past occurrence of sea ice. Further, if such proxies are also able

to discriminate between different sea ice scenarios, then there is the additional potential to improve on the somewhat generic terms that are frequently used to describe past sea ice conditions (extreme, extensive, etc) which, while understandable given the nature of the proxies from which they are derived, are not especially informative. In the particular case of the Younger Dryas, the application of sea ice-specific proxies that also provide more specific details of the sea ice conditions should further help identify or confirm the role of seasonality during abrupt climate changes (Manabe and Stouffer, 2000; Gildor and Tziperman, 2003; Denton et al., 2005; Lie and Paasche, 2006).

The main aim of the current study was to use the presence of the IP_{25} sea ice proxy and other biomarkers 1) to identify, unambiguously, sea ice occurrence during the Younger Dryas stadial in northern Norway, 2) to better define the nature of the sea ice conditions, 3) to identify any fluctuations within these and 4) to make any sea ice determinations more quantitative by comparing the biomarker-based proxy data with predictions of sea ice concentrations derived from modelling approaches carried out previously (Müller et al., 2011). In addition, these outcomes have the potential to provide insights into the mechanism(s) responsible for initiating the Younger Dryas and for establishing a more detailed understanding of the oceanographic transitions that occurred within this stadial. In order to achieve these aims, we chose to investigate a sediment core for which a reasonably comprehensive suite of other oceanographic proxy and geochemical data had already been collected and discussed (Knies et al., 2003; Ebbesen and Hald, 2004; Knies, 2005).

4.2 Regional setting

Two water masses, the Atlantic water of the North Atlantic Current (NAC) and the coastal water of the Norwegian Coastal Current (NCC), dominate the oceanographic regime in the study area (Figure 4.1a). The warm (> 2 °C) and saline (> 35‰) NAC (Hopkins, 1991) flows northward adjacent to, and beneath, the less saline (32-35‰) NCC by following the bathymetry of the northern Norwegian shelf (Loeng, 1991). The shelf topography, which is dominated by relatively shallow to intermediate glacial troughs, strongly steers the in- and outflow of both water masses (Moseidjord et al., 1999). Due to the open ocean connection, the water column is well-oxygenated (95-105% of saturation) (Hald and Vorren, 1984). Almost half of the shelf water flow makes a right turn into Andfjorden along the western slope and flows out again on the eastern slope (Nordby et al., 1999; Slagstad et al., 1999). When hitting the northward flowing NAC along the shelf break again, the flow is forced to change direction, which causes a topographically-steered upwelling via vertical mixing (Slagstad et al., 1999; Wassmann et al., 1999). The upwelling facilitates primary production rates of up to 190 g C m^{-2} yr^{-1} in outer Andfjorden by supplying nutrient-rich water masses to the euphotic zone (Slagstad et al., 1999). Low phytoplankton concentrations have previously been reported, however, as shown by low chlorophyll biomass (Wassmann et al., 1999), probably due to substantial grazing and degradation of phytoplankton-derived organic matter (Verity et al., 1999; Wassmann et al., 1999). Consequently, advection of particulate organic matter and influences from various water masses play important roles for the ecology and particulate fluxes in Andfjorden (Wassmann et al., 1996). In contrast, the influence of continental input, with regard to nutrient supply and biogenic production, is rather small in northern Norway (Wassmann et al., 1996).

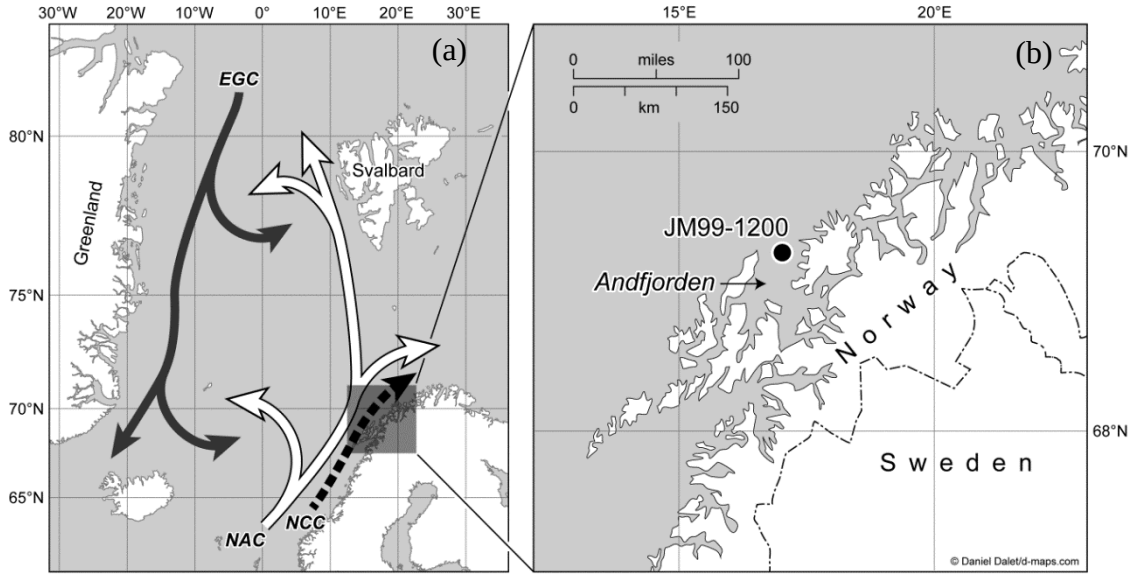

Figure 4.1: (a) Simplified map showing the surface water currents in the Nordic Seas. Black solid arrows indicate the East Greenland Current (EGC), white arrows the North Atlantic Current (NAC), and the black dashed arrow represents the Norwegian Coastal Current (NCC); (b) Detailed map of the Andfjorden area with the location of core JM99-1200.

Andfjorden, where the current study is based, is a glacial trough on the continental shelf off Tromsø, northern Norway (Figure 4.1b) and represents a good setting for palaeoenvironmental studies for a number of reasons. Firstly, high sedimentation rates (up to 500 cm kyr^{-1}) permit high-resolution studies to be carried out. Secondly, since the region is influenced by the NAC, which contributes to the formation of North Atlantic Deep Water in the Nordic Seas, it is a very sensitive location to climatic changes (e.g. Hald and Hagen, 1998). Current surface-water temperatures in Andfjorden range between 9 – 12˚C in August and between 2 – 6˚C in February (Hald and Vorren, 1984).

4.3 Material and methods

4.3.1 Field methods and chronology

The piston core under investigation, JM99-1200, was recovered from Andfjorden off northern Norway (69.16˚N, 16.25˚E; water depth 475 m; core length 1115 cm; Figure 4.1b) on board the R/V *Jan Mayen* in November 1999 and stored *in situ* (5˚C) until sampled for analysis. Individual sub-samples for biomarker analysis were taken at 1-5 cm intervals from 102 to 790 cm, freeze-dried and stored at -20˚C prior to extraction.

An age model for JM99-1200 was first developed by Knies et al. (2003) and was based on linear interpolation between seven accelerator mass spectrometry (AMS) ^{14}C dates. This age model was improved by Ebbesen and Hald (2004) using additional AMS ^{14}C dates and the Vedde Ash tephra horizon identified at 436.5 cm (time marker corresponding to 11.980 ice-core yr; Grönvold et al., 1995). For the current study, the AMS dates have been further recalibrated by Dr. Katrine Husum, using Calib version 6.0 (Stuiver et al., 2005) and the marine calibration curve marine09 (Hughen et al., 2004; Reimer et al., 2009) (Table 4.1). A regional ΔR (the difference between marine reservoir age of the local region and model ocean) was selected for each date (Ebbesen and Hald, 2004 and references herein). In addition, it was assumed that ΔR in northern Norway was higher during the Younger Dryas (GS-1) than it was during the Allerød (GI-1a) and early Holocene (Bondevik et al., 1999; Ebbesen and Hald, 2004; Bondevik et al., 2006). Linear sedimentation rates varied between 30 – 430 cm kyr^{-1} (Figure 4.5a). As pointed out previously by Knies et al (2003) and Knies (2005), documentation of proxy data as accumulation rates was not recommended in this case due to highly fluctuating sedimentation rates and an insufficient number of AMS^{14}C dates. Therefore, biomarker data presented in this study were given as concentration profiles normalised

to sediment dry weight (μg g^{-1} dry sed). Knies (2005) also pointed out the low fluctuating TOC content through geologic time (~0.5% - ~1.1%; Figure 4.5c), despite highly fluctuating sedimentation rates.

Table 4.1. Radiocarbon dates and calibrated ages in core JM99-1200.

Core depth (cm)	**Material**	**Lab. ref**	**Uncorrected 14C Age (BP)**	**Reservoir correction (yr)**	**95.4% (2σ) cal. age ranges**	**Age used (cal. yr BP)**	**Located correction ΔR**
59	*Cylichna alba*	Tua-2921	5.965 ± 60	400	6.179 – 6.466	6.323	64+/-35
280.5	shell fragments	Tua-3728	10.350 ± 85	400	*	*	200+/-50
281.8	*Nuculana pernula*	KIA-11165	10.130 ± 50	400	10.640 – 11.106	10.873	200+/-50
300.5	shell fragments	Tua-3729	10.510 ± 85	400	11.132 - 11.726	11.429	200+/-50
436.5	Tephra		Vedde Ash			11.980	
457.5	shell fragments	Tua-3730	11.165 ± 90	400	12.361 – 12.819	12.590	200+/-50
511	*Nuculana pernula*	TUa-2922	11.460 ± 85	400	12.663 – 13.097	12.880	64+/-35
655.5	*Bathuarca glacialis*	TUa-2923	11.830 ± 85	400	13.085 – 13.427	13.256	64+/-35
723.5	*Bathuarca glacialis*	Tua-2924	12.160 ± 80	400	13.347 – 13.758	13.553	64+/-35
788	*Bathuarca glacialis*	KIA-11109	12.425 ± 55	400	13.637 – 13.992	13.815	64+/-35
855	*Bathuarca glacialis*	Tua-3030	12.575 ± 100	400	13.700 – 14.246	13.973	64+/-35

*Dating excluded from the age model.

4.3.2 Experimental

Each of the biomarkers of interest (hydrocarbons and sterols) required extraction from the sample matrix and separation into individual fractions prior to analysis by GC-MS. For a detailed description of the extraction and purification techniques shown in Figure 4.2, refer to Chapter 2 (Methods).

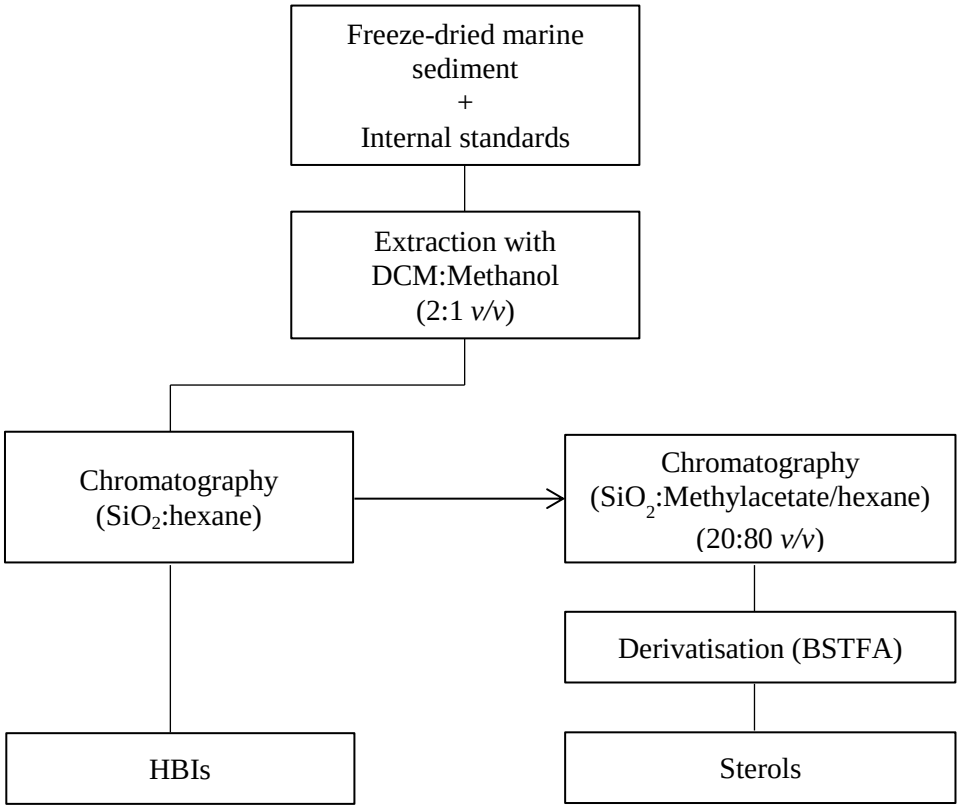

Figure 4.2: Sample extraction flow diagram for lipid biomarkers.

Briefly, following addition of the internal standards (7-hexylnonadecane; 10 μL; 10 μg mL^{-1} and 9-octylheptadec-8-ene; 10 μL; 10 μg mL^{-1}) for quantification, the freeze dried sediments were extracted with DCM/Methanol (3 x 3 mL; 2:1 *v/v*) and then purified by open column silica chromatography with hexane mobile phase (6 mL) used to yield apolar lipids. Methylacetate/hexane (20:80, 6 mL) was used to elute sterols. Prior to analysis by GC-MS, sterols were derivatised (BSTFA; 50 μL; 70˚C; 1h). Analytical reproducibility was monitored using a standard sediment with known abundances of biomarkers for every 14 – 16 sediment samples extracted (analytical error of 7%, n = 15).

Calculation of the PIP_{25} and DIP_{25} indices was achieved using the methods described in Chapter 2. In this study, the mean IP_{25} concentration value of all samples analysed divided by the mean phytoplankton biomarker (brassicasterol) concentration value, yielded a c factor value of 0.1141.

4.4 Results

4.4.1 Pilot study

An initial pilot study consisted of the analysis of 80 samples for IP_{25} content, from 60 to 790 cm depth covering the period from 6.34 to 13.82 kyr BP. Additionally, samples covering the Younger Dryas interval (11.5 – 12.9 cal. kyr BP) were extracted and analysed in duplicate (0.5 ± 0.1 g) to check on the reproducibility of the method. This set of samples was sub-sampled before 2005 from archived material in collaboration with the Geological Survey of Norway (NGU), freeze dried and stored at ambient temperature.

In all 80 samples analysed in the pilot study, IP_{25} was found to be present in 25 horizons, all of which corresponded to the Younger Dryas period (ca. 11.7 – 12.7 cal. kyr BP, Figure 4.3a). In contrast, IP_{25} was absent (or below the limit of detection) in the remaining 55 horizons covering the period from ca. 6.34 to 11.7 cal. kyr BP and from ca. 12.8 to 13.8 cal. kyr BP. The results (Figure 4.3a) showed an increasing concentration trend in IP_{25} from ca. 12.7 up to 12.4 cal. kyr BP, before decreasing slightly at ca. 12.08 cal. kyr BP. After this period, IP_{25} concentrations increased again at ca. 12 to 11.7 cal. kyr BP, after which IP_{25} was absent. The availability of extra sediment material in most of the horizons covering the Younger Dryas period allowed duplicate analyses to be performed. The reproducibility of the method, given by the close resemblance between both IP_{25} profiles (Figure 4.3b), was thus demonstrated.

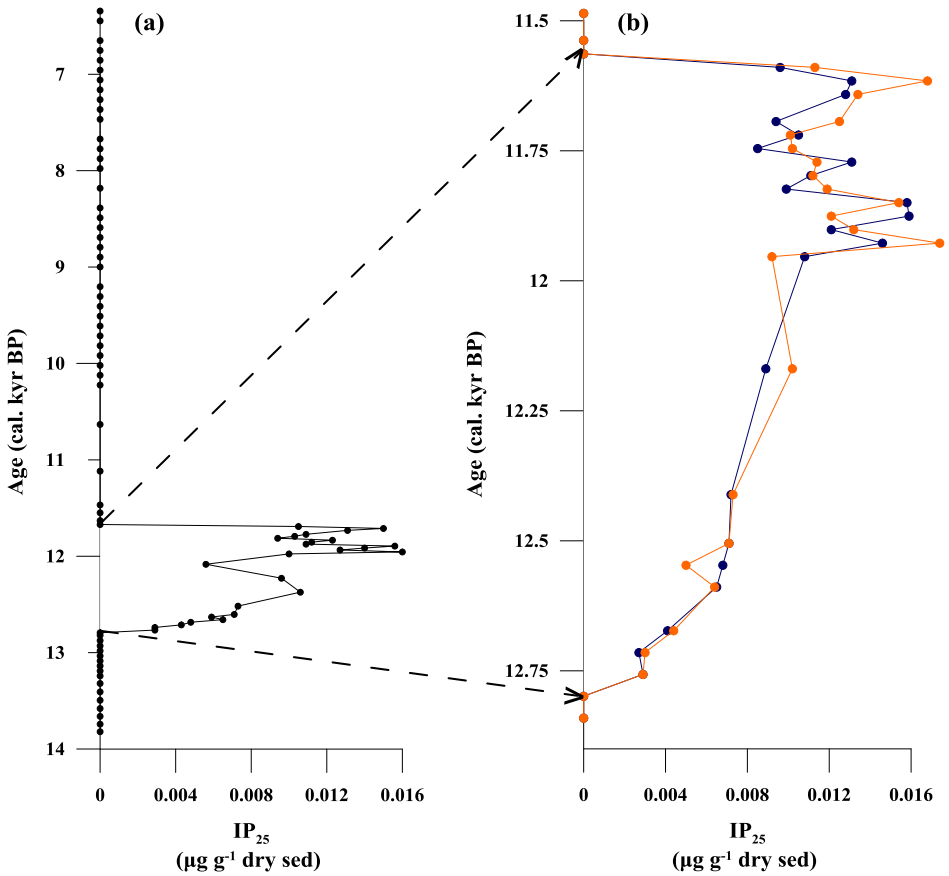

Figure 4.3: Individual temporal concentration profile of IP_{25} for the pilot study of JM99-1200 core: (a) for the period ca. 6.34 – 13.82 cal. kyr BP; (b) for two replicate IP_{25} analysis during the period ca. 11.5 – 12.9 cal. kyr BP.

4.4.2 Full study

In an attempt to obtain a higher resolution study, 123 additional downcore sediment samples were analysed for the sea ice biomarker IP_{25} and the structurally related HBI diene II (Chapter 2). Samples were also analysed for the sterols 24-methylcholesta-5,22E-dien-3β-ol (brassicasterol) and 24-methylcholesta-5,24(28)-dien-3β-ol (24-methylenecholesterol), both of which are commonly synthesised by marine algae (Volkman et al., 1998). Sampling and analysis was carried out at 5 cm intervals during the Holocene section of the core (ca. 7.2 – 11.5 cal. kyr BP), corresponding to an effective age resolution of ca. 200 – 400 yr. A higher resolution study of the Allerød – Younger Dryas intevals (ca. 11.5 – 13.8 cal. kyr BP) was achieved by sampling at 1 cm intervals, equivalent to a temporal resolution of ca. 5 – 80 yr. This set of samples was freshly sub-sampled especially for this study from archived material, freeze dried and stored in the freezer until needed for analysis.

IP_{25} was found to be present in 96 samples and absent (or below the limit of detection: 0.92 ng g^{-1} dry sed) in the remaining 27, even after further concentration of the sediment extracts. The presence of IP_{25}, moreover, was limited to one continuous period in the sequence from ca. 12.9 to 11.5 cal. kyr BP (Figure 4.4a) with no IP_{25} detected from ca. 13.8 to 12.9 cal. kyr BP or after ca. 11.5 cal. kyr BP and into the Holocene to ca. 7.2 cal. kyr BP. After ca. 12.9 cal. kyr BP, the concentration of IP_{25} increased rapidly (from not detectable) and reached its maximum value at ca. 12.66 cal. kyr BP, before decreasing slightly to an approximately constant value until ca. 11.9 cal. kyr BP. After ca. 11.9 cal. kyr BP, IP_{25} concentrations fell sharply and remained relatively low for the next ca. 400 yr. The concentration profile of the structurally related HBI diene II exhibited extremely similar characteristics to those described for IP_{25}, especially in terms of intervals of presence/absence (Figure 4.4b). Thus, diene II was present from ca. 12.9 to

11.5 cal. kyr BP and absent either side of this interval, suggesting co-production with IP_{25} by sea ice diatoms, as reported previously (Belt et al., 2007; Belt et al., 2008; Vare et al., 2009).

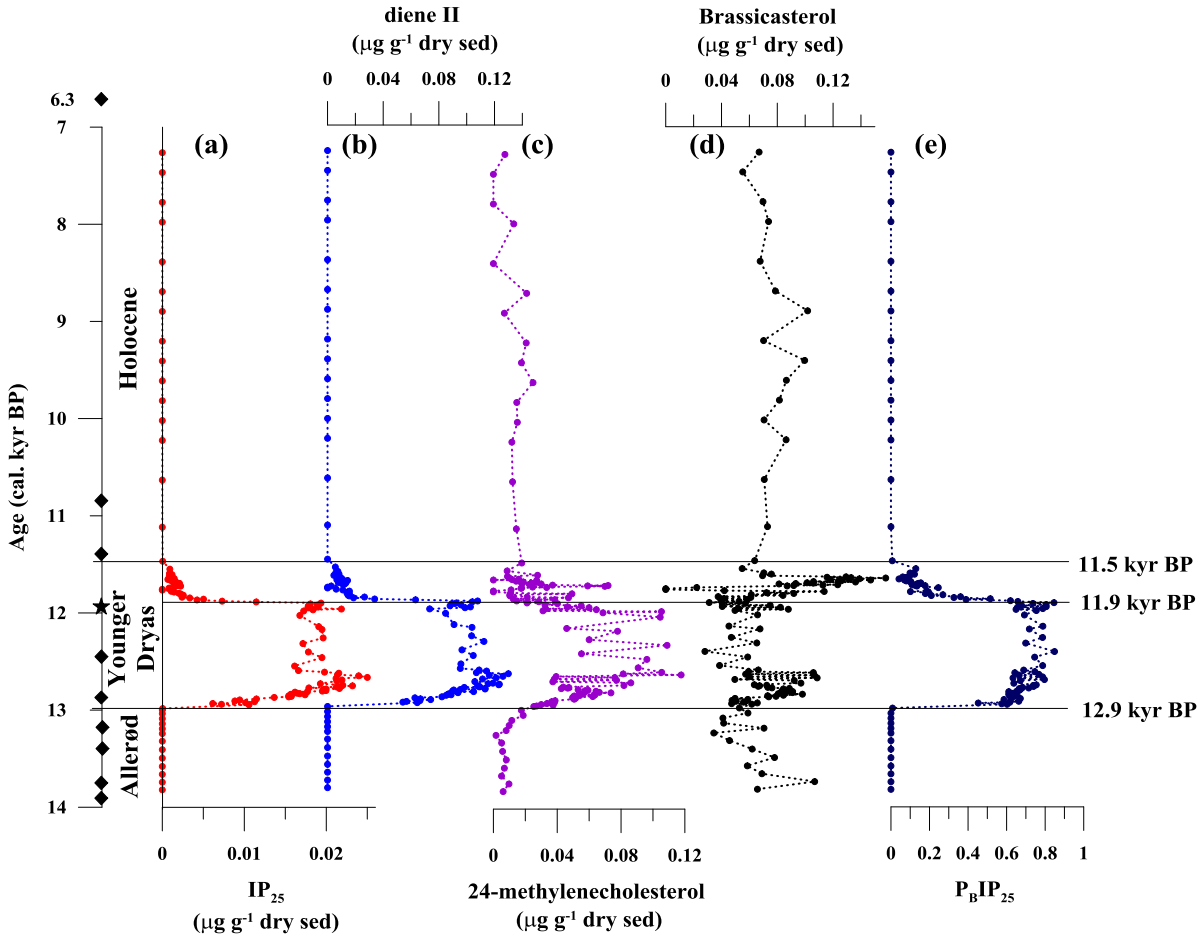

Figure 4.4: Individual and combined temporal concentration profiles of biomarkers in the JM99-1200 core (123 sampling points): (a) IP_{25}; (b) diene II; (c) 24-methylenecholesterol; (d) brassicasterol; (e) P_BIP_{25} index. The horizontal solid lines at ca. 12.9 cal kyr BP and ca. 11.5 cal kyr BP indicate the onset and the termination of the Younger Dryas, respectively. The horizontal solid line at ca. 11.9 ca. kyr BP represents a shift in sea ice conditions during the late Younger Dryas. The diamonds mark the AMS ^{14}C dates and the arterisk indicates the Vedde Ash tephra horizon used in the age model.

As expected, the representation of IP_{25} results as fluxes (Figure 4.5b) yielded a profile highly influenced by the sedimentation rates which, in turn, were derived from the age model (Figure 4.5a). As pointed out previously by Knies et al. (2003) bulk and

compound-specific accumulation rates in Andfjorden simply follow the fluctuations in sedimentation rates and would therefore distort interpretation of biogeochemical processes and their changes from bulk and molecular geochemical data. In reality, sedimentation rates do not undergo step changes as indicated by Figure 4.5b. Therefore in this case, sedimentation rates were considered to provide too severe an overprint on biomarker data and as such, all results for this study were given as concentrations of biomarkers per gram of dried sediment.

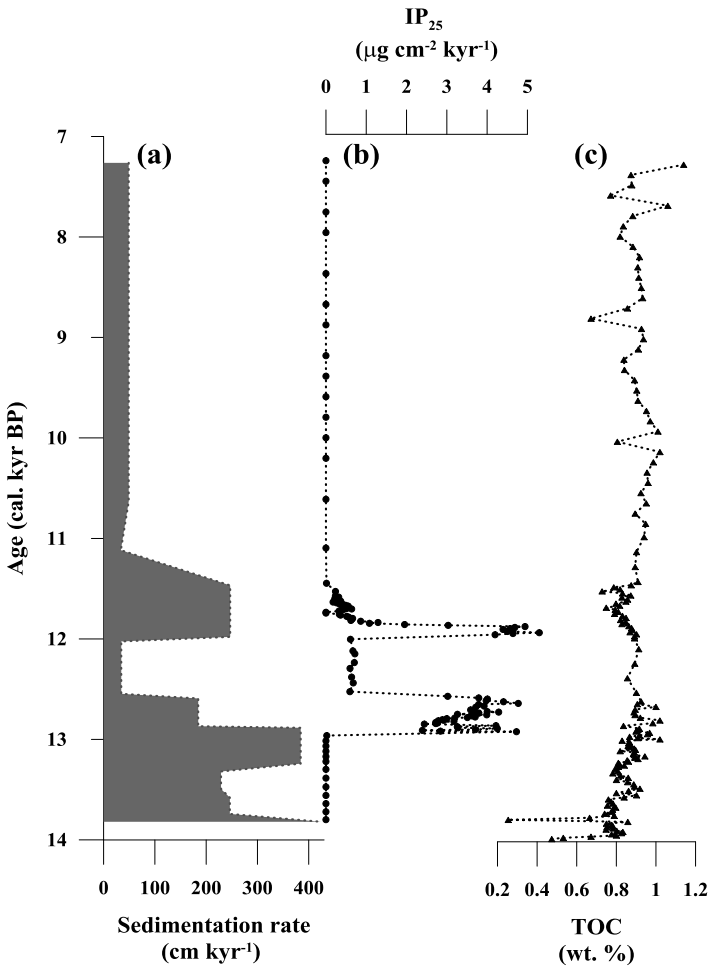

Figure 4.5: (a) Sedimentation rates (cm kyr^{-1}); (b) IP_{25} fluxes (μg cm^{-2} kyr^{-1}); (c) total organic carbon (TOC, wt. %; Knies 2005) of core JM99-1200.

In contrast to IP_{25} and diene II, the concentration profiles of the two sterols (brassicasterol and 24-methylenecholesterol) showed clear differences compared to

those of IP_{25} and diene II. Firstly, both sterol biomarkers were present throughout the entire sequence, consistent with a previous lower resolution study by Knies (2005) and concentrations were quite variable between the two sterols and at different time intervals. Secondly, concentrations of brassicasterol were relatively constant throughout the sequence, although some (mainly) positive departures were observed at ca. 12.9 to 12.7 cal. kyr BP and ca. 11.9 to 11.5 cal. kyr BP (Figure 4.4d). For 24-methylenecholesterol the overall concentration profile more closely resembled those of IP_{25} and diene II, but some clear differences were also evident. For example, concentrations of 24-methylenecholesterol were highest from ca. 12.9 to 11.9 cal. kyr BP, but with a much greater degree of variation than that found for IP_{25} and diene II (Figure 4.4c). The reduced concentrations found for IP_{25} and diene II from ca. 11.9 to 11.5 cal. kyr BP was seen in the 24-methylenecholesterol profile; however, unlike IP_{25} and diene II, 24-methylenecholesterol was also detected after 11.5 cal. kyr BP into the Holocene (Figure 4.4).

The determination of both IP_{25} and brassicasterol concentrations enabled the calculation of the so-called PIP_{25} or 'IP_{25} – phytoplankton' index, proposed by Müller et al. (2011) to indicate more detailed sea surface conditions and, sea ice, in particular. The P_BIP_{25} (subscript B refers specifically to brassicasterol) profile closely resembles that described previously for the IP_{25} and diene II biomarkers (Figure 4.4e) and can be classified according to four intervals. Before ca. 12.9 cal. kyr BP and after ca. 11.5 cal. kyr BP, P_BIP_{25} values were zero as a consequence of the absence of any detected IP_{25}. At ca. 12.9 cal. kyr BP, the P_BIP_{25} index increased abruptly (< 40 yr) and remained in the range 0.6 – 0.8 from ca. 12.9 to 11.9 cal. kyr BP. Finally, P_BIP_{25} values decreased sharply after ca. 11.9 cal. kyr BP and stayed less than 0.2 from ca. 11.9 – 11.5 cal. kyr BP.

4.4.3 Comparison of results between the pilot study and the full study

Comparison of results obtained between the pilot study and the full study for the same core showed two IP_{25} profiles with different trends during the Younger Dryas period. As can be noticed in Figure 4.6, during the early-mid Younger Dryas, IP_{25} concentrations were notably lower in the pilot study than in the high-resolution study. The fact that IP_{25} was absent or below the limit of detection during the early Younger Dryas in the pilot study and present between the early-mid Younger Dryas but at lower concentrations than the full study, pointed to possible degradation of the samples analysed for the pilot study. This set of samples (pilot study) had been stored at ambient temperature probably affecting the chemical composition of sediments as shown by Grimalt et al. (1988) where they observed alteration in the hydrocarbon composition of sediments during storage at ambient temperature for short periods of time (1 month). Also, the exposure of the marine sediments to light, could potentially have resulted in chemical processes, such as photodegradation, that could have led to degradation of the organic matter (including IP_{25}) contained in the samples. However, Rontani et al. (2011) recently showed the low photoreactivity of the IP_{25} compared to the more unsaturated HBIs although without detailed information on storage this observation cannot be ruled out. Conversely, IP_{25} concentrations were much higher in the pilot study during the late Younger Dryas compared to that of the full study. However, the reason why this could have happened is not understood yet.

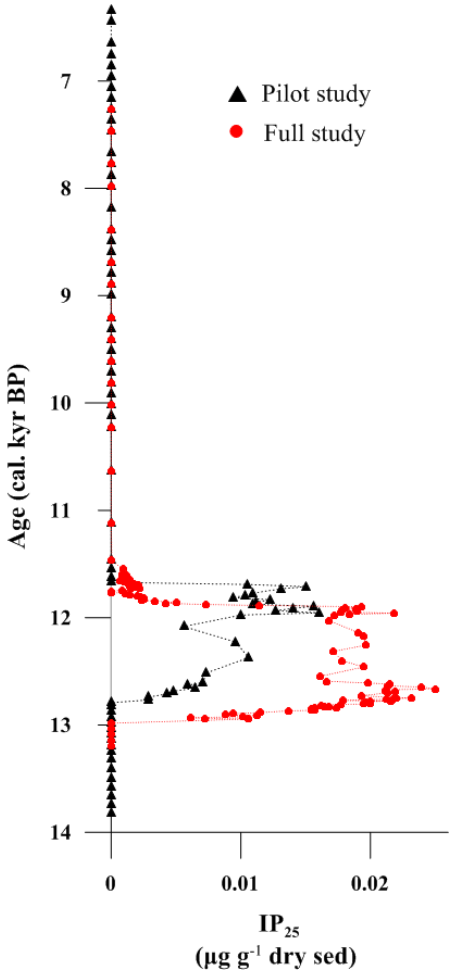

Figure 4.6: IP_{25} concentrations (µg g^{-1} dry sed) for core JM99-1200 in both the pilot and full studies.

Previous studies have noted that degradation of organic matter in sediment samples can occur under the influence of parameters such as the ambient atmosphere (Harada et al., 2012); however, the extent to which these parameters influence the preservation of chemical compounds, such as IP_{25}, and encourage the degradation of organic matter it is not completely understood. Therefore, since samples obtained for the pilot study were not properly stored and samples for the full study were specifically sampled from fresh and well-stored material for this study, only the results obtained from the latter study were used. Results initially obtained in the pilot study were discarded and not taken into account for environmental reconstructions. Hence, the discussion part of this chapter will be based on results obtained from the full study. The disparity of results obtained

with samples from the same core and depths, but sampled in different periods and stored in different ways, shows the great importance of proper storage and handling of sediment samples for organic geochemical analysis.

4.5 Discussion

Previously, a number of investigations into the marine environment for northern Norway have been carried out. For example, based on geotechnical and sediment-petrographical investigations, Vorren and Plassen (2002a) described eight main glacial events between ca. >22 – 9.5 ^{14}C kyr BP in northern Norway, with the final deglaciaton from the shelf break occurring at the end of the last glacial period (14.6 ^{14}C kyr BP). They also attributed atmospheric warming as the likely main cause for the melting of the ice sheets. In the same region, the end of the deglaciation was set to ca. 11.7 ^{14}C kyr BP based on stratigraphy (Fimreite et al., 2001), while in a more recent study based on foraminifera, Risebrobakken et al. (2011) showed that the melting of ice sheets and glaciers were responsible for cooling of the upper part of the water column at 12 – 8.5 kyr BP in the Nordic Seas.

With respect to the study location described in the current study and, more specifically, for the JM99-1200 core, previous studies have focused on the climate conditions of the northeast North Atlantic, especially during the Younger Dryas (Ebbesen and Hald, 2004). Initially, Knies et al. (2003) examined relative percentages of biogenic carbonate and marine organic carbon to explain changes in biogenic sedimentation and palaeoproductivity, while Ebbesen and Hald (2004) estimated SST inferred from planktic foraminifera. A further study was based on organic geochemical parameters (Knies, 2005) such as bulk organic proxies (Rock-Eval pyrolysis and $\delta^{13}C_{org}$ and $\delta^{15}N$ stable isotopes) and organic biomarkers (*n*-alkanes, alkenones and sterols). Analysis of

biomarkers from marine (e.g. brassicasterol, dinosterol) and terrigenous (e.g. C_{25} – C_{31} *n*-alkanes) origin was used to infer past climate changes in northern Norway and it was suggested that changes in sedimentary geochemical signatures during the last glacial - interglacial transition were mainly climate-induced rather than reflecting different preservation states of individual biomarkers.

Thus, these studies of northern Norway have focused mainly on somewhat broad oceanographic signatures of the marine environment as well as identifying the climate conditions of this area during different geological time intervals including the last deglaciation. Few studies have aimed to identify, uniquely, the occurrence or role of sea ice, despite the key role that it plays in controlling the climate system and its variability (e.g. Aagaard and Carmack, 1989; Thomas and Dieckmann, 2010). Exceptionally, Knies (2005) provided evidence for the occurrence of severe sea ice conditions in northern Norway during the Younger Dryas on the basis of a relative enhancement of the sterol biomarker 24-methylenecholesterol, believed to be produced by sea ice-dwelling diatoms.

4.5.1 Sea ice variability during the Younger Dryas

In the current study, these initial investigations were extended to provide a more comprehensive account of the palaeoceanography of the region and, in particular, of the identification and classification of the sea ice conditions throughout the Allerød – Younger Dryas – Holocene transitions based on temporal changes to a suite of biomarkers including IP_{25}.

The first point to note within the IP_{25} record is the occurrence of alternating intervals of absence and presence (Figure 4.4a) which contrasts the outcomes from previous IP_{25}-

based sea ice reconstruction studies in the Arctic and sub-Arctic regions, where IP_{25} has either been absent or present (but variable) throughout the entire record (e.g. Massé et al., 2008; Andrews et al., 2009; Müller et al., 2009; Belt et al., 2010; Vare et al., 2010). This study represents the first example of such a scenario and is interpreted in terms of particularly strongly contrasting sea ice conditions during the interval under study. It was also noted that the temporal concentration profile of the structurally related HBI diene II (Figure 4.4b) was qualitatively very similar to that of IP_{25}, lending further support to the suggestion that this biomarker is also produced by sea ice diatoms during the spring (Belt et al., 2007).

In the early part of the record, from ca. 13.8 – 12.9 cal. kyr BP (Allerød), IP_{25} was absent (Figure 4.4a) suggesting ice-free or permanent ice conditions during this interval. Previously, a marked and abrupt increase in *n*-alkane concentrations during the Inner Allerød Cold Period (ca. 13.5 – 13.0 cal. kyr BP) was observed within this interval which was explained in terms of a possible re-advance of the ice sheet in the study area (Knies, 2005) and this observation coincided with a short term reduction in SSTs (Ebbesen and Hald, 2004). The precise origins of *n*-alkanes, however, can be difficult to identify unambiguously and the absence of IP_{25} neither confirms nor rejects the possibility of some re-advance of the ice sheet at this time, since this scenario would have likely prevented any formation of IP_{25}. However, reduced brassicasterol concentrations during this interval (ca. 13.5 – 13.0 cal. kyr BP) provide some support to the possibility of glacial re-advance, since this would have limited phytoplankton production. Previously, Fahl and Stein (2012) interpreted low abundances of IP_{25} during the Allerød for a core from the Laptev Sea as representing low sea ice occurrence, but the observations here and those of Knies (2005) indicate a possible short-term re-advance of the ice sheet given the proximity of the JM99-1200 core site to the Norwegian coast.

IP_{25} first appeared in the record at ca. 12.9 cal. kyr BP and concentrations increased sharply, in less than ca. 40 yr, coincident with the onset of the Younger Dryas cold period, as reported in previous studies of this core (Ebbesen and Hald, 2004; Knies, 2005) and for other Arctic regions (e.g. Mayewski et al., 1993; Bakke et al., 2009). Interestingly, this first incidence of IP_{25} in the record occurred around the same time as a short-term, but significant increase in local SST (Figure 4.7d) and global atmospheric temperatures (Figure 4.7e), indicating that the sharp response in sea ice probably resulted from freshwater forcing following a large meltwater release (e.g. Manabe and Stouffer, 2000) during warmer summers and freezing of fresher surface waters during winter.

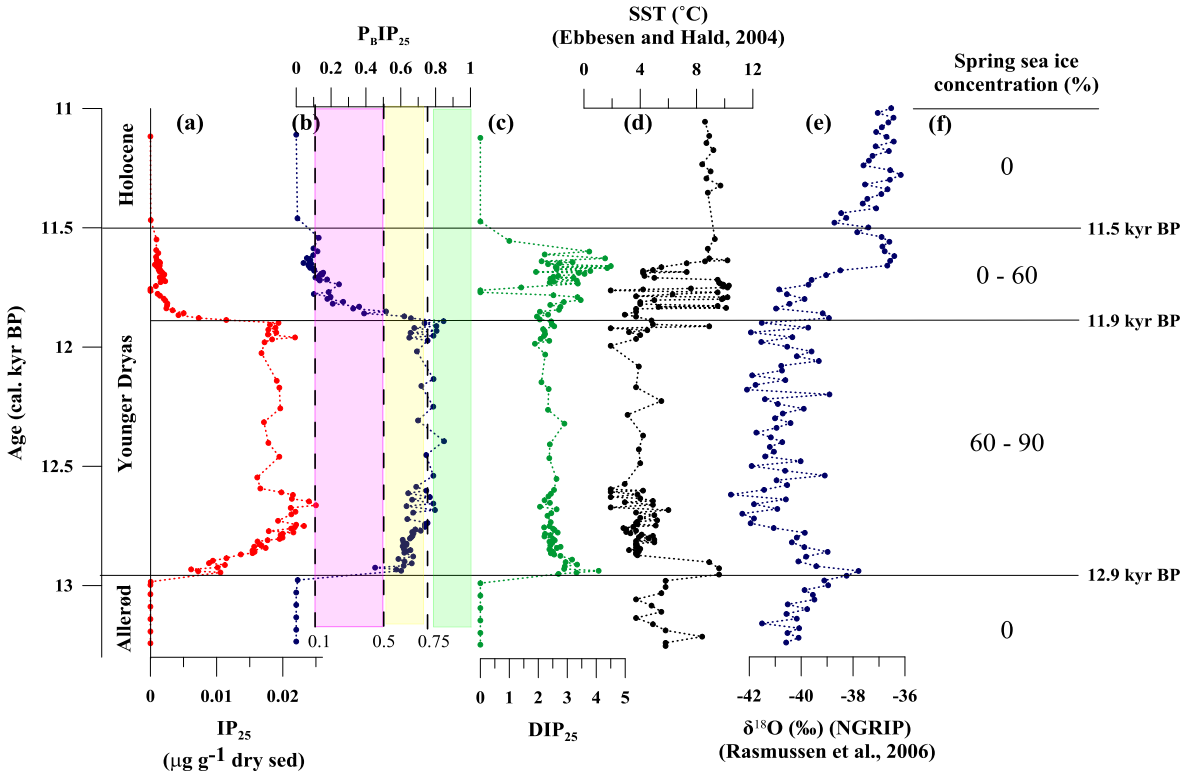

Figure 4.7: Temporal palaeoclimate profiles for the JM99-1200 core for the period ca. 13.25 – 11 cal. kyr BP: (a) IP_{25} concentrations; (b) P_BIP_{25} index; (c) DIP_{25} index; (d) estimated mean SST (˚C). General deviation of SST is ± 1 ˚C (Ebbesen and Hald, 2004); (e) $\delta^{18}O$ data from the NGRIP core (Rasmussen et al., 2006); (f) Spring sea ice concentration (%) (calculated according to the correlated satellite data with P_BIP_{25} data (Müller et al., 2011)). The horizontal solid lines at ca. 12.9 cal. kyr BP and ca. 11.5 cal. kyr BP indicate the onset and the termination of the Younger Dryas, respectively. The horizontal solid line at ca. 11.9 cal. kyr BP represents a major shift in the sea ice conditions during the late Younger Dryas.

During the Younger Dryas (ca. 12.9 – 11.5 cal. kyr BP), IP_{25} abundances could be divided into two main sections (Figure 4.4a and Figure 4.7a). During the first interval (ca. 12.9 – 11.9 cal. kyr BP), increasing IP_{25} concentrations (ca. 12.9 – 12.66 cal. kyr BP) indicated higher frequencies of seasonal sea ice occurrence consistent with increasing rates of fresh surface water, declining SSS and SST and the presence of polar planktic foraminifera reported previously (Hald and Aspeli, 1997; Ebbesen and Hald, 2004). Following this relatively short interval, IP_{25} concentrations decreased slightly, before remaining fairly constant for the subsequent ca. 700 yrs up to ca. 11.9 cal. kyr BP. At the same time, concentrations of 24-methylenecholesterol were also elevated relative to pre- and post-Younger Dryas values, while brassicasterol concentrations were at their lowest levels for the entire record (Figure 4.4c and Figure 4.4d). Previously, Knies (2005) found similar (lower resolution) sterol profiles during this interval and suggested that enhanced 24-methylenecholesterol and reduced brassicasterol abundances during the Younger Dryas were consistent with the prevalence of seasonal sea ice during severe climate conditions, since these two biomarkers were considered to be representative of sea ice diatoms and phytoplankton, respectively. The outcomes of these proxy data are also consistent with minimum SSTs, low sedimentation rates, low foraminiferal fluxes (Ebbesen and Hald, 2004) and low primary productivity estimates, inferred from biogenic carbonate and marine organic carbon in the same record (Knies et al., 2003). The new proxy data are also consistent with low primary productivity and extended sea ice cover for a study carried out in the south-western Barents Sea (Aagaard-Sørensen et al., 2010).

At ca. 11.9 cal. kyr BP, there was a rapid decrease in IP_{25} concentrations and values remained low up to ca. 11.5 cal. kyr BP, indicating a major change to the spring sea ice occurrence at this time with less frequent, more variable or shorter seasonal sea ice occurrence. This abrupt change in the IP_{25} profile was accompanied by a decrease in 24-

methylenecholesterol (Figure 4.4c) and an increase in SSTs (ca. 2 -10 ˚C; Figure 4.7d) consistent with a reversal in the sea ice conditions compared to the early-mid Younger Dryas. At the same time, higher brassicasterol concentrations, compared to the early Holocene (Figure 4.4d), likely reflect the rapid settling of significantly enhanced primary produced organic matter due to scavenging on detritus (and increased sedimentation rates) (Knies, 2005) and, in terms of production, this period was probably the most productive interval during the last ca. 13.8 cal. kyr BP. Higher phytoplankton blooms would have been promoted by the occurrence of reduced sea ice and the input of additional nutrients resulting from sea ice and ice sheet melt. In addition, the variability in the sterol and SST records may also reflect the instability of the thermohaline circulation towards the end of the Younger Dryas and into Preboreal times, also as a result of variations in meltwater input from melting ice-sheets (Bauch et al., 2001).

After ca. 11.5 cal. kyr BP, IP_{25} was again absent, suggestive of ice-free conditions following the termination of the Younger Dryas cold period as described in numerous previous studies (e.g. Alley et al., 1993; Gulliksen et al., 1998; Alley, 2000; Ebbesen and Hald, 2004). The absence of IP_{25} in the record continued into the early-mid Holocene (ca. 7.2 cal. kyr BP), suggesting continued ice-free conditions, reflecting the longer term influence of Atlantic waters (Knies, 2005; Hald et al., 2007). The occurrence of reduced 24-methylenecholesterol concentrations and increased abundances of other sterols (this study and Knies, 2005) also indicates ice-free conditions during this period, as does the absence of IRD in a core from the south-western Barents Sea (Aagaard-Sørensen et al., 2010), although the occurrence of winter sea ice in this region cannot be excluded on the basis of low IRD (Risebrobakken et al., 2010).

Exceptionally, within the 11.9 – 11.5 cal. kyr BP interval, a noticeable feature appeared at ca. 11.76 – 11.75 cal. kyr BP, where IP_{25} and the other biomarkers described herein (Figure 4.4), were absent despite the presence of reasonable OM content as revealed by our GC-MS analyses and TOC data reported previously (Knies, 2005) (Figure 4.5). The effective shutdown in production of sea ice diatom and phytoplankton biomarkers during this short interval possibly resulted from severe climate conditions during an extremely short-term period (ca. 10 yr) with permanent sea ice cover. Significantly, these absences in biomarkers were accompanied by a sudden and dramatic drop in mean SST (ca. 2 ˚C; calculated using material from the same core and age model as employed here; Figure 4.7d) which was preceded and succeeded by high amplitude SST oscillations from ca. 4 – 10 ˚C. Interestingly, Taylor et al. (1997) identified a ca. 10-year cooling event by a large increase in non-sea-salt sulphate which likely resulted from a volcanic eruption recorded at Summit, Greenland, at a similar time period (11.66 kyr BP), although the accuracy of the respective age models may prevent any correlations between these two observations being made with great certainty. It was also suggested, however, that this short-term cooling was probably not the trigger for a warmer climate state, which is also supported by our data.

4.5.2 Quantitative sea ice coverage during the last deglaciation – application of the PIP_{25} index

In this study and in several others previously (e.g. Massé et al., 2008; Vare et al., 2009; Belt et al., 2010), temporal changes to IP_{25} abundances have been interpreted as reflecting qualitative directional changes to seasonal sea ice occurrence. With the aim of making IP_{25}-based sea ice reconstructions more quantitative or, at least, more accurate

in terms of defining ice conditions, Müller et al. (2011) proposed the use of the so-called PIP_{25} index whereby, the concentration of IP_{25} was compared to that of a common phytoplankton sterol biomarker (e.g. brassicasterol). While the general applicability of the PIP_{25} index needs further investigation, the principles behind it are clear and worthy of testing, where possible. The PIP_{25} index was calculated according to Equation 4.1, whereby [IP_{25}] and [P] represent the respective concentrations of IP_{25} and a phytoplankton biomarker P, while c was used to modify the concentrations of P due to its significantly increased magnitude compared to that of IP_{25}; the c factor was calculated from the ratio of the mean IP_{25} and P concentrations. As a result, PIP_{25} values range from 0-1 and Müller et al. (2011) have suggested that individual ranges can be classified according to different oceanographic or sea ice scenarios. Thus, high (> 0.75) PIP_{25} values are indicative of severe sea ice cover, medium values (0.5 – 0.75) suggest seasonal or stable ice edge conditions, while $PIP_{25} < 0.5$ suggests infrequent or ice-free conditions. Of course, since the derivation of the PIP_{25} is largely empirical, the boundaries between these classifications should be considered with some flexibility; however, the rationale behind them is clear and largely reflects the relative favorability in conditions for production of both types of biomarker. For example, PIP_{25} is necessarily zero under ice-free conditions since IP_{25} is not biosynthesised in the absence of sea ice. In contrast, during periods where there is a marginal ice zone or stable ice edge, the formation of both biomarkers is favored, resulting in PIP_{25} values of ca. 0.5 – 0.75.

Equation 4.1

$$PIP_{25} = IP_{25} / (IP_{25} + (P \times c)).$$

In the current study, PIP_{25} values were calculated from the respective IP_{25} and brassicasterol data and this resulted in a P_BIP_{25} profile that can be divided into four

intervals (Figure 4.4e and Figure 4.7b). Before ca. 12.9 cal. kyr BP (Allerød) and after ca. 11.5 cal. kyr BP (Holocene), P_BIP_{25} values were zero due to the absence of IP_{25} during both periods, indicating ice-free conditions during these warm periods, as expected. Conversely, the absence of IP_{25} (and thus P_BIP_{25} = 0) can also imply permanent sea-ice cover; however, such an interpretation in this instance can be ruled out on the basis of elevated concentrations of other biomarkers, notably the sterols which demonstrates the value of interpreting PIP_{25} data alongside that of the individual biomarkers (Belt and Müller, 2013). The occurrence of permanent sea ice cover also seems unlikely given the observation of sub-polar foraminifera (Bauch et al., 2001) and low IRD (especially after the Younger Dryas) (Aagaard-Sørensen et al., 2010) from nearby locations during these intervals.

During the Younger Dryas, two main features of the P_BIP_{25} profile were identified (Figure 4.7b). Firstly, from ca. 12.9 – 11.9 cal. kyr BP the majority of the P_BIP_{25} values were high and fairly constant (0.6 – 0.8). According to the classification of Müller et al. (2011), such P_BIP_{25} values indicate the occurrence of either seasonal or marginal ice zone conditions with some brief excursions (e.g. at ca. 12.4 cal. kyr BP) indicative of more severe sea ice cover. Since the boundary conditions that categorise these scenarios are rather poorly defined, the P_BIP_{25} data, like the presence of IP_{25} alone, are not sufficient to distinguish between them with absolute confidence. Further, PIP_{25} values are somewhat sensitive to the c-factor used in their calculation, which further limits defining precisely the sea ice conditions using this method alone; however, failure to observe enhanced concentrations of brassicasterol and other phytoplankton biomarkers during this period, more strongly suggests the occurrence of extended seasonal sea ice conditions, since a marginal ice zone scenario generally results in enhanced primary production (Smith et al., 1985; Sakshaug, 1997) with associated increased lipid profiles relative to open water environments.

During the second part of the Younger Dryas, between ca. 11.9 – 11.5 cal. kyr BP, P_BIP_{25} values decreased sharply, with mean P_BIP_{25} values of ca. 0.1, suggesting a change from extended to reduced sea ice occurrences or short-term seasonal sea ice. Interestingly, the rapid (< 40 yr) change in sea ice conditions at the onset of the Younger Dryas at ca. 12.9 cal. kyr BP is even more apparent in the P_BIP_{25} index compared to the IP_{25} data alone. In contrast, both the P_BIP_{25} and IP_{25} records indicate a more gradual (ca. 400 yr) decline in sea ice cover between ca. 11.9 and 11.5 cal. kyr BP.

Since one of the aims of this study was to extend the sea ice record beyond that of general descriptions and make the identifications more quantitative, one of the further outcomes of the study by Müller et al. (2011) were applied, who demonstrated a reasonably good correlation between P_BIP_{25} proxy data and sea ice concentrations (%) derived from satellite data. Accordingly, P_BIP_{25} values in the range 0.6 – 0.8 during the interval ca. 12.9 – 11.9 cal. kyr BP yielded sea ice concentrations of 60 – 90% (Figure 4.7f), while between ca. 11.9 and 11.5 cal. kyr BP, the P_BIP_{25} data (0.1 – 0.6) suggested significantly reduced and also more variable sea ice cover (0 – 60%; Figure 4.7f). Such quantitatve estimates provide further evidence for contrasting seaonal sea ice conditions between the early/mid and late Younger Dryas for northern Norway.

4.5.3 Diene II/IP_{25} ratios (DIP_{25} index): further insights into seasonal sea ice conditions?

Thus far, the environmental significance of the HBI diene II (hereafter referred to as diene II) was not specially considered, other than to note that its temporal concentration profile aligns reasonably closely with that of IP_{25} (Figure 4.4b). Previously, the occurrence of IP_{25} and diene II has been observed in a number of Arctic marine sediments (Belt et al., 2007; Vare et al., 2009) and, in one instance, a small enhancement of diene II relative to IP_{25} was suggested to be consistent with reduced sea ice (Vare et al., 2009) or generally warmer conditions given the previously reported temperature dependence of unsaturation in HBIs (Rowland et al., 2001); however, this was not investigated further in any great detail and now seems an unlikely explanation given that bottom ice temperatures (where sea ice diatoms grow) are largely invariant of sea ice surface temperatures, ice thickness, etc. In addition, the stable isotopic composition of diene II, like that for IP_{25}, has also been shown to be consistent with a sea ice origin (Belt et al., 2008; Brown, 2011), for the Canadian Arctic, at least.

Given the structural, isotopic and co-occurrence characteristics between IP_{25} and diene II, in the current study, the abundance relationships between the two biomarkers were compared in more detail starting with the examination of IP_{25} and diene II data for three Holocene cores from different regions of the Arctic obtained previously. Indeed, a similar analysis was performed by Massé et al. (2011) to support the use of diene II as a proxy for the past occurrence of Antarctic sea ice when detected in Antarctic sediments, since IP_{25} is absent in the Southern Ocean. Two of the core locations represented different regions of the Canadian Arctic Archipelago and different timescales (Barrow Strait and Dease Strait; ca. 7 – 10 kyr) (Vare et al., 2009; Belt et al., 2010), while a third study site was from the North Icelandic Shelf (1.2 kyr) (Massé et al., 2008). For each

location, relative abundances of diene II and IP_{25} showed a remarkably strong linear correlation (Figure 4.8) providing compelling evidence for co-production of both biomarkers by sea ice diatoms. Still, relatively little is known about the environmental controls over IP_{25} (and other HBIs) production by sea ice diatoms (a review of this topic is given by Belt and Müller, 2013), but the strong linear relationship between the abundances of diene II and IP_{25} was interpreted as a high degree of consistency in the nature of the sea ice conditions for each of the individual locations studied. For each core site, however, there was a change in the relative concentrations of the two biomarkers (as measured by the gradient of the correlations; Figure 4.8) that further suggested that the magnitude of this relationship could be used to further characterise the sea ice conditions from each region. Thus, diene II/IP_{25} ratios (hereafter referred to as DIP_{25}) were between ca. 1 – 2 for the Canadian Arctic and ca. 3 for North Iceland, which experience predominantly landfast and drift ice, respectively. The extent to which this parameter may be used in the future to identify either the source or the nature of sea ice conditions will require a more comprehensive analysis from different Arctic regions. Nevertheless, the clear linear relationship between the abundances of diene II and IP_{25} shown here provides the basis for refining the application of the IP_{25} proxy even further.

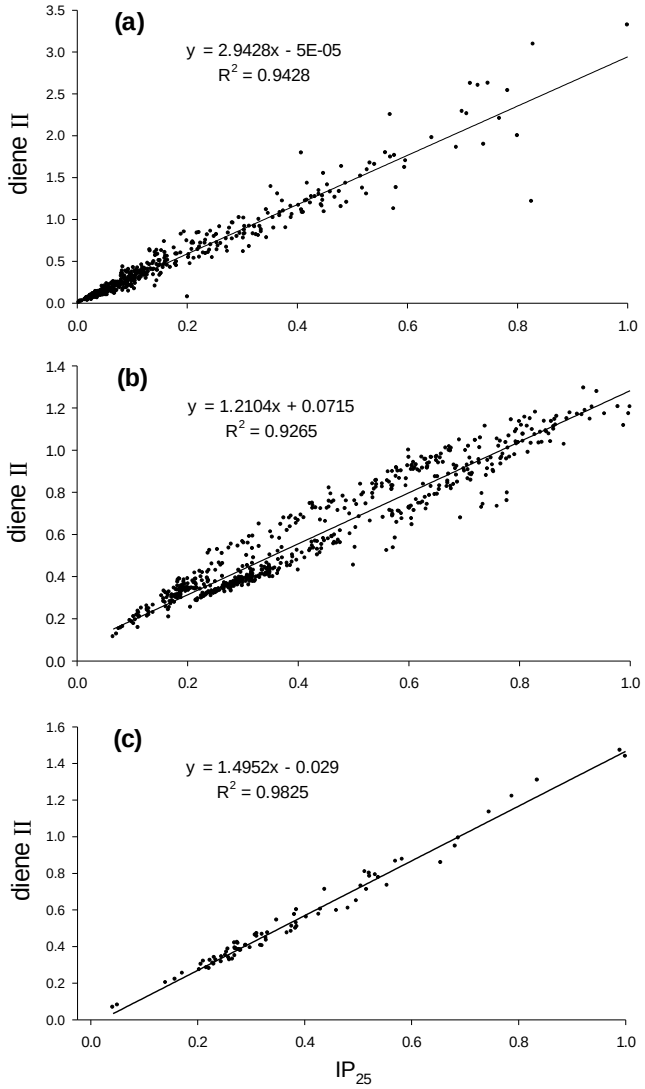

Figure 4.8: Concentrations of diene II *vs* IP_{25} in marine sediment cores from three different regions of the Arctic: (a) the North Icelandic Shelf (471 sediment samples) (Massé et al., 2008); (b) Barrow Strait (618 sediment samples) (Vare et al., 2009); (c) Dease Strait (80 sediment samples) (Belt et al., 2010). Concentrations were normalised to the maximum value of IP_{25} measured in each core.

When the equivalent comparison for the biomarker data obtained for the JM99-1200 core was made, the abundances of diene II and IP_{25} also showed a strong linear correlation between ca. 12.8 – 11.9 cal. kyr BP (Figure 4.9a), consistent with the observations made for the cores from the Canadian Arctic and North Iceland; however, there were significant deviations in this relationship from ca. 12.9 – 12.8 cal. kyr BP and ca. 11.9 – 11.5 cal. kyr BP (Figure 4.9b). The interpretation that the near constant

DIP_{25} index between 12.8 – 11.9 cal. kyr BP reflects relatively stable sea ice conditions during this interval was supported by low and consistent SSTs for the same interval (Ebbesen and Hald, 2004) (Figure 4.7d). In contrast, significantly weaker correlations were observed between diene II and IP_{25} between ca. 12.9 – 12.8 cal. kyr BP and 11.9 – 11.5 cal. kyr BP as illustrated by the weaker linear correlation (Figure 4.9b) between them and the extreme variability in DIP_{25} values (Figure 4.7c). This variability suggested periods of highly unstable or variable sea ice conditions and that, transitions to/from consistent DIP_{25} values indicated major changes to the sea ice regime. These observations and hypothesis were supported by highly fluctuating SSTs (2 – 10 ˚C; Figure 4.7d) as well as extremely variable sterol concentrations (Figure 4.4c and Figure 4.4d) during both periods, which also suggested a high degree of instability in the sea surface conditions. Although the interpretation of the DIP_{25} index will require further validation, ideally through measurements for which known stability or variability in sea ice conditions have already been established, there was an excellent agreement between the proposed interpretations and the ranges in sea ice concentrations predicted from the P_BIP_{25}-values (Figure 4.7f) and their correlations with satellite data presented previously (Müller et al., 2011).

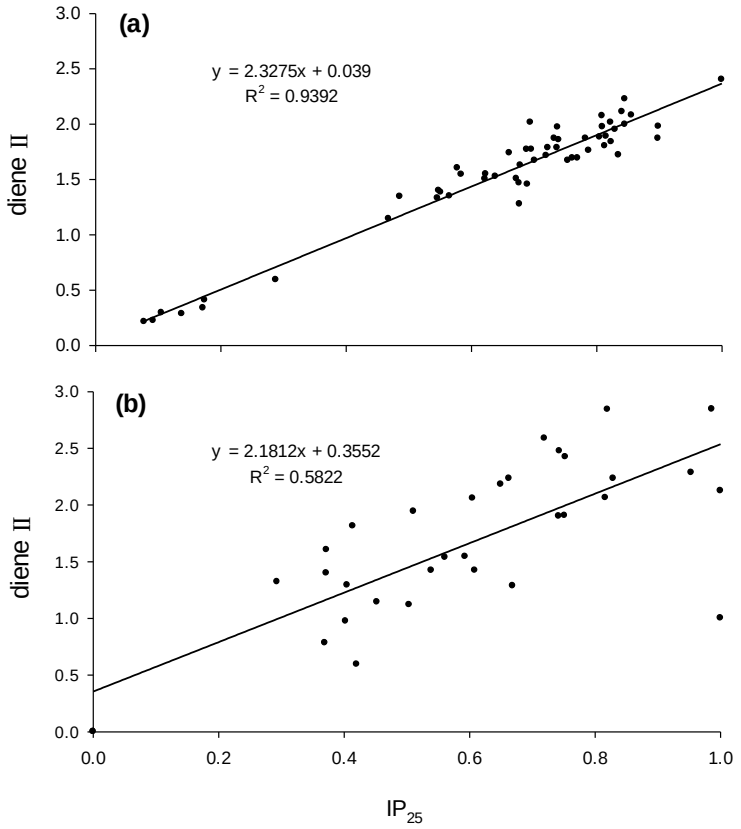

Figure 4.9: Concentrations of diene II *vs* IP_{25} for the JM99-1200 core during different time intervals: (a) ca. 12.8 – 11.9 cal. kyr BP (55 sediment samples); (b) ca. 12.9 – 12.8 cal. kyr BP and ca. 11.9 – 11.5 cal. kyr BP (33 sediment samples). Concentrations were normalised to the maximum value of IP_{25} observed for each dataset.

Previously, Taylor et al. (1993) showed that the climate system tends to undergo rapid changes or "flickering" during transitions, such as at the end of the Younger Dryas. According to our DIP_{25} profile, two "flicker" points were observed in the JM99-1200 core, the first of which coincided with the onset of the Younger Dryas (between ca. 12.9 – 12.8 cal. kyr BP). This initial transition from ice-free to stable sea ice conditions occurred relatively quickly (less than ca. 120 yr) and was followed by a period of ca. 900 yr where sea ice conditions were relatively stable (consistent DIP_{25} values; Figure 4.7c). A second, and more pronounced "flicker" point, was observed during the late Younger Dryas (beginning ca. 11.9 cal. kyr BP), and this instability in the sea ice regime continued until the onset of the Holocene (ca. 11.5 cal. kyr BP). A similar, two interval sea ice scenario, was also suggested by Bakke et al. (2009) following analysis

of a lake sediment core from western Norway and a marine core from the Faeroe-Shetland channel. Combined geochemical and physical data from the lake core provided evidence for a stable early Younger Dryas followed by a second interval, beginning ca. 12.15 cal. kyr BP, where there were rapidly changing signals from glacial meltwater, and this period of instability continued until the transition into the Holocene (ca. 11.7 cal. kyr BP). This so-called "flickering" in climate conditions was also seen in the accompanying marine record (albeit ca. 100 yr later) with high amplitude changes in SST and salinity, which were further interpreted as indicating variable sea ice cover. Thus, in contrast to the early Younger Dryas, where the combined proxy records indicated a stable and extensive sea ice cover, Bakke et al. (2009) suggested that the short-term changes in proxy data during the late Younger Dryas (after ca. 12.15 cal. kyr BP) indicated a reduction in sea ice extent resulting from a greater influx of warm Atlantic water into the region. Clearly, the biomarker data presented in the current study from northern Norway (JM99-1200) lend further support to these suggestions and, in addition, provided more detailed descriptions of the sea ice conditions in the two sub-intervals within the Younger Dryas.

4.6 Conclusions

In contrast to previous IP_{25}-based sea ice reconstructions for the Arctic, this study represents the first example where the occurrence of this biomarker had been restricted to a relatively short-term and discrete geological interval and has provided unequivocal evidence for the occurrence of seasonal, rather than permanent, sea ice conditions for northern Norway during the Younger Dryas. In addition, the alternating absence/presence of IP_{25} in the record further illustrates the selectivity of this biomarker to a specific source or environment (diatoms in sea ice), which contrasts with the more

generic nature of many other biomarker or geochemical proxies. The rapid appearance of IP_{25} at ca. 12.9 cal. kyr BP provides further evidence that the onset of the Younger Dryas was extremely rapid, before reasonably consistent sea ice conditions prevailed until ca. 11.9 cal. kyr BP. During the latter part of the Younger Dryas (ca. 11.9 – 11.5 cal. kyr BP), environmental conditions changed again, and sea ice conditions were much more variable during this ca. 400 yr period including an extremely short interval of permanent or near-permanent sea ice cover at ca. 11.75 cal. kyr BP. The absence of IP_{25} in the record after ca. 11.5 cal. kyr BP signifies the onset of ice-free conditions at the beginning of the Holocene. When IP_{25} abundances were combined with those of the phytoplankton biomarker brassicasterol, the resulting P_BIP_{25} data provides additional descriptions of the sea ice conditions and estimates of sea ice concentrations from previously established modelled correlations; for example, substantially higher sea ice concentrations during the early Younger Dryas (ca. 70-95% from ca. 12.9 – 11.9 cal. kyr BP). As part of this study, it was also shown that the co-occurrence of the HBI diene II, previously identified in sediments from other Arctic regions, had the potential to be used alongside IP_{25} (DIP_{25} index) to further characterise the sea ice conditions and, in particular, to demonstrate contrasting and short-term variability in sea ice cover. The application of, and mutual agreement between, a series of organic geochemical proxy measures described herein, therefore increased the confidence in their palaeoclimatic interpretation and these results were further complemented by other proxy data obtained previously.

CHAPTER FIVE

5 Results (2): Seasonal sea ice conditions in the western Barents Sea following the last deglaciation

5.1 Introduction

Chapter five describes a biomarker based analysis of a sediment core from Kveithola Trough, western Barents Sea (JM09-KA11-GC; Figure 5.2). Data from this biomarker approach, including quantification of IP_{25}, a di-unsaturated HBI alkene and sterols, for palaeo sea ice reconstructions, are presented and interpreted. Comparisons are also made with other proxy studies for the same core and those obtained close to the study area. Amongst the outcomes, the presence of seasonal sea ice conditions during the Younger Dryas is further confirmed.

During the last glacial maximum the Barents Sea shelf area was covered by the Svalbard-Barents Sea Ice Sheet (e.g. Elverhøi and Solheim, 1983; Mangerud et al., 1998; Ingólfsson and Landvik, 2013) which following retreat, allowed the transport of Atlantic waters towards the Arctic Ocean. Numerous studies have focused on studying variations in Atlantic water inflow into the northern north Atlantic during the last deglaciation and the Holocene (e.g. Hald et al., 2007; Andersson et al., 2010). Furthermore, changes in the West Spitsbergen Current (WSC) that branches off the Norwegian Atlantic Current have been documented (e.g. Rasmussen et al., 2007; Ślubowska-Woldengen et al., 2007; Rasmussen et al., 2012) as well as variations north of Svalbard (e.g. Koç et al., 2002; Ślubowska et al., 2005). Oceanographic variations during the last deglaciation have also been reported in the Barents Sea region (e.g. Hald

and Aspeli, 1997; Duplessy et al., 2001; Sarnthein et al., 2003b; Aagaard-Sørensen et al., 2010; Risebrobakken et al., 2010).

The main aim of the current study was to use a biomarker-based approach, including the use of the sea ice biomarker IP_{25}, to reconstruct the palaeo sea ice conditions in the western Barents Sea margin following the last deglaciation. Further, the comparison of biomarker data with other proxy-based studies for the same core allowed to better define the overall oceanographic conditions.

5.2 Regional setting

The Barents Sea is a relatively shallow continental shelf with an average water depth of 230 m. The total area of the Barents Sea is 1.4 million km^2 (Loeng, 1991; Sakshaug, 1997; Loeng and Drinkwater, 2007). The ocean Polar Front, which is the boundary between Atlantic and Arctic waters, divides the Barents Sea into the northern and southern parts in the western part of the Barents Sea at latitudes of 75 – 76˚N (e.g. Loeng and Drinkwater, 2007) (Figure 5.1). The southern part of the Barents Sea is characterised by Atlantic surface waters (temperature > 2˚C; salinity > 35‰). The influx of Arctic water to the Barents Sea forms its northern part and can be transported to the Barents Sea by two main routes, between Spitsbergen and Frans Josefs Land and, to a greater extent, between Frans Josefs Land and Novaya Zemlya (Loeng, 1991) (Figure 5.1). A small amount of Arctic water enters through the Kara Sea (Loeng et al., 1997). Polar waters are characterised by salinities in the range 34.3 – 34.7‰ and temperatures below 0˚C due to meltwater from sea ice. In summer, a 5 – 20 m layer of melt water covers the polar water, while in winter, the upper 150 m of the water column is formed by Arctic waters (Loeng, 1991). Tides and winds are the main reason for climatic variability in the Barents Sea (Slagstad and McClimans, 2005).

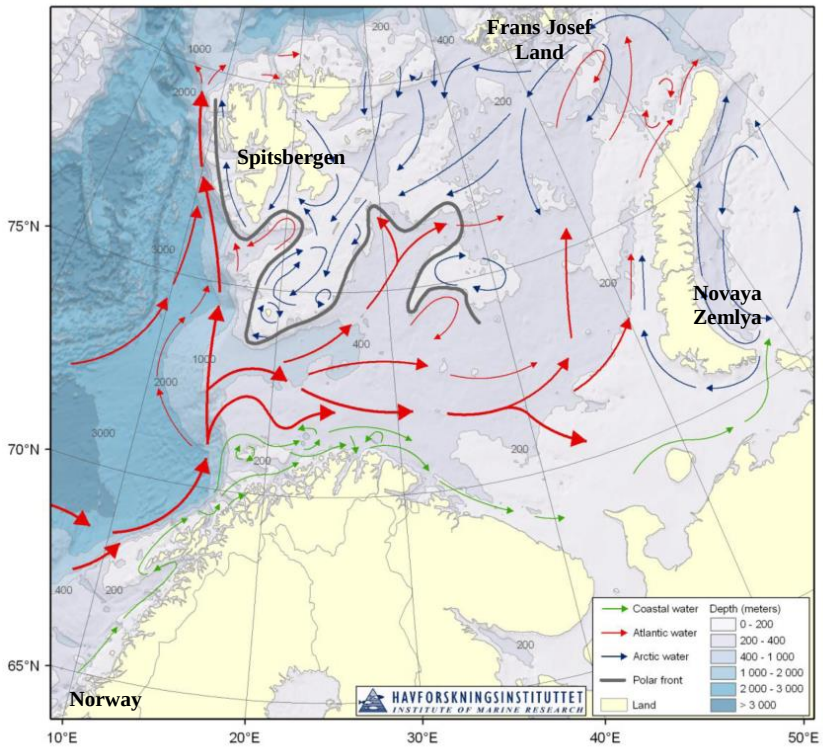

Figure 5.1: The main features of the circulation and bathymetry of the Barents Sea; grey line defines the Polar Front (modified from Stiansen and Filin, 2006).

The main water mass in the Barents Sea (by volume and flux) is Atlantic water coming from the Norwegian Sea (Figure 5.1) which is almost continuously transported northwards into the Barents Sea changing its temperature and salinity, most probably also affecting the variability of the Barents Sea climate (Loeng, 1991). The ice drift in the Barents Sea is mainly wind-driven (Vinje and Kvambekk, 1991). The presence of cold polar waters results in an annual average of about 40% of the Barents Sea being ice covered. However, there is also a large variation of the ice conditions in this region (e.g. Vinje and Kvambekk, 1991; Divine and Dick, 2006). The ice reaches its minimum in August/September, when the ice edge retreats to the northern shelf break. In October, new ice starts to form, usually reaching its maximum in March/April where approximately 60% (varying from 0.77 – 1.1 million km^2) of the Barents Sea is ice

covered, with ice-free conditions in the southern and western areas (Vinje and Kvambekk, 1991; Loeng and Drinkwater, 2007).

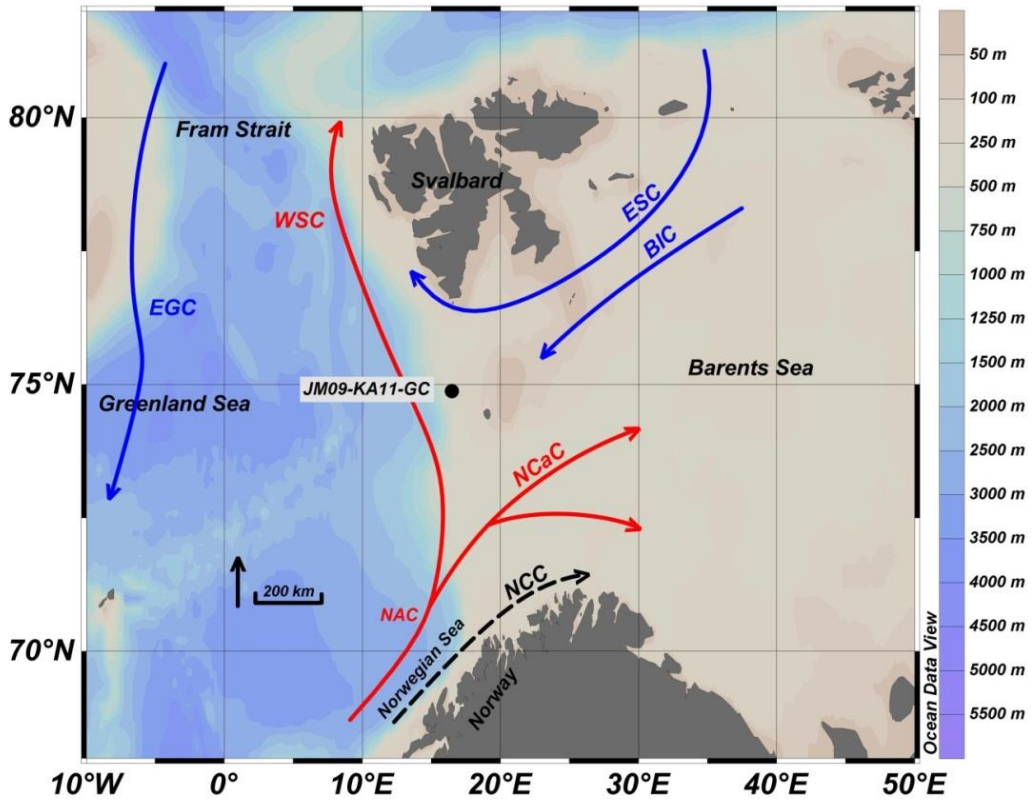

Figure 5.2: Map of the sampling location JM09-KA11-GC with main surface water currents. Atlantic waters are carried northwards along the Norwegian continental shelf break by the North Atlantic Current (NAC) and continue into the Arctic Ocean via the West Spitsbergen Current (WSC) and into the Barents Sea as the North Cape Current (NCaC). Also shown in the map are the Norwegian Coastal Current (NCC) and the cold water East Greenland Current (EGC), East Spitsbergen Current (ESC) and Bear Island Current (BIC).

Kveithola, where the current study is based, is a small trough extending westwards from Spitsbergenbanken in the western Barents Sea. The trough is approximately 100 km long and 15-20 km wide, with water depths ranging between 200 – 400 m (Rüther et al., 2012). Within the Norwegian Sea, Atlantic waters are carried northwards along the Norwegian continental shelf break by the North Atlantic Current (NAC) and continue into the Arctic Ocean via the West Spitsbergen Current (WSC) and to the Barents Sea via the North Cape Current (NCaC) (Figure 5.2). These bring heat and salt to the high northern latitudes, which greatly influences the climate of the region (e.g. Sarnthein et al., 2003b; Ślubowska et al., 2005). Presently, the south-western Barents Sea (including the study site) is dominated by warm and saline Atlantic water, while the northern Barents Sea is dominated by cold and less saline Arctic waters. Further, the study area under investigation currently lies close to the modern day maximum sea ice extent (Figure 5.3). Kveithola Trough is characterised as a sediment trap during the last deglaciation, although modern accumulation rates are low (5 cm kyr^{-1}) (Elverhøi et al., 1989). Hence, the Kveithola Trough is considered to be a key area for understanding the ice dynamics and the timing of deglaciation of the north-western Barents Sea (e.g. Rüther et al., 2012).

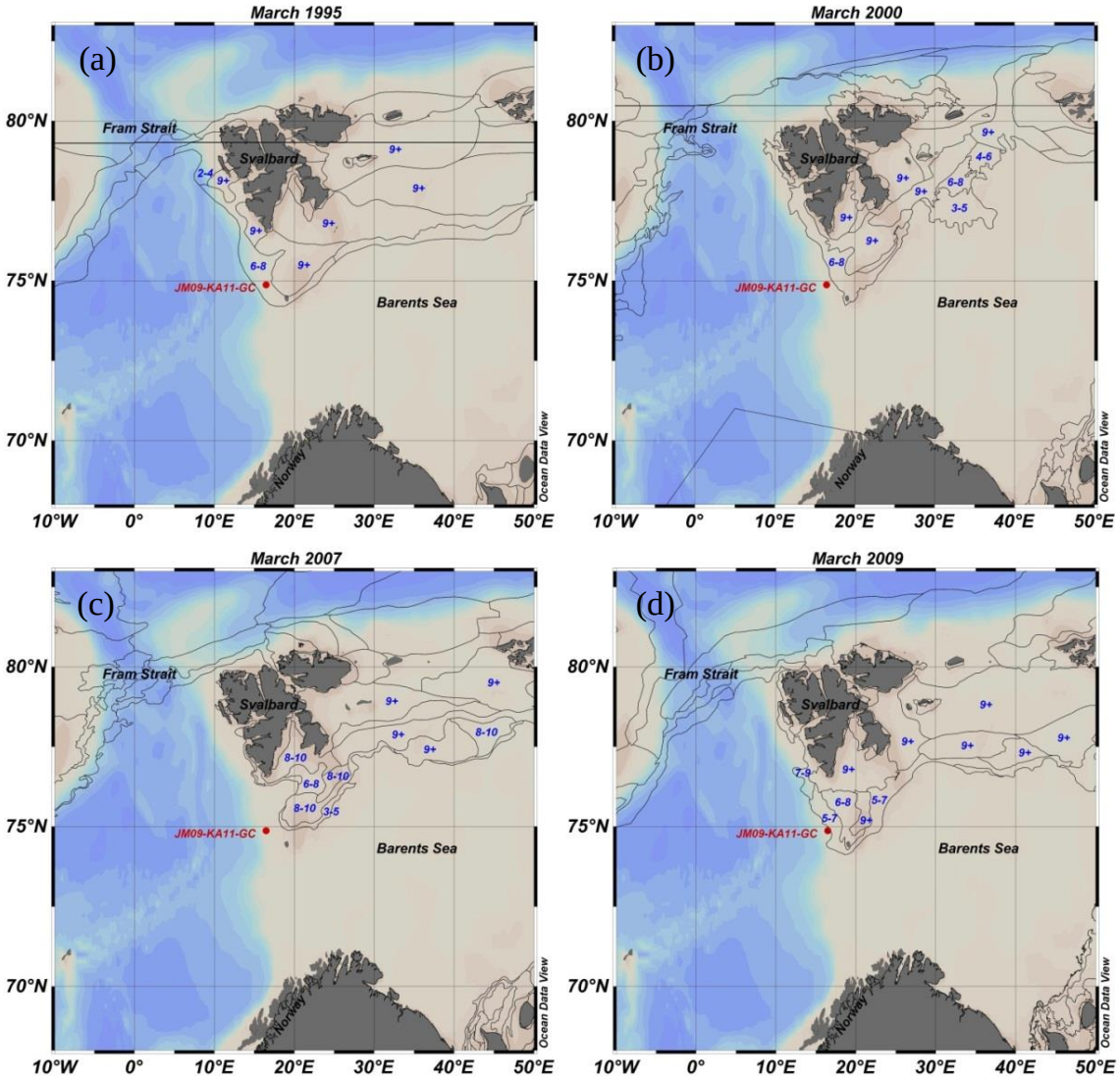

Figure 5.3: Maps showing the sampling location (JM09-KA11-GC) and sea ice concentrations (in tenths), corresponding to: (a) March 1995; (b) March 2000; (c) March 2007; (d) March 2009 (bottom right). Data obtained from the U.S. National Ice Center. The selected years illustrate the contrasting sea ice conditions from zero ice cover to sea ice edge conditions. The maximum sea ice extent in most years occurs during March.

5.3 Material and methods

5.3.1 Field methods and chronology

The gravity core under study, JM09-KA11-GC, was retrieved from Kveithola Trough, western Barents Sea, (74.52˚N, 16.29˚E; water depth 345 m; core length 3.86 m; Figure 5.2) on board the R/V *Jan Mayen* in 2009 and stored *in situ* (5˚C) until sampled for analysis. Individual sub-samples for biomarker analysis were taken at 0.5 – 1 cm intervals from 0 to 386 cm, freeze-dried and stored at -20˚C prior to analysis.

An age model for JM09-KA11-GC was first constructed by Rüther et al. (2012). A total of eight AMS ^{14}C age determinations were performed. Five additional AMS ^{14}C dates were obtained after that and a new depth-age model was developed by linear interpolation (Berben et al., 2013; Groot et al., 2013). Linear sedimentation rates varied between 4 – 240 cm kyr^{-1} (Figure 5.6a) giving an effective temporal resolution of 3 – 300 yr.

Note: Following submission of this thesis a minor revision of the age model was performed. Further information is given by Berben et al. (2013) and Aagaard-Sørensen et al. (in prep).

5.3.2 Experimental

Analysis of biomarkers (hydrocarbons and sterols) required extraction from the sample matrix and separation into individual fractions prior to GC-MS analysis. A complete description of the experimental procedure shown in Figure 5.4, is given in Chapter 2 (Methods). However, the following amendments and other observations are noted.

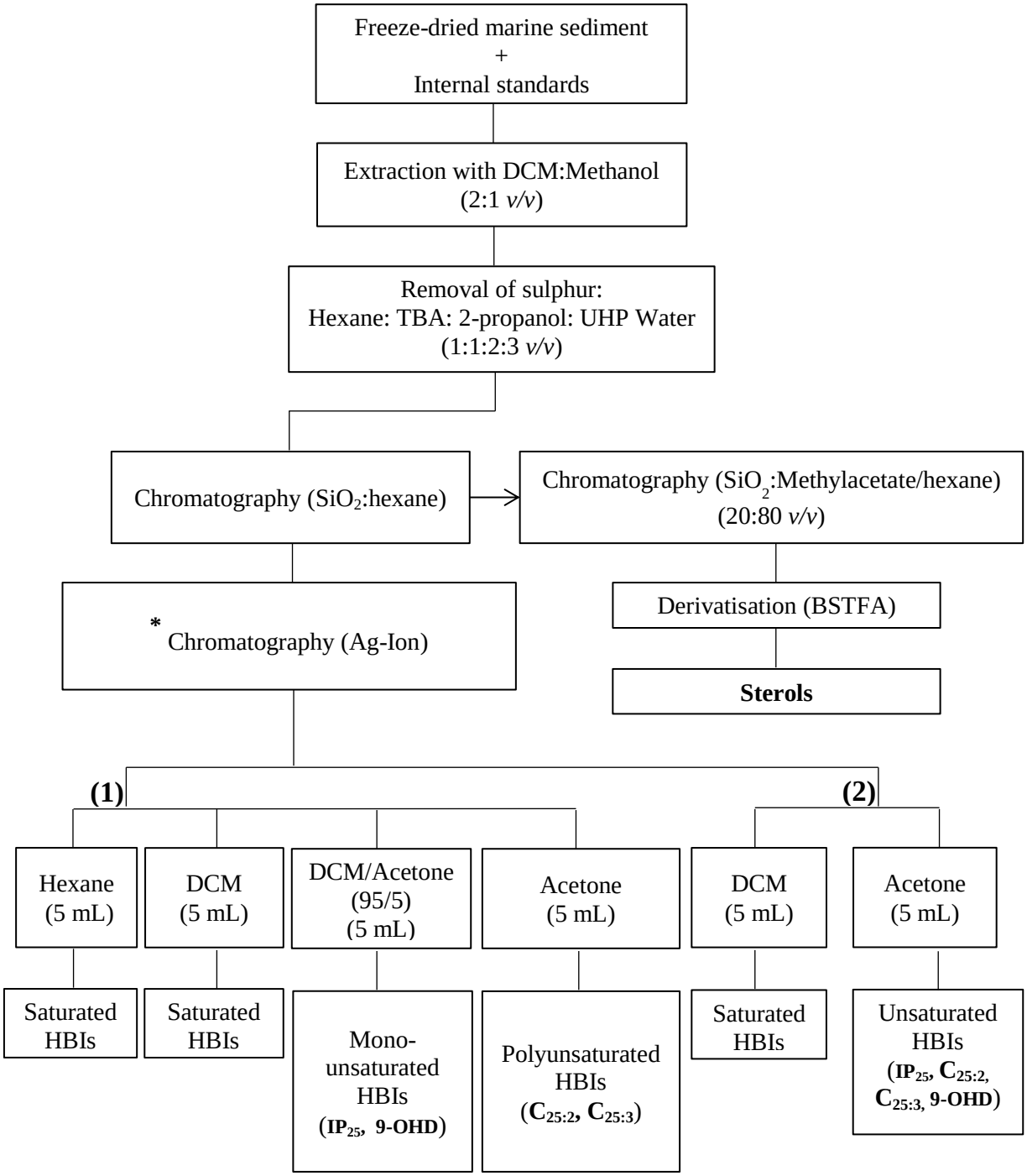

Figure 5.4: Sample extraction flow diagram for lipid biomarkers. * Two different approaches regarding Ag-Ion chromatography were adopted depending on level of purification and biomarkers required for GC-MS analysis.

Following addition of the internal standards for quantification (7-hexylnonadecane; 10 µL; 10 µg mL^{-1} and 9-octylheptadec-8-ene; 10 µL; 10 µg mL^{-1}), the freeze dried sediments were extracted with DCM/Methanol (3 x 3 mL; 2:1 *v/v*). Since many TOEs were found to contain high concentrations of elemental sulphur (GC-MS) that interfered with the gas chromatographic analyses, this was removed from the primary extracts before further purification (Chapter 2). Having removed sulphur, extracts were further purified using column chromatography (silica), with apolar lipids (hexane; 6 mL) and sterols (20:80 methylacetate/hexane; 6 mL) collected as two single fractions. In some cases, the identification or quantification of some HBIs in these partially purified extracts was made difficult due to a combination of low concentrations and the occurrence of other highly abundant co-eluting organic compounds that prevented further concentration of the extracts. Depending on which biomarkers were needed for analysis and on degree of purification required (Figure 5.4), two different approaches were adopted (a detailed description of these techniques is given in Chapter 2) by using Ag-Ion chromatographic material. The use of different solvents allowed the elution of different biomarkers (Figure 5.4). Sterols were derivatised (BSTFA; 50 µL; 70°C; 1h) prior to analysis by GC-MS. Analytical reproducibility was monitored using a standard sediment with known abundances of biomarkers for every 16 - 18 sediment samples extracted (analytical error of 10%, n = 11).

TOC data were determined at the University of Tromsø using a Leco CS 200 analyser. Briefly, sediment samples were repeatedly treated with 10% (vol.) hydrochloric acid (HCl) to remove carbonate, then washed repeatedly with distilled water to remove traces of HCl and finally dried overnight (50˚C) before being analysed.

Regarding the quantification of the $C_{25:2}$ HBI (6/17) (diene II) by GC-MS, poor chromatographic resolution of di-unsaturated HBIs was observed, which made it

difficult to obtain reliable manual integration data for this biomarker (Figure 5.5). Therefore, baseline-to-baseline manual peak integrations were carried out to include all C_{25} dienes in a single measurement. The C_{25} dienes included isomers with unsaturation at positions 5/6 and 23/24 ($C_{25:2}$ (5/6), Brown, 2011), diene II (Chapter 2), and a further $C_{25:2}$ HBI reported by Brown (2011), following GC-MS analysis of an Arctic sea urchin extract. Hydrogenation of the latter, followed by analysis by GC-MS confirmed the same $C_{25:0}$ parent structure compared to previously reported $C_{25:2}$ HBIs, although the lack of sufficient material prevented structural identification by NMR spectroscopy. On the basis of the relative peak heights of these three HBI dienes, diene II appeared to be the most abundant, although all three were included in the integrated data (Figure 5.5). Thus, diene concentrations are referred to, collectively, as ΣDienes.

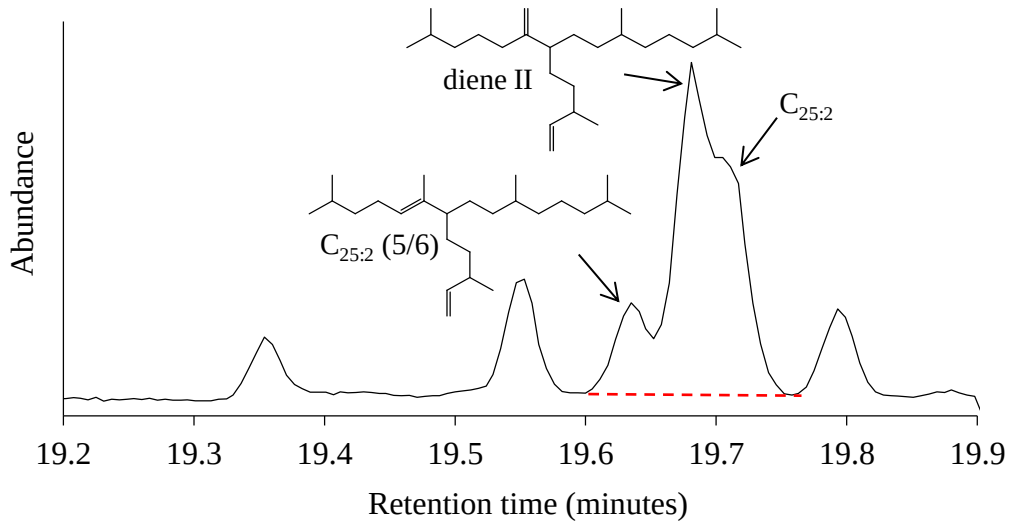

Figure 5.5: Partial GC-MS chromatogram (SIM *m/z* 348.3) of a silica and Ag-Ion purified JM09-KA11-GC sediment extract. Red dotted line shows the approach adopted for manual integration of the $C_{25:2}$ HBI diene II peak (middle main peak), which also included two other compounds identified as $C_{25:2}$ (5/6) (left minor peak, Brown, 2011) and an extra $C_{25:2}$ with identical $C_{25:0}$ parent structure to previously reported $C_{25:2}$ HBIs but yet, unidentified by NMR.

All biomarkers concentrations (μg g^{-1} dry sed) were normalised to TOC content (μg g^{-1} OC) as TOC data for this core showed a highly fluctuating profile (~0.8 – 1.7%; Figure 5.6b). Biomarker concentrations were also converted to fluxes (μg cm^{-2} kyr^{-1}) as described in Chapter 2, Section 2.2.7.1.

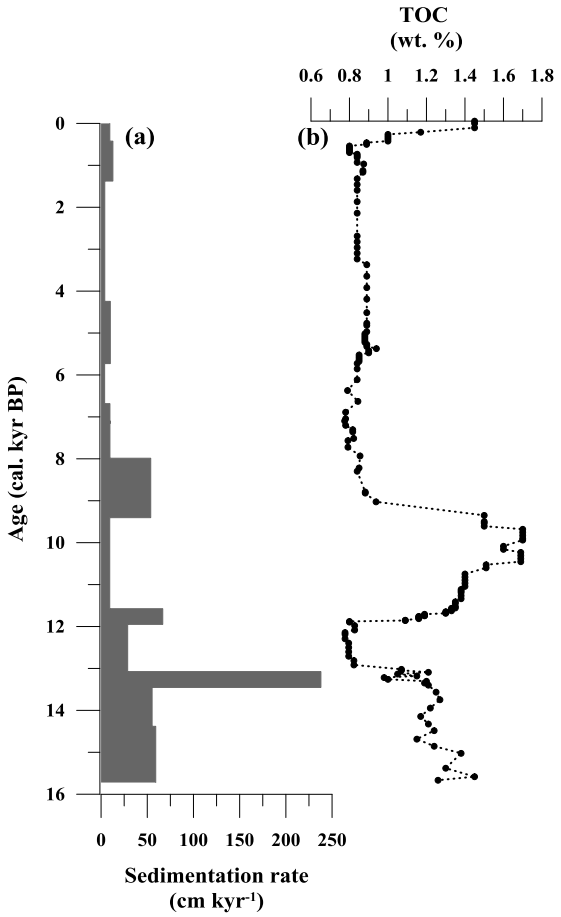

Figure 5.6: (a) Sedimentation rates (cm kyr^{-1}); (b) Total organic carbon (TOC, wt. %) of core JM09-KA11-GC.

Calculation of the PIP_{25} and DIP_{25} indices was carried out as described in Chapter 2. Concerning the PIP_{25} index, a c factor value of 0.0179 was obtained by dividing the mean IP_{25} concentration (all samples) by the mean phytoplankton biomarker (brassicasterol) concentration. Regarding the calculation of the DIP_{25} ratio, since the peak integrations included (at least) three $C_{25:2}$ HBIs (as previously explained) the ratio was named ΣDIP_{25}.

5.4 Results

Overall, a total of 152 downcore sediment samples were analysed for the sea ice biomarker IP_{25}, the structurally related HBI diene II and other lipid biomarkers, including the two sterols, 24-methylcholesta-5,22E-dien-3β-ol (brassicasterol) and 24-methylcholesta-5,24(28)-dien-3β-ol (24-methylenecholesterol) commonly found in marine algae (Volkman et al., 1998). Sampling was carried out according to the age model, in order to achieve decadal to centennial resolution.

IP_{25} was present in some (but not all) horizons, consistent with the core location and known ice cover (Figure 5.3). From the late Oldest Dryas, Bølling – Allerød interstadials and up to the beginning of the Younger Dryas (ca. 15.7 – 13.1 cal. kyr BP, P-I), TOC normalised IP_{25} concentrations showed a slight increasing trend up to ca. 13.1 cal. kyr BP. In general, however, IP_{25} concentrations were relatively low although higher than those observed during the Holocene (Figure 5.7a). At the end of the Allerød period and at the onset of the Younger Dryas stadial at ca. 13.1 cal. kyr BP (P-II), the concentration of IP_{25} increased more rapidly up to ca. 12 cal. kyr BP. Highest IP_{25} concentrations recorded for the entire record were observed at both ca. 12.45 and 12 cal. kyr BP. After ca. 12 cal. kyr BP, IP_{25} concentrations fell sharply towards the transition to the current interglacial at ca. 11.7 cal. kyr BP. At this point IP_{25} concentrations remained relatively low but stable up to ca. 9.5 cal. kyr BP (P-III). From ca. 9.5 – 1.6 cal. kyr BP (P-IV), IP_{25} was mainly absent (or below the limit of detection: 0.05 ng g^{-1} dry sed), although some minor positive departures were observed around ca. 6.5, 5.5 – 4.5 and 3.5 – 2.5 cal. kyr BP (Figure 5.7a). During the last ca. 1.6 cal. kyr BP of the record (P-V), IP_{25} was present more consistently, although still at relatively very low concentrations. The concentration profile of ΣDienes (believed to consist mainly of diene II) showed a similar trend to that of IP_{25}, especially between ca. 15.7 – 11.7 cal.

kyr BP (Figure 5.7b) suggesting co-production of diene II (and possibly other HBI dienes) and IP_{25} by sea ice diatoms, as suggested previously (Belt et al., 2007; Belt et al., 2008; Vare et al., 2009; Brown, 2011).

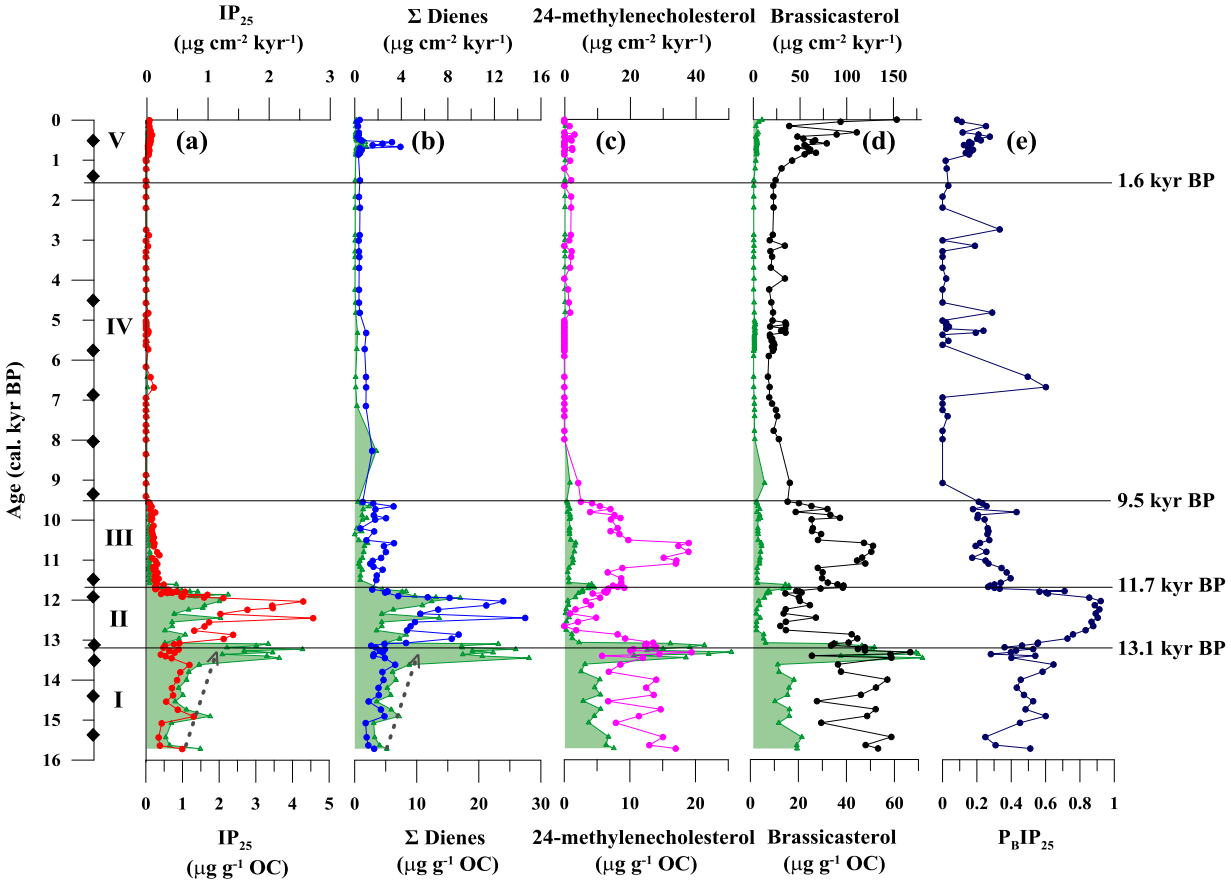

Figure 5.7: Individual and combined temporal concentration profiles (fluxes plotted in green) of biomarkers in the JM09-KA11-GC core: (a) IP_{25}; (b) ΣDienes; (c) 24-methylenecholesterol; (d) brassicasterol; (e) P_BIP_{25} index. The horizontal solid lines at ca. 13.1 cal. kyr BP and ca. 11.7 cal. kyr BP indicate the onset and the termination of the Younger Dryas, respectively. The horizontal solid lines at ca. 9.5 cal. kyr BP and ca. 1.6 cal. kyr BP represent shifts in the sea ice conditions during the early-mid and mid-late Holocene boundaries, respectively. The diamonds mark the AMS ^{14}C dates used in the age model.

During the late Oldest Dryas – Bølling – Allerød periods (P-I), concentrations of 24-methylenecholesterol and brassicasterol fluctuated significantly from ca. 15.7 to 13.1 cal. kyr BP (Figure 5.7c and Figure 5.7d). At the boundary between the Allerød and Younger Dryas periods, both sterol concentrations decreased up to ca. 12.7 cal. kyr BP and remained relatively low throughout the Younger Dryas cold period up to 11.7 cal. kyr BP (P-II). Brassicasterol and 24-methylenecholesterol concentrations increased again during the early Holocene up to ca. 10 cal. kyr BP before decreasing again to ca. 9.5 cal. kyr BP (P-III). Between ca. 9.5 – 1.6 cal. kyr BP (P-IV) brassicasterol concentrations were at their lowest for the entire record, while 24-methylenecholesterol was absent between ca. 8 – 5 cal. kyr BP and then present again at very low concentrations up to ca. 1 cal. kyr BP.

24-methyelenecholesterol and brassicasterol profiles were very similar (Figure 5.7c and Figure 5.7d), even during the Younger Dryas, where concentrations of both sterols were fairly low. However, some differences were observed, such as during ca. 11 cal. kyr BP (P-III) where 24-methylenecholesterol concentrations increased more than those of brassicasterol. In addition, during the last ca. 1.6 cal. kyr BP (P-I) brassicasterol increased rapidly towards the present, while 24-methylenecholesterol was either absent or present at very low concentrations. The observation that both sterol profiles were quite similar and differed from those of IP_{25} and ΣDienes (Figure 5.7), contrasts with that found previously, where 24-methylenecholesterol was more abundant during the Younger Dryas and similar to IP_{25} (Chapter 4). Previously, 24-methylenecholesterol was reported as the main sterol in sea ice diatom communities during the spring bloom in McMurdo, Antarctica (Nichols et al., 1993). A recent study by Belt et al. (2013b) shows the presence of a number of sterols, including 24-methylenecholesterol and brassicasterol, in sea ice samples from Resolute Passage in the Canadian Arctic Archipelago and the Amundsen Gulf. Although 24-methylenecholesterol is one of the

most common sterols in diatoms (Rampen et al., 2010), this biomarker is not considered source specific, since some dinoflagellates and prasinophytes also produce it (Volkman, 1986). Further, the observed similarity of brassicasterol and 24-methylenecholesterol profiles in the JM09-KA11-GC core, reflects the poor source specificity of both biomarkers.

The IP_{25} and brassicasterol concentration data were combined to generate PIP_{25} indices (Müller et al., 2011) in an attempt to provide more quantitative palaeo sea ice estimates. The P_BIP_{25} (subscript B refers specifically to brassicasterol) profile showed some similarities to those of IP_{25} and ΣDienes. Between ca. 15.7 – 13.1 cal. kyr BP P_BIP_{25} values ranged between ca. 0.2 – 0.6, after which a sharp increase during the Younger Dryas was observed (ca. 0.8 – 0.9). Towards the end of the Younger Dryas, P_BIP_{25} values decreased rapidly again to ca. < 0.4 followed by a further decreasing trend up to ca. 9.5 cal. kyr BP (Figure 5.7e). Between ca. 9.5 – 1.6 cal kyr BP, P_BIP_{25} values were at their lowest for the entire studied period, although some positive departures were observed, coinciding with periods where IP_{25} was present at very low concentrations at ca. 6.5, 5.5 – 4.5 and 3.5 – 2.5 cal. kyr BP. During the last millennium, P_BIP_{25} values increased again, but the actual values remained relatively low. Finally, biomarker concentration profiles broadly align with fluxes throughout the record (Figures 5.7 and Figure 5.8), except around ca. 13.5 – 13 cal. kyr BP (Figure 5.7) where enhanced fluxes, relative to concentrations, were observed as a result of very high sedimentation rates (Figure 5.6a).

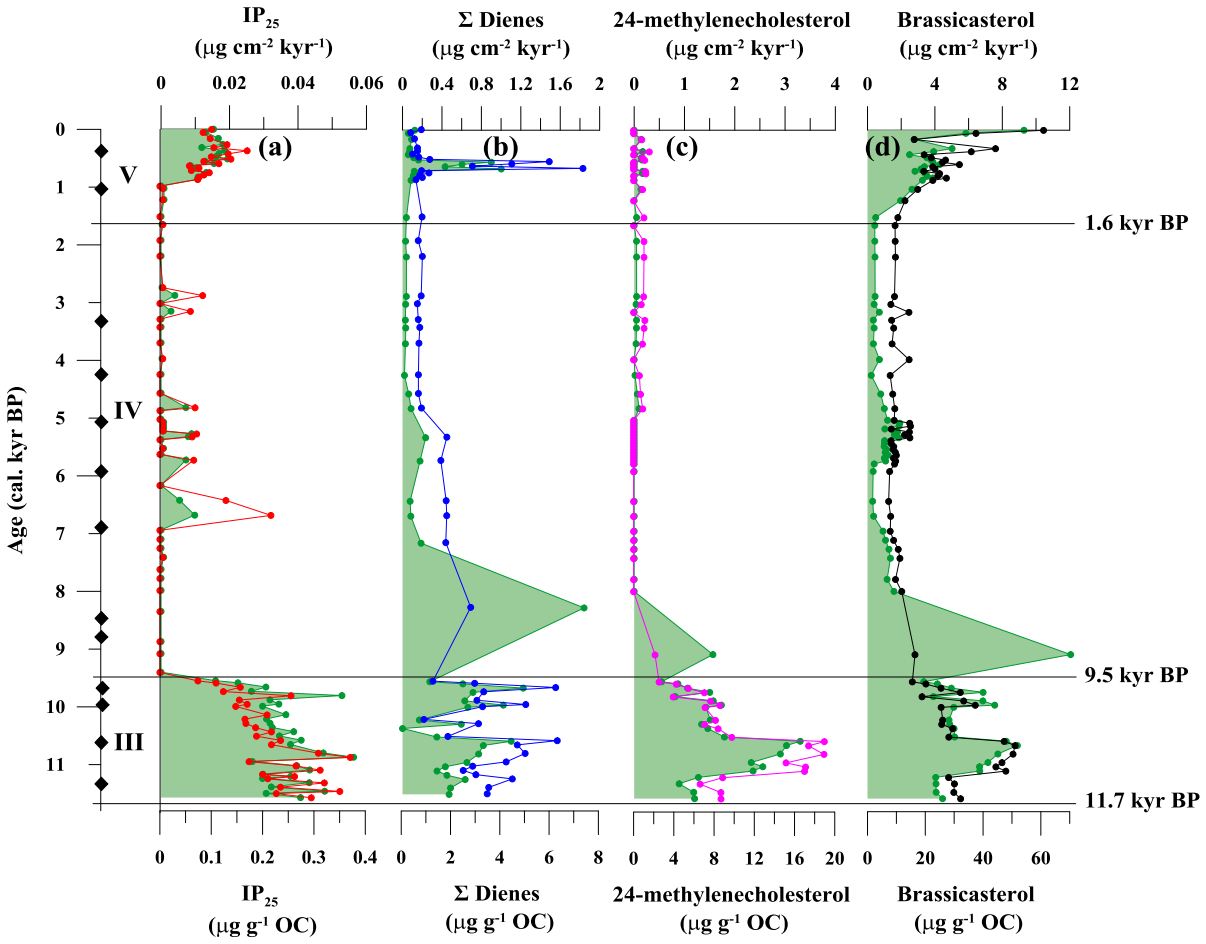

Figure 5.8: Individual and combined temporal concentration profiles (fluxes plotted in green) of biomarkers in the JM09-KA11-GC core during the last ca. 11.7 cal. kyr BP: (a) IP_{25}; (b) ΣDienes; (c) 24-methylenecholesterol; (d) brassicasterol. The horizontal solid line at ca. 11.7 cal. kyr BP indicates the termination of the Younger Dryas. The horizontal solid lines at ca. 9.5 cal. kyr BP and ca. 1.6 cal. kyr BP represent shifts in the sea ice conditions during the early-mid and mid-late Holocene boundaries, respectively. The diamonds mark the AMS ^{14}C dates used in the age model.

5.5 Discussion

Previously, many studies have been focused on the Norwegian-Svalbard region. These include, for example, reconstructions of Atlantic water inflow around west Svalbard during the late glacial – early Holocene transition (Ebbesen et al., 2007), the Holocene (Rasmussen et al., 2012) as well as on the Norwegian-Svalbard continental margin (Hald et al., 2007) along with palaeoceanographic reconstructions of the south-west Svalbard margin during the last deglaciation (Rasmussen et al., 2007). Similarly, studies of the south-western Barents Sea area included seafloor geomorphology investigations

(Andreassen et al., 2008; Winsborrow et al., 2010) as well as palaeoceanographic studies covering the late Weichselian – early Holocene transition (Aagaard-Sørensen et al., 2010), early Holocene (Wohlfarth et al., 1995) and the entire Holocene (Risebrobakken et al., 2010). A further study, located close to that of the current study, was focused on the palaeoceanographic conditions during the Holocene (Sarnthein et al., 2003b).

Regarding the study area described in this chapter and, more specifically, for the JM09-KA11-GC core, one previous study focused on acoustic characteristics, lithology and physical properties (Rüther et al., 2012). In a further study, benthic and planktic foraminiferal fauna, stable isotopes ($\delta^{13}C$, $\delta^{18}O$), geochemical (e.g. %TOC) and geophysical (e.g. IRD) parameters, covering the late Oldest Dryas, the Bølling – Allerød interstadials and the Younger Dryas have been investigated (Aagaard-Sørensen et al., *In prep*). Further, within the changing Arctic and Subarctic Environment network (CASE, EU FP7), the Holocene section of the JM09-KA11-GC core has been investigated using benthic and planktic foraminifera and stable isotopes ($\delta^{13}C$, $\delta^{18}O$) (Berben et al., 2013; Groot et al., 2013) as well as dinocyst assemblages (Dylmer, submitted). The biomarker data presented here are discussed alongside these existing investigations.

5.5.1 Sea ice conditions during the last ca. 15.7 cal. kyr BP

Based on the age model, biomarker data presented here and comparisons with other proxy data, it is proposed that the palaeoceanographic conditions at the JM09-KA11-GC core location covering the last ca. 15.7 cal. kyr BP can be divided into five distinct periods (Figure 5.7):

5.5.1.1 Period I: 15.7 – 13.1 cal. kyr BP (late Oldest Dryas – Bølling – Allerød)

Period I (P-I) corresponds to the late part of the Oldest Dryas stadial and the Bølling – Allerød interstadials (Figure 5.7). Overall, the IP_{25} and ΣDienes profiles show an increasing trend from ca. 15.7 cal. kyr BP to ca. 13.1 cal. kyr BP with intermediate concentrations compared to the rest of the record. The presence of IP_{25} suggests the presence of seasonal sea ice at that time. In contrast, the sterol concentrations were high but rather variable during the whole interval. Together these observations suggest overall quite variable seasonal sea ice as well as open-water conditions. Relatively low bottom and subsurface water temperatures and salinities were reported in a study of the same core by Aagaard-Sørensen et al. (*In prep*) where a strong influence of meltwater was inferred by planktic foraminifera further suggesting the presence of sea ice/icebergs. During the Bølling – Allerød, primary productivity increased markedly, as shown by relative abundances of benthic fauna, while water temperatures and salinities rose periodically, in response to a changing influx of Atlantic water (Aagaard-Sørensen et al., *In prep*), suggesting the presence of sea ice and the Polar Front at, or in close proximity to, the core site. These observations were further supported by the biomarker data, where high but variable sterol concentrations (especially brassicasterol) and

relatively high IP_{25} concentrations (Figure 5.7a), suggested that this period was characterised by enhanced primary productivity and ice edge conditions. In addition, the high degree of variability in the concentrations might reflect movements of the ice edge in the area under study consistent with modern day conditions (Figure 5.3). Previously, the benthic foraminifera *Nonionellina labradorica* has been related to Polar Front conditions associated with high primary productivity (e.g. Jennings et al., 2004; Wollenburg et al., 2004; Jennings et al., 2011). However, and unlike the biomarker data, which points to enhanced primary productivity during this period, low relative abundances of *N. labradorica* are observed (Figure 5.9f). This observation suggests that the influence of enhanced freshwater conditions as well as higher turbidity and sedimentation rates possibly disfavoured the proliferation of this species during this period (Aagaard-Sørensen et al., *In prep*) at times when primary productivity was high.

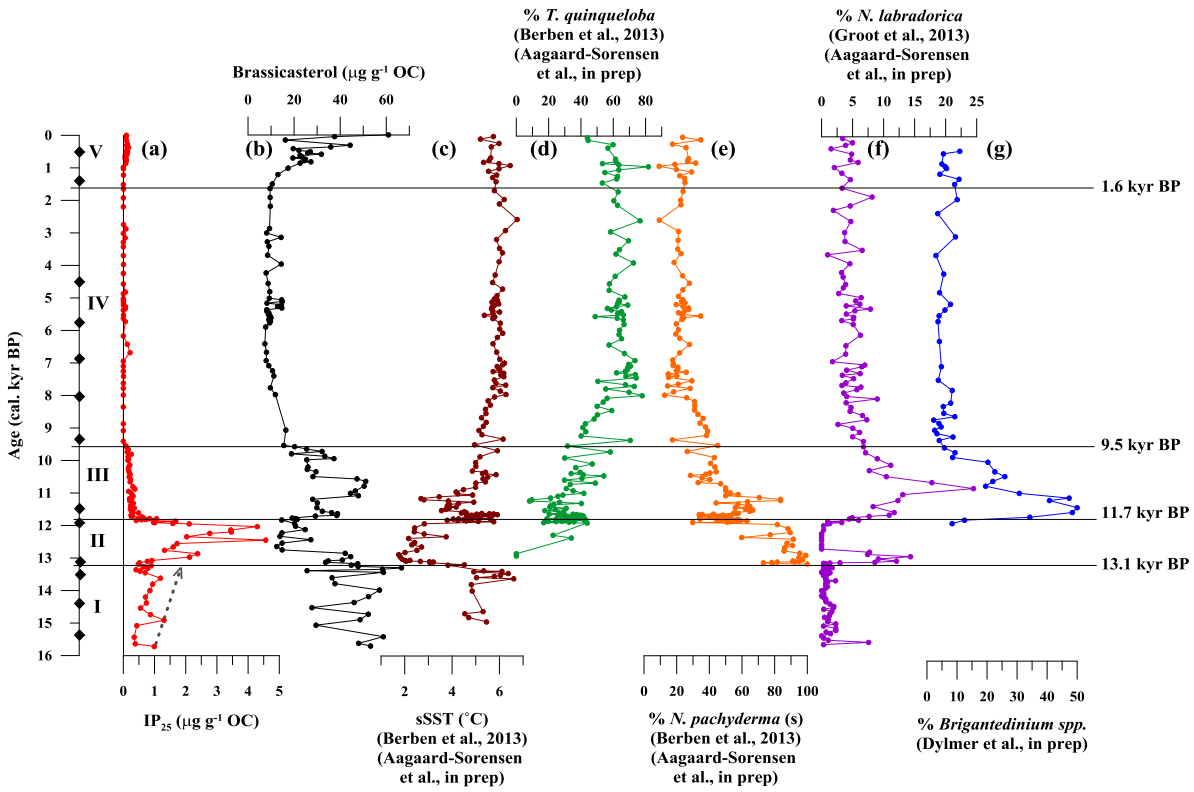

Figure 5.9: Temporal palaeoclimate profiles for the JM09-KA11-GC core: (a) IP_{25}; (b) Brassicasterol; (c) Reconstructed summer Sea Surface Temperature (˚C) estimates; (d) % *Turborotalia quinqueloba*; (e) % *Neogloboquadrina pachyderma*; (f) % *Nonionellina labradorica*; (g) % *Brigantedinium spp*. The horizontal solid lines at ca. 13.1 cal. kyr BP and ca. 11.7 cal. kyr BP indicate the onset and the termination of the Younger Dryas, respectively. The horizontal solid lines at ca. 9.5 cal. kyr BP and ca. 1.6 cal. kyr BP represent shifts in the sea ice conditions during the early-mid and mid-late Holocene boundaries, respectively. The diamonds mark the AMS ^{14}C dates used in the age model.

5.5.1.2 Period II: ca. 13.1 – 11.7 cal. kyr BP (Younger Dryas)

P-II included the Younger Dryas period, (further information about this cold stadial is given in Chapter 4). Changes in all biomarker data occurred at the onset and end of the Younger Dryas, at ca. 13.1 and 11.7 cal. kyr BP, respectively, although these were clearer in the IP_{25} and ΣDienes profiles. Both biomarkers were present at their highest concentrations during this interval (Figure 5.7a and Figure 5.7b) suggesting higher frequencies or concentrations of seasonal sea ice. In contrast, both brassicasterol and 24-methylenecholesterol (Figure 5.7c and Figure 5.7d) showed a marked reduction in their concentrations during this period, suggesting that primary productivity was inhibited

during a period of greater sea ice cover. These observations are consistent with a substantial increase of the cold water foraminifera species *Neogloboquadrina pachyderma (s)* (e.g. Bé and Tolderlund, 1971) (Figure 5.9e), a decrease of the subpolar species *Turborotalia quinqueloba* (e.g. Bé and Tolderlund, 1971; Carstens et al., 1997) (Figure 5.9d), low IRD and minimum SST reconstructed from the same core (Aagaard-Sørensen et al., *In prep*) (Figure 5.9c) and the likely prevalence of seasonal sea ice conditions during severe climatic conditions. In contrast, high concurrent bottom water temperatures, as a result of a strong influx of subsurface Atlantic water below a layer of Polar surface water were also observed as shown by an increased dominance of the benthic species *Cassidulina neoteretis* (Aagaard-Sørensen et al., *In prep*) which is often associated with chilled Atlantic waters (e.g. Jennings et al., 2004; Wollenburg et al., 2004). This observation is also seen in a previous study of a nearby location north of the current study (Rasmussen et al., 2007).

Towards the transition between the end of the Younger Dryas stadial and the onset of the Holocene (ca. 12.1 – 11.7 cal. kyr BP), IP_{25} and ΣDienes concentrations decreased sharply (Figure 5.7a and Figure 5.7b), pointing to a shift in the seasonal sea ice conditions from more severe towards lower frequencies of spring sea ice, and this is supported by increasing 24-methylenecholesterol and brassicasterol concentrations (Figure 5.7c and Figure 5.7d). The abrupt decrease in IP_{25} and ΣDienes concentrations also coincided with a rapid increase in SST (from ca. 3 to 6 ˚C; Figure 5.9c) and a depletion in $\delta^{18}O$ (Berben et al., 2013), indicating a surface warming. Such a warming was also reported in previous studies from the Storfjorden Trough (76˚N) (Rasmussen et al., 2007) and over the slope south of Svalbard (75˚N) close to the core site (Sarnthein et al., 2003b). This abrupt transition was also seen in a study by Hald et al. (2007), where a shift from polar foraminifera and cool SST to subpolar fauna and temperatures, similar or warmer than those of the present, was observed across a core

transect (60 – 77˚N). Hald et al. (2007) also noted a more gradual change in both fauna and temperatures in the northernmost locations (where the current study is based, 74.5˚N), which was explained in terms of a higher heat loss to the atmosphere or the existence of colder water conditions due to the influence of the remnants of the last glacial towards the north.

5.5.1.3 Period III: 11.7 – 9.5 cal. kyr BP (early Holocene)

After the abrupt Younger Dryas – early Holocene transition (ca. 11.7 cal. kyr BP), IP_{25} concentrations remained consistently low until ca. 9.5 cal. kyr BP (Figure 5.8a and Figure 5.8a). In contrast to P-I and P-II, where IP_{25} and ΣDienes showed very similar profiles, there appeared to be less consistency during P-III (Figure 5.7a and Figure 5.8b). In contrast to the lower IP_{25} and ΣDienes concentrations, sterols increased towards the end of the Younger Dryas, reaching maxima at ca. 10.7 cal. kyr BP before decreasing slightly up to ca. 9.5 cal. kyr BP (Figure 5.8c and Figure 5.8d). These combined biomarker observations indicate a period characterised by the presence of seasonal sea ice conditions that would have been less severe compared to the Younger Dryas, but would have promoted enhanced primary productivity. Indeed, the presence of IP_{25} and ΣDienes (albeit low concentrations) and relatively high concentrations of both sterols, especially around ca. 10.5 – 11 cal. kyr BP suggests that, during the early Holocene, the study area was probably characterised by periods of sea ice edge conditions or close to the marginal ice zone, since this scenario results generally in enhanced primary production (Smith et al., 1985; Sakshaug, 1997). This conclusion is also supported by relatively high abundances of the benthic species *N. labradorica* (Groot et al., 2013) (Figure 5.9f). Higher productivity in surface waters is also supported by increased relative abundances of the dinoflagellate species *Brigantedinium*

spp (Dylmer, submitted) (Figure 5.9g) although this can also be found in broader environmental settings (e.g. Marret and Zonneveld, 2003).

The initial warming at the Younger Dryas – Holocene transition that was observed in this study (Figure 5.9c) and by Sarnthein et al. (2003b), was succeeded by a short-term cooling interval at ca. 11.2 cal. kyr BP, possibly as a result of a large meltwater input from melting ice-sheets during the Younger Dryas (Bauch et al., 2001). Following this short-term cooling, SST increased again towards the end of P-III. This warm-cold-warm oscillation in P-III was not observed in the IP_{25} record (Figure 5.8a) or the carbon isotope data ($\delta^{13}C$) (Berben et al., 2013) but could also be seen in the oxygen isotope data for the same core ($\delta^{18}O$) (Berben et al., 2013) and in a study from western Svalbard (Rasmussen et al., 2012). Previous studies from several terrestrial and marine records correlated these events with the Pre-Boreal Oscillations of the early Holocene (e.g. Björck et al., 1997; Nesje et al., 2004) and attributed this temperature variability to the final stage of the deglaciation of the Fennoscandian and Svalbard ice sheets (Hald et al., 2007). A widespread cooling in the north Atlantic region around ca. 11.3 cal. kyr BP was suggested to be driven by a meltwater outburst hampering the thermohaline circulation in the north Atlantic (Hald and Hagen, 1998; Husum and Hald, 2002). It is not clear why this change was not observed in the IP_{25} record, although, one possible explanation could be that the sea ice conditions were not favourable for diatom growth.

The Holocene Thermal Maximum has been recorded in many previous studies from the northern North Atlantic area and linked to the increased summer (June) insolation at high latitudes (Koç et al., 1993; Kaufman et al., 2004; Hald et al., 2007). However, the reconstructed summer SST (Figure 5.9c) show a small warming profile after the Younger Dryas and up to ca. 8 cal. kyr BP, remaining relatively stable throughout the rest of the Holocene. As suggested by Andersson et al. (2010) this temperature trend

may simply reflect that temperatures on subsurface waters were stable and only the upper surface layers were affected by maximum insolation. However, reconstructed sSST also reflects the planktic foraminiferal fauna data, with relatively low abundances of *T. quinqueloba* (Figure 5.9d) compared to other studies in the same region (e.g. Sarnthein et al., 2003b; Ebbesen et al., 2007; Hald et al., 2007; Risebrobakken et al., 2010). Nevertheless, the close proximity of the study site to the Arctic Front compared to other studies might have caused the difference in the foraminiferal fauna or might also be ascribed to the state of preservation (Berben et al., 2013).

The declining IP_{25} trend (Figure 5.8a) observed during this period, before disappearing at ca. 9.5 cal. kyr BP, points to a transition from a favourable marginal ice zone scenario to reduced seasonal sea ice conditions and finally open water conditions with increased Atlantic water inflow (Berben et al., 2013), which is consistent with previous observations during this time interval (e.g. Risebrobakken et al., 2010).

5.5.1.4 Period IV: ca. 9.5 – 1.6 cal. kyr BP (mid-late Holocene)

During P-IV, IP_{25} was mainly absent, indicating ice-free conditions during the spring, although some periods of low seasonal sea ice (low IP_{25}) were recorded between ca. 6.5, 5.5 – 4.5 and 3.5 – 2.5 cal. kyr BP (Figure 5.8a). A previous study across the northern north Atlantic of a core transect (60 – 77˚N) revealed cooling in the northern locations (72 – 77˚N) around ca. 7.5, 6.5, 5.5-3, 1 cal. kyr BP (Hald et al., 2007) and these were related to enhanced influence of Arctic waters. At present, the western Barents Sea is characterised by sharp gradients between cold Arctic waters and warm Atlantic waters (Hald et al., 2007). As a result, a large inter-annual variability in sea ice conditions exists around the study area and sea ice can be present, absent or close to the study site (Figure 5.3). Therefore, periods of ice-free or low seasonal sea ice conditions recorded

in this core during P-IV, could be due to small northward or southward movements of the Polar Front relative to the study area. Interestingly, the cooling around ca. 6.5 cal. kyr BP was also recorded in the western Barents Sea (Hald et al., 2007) and was linked to increased tidewater glacier activity on western central Svalbard, deduced from an IRD record in the van Mijenfjorden. Furthermore, a study from northern Norway also showed a cooling around this period (Hald and Aspeli, 1997). However, the very low IP_{25} data might also be attributed to allochthonous input from the Barents shelf. Indeed, a previous study very close to the core site during the Holocene pointed to the existence of lateral sediment transport (Sarnthein et al., 2003b). Evidence for the allochthonous input of IP_{25} into marine sediments around the Bear Island Trough, close to the current study site, has been reported for the first time by Navarro-Rodriguez et al. (2013).

In general, however, stable SSTs were recorded during this period (Figure 5.9c), as well as low biomarker concentration data (Figure 5.8) point to a rather stable period, mostly characterised by increasing influence of Atlantic waters (Risebrobakken et al., 2010; Berben et al., 2013) and open-water conditions, with little or no influence of sea ice (Hald and Aspeli, 1997). This stability in the oceanographic conditions is also reflected by planktic and benthic foraminifera (Berben et al., 2013; Groot et al., 2013) (Figure 5.9d, Figure 5.9e and Figure 5.9f) and dinocyst assemblages (Dylmer, submitted) (Figure 5.9g).

The 8.2 kyr event was a cold spell recorded in Greenland ice cores (e.g. Johnsen et al., 2001) as well as marine (e.g. de Vernal et al., 1997; Wang et al., 1999; Bond et al., 2001) and terrestrial (e.g. Baldini et al., 2002) sediment cores. Unlike many previous studies close to the area under study, where the 8.2 kyr event was also recorded (e.g. Sarnthein et al., 2003b; Hald et al., 2007), the biomarker data for core JM09-KA11-GC did not show a cooling or the presence of sea ice during this period. The reason why this

well-known cold event was not reflected by the biomarker data may be due to the low temporal resolution of the study: there is only one data point available for IP_{25} and ΣDienes and none for sterols biomarkers from ca. 8 – 9 kyr BP (Figure 5.8). However, neither planktic/benthic (Figure 5.9d, Figure 5.9e and Figure 5.9f) (Berben et al., 2013; Groot et al., 2013) foraminiferal fauna nor dinocyst assemblages (Dylmer, submitted) (Figure 5.9g) obtained for the same core showed a cooling at this time interval possibly due also to low temporal resolution.

Further, a general cooling trend from the early to the mid-late Holocene has been recorded at high-latitudes (e.g. Hald and Aspeli, 1997; Ślubowska et al., 2005; Hald et al., 2007; Risebrobakken et al., 2010; Rasmussen et al., 2012). Indeed, stable isotope $\delta^{18}O$ trends based on planktic (Berben et al., 2013) and benthic (Groot et al., 2013) foraminifera showed a slightly decreasing trend from lower to higher isotopic values towards the late Holocene following the decrease in summer (June) insolation at high latitudes (Koç et al., 1993; Hald et al., 2007) . However, this was not reflected in summer sea surface (Figure 5.9c) and bottom temperature reconstructions (Groot et al., 2013), either because the cooling seen was within the error bars of the transfer function, the temperature decrease was too small to affect the foraminiferal assemblages or because the two SST reconstructions correspond to a different seasonal signal (Groot et al., 2013).

An interesting feature about the P-IV concerns the very low brassicasterol concentrations recorded during this interval which, together with low or absent IP_{25} might, according to Müller et al. (2011), indicate permanent sea ice conditions other than open water conditions. However, this could not have been the case for the study area at this time period due to high SST (Figure 5.9c) and high abundances of the planktic foraminifera *T. quinqueloba* (Figure 5.9d). Instead, the low sterol

concentrations (Figure 5.8), presumably reflect lower primary production in general. This is supported further by the low TOC (Figure 5.6b). The stability of the water column in Atlantic waters depends on the formation of a temperature-dependent thermocline and results in a fairly late spring bloom (Sakshaug, 1997). Additionally, late and prolonged phytoplankton blooms in permanently ice-free Atlantic waters would maximise grazing by zooplankton and therefore minimise sedimentation (e.g. Hassel et al., 1991). Therefore, an alternative to permanent ice cover inhibiting primary productivity could be a scenario where by a northward movement of the Polar Front and increased influence of Atlantic waters, could have resulted in a late phytoplankton bloom together with enhanced grazing. This, in turn, could have resulted in low organic matter sedimentation to the seafloor, thus resulting in low occurrences of biomarkers in sediments.

5.5.1.5 Period V: ca. 1.6 – 0 cal. kyr BP (late Holocene)

During the last part of the Holocene (P-V) IP_{25} was absent (or present yet at very low concentrations), while the ΣDienes concentration showed a peak around ca. 0.5 cal. kyr BP (Figure 5.8a and Figure 5.8b). Regarding the sterols, 24-methylenecholesterol was absent or present at very low concentrations (Figure 5.8c). Increasing brassicasterol concentrations towards the present (Figure 5.8d), coincided with an increase of the planktic foraminifera species *Globigerinita uvula* (Berben et al., 2013) which indicates cold-water conditions and high food supply (e.g. Boltovskoy et al., 2000; Bergami et al., 2009). Further, *G. uvula* was found as a dominant species in coastal waters in the south-western Barents Sea, and was also related to slightly reduced salinities (Husum and Hald, 2012). These observations suggested a period characterised by the presence of cold waters and seasonal sea ice as a result of high seasonality, where open-water

conditions would have favoured primary productivity. Similarly, a study located on the west margin of Svalbard by Jernas et al. (2013), also pointed to strong seasonality (spring/summer) during this time period. Furthermore, Groot et al. (2013) also observed more unstable conditions compared to the mid Holocene for the same core (JM09-KA11-GC), with episodes of enhanced productivity.

Currently (ca. last 20 yr), the core site is characterised by rather large year-by-year sea ice variability as shown in Figure 5.3 (with maximum sea ice extent generally observed in March). Therefore, the absence or presence of IP_{25} at very low concentrations and increasing brassicasterol concentrations during the last ca. 1.6 cal. kyr BP could indicate that this area experienced sea ice conditions similar to those of the present day, with alternating periods of ice-free conditions and low occurrences of seasonal sea ice reflected by sea ice being in or close to the core site. Similar conditions have also been observed based on satellite imagery and biomarker reconstructions (Navarro-Rodriguez et al., 2013).

5.5.2 Application of the PIP_{25} index

A P_BIP_{25} profile was obtained for the JM09-KA11-GC core site (Figure 5.7e and Figure 5.10b) by combining the concentrations of the sea ice biomarker IP_{25} with those of the phytoplankton biomarker brassicasterol (B referred to brassicasterol). Furthermore, estimates of spring sea ice concentrations were also made (Figure 5.10e) using the correlation of the PIP_{25} proxy data with sea ice concentrations (%) derived from satellite data by Müller et al. (2011). During P-I P_BIP_{25} values fell within the range ca. 0.2 – 0.7 (Figure 5.10b), suggesting a period of alternating less frequent and seasonal sea ice or stable ice edge conditions, respectively (10 – 60%), and this is supported further by

individual biomarker profiles. During the Younger Dryas (ca. 13.1 – 11.7 cal. kyr BP, P-II) the P_BIP_{25} values were mainly higher (ca. 0.4 – 0.9) with maximum values of ca. 0.9 during the mid-Younger Dryas before sharply decreasing towards the Younger Dryas/Holocene transition (Figure 5.10b). Sea ice concentrations were estimated to be between 50 – 99% (Figure 5.10e) suggesting a period characterised by severe sea ice conditions and lower primary productivity. At the transition between the Younger Dryas and the Holocene (ca. 11.7 cal. kyr BP), lower P_BIP_{25} values compared to the Younger Dryas (ca. 0.3) suggested a shift in the sea ice conditions from more severe to less seasonal sea ice conditions, consistent with the IP_{25} and ΣDienes data (Figure 5.7a and Figure 5.7b). During the early Holocene, P_BIP_{25} values remained low up to ca. 9.5 cal. kyr BP, suggesting less severe sea ice conditions compared to the Younger Dryas with lower sea ice concentrations (1 – 40%). This observation contradicts the suggested marginal ice zone scenario based on individual biomarker data, as well as other proxy data presented for the same core (Figure 5.9), which further confirms the need to consider individual and combined biomarker profiles for sea ice reconstructions (Müller et al., 2011; Belt and Müller, 2013). During the mid-late Holocene the P_BIP_{25} index was predominantly 0, although some positive departures of different P_BIP_{25} values were observed at ca. 6.5 cal. kyr BP (P_BIP_{25} = 0.6), ca. 5.5 – 4.5 and 3.5 – 2.5 cal. kyr BP (P_BIP_{25} = 0.1 – 0.4) suggesting moderate frequencies of seasonal sea ice conditions, and infrequent or less seasonal sea ice conditions, respectively. P_BIP_{25} values of 0 result from the absence of IP_{25} and can indicate either ice-free or permanent sea ice conditions. However, the presence of low IRD (Aagaard-Sørensen et al., *In prep*) as well as SST of ca. 5˚C and high abundances of the sub-polar species *T. quinqueloba* (Figure 5.9d) rejects the latter observation, pointing to ice-free conditions during this period, with alternating low occurrences of seasonal sea ice at ca. 6.5, 5.5 – 4.5 and 3.5 – 2.5 cal. kyr BP. These minor P_BIP_{25} excursions (also observed in the IP_{25} profile)

could also be due to advected material as previously mentioned. Finally, during the last ca. 1.6 cal. kyr BP, the P_BIP_{25} data suggest a period of lower frequencies of seasonal sea ice compared to the early Holocene. Estimated spring sea ice concentration values of 0 – 15% during this period (Figure 5.10e), compare relatively well with satellite-derived sea ice concentrations for this area, with values between 0 – 5% (Navarro-Rodriguez et al., 2013). Interestingly, the distinction of different sea ice conditions during the late Oldest Dryas and Bølling – Allerød periods and the transition between the Younger Dryas and the Holocene was more obvious in the P_BIP_{25} index than in the IP_{25} profile alone.

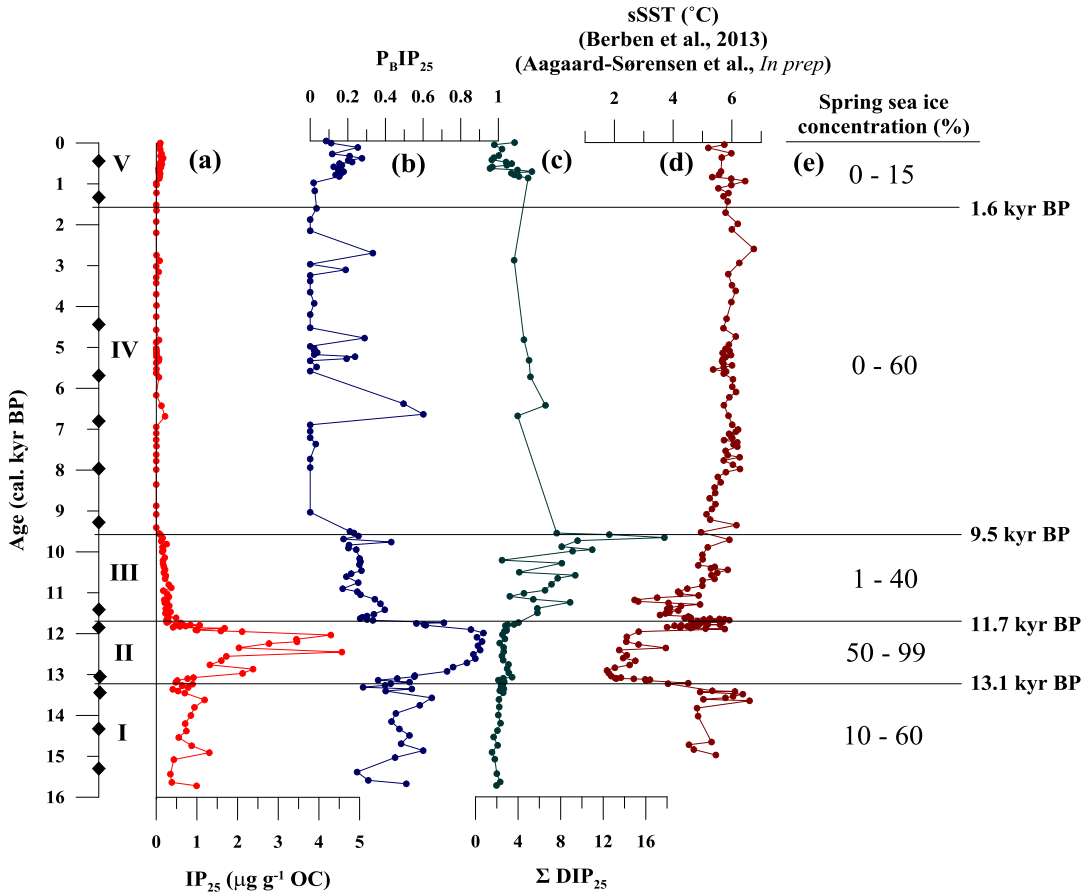

Figure 5.10: Temporal palaeoclimate profiles for the JM09-KA11-GC core: (a) IP_{25}; (b) P_BIP_{25} index; (c) Σ DIP_{25} ratio; (d) Reconstructed summer Sea Surface Temperature (˚C) estimates (Berben et al., 2013; Aagaard-Sørensen et al., *In prep*); (e) Spring sea ice concentration (%) (calculated according to the correlated satellite data with P_BIP_{25} data (Müller et al., 2011)). The horizontal solid lines at ca. 13.1 cal. kyr BP and ca. 11.7 cal. kyr BP indicate the onset and the termination of the Younger Dryas, respectively. The horizontal solid lines at ca. 9.5 cal. kyr BP and ca. 1.6 cal. kyr BP represent shifts in the sea ice conditions during the early-mid and mid-late Holocene boundaries, respectively. The diamonds mark the AMS ^{14}C dates used in the age model.

One potential limitation of the P_BIP_{25} approach, as pointed out by Belt and Müller (2013), concerns the use of the c factor that is used to account for substantial differences in biomarker concentrations. Belt and Müller (2013) suggested that, depending on the section of the core analysed, this c factor could be significantly altered, which could, in turn, affect the PIP_{25} profile and, therefore, the interpretations of the sea ice conditions. The study of this core (JM09-KA11-GC), which covered different time periods with clearly different climatic conditions (e.g. Younger Dryas, Holocene) allowed for a further evaluation of the c factor used in the PIP_{25} calculations. A c factor value of 0.0179 was obtained when taking into account the IP_{25} and brassicasterol values of the entire core (ca. 15.7 – 0 cal. kyr BP), and this c factor yielded the P_BIP_{25} profile presented previously (Figure 5.10b). However, if only the Holocene section (ca. 11.7 – 0 cal. kyr BP) of the core is taken into account, a c factor of 0.0047 is calculated, which is ca. 4 times lower than the one obtained for the whole core. A consequence of this is an increase in all Holocene P_BIP_{25} values compared to the previous P_BIP_{25} profile (data points after ca. 11.7 cal. kyr BP were not taken into account, Figure 5.11c) and different sea ice interpretations. For example, previously the interpretation of P_BIP_{25} values during the mid-late Holocene interval (P-IV) indicated a period of alternating ice-free or less sea ice conditions. However, if only the Holocene section of the core is considered, the P_BIP_{25} indices indicate a period characterised by varying ice-free and seasonal or stable ice edge conditions or even more severe sea ice conditions (Figure 5.11c), which is not consistent with other proxy data. Similarly, if P_BIP_{25} data were based only on values of IP_{25} and brassicasterol for the older part of the core comprising the late Oldest Dryas – Bølling – Allerød/Younger Dryas periods, the c factor becomes ca. twice that obtained when considering the whole core (c factor = 0.0337) with consequential lowering of P_BIP_{25} values (Figure 5.11d) which also influences the interpretation of the sea ice conditions. In addition, if this core extended further back in time, and for

example higher IP_{25} concentrations than those found during the Younger Dryas were recorded, the c factor obtained would be bigger than the c factor obtained for this study. Therefore, the full range of biomarker concentrations needs to be known with confidence (i.e. all available material). Even then, the interpretation of the P_BIP_{25} index should always be carried out alongside other proxy and biomarker data as, pointed out previously (Belt and Müller, 2013; Cabedo-Sanz et al., 2013).

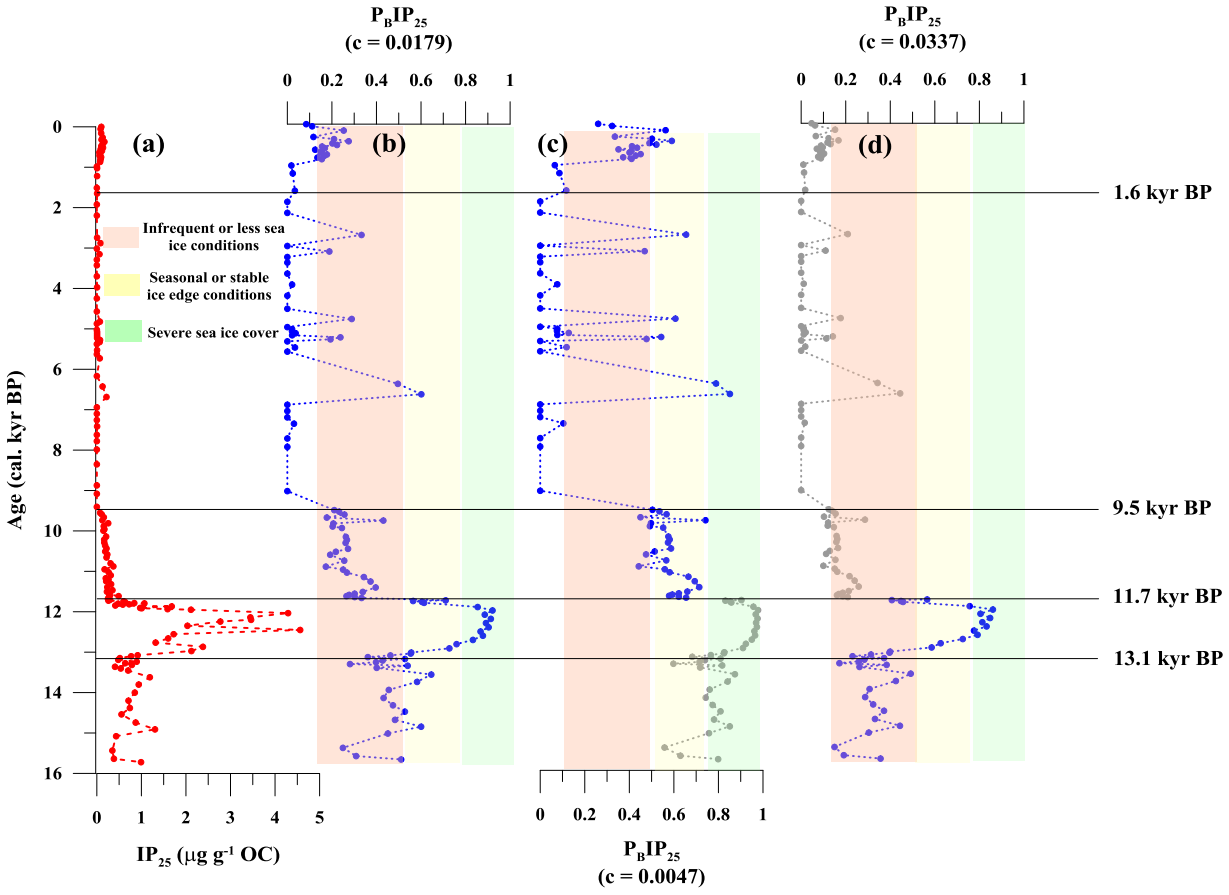

Figure 5.11: (a) Temporal IP_{25} profile; (b) P_BIP_{25} profile obtained by using a c factor (c = 0.0179) that included all IP_{25} and brassicasterol values for the whole studied interval; (c) P_BIP_{25} profile obtained by using a c factor (c = 0.0047) that excluded the late Oldest Dryas – Bølling – Allerød – Younger Dryas IP_{25} and brassicasterol values. (d) P_BIP_{25} profile obtained by using a c factor (c = 0.0337) that excluded the Holocene IP_{25} and brassicasterol values.

5.5.3 Application of the DIP_{25} ratio

Regarding the use of the DIP_{25} index (described in Chapter 4) and in order to expand upon this initial investigation, relative abundances of IP_{25} and ΣDienes obtained for the JM09-KA11-GC core were used to calculate ΣDIP_{25} ratios. (Note: when IP_{25} was absent, e.g. between ca. 9.5 – 1.6 cal. Kyr BP, the ΣDIP_{25} ratio could not be calculated). Further, linear correlations between both biomarkers were calculated for each period (Figure 5.12). During P-I and P-II, ΣDIP_{25} values were fairly constant compared to the rest of the core (Figure 5.10c), supported by strong linear correlations between the two biomarkers (Figure 5.12e). In contrast, a weaker linear correlation was observed between IP_{25} and ΣDienes during P-III (Figure 5.12c) as shown by highly variable ΣDIP_{25} values (Figure 5.10c). Indeed, the weakest linear correlation between both biomarkers for the entire studied period was observed in P-III, possibly suggesting a period characterised by highly variable or unstable sea ice conditions, coinciding with a rapid warm-cold-warm oscillation recorded in this core and associated to meltwater events and found in other studies (e.g. Nesje et al., 2004; Hald et al., 2007). Interestingly, a significant change in ΣDIP_{25} values at the transition between the Younger Dryas and Holocene (ca. 11.7 – 9.5 cal. kyr BP; Figure 5.10c) coincided with a change in the sea ice conditions (inferred by individual biomarker and proxy data) from more stable (and severe) to more variable (and less frequent) seasonal sea ice conditions, respectively. This observation further supports the previous suggestion that transitions to/from consistent ΣDIP_{25} values could indicate major changes to the sea ice regime (Chapter 4). For P-IV, IP_{25} was mostly absent and this prevented an adequate assessment of the ΣDIP_{25} ratio and potential correlation for this interval (Figure 5.12b). Nevertheless, stable SST (Figure 5.10d), TOC, biomarker and proxy data suggests a period of relatively stable (and mild) climatic conditions. During P-V, the ΣDIP_{25} ratio

was relatively variable showing a weaker IP_{25} – ΣDienes linear correlation (Figure 5.12a) compared to P-I and P-II (although stronger compared to P-III), suggesting a period characterised by some variability in the sea ice conditions although to a lesser extent than during P-III. This is also reflected by (estimated) calculated spring sea ice concentration ranges for the two intervals (Figure 5.10e; P-III: 1 – 40%, P-V: 0 – 15%). An alternative to the explanations for changes to the ΣDIP_{25} ratio described above may potentially be found in the analytical measurement. In particular, the reliability of the measurement of ΣDienes, given their chromatographic co-eluting (Figure 5.5). For example, intervals where the two biomarkers are more poorly correlated may simply reflect the challenges associated with accurately measuring the $C_{25:2}$. However, the strong correlation observed at least in two intervals (Figure 5.12d and Figure 5.12e), suggests that this is not always a major factor, if ever.

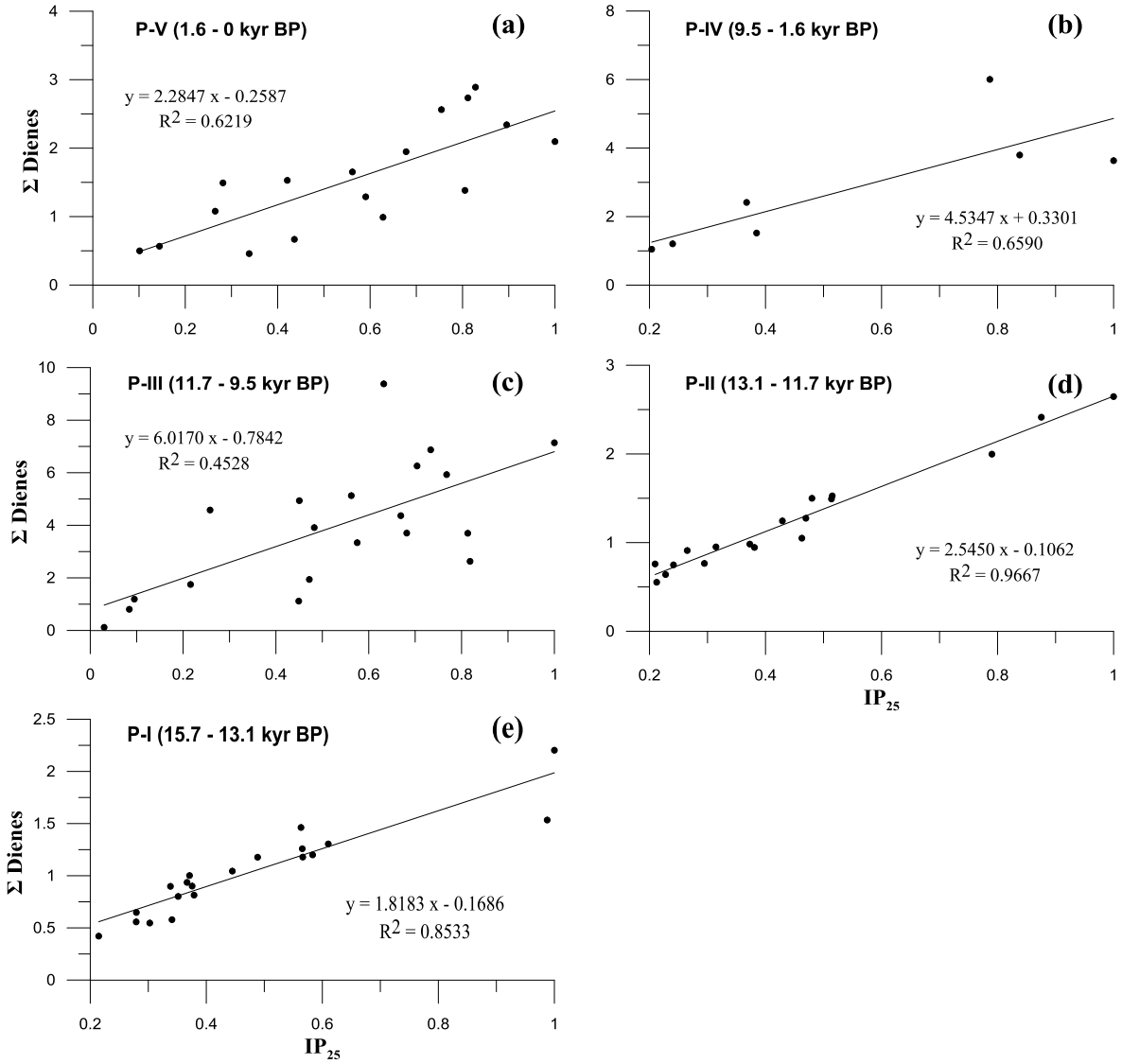

Figure 5.12: Relative abundances of ΣDienes *vs* IP_{25} for the JM09-KA11-GC core during different time intervals: (a) ca. 1.6 – 0 cal. kyr BP (17 sediment samples); (b) ca. 9.5 – 1.6 cal. kyr BP (7 sediment samples); (c) ca. 11.7 – 9.5 cal. kyr BP (20 sediment samples); (d) ca. 13.1 – 11.7 cal. kyr BP (18 sediment samples); (e) ca. 15.7 – 13.1 cal. kyr BP (20 sediment samples). Relative abundances were normalised to the maximum values of IP_{25} observed for each dataset.

In addition to ΣDIP_{25} values obtained from relative abundances (manual peak integrations of SIM chromatograms) of both biomarkers (Figure 5.10c and red dotted line in Figure 5.13) the ΣDIP_{25} ratio was also calculated from ΣDienes and IP_{25} concentrations (black dotted line in Figure 5.13). Biomarker concentrations include factors such as the response factor between the internal standard and the biomarker and the sediment mass. Regarding ΣDienes concentrations, these included the response

factor between the internal standard (9-OHD) and diene II (Chapter 3), but the unknown response factors for the other two $C_{25:2}$ overlapped with diene II (Figure 5.5) are not considered. Both ΣDIP_{25} profiles (derived from abundances and concentrations) showed a relatively similar trend (Figure 5.13), although ΣDIP_{25} values were higher when obtained from concentrations, indicating that the response factor of the other two $C_{25:2}$ HBIs did have an effect on the calculation of the ΣDIP_{25} ratio. Indeed when subtracting ΣDIP_{25} values obtained from biomarker concentrations from those obtained from relative abundances (blue line in Figure 5.13) fairly constant DIP_{25} values were observed from ca. 15.7 to 12 cal. kyr BP, after which ΣDIP_{25} values increased but also remained stable up to ca. 9.5 cal. kyr BP. This observation further suggested that challenges associated with the correct measurement of $C_{25:2}$ were not a major factor and that both approaches can provide similar outcomes.

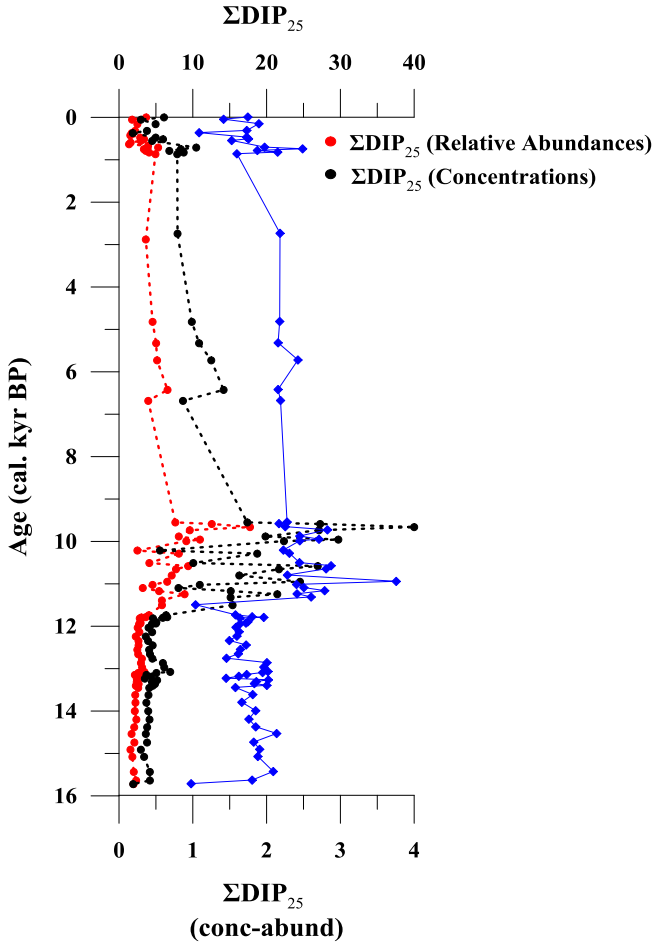

Figure 5.13: Red dotted line represents the ΣDIP_{25} ratio (top axis) calculated based on relative abundances of ΣDienes and IP_{25}. Black dotted line represents the ΣDIP_{25} ratio (top axis) calculated based on ΣDienes and IP_{25} concentrations. Blue line indicates ΣDIP_{25} values (bottom axis) obtained when subtracting ΣDIP_{25} ratio calculated based on concentrations from that based on relative abundances.

5.6 Conclusions

Five distinct periods of varying palaeoceanographic conditions have been identified in the Kveithola Trough during the last ca. 15.7 cal. kyr BP based on a multi proxy approach. P-I covers the late part of the Oldest Dryas and the Bølling – Allerød interstadials (ca. 15.7 – 13.1 cal. kyr BP). The presence of seasonal sea ice throughout the whole period, as inferred by the presence of IP_{25}, was observed. During the Bølling – Allerød ice edge conditions and enhanced primary productivity probably dominated in the study area. P-II comprises the Younger Dryas (ca. 13.1 – 11.7 cal. kyr BP) characterised by low primary productivity as a result of seasonal sea ice conditions

during severe climatic conditions. A shift in the IP_{25} concentrations from higher to lower represented a change in the sea ice conditions at the Younger Dryas – early Holocene boundary. P-III includes the early Holocene (ca. 11.7 – 9.5 cal. kyr BP) characterised with less severe seasonal sea ice conditions compared to the Younger Dryas. High sterol concentrations together with high abundances of *N. labradorica* and *Brigantedinium spp.* suggest enhanced primary productivity and sea ice edge conditions at, or in close proximity to, the core site. P-IV included the mid-late Holocene (ca. 9.5 – 1.6 cal. kyr BP) which was characterised by predominantly ice-free and rather stable climatic conditions as suggested by all the proxy data (e.g. SST, benthic and planktic foraminifera, dinocysts). Low brassicasterol concentrations and low TOC data during this interval also suggested a northward movement of the Polar Front and increased Atlantic water influence. During P-V (ca. 1.6 – 0 cal. kyr BP) low or absent IP_{25}, increasing brassicasterol concentrations and increasing abundance of *G. uvula* indicates the presence of cold waters and sea ice conditions similar to those of the present day. In general, the good agreement between all biomarker and proxy data presented for the JM09-KA11-GC core further shows the advantage of using a multi-proxy approach for palaeo sea ice reconstructions.

Further, the use of the PIP_{25} index provided estimates of sea ice concentrations derived from satellite data and additional information regarding sea ice conditions. The ΣDIP_{25} ratio also allowed to further characterise sea ice conditions. For example, high sea ice concentrations and more stable sea ice conditions were found during the Younger Dryas (P-II; 50 – 99%) compared to other intervals such as the early Holocene (P-III; 1 – 40%) or late Holocene (P-V; 0 – 15%), with less and more variable sea ice conditions. The use of a c factor in the PIP_{25} index has also been shown to greatly influence the interpretation of the sea ice conditions, being a potential limitation of this approach.

CHAPTER SIX

6 Results (3): Environmental and drift ice conditions in south-east Greenland: from recent to ancient sediments.

6.1 Introduction

Sea ice in the Arctic has undergone dramatic changes in recent years, with significant thinning and reduction of total area (e.g. Polyak et al., 2010). In 2012, the summer sea ice loss was at its largest for the 34-year satellite record (Schiermeier, 2012). At the same time, there has been an increased loss of mass from the Greenland Ice Sheet (GIS) (e.g. Hanna et al., 2008; Rignot et al., 2008; Van de Wal et al., 2008). Many studies since the 1970s have aimed to study the variability in climatic conditions and evaluate their impact on future climate (e.g. Caseldine et al., 2010; Polyak et al., 2010). The East Greenland Shelf is a very sensitive area to changes in sea ice and freshwater outflow from the Arctic Ocean (e.g. Jennings and Weiner, 1996). The East Greenland Current (EGC), which flows adjacent to the east Greenland shelf, is one of the main sea ice and freshwater export pathways from the Arctic Ocean (Aagaard and Coachman, 1968). Denmark Strait (Figure 6.1) represents a particularly sensitive area for palaeoceanographic and palaeoclimatic studies since it corresponds to where the cold and low-saline EGC meets the warm Irminger Current (IC) to form the oceanic Polar Front (e.g. Andrews et al., 1998; Andresen and Björck, 2005). Previous palaeoclimatic and palaeoceanographic studies have focused on different time-scales, such as the Holocene (e.g. Jennings and Weiner, 1996; Jennings et al., 2002b; Andersen et al., 2004a; Solignac et al., 2006; Andrews et al., 2010; Jennings et al., 2011), the Younger Dryas (e.g. Jennings et al., 2006) and older (e.g. Andrews et al., 1998).

This chapter describes a further investigation into this sensitive region and is divided into two parts. The main aim of the first part of the chapter (Part A) was to carry out a multi-proxy based study of three short gravity cores from the outer Kangerdlugssuaq Trough, within Denmark Strait, south-east Greenland (PO175GKC cores; Figure 6.1). These cores span the last ca. 150 yr, presenting the opportunity to study recent oceanographic changes through comparison of compiled proxy data. Comparisons are made between a variety of mineralogical determinations and biomarker analyses and these are further compared to historical and instrumental data. The outcomes presented provide a better understanding of the ice sheet-ocean interactions in the Denmark Strait area in recent times. These outcomes, in turn, provided an opportunity to develop a model from which longer term palaeoceanographic reconstructions could be tested. Thus, the second part of this chapter (Part B) was based on a multi-proxy based study of a sediment core, also located within the Kangerdlugssuaq Trough (JM96-1213), over an extended timescale (ca. 16.3 – 10.9 cal. kyr BP). The aims of Part B of the chapter were 1) to test the model provided in Part A for longer term palaeoceanographic reconstructions in the same study area, 2) to enable modifications of the model to be made (where needed) and finally, 3) to elucidate the palaeoclimatic conditions in the Kangerdlugssuaq Trough during the studied interval.

6.2 Regional setting

The two main currents that characterise the Denmark Strait area are the East Greenland Current (EGC) and the Irminger Current (IC) (Figure 6.1 and Figure 6.2). The EGC is a cold, low-salinity polar water current that flows southward from the Arctic Ocean as an extension of the Trans-Polar Drift (TPD) (Figure 6.2) along the Greenland margin carrying sea ice and freshwater from the Arctic Ocean. Freshwater and icebergs discharged from the Greenland Ice Sheet (GIS) are incorporated to the EGC as it flows southwards (Aagaard and Coachman, 1968; Rudels et al., 2002). The IC is a branch of the North Atlantic Current (NAC) that flows northward, carrying warm and saline Atlantic waters from the south (Figure 6.1 and Figure 6.2). The IC splits close to Denmark Strait; one branch flows northwards and clockwise along the west Iceland shelf and another is directed southwards and counter clockwise along south-east Greenland, entering the Kangerdlugssuaq Trough as an intermediate layer between the polar water and the Atlantic intermediate water of the EGC (e.g. Jennings et al., 2011). Rudels et al. (2002) showed that most of the Denmark Strait Overflow Water is carried by the EGC and that the rest is derived from the Iceland Sea. Changes in the extent of the IC have been linked to phases of the North Atlantic Oscillation (NAO) (Hurrell et al., 2003) where, in general, positive (negative) NAO result in reduced (increased) IC flow (e.g. Myers et al., 2007).

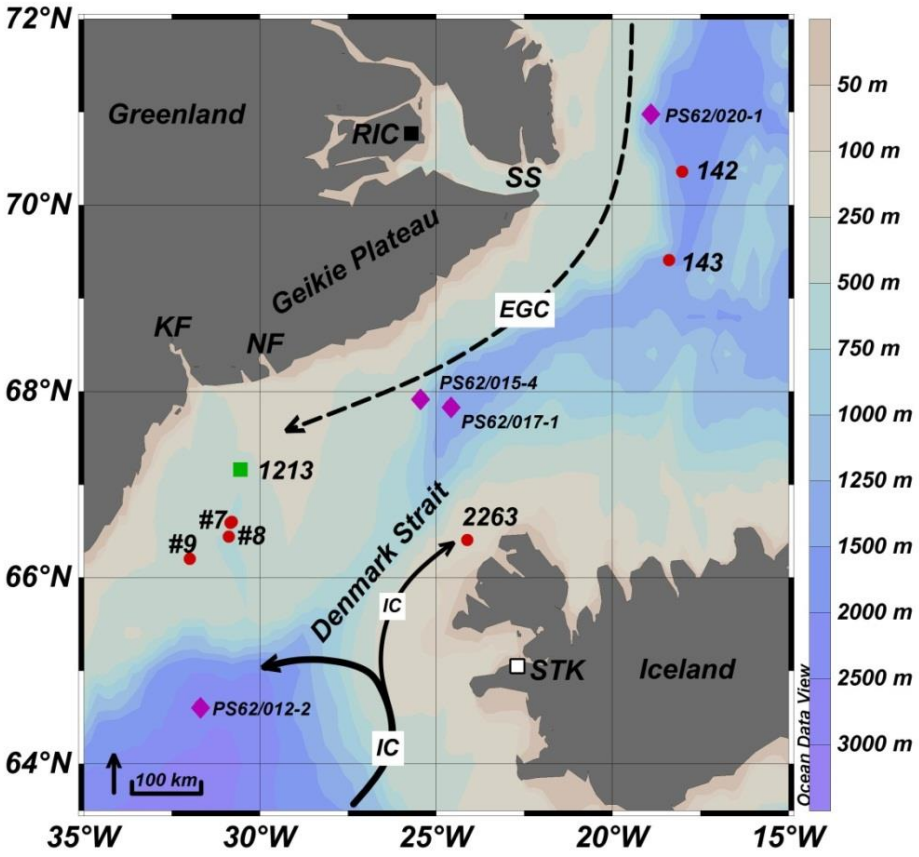

Figure 6.1: Location map showing the cores under study: PO175GKC#7, #8, #9 and JM96-1213. Other locations mentioned in this chapter are: HH11-142/143; MD99-2263. Core sites studied by Müller et al. (2011) and mentioned in this chapter are: PS62/020-1; PS62/015-4; PS62/017-1 and PS62/012-2. Main surface water currents are the cold East Greenland Current (EGC) carried southwards along the east coast of Greenland and the relatively warm Irminger Current (IC), a branch of the north Atlantic current that flows northward carrying Atlantic waters. Rendland Ice Cap (RIC), Scoresby Sund Fjord (SS), Kangerdlugssuaq Fjord (KF), Nansen Fjord (NF), Stykkisholmur (STK).

Kangerdlugssuaq Trough, where the study is based (PO175GKC and JM96-1213 cores), is formed as a continuation of the Kangerdlugssuaq Fjord onto the continental shelf (Figure 6.1). Kangerdlugssuaq Fjord is a large fjord that drains Kangerdlugssuaq glacier, one of the main outlets of the GIS (Luckman et al., 2006), that maintains a *sikkusaq*, a mélange of sea ice and icebergs at the tidewater terminus (Dwyer, 1995). Estimated fluxes of iceberg calving across the Kangerdlugssuaq Trough are in the range of 30 – 100 km^3 yr^{-1} (Bigg, 1999). Calving rates of 18 km^3 yr^{-1} were estimated during the 1990s (Andrews et al., 1994). Kangerdlugssuaq Trough and Fjord are directly

influenced by modified intermediate Atlantic water linked with inflow of waters from the IC (Syvitski et al., 1996; Jennings et al., 2006). The trough reaches the shelf edge at 450 m water depth. Additionally, 19 tidewater glaciers descend to sea level from the Geikie Plateau (Nuttall, 1993) and several large tidewater glaciers contribute icebergs into the fjords that lead into Scoresby Sound (e.g. Seale et al., 2011).

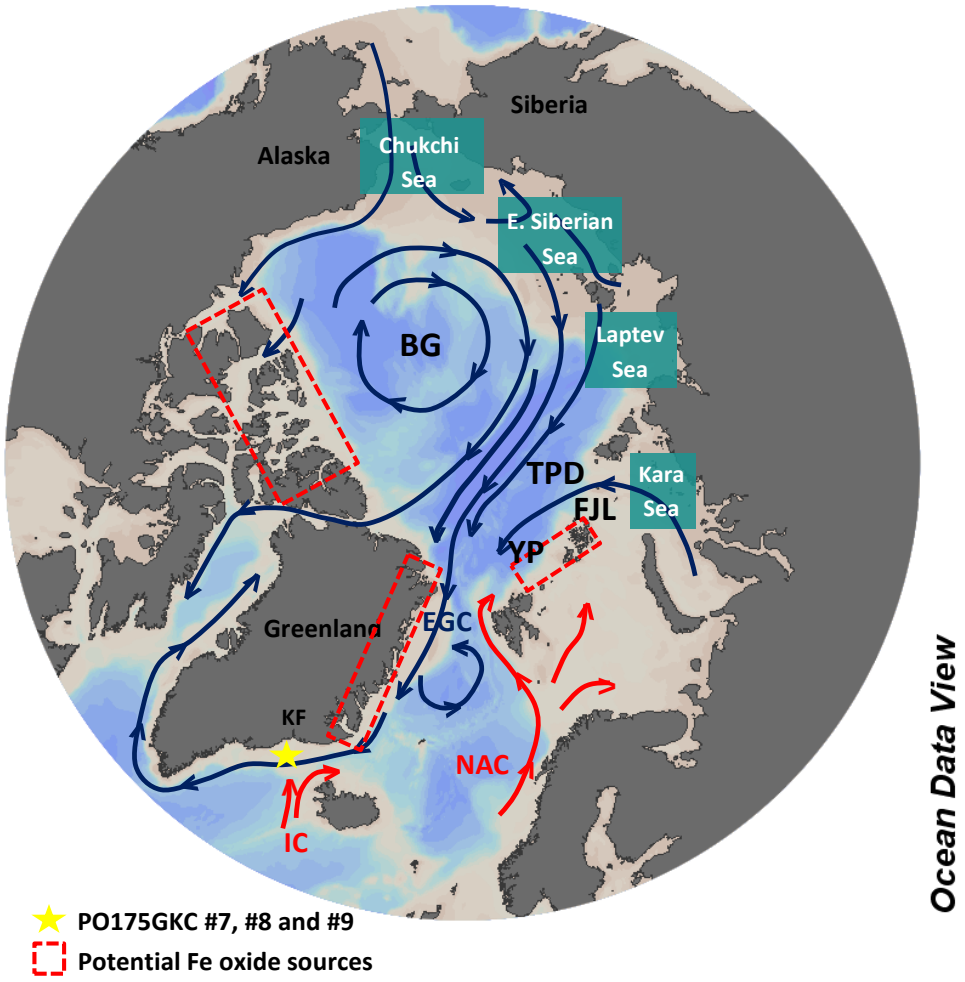

Figure 6.2: Simplified map showing the main Arctic Ocean circulation pattern and the potential Fe oxide sources (red dotted squares) that reached the study area (yellow star). East Greenland Current (EGC), Irminger Current (IC), North Atlantic Ocean (NAC), Beaufort Gyre (BG), Transpolar Drift (TPD), Yermak Plateau (YP), Franz Josef Land (FJL), Kangerdlugssuaq Fjord (KF).

Sea ice forms in the fjords and the coast of east Greenland as landfast ice, which contrasts with the belt of drifting sea ice from the Arctic Ocean along the east coast of Greenland via Fram Strait (Schmith and Hansen, 2003; Rogers et al., 2005) (Figure 6.4). The movement of icebergs onto the shelf is restricted by the presence of sea ice. In severe years, the presence of a perennial sea ice cover impedes iceberg calving from glaciers (Reeh et al., 1999; Reeh et al., 2001; Reeh, 2004). Inspection of Danish Meteorological Institute sea ice charts from 2000 to 2009 by Jennings et al. (2011) indicated 6.5 – 8.5 months of sea ice cover around core site JM96-1213 with ice-free conditions beginning in July/August and new ice cover re-established by late October to late December. Similarly, examination of sea ice charts from the US National Ice Center from 2000 to 2011 in this study indicates around 7 months of sea ice cover at site PO175GKC, with ice-free conditions starting in July or August and newly-formed sea ice during January. An example of current sea ice conditions is shown in Figure 6.3, which shows the sea ice extent (in tenths) during March and August in 2000. During March 2000, the whole study area was covered by sea ice, with higher concentrations of sea ice found close to land. In the summer (August 2000) a reduced sea ice cover was observed, especially along the Kangerdlugssuaq Trough, due, in part, to the inflow of Atlantic waters.

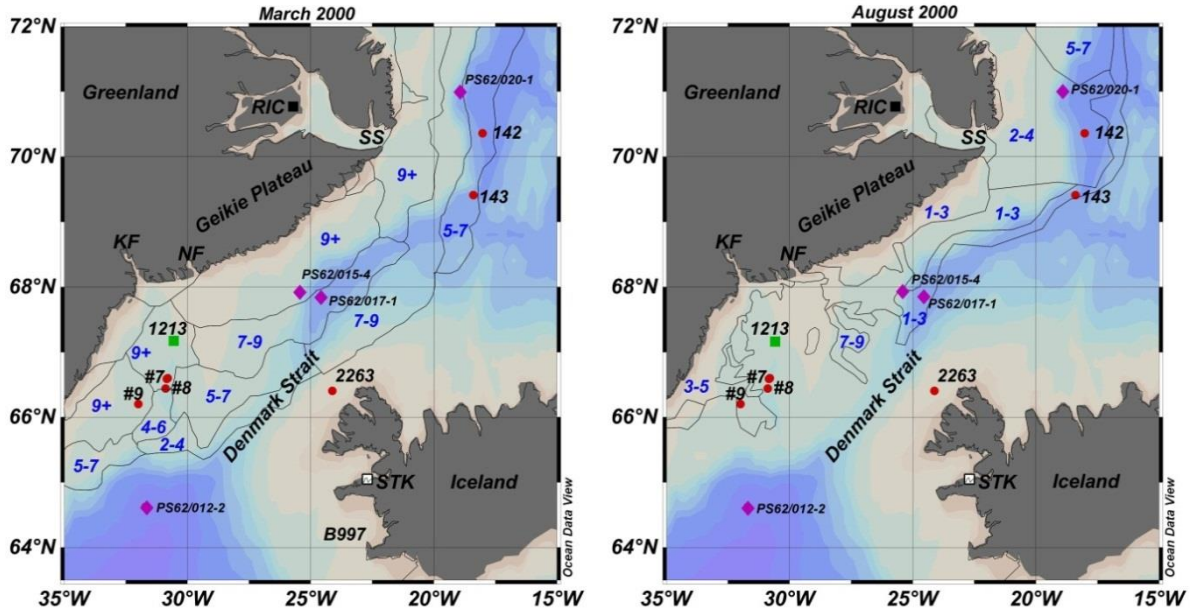

Figure 6.3: Total concentration of sea ice in the area in tenths during March and August AD 2000, according to the U.S. National Ice Center. The reduced summer sea ice cover along the Kangerdlugssuaq Trough is due, in part, to the inflow of Atlantic water. Locations mentioned in this chapter are also shown. Rendland Ice Cap (RIC), Scoresby Sund Fjord (SS), Kangerdlugssuaq Fjord (KF), Nansen Fjord (NF), Stykkisholmur (STK)

An image taken by the Moderate Resolution Imaging Spectroradiometer (MODIS) on NASA's Aqua satellite shows the modern sea ice conditions (27th March 2010) along the south-east coast of Greenland (Figure 6.4a). Drift ice is multiyear ice carried southwards as sea ice or icebergs from the Arctic Ocean by the EGC following the east coast of Greenland. A magnified image of the study area (Figure 6.4b) shows clearly that this area is characterised by two well-delimited sea ice types; landfast sea ice formed along the east coast of Greenland and sea ice drifting from further north.

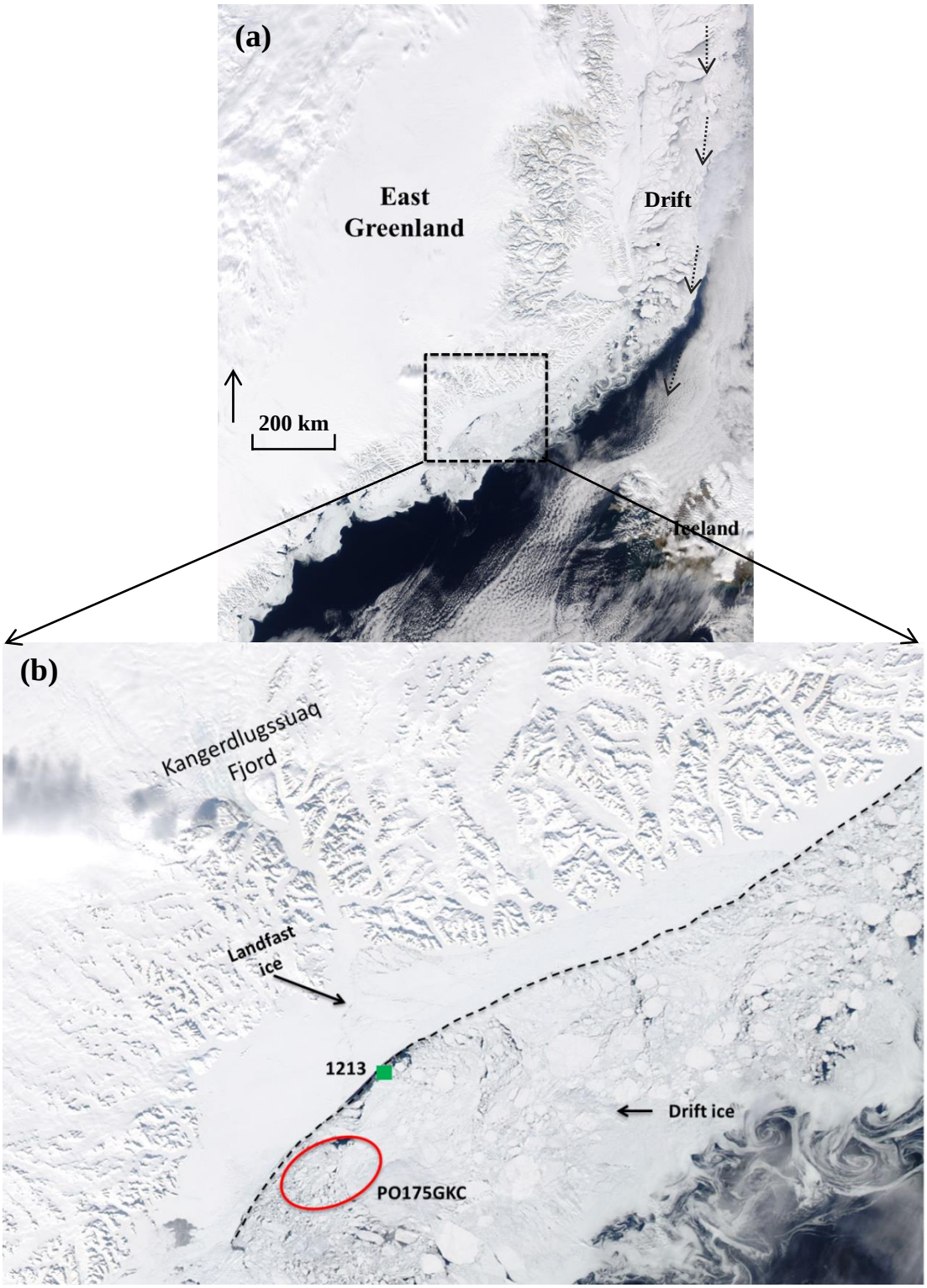

Figure 6.4: (a) Moderate Resolution Imaging Spectroradiometer (MODIS) image of the south-east coast of Greenland sea ice cover, 27th March 2010, indicating land fast ice and the predominant southward transit of drift ice along the east coast of Greenland; (b) Magnified image of the study area. The red circle represents the region where the short cores (PO175GKC) were taken.

6.3 Historical data

Extensive instrumental and observational records of sea ice conditions and air temperatures are available for both the Greenland and Iceland side of Denmark Strait.

In addition, historical observations of "storis" (Figure 6.5b), which is multiyear ice from the Arctic Ocean that is advected to south-west Greenland by the EGC exist from 1820 (Schmith and Hansen, 2003). Observational sea ice data from Iceland goes even further back in time (ca. 1000 yr) (Koch, 1945; Björnsson, 1969) and several studies have attempted to reconstruct the climate in the last few centuries on a more solid historical basis (Ogilvie et al., 2000; Ogilvie and Jónsdóttir, 2000; Ogilvie and Jónsson, 2001). Thus, the Koch index represents the sea ice extent observed near the coasts of Iceland (Koch, 1945) and a revised version of the Koch index of sea ice cover (Figure 6.5b) has been carried out by Wallevik and Sigurjonsson (1998).

Air temperatures at Stykkisholmur (west Iceland) and Angmagssalik (south-east Greenland) are very well correlated (Figure 6.5a), although the Iceland record extends further back in time. Significantly, both records show variability during the last century. For example, a marked increase in Mean Annual Temperature (MAT) occurs on both sides of the Denmark Strait (Figure 6.5a) at ca. AD 1920, peaking at ca. AD 1940 before decreasing up to ca. AD 1970. The minimum in MAT at ca. AD 1970, has been associated with the Great Salinity Anomaly (Dickson et al., 1988; Belkin et al., 1998). As expected, the MAT record for East Greenland (as well as Iceland) shows an inverse correlation to that of the storis record (Figure 6.5). Thus, higher temperatures coincided with less multiyear ice exported from the Arctic Ocean and viceversa. The main historical observations during the studied interval are heavy ice years between AD 1860 – 1920 (e.g. Gray, 1881), less ice after AD 1920, with some "ice years" excursions between AD 1960 – 1970 (Figure 6.5). The variability of temperatures and drift ice has

also been related to variations in both the NAO (Figure 6.9f) and Arctic Oscillation (AO) indices (Thompson and Wallace, 1998; Wang and Ikeda, 2000; Hurrell et al., 2003; Darby and Bischof, 2004; Hanna et al., 2004).

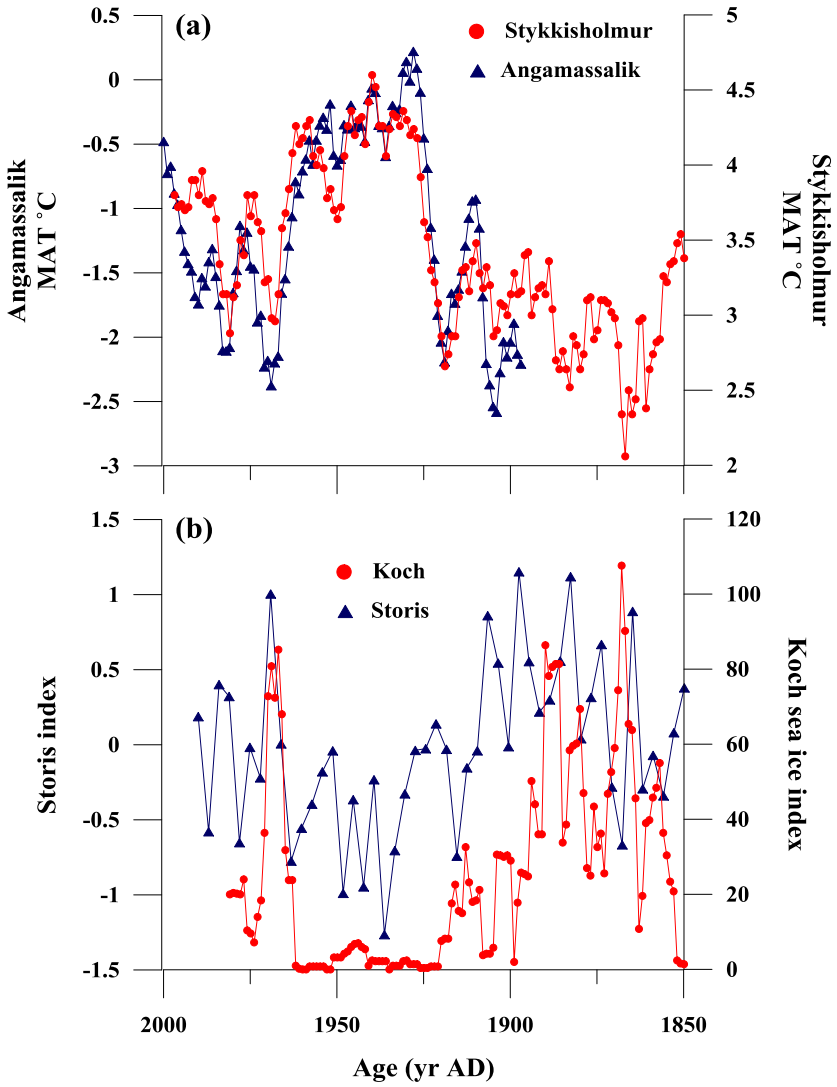

Figure 6.5: (a) Mean annual temperature (MAT) at Stykkisholmur, west Iceland (red line),and Angamassalik, south-east Greenland (red line); (b) Indices of sea ice off south-west Greenland and in Iceland waters. The red line represents the revised Koch sea ice index (Wallevik and Sigurjonsson, 1998) and the blue line corresponds to the storis index (Schmith and Hansen, 2003).

6.4 Part A: Recent sediments: last ca. 150 yr

6.4.1 Material and methods

6.4.1.1 Field methods and chronology

The short gravity core PO175GKC#9 (hereafter GKC#9) which represents the main focus of this study, was retrieved from the margin of the Kangerdlugssuaq Trough, (66.2˚N, 32.0˚W; water depth 313 m; core length 20 cm; Figure 6.1) on board the German research vessel *Posseidon* in 1990. Two other short gravity cores, PO175GKC#7 (hereafter GKC#7; 66.6˚N, 30.8˚W; water depth 325 m; core length 20 cm; Figure 6.1) and PO175GKC#8 (hereafter GKC#8; 66.4˚N, 30.9˚W; water depth 300 m; core length 20 cm; Figure 6.1) were obtained during the same cruise. The cores were stored (vertically and refrigerated; 4˚C) at the Institute of Arctic and Alpine Research (INSTAAR), and were sampled at 1 cm intervals in 2011 and kept in the freezer (-20˚C) prior to analysis. Surface sediment material from two multicores offshore East Greenland and further north than the GKC cores were collected in 2011 (HH11-142, 70.36˚N, 18.02˚W; water depth 1689 m and HH11-143, 69.41˚N, 18.39˚W; water depth 1332 m) aboard the RV *Helmer Hanssen* as part of the Changing Arctic and sub-Arctic Environment (CASE) International Training Network research project. Surface sediment material from each multicore was stored frozen (-20ºC) prior to freeze drying and analysis in the laboratory.

An age model for GKC#9 core was developed using ^{210}Pb and ^{137}Cs radioisotopes (Alonso-Garcia et al., 2013). A core top age of 1990 cal. yr AD was assumed and a mean linear sedimentation rate of 0.14 cm yr^{-1} was obtained. The chronology obtained for GKC#9 was then expanded to the two adjacent cores (GKC#7 and GKC#8) based on correlations between calcite wt% records. The calcite wt% showed a similar pattern

in GKC#8 and GKC#9, while GKC#7 was rather different (Alonso-Garcia et al., 2013). Therefore, GKC#8 and GKC#9 records span the interval from AD 1990 to ca. 1850, with a sampling interval of ca. 7 yr cm^{-1} and GKC#7 covers the period from AD 1998 – 1945.

6.4.1.2 Experimental

Analysis of the IP_{25}, diene II and sterol biomarkers (24-methylenecholesterol and brassicasterol) was performed using methods described in Chapter 2.

Regarding analysis of the GKC cores specifically, and due to the low abundances of all biomarkers, extractions were performed on 5 g of dried sediment which required a corresponding scaling adjustment of the solvent volumes and chromatographic conditions. A complete description of the experimental procedure shown in Figure 6.6 is given in Chapter 2.

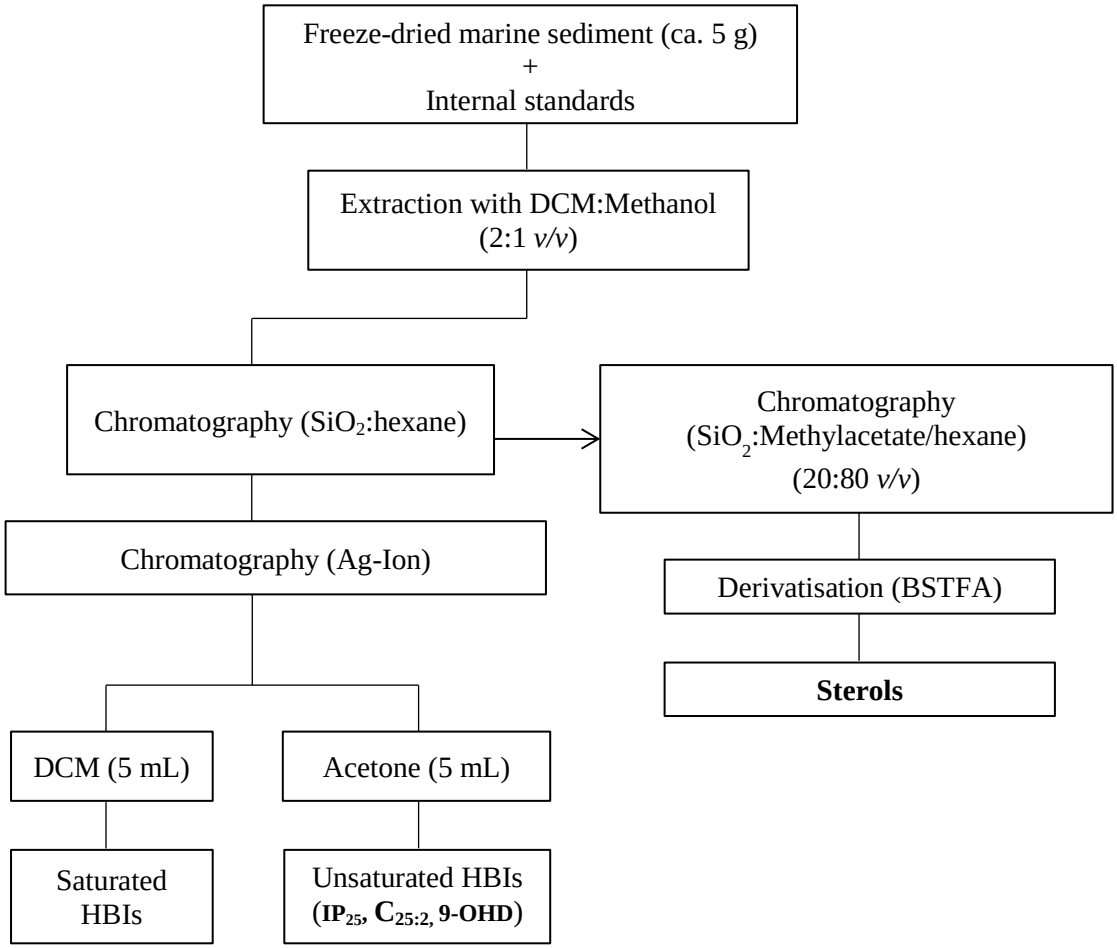

Figure 6.6: Sample extraction flow diagram for lipid biomarkers.

Briefly, three internal standards were added to each freeze-dried sediment sample (ca. 5 g) to permit quantification. 7-hexylnonadecane (7-HND, 10 µL; 10 µg mL^{-1}) and 9-octylheptadec-8-ene (9-OHD, 10 µL; 10 µg mL^{-1}) were added for quantification of IP_{25} and diene II while 5α-androstan-3β-ol (10 µL; 10 µg mL^{-1}) was added for quantification of sterols. Samples were then extracted using DCM/methanol (3 x 15 mL; 2:1 *v/v*) and ultrasonication. Following removal of the solvent (N_2), the resulting total organic extracts (TOE) were purified using column chromatography (SiO_2; 2 silica columns were used for each sample), with IP_{25} (hexane; 6 mL) and sterols (20:80 methylacetate/hexane; 6 mL) collected as two separate fractions. Since the concentration of IP_{25} was generally very low and identification and quantification was often difficult due to the abundance of other hydrocarbons, hexane extracts were further fractionated into saturated and unsaturated components using glass pipettes containing Ag-Ion stationary phase (Supelco discovery® Ag-Ion). Ag-Ion columns were first conditioned (5 column volumes acetone, then 5 column volumes DCM) before addition of partially purified hexane extracts in DCM (100 µL). Elution of saturated and unsaturated hydrocarbons (including IP_{25}) was achieved with DCM (5 column volumes) and acetone (5 column volumes), respectively. Analysis of each fraction was carried out using GC-MS (Chapter 2). Sterols were derivatised (BSTFA; 50 µL; 70°C; 1h) prior to analysis by GC-MS. Analytical reproducibility was determined using a standard sediment with known abundances of biomarkers (± 7%).

Additional biomarker data of surface sediments was obtained from two multicores (HH11-142 and 143) and from a box core collected from north-west Iceland (Andrews et al., 2009) (MD99-2263; Figure 6.1).

Total organic carbon (TOC) of the sediment horizons were determined by Andrew Tonkin (Plymouth University) using ca. 10-20 mg of sediment and a LECO 900 CHN

analyser. Inorganic carbonates were removed with hydrochloric acid (10%; 1 mL) (Belt et al., 2010). Acetanilide was used as a calibration standard.

6.4.2 Results

A total of 20 downcore sediment samples (1 cm resolution) for each of GKC#8 and GKC#9 cores in addition to 2 sediment samples from core GKC#7 were analysed for the sea ice biomarker IP_{25}, a structurally related HBI diene II and the sterols 24-methylcholesta-5,22E-dien-3β-ol (brassicasterol) and 24-methylcholesta-5,24(28)-dien-3β-ol (24-methylenecholesterol).

IP_{25} was identified in 10 out of 20 samples in GKC#9 and in all but 1 sediment sample in GKC#8. It was also found in the 2 samples from GKC#7. The temporal abundance profiles of IP_{25} (TOC normalised) were similar for GKC#9 and GKC#8 although concentrations were slightly higher in the latter (Figure 6.7a), probably reflecting slightly different burial efficiencies between the two core sites. For both GKC#9 and GKC#8, IP_{25} was absent (or below the limit of detection: 0.03 ng g^{-1} dry sed) and concentrations were at their minimum values from ca. AD 1850 – 1910, respectively, before increasing to ca. AD 1990. In GKC#7, IP_{25} concentrations were very low (ca. 50 – 100 ng g^{-1}OC; Table 6.1). Similar temporal profiles were observed for diene II in both GKC#9 and GKC#8 cores (Figure 6.7b), consistent with this lipid being co-produced by Arctic sea ice diatoms (e.g. Belt et al., 2007; Vare et al., 2009; Cabedo-Sanz et al., 2013). Despite these relative temporal abundance changes, however, absolute concentrations of both biomarkers were extremely low, especially when compared with those found for locations slightly further north of GKC#9 and GKC#8 along the east Greenland margin and from north-west Iceland (Table 6.1).

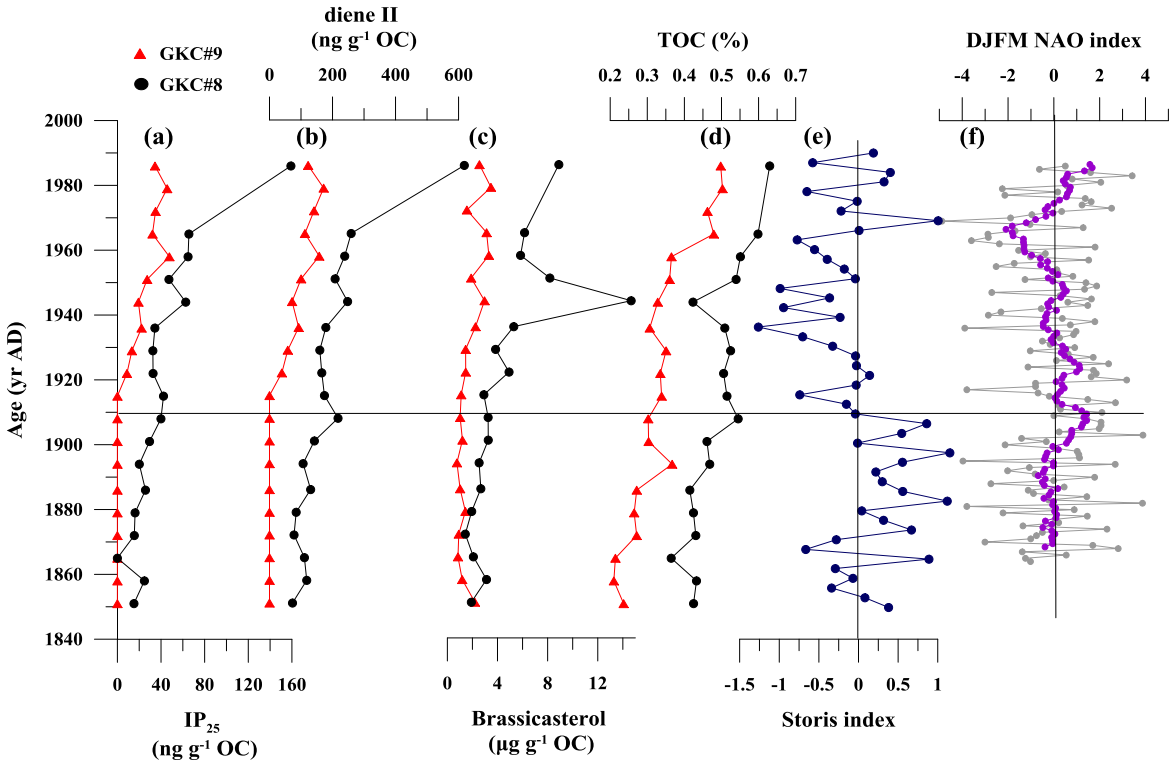

Figure 6.7: Individual temporal concentration profiles of biomarkers (TOC normalised) in the GKC#9 (20 sampling points) and GKC#8 cores (18 sampling points): (a) IP_{25}; (b) diene II; (c) brassicasterol; (d) TOC (%); (e) Storis index (Schmith and Hanssen, 2003); (f) winter NAO index record (Hurrel et al, 2003).The horizontal solid line at AD 1910 indicate a prominent shift in sea ice conditions during the last ca. 150 yr.

For example, the maximum IP_{25} concentration in the current study was 160 ng g^{-1}OC compared with values of ca. 4 µg g^{-1}OC from surface sediments from ca. 68˚N; 25˚W (Müller et al., 2011) (PS62/015-4; PS62/017-1; Figure 6.8) and ca. 400 ng g^{-1}OC from ca. 70˚N; 18˚W (HH11-142/143; Figure 6.8; this study). In contrast, IP_{25} was not identified in surface sediments from ca. 65˚N; 32˚W (PS62/012-2; Figure 6.8) (Müller et al., 2011). Finally, the concentration of IP_{25} in surface sediment material from north-west Iceland (surface grab, MD99-2263; this study) was found to be ca. 2 µg g^{-1}OC, similar to the values found by Müller et al. (2011) for sediments from ca. 70˚N; 18˚W (Müller et al., 2011) (PS62/020-1; Figure 6.8).

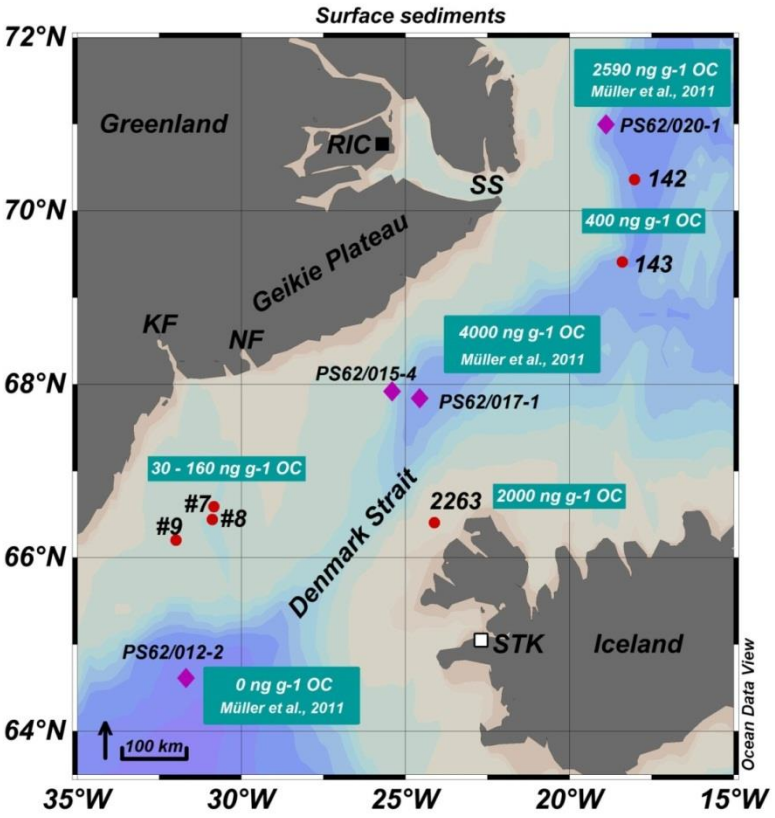

Figure 6.8: IP_{25} concentrations for surface sediments analysed in the study area, including those previously studied by Müller et al. (2011). Rendland Ice Cap (RIC), Scoresby Sund Fjord (SS), Kangerdlugssuaq Fjord (KF), Nansen Fjord (NF), Stykkisholmur (STK).

Relative concentration changes to the general phytoplankton biomarker brassicasterol in GKC#9 and GKC#8 were similar to those of IP_{25} and diene II (Figure 6.7c), with increases after ca. AD 1910; however, absolute concentrations (GKC#9; ca. 2-4 μg g^{-1}OC) were also extremely low compared to many other Arctic and sub-Arctic locations and generally ca. 2 orders of magnitude lower than other locations along the east Greenland margin (Müller et al., 2011) and north-west Iceland (MD99-2263; 308 ng g^{-1}OC; this study) (Table 6.1). In contrast, the lipid biomarker 24-methylencholesterol was absent or below the limit of detection in all the samples analysed for this study.

Table 6.1: TOC normalised concentrations of IP_{25} and brassicasterol in surface and near surface sediments from GKC#7, GKC#8 and GKC#9 and other locations near to the area under study.

Core name	IP_{25} (ng g^{-1} OC)	Brassicasterol (µg g^{-1} OC)
GKC#8 (0.5 cm depth)	160	9
GKC#9 (0.5 cm depth)	34	3
GKC#7 (1.5 cm depth)	50	5
GKC#7 (5.5 cm depth)	100	4
HH11-142-MC	310	410
HH11-143-MC	400	64
PS62/020-1	2590	117
PS62/015-4	3880	135
PS62/017-1	4110	234
MD99-2263	2000	308
PS62/012-2	0	111

6.4.3 Discussion

6.4.3.1 Surface sediments: IP_{25} concentrations *versus* satellite data

In order to perform an assessment of IP_{25} concentrations in surface sediments around the Denmark Strait area and to compare them with modern-day sea ice conditions, sea ice concentrations (%) were obtained from satellite data from the U.S. National Ice Center. A 12 year (2000 – 2011) monthly average sea ice concentration record was obtained (Figure 6.9). This sea ice record (satellite) shows that the percentage of sea ice for northerly locations (HH11-142/143; PS62/020-1; PS62/015-4 and PS62/017-1) is more than ca. 2 times higher compared to the PO175GKC core sites (Figure 6.9). The sea ice also extends further into the summer for the northerly locations but normally disappears from PO175GKC sites by July/August (and sometimes June). The core located in north-west Iceland (MD99-2263; Figure 6.1) also receives some sea ice from January to June, although to a lesser extent than that of the other core sites. No sea ice has been observed in southerly locations (PS62/012-2) for this interval.

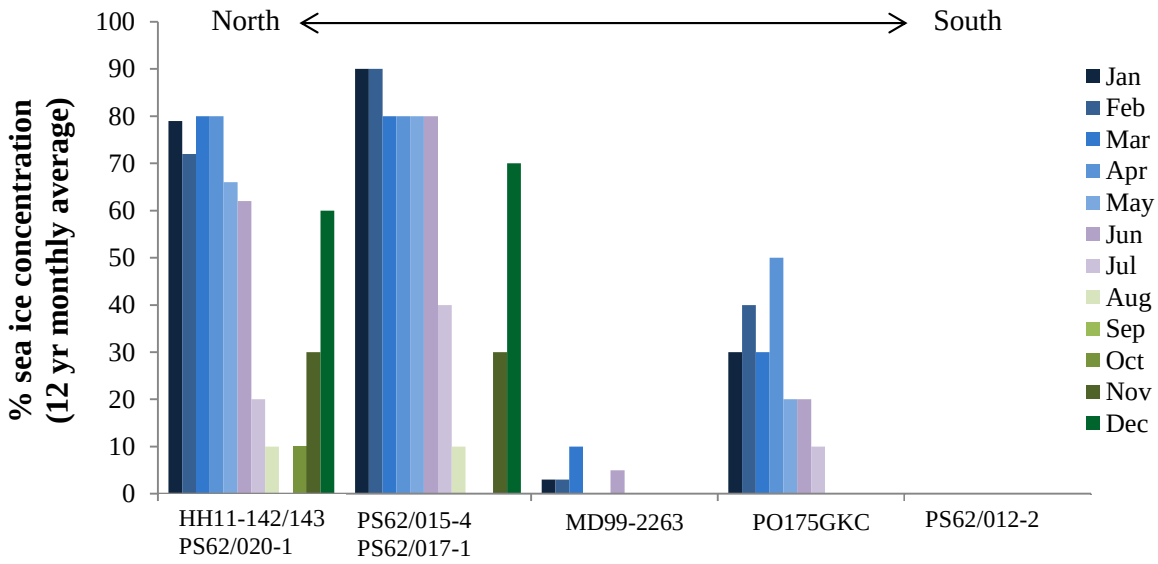

Figure 6.9: Sea ice concentration (%) based on a 12 year (2000 – 2011) monthly average obtained from satellite data from the U.S. National Ice Center, for each of the locations studied.

Satellite data were then compared to IP_{25} concentrations (TOC normalised) from surface sediments (Figure 6.8 and Figure 6.9). IP_{25} concentrations from the PO175GKC sites were lower than for the other locations from further north (HH11-142/143; PS62/020-1; PS62/015-4 and PS62/017-1) and IP_{25} was absent in a core from further south (PS62/012-2), consistent with a general reduction in sea ice from north to south along east Greenland. However, some anomalies were observed. For example, IP_{25} concentrations for north-west Iceland were ca. 10 times higher than those found for the PO175GKC core sites and ca. 5 times higher than for the northern locations (HH11-142/143; Figure 6.8) even though, according to the satellite data, there has been more sea ice recorded in the PO175GKC and northern areas compared to north-west Iceland (Figure 6.7). Further, IP_{25} concentrations were much higher in northern locations compared to the GKC sites yet this is not reflected by the satellite data where the GKC sites show sea ice concentrations that are ca. half those of northern locations (Figure 6.7). These outcomes suggest that the concentration of IP_{25} in this area does not simply reflect sea ice concentration, but perhaps is a better indicator of more specific sea ice conditions such as drift ice input from the north *versus* less productive or other types of ice. In order to examine this hypothesis, comparison of biomarkers with other proxy data covering the last ca. 150 yr was carried out (Figure 6.1).

6.4.3.2 Recent sediments: General considerations

6.4.3.2.1 Biomarker data

In general, and during the whole studied interval (last ca. 150 yr), for both GKC#8 and GKC#9 cores, concentrations of IP_{25} and diene II were very low or not detectable (Figure 6.7a and Figure 6.7b). Similarly, brassicasterol and TOC data were also low (Figure 6.7c and Figure 6.7d), suggesting that summer productivity has been significantly inhibited at GKC#9 and GKC#8 during the last ca. 150 yr, probably due to severe sea ice conditions. These observations, together with the outcomes observed by assessment of IP_{25} concentrations in surface sediments and satellite data, suggest that any IP_{25} recorded in this area, was probably advected from elsewhere through drift ice and not as a result of local production in first year ice. This conclusion is supported by very low brassicasterol concentrations, since poor open water conditions would prevent this biomarker being abundant. In contrast, locations further north (HH11-142/143, PS62/020-1, PS62/015-4 and PS62/017-1; Figure 6.1) and south (PS62/012-2; ice-free) in the drift ice corridor and north-west Iceland (MD99-2263; drift ice only) all represent more favourable conditions for phytoplankton production (i.e. high brassicasterol, Table 6.1).

6.4.3.2.2 Overview of proxy data obtained for the same study

Other proxy data obtained for the GKC#9 core included a variety of mineralogical determinations including quantitative x-ray diffraction (qXRD, provided by Prof. John T. Andrews, University of Colorado), ice-rafted debris (IRD) including hematite stained grains (HSG, provided by Dr. Montserrat Alonso-García, University of South Florida), Fe oxide measurements (provided by Prof. Dennis Darby, Old Dominion University) and quartz data (provided by Prof. John T. Andrews, University of Colorado). Detailed

interpretations of mineralogical data are discussed by Alonso-Garcia et al. (2013) and an overview is given here.

The qXRD mineralogical data suggest that most of the IRD probably came from Nansen and Kangerdlugssuaq Fjords during the last ca. 150 yr. IRD has been used in many previous studies as a tracer for sediment transport in sea ice (e.g. Eiríksson et al., 2000; Moros et al., 2006; Andrews and Eberl, 2007). Total IRD concentration (Figure 6.10d) showed a long-term decreasing trend in ice-rafting towards the present, although several peaks in IRD concentration were also recorded. HSG (63-150 μm; Figure 6.10c) are quartz and feldspar grains with a red coating composed of Fe oxides, mainly hematites, that derive primarily from the red bed deposits in NE Greenland and the Arctic coasts (Bond and Lotti, 1995). It is likely that a significant amount of the HSG found in GKC samples were wind-blown to the top of terrestrial glaciers or sea ice rather than IRD incorporated at the bottom of the glacier. As such, higher abundances of HSG would suggest stronger ice export via the EGC. Both, total IRD concentration and relative abundances of HSG showed opposite trends on long-term and decadal scales (Figure 6.10c and Figure 6.10d). Quartz wt% (< 2 mm from XRD; Figure 6.10e) is used as a proxy for drift ice transport and grain size (e.g. Andrews and Eberl, 2007; Andrews, 2011; Andrews and Jennings, 2013). Quartz is generally higher in surface samples from Scoresby Sund and further north along the NE Greenland shelf than in Kangerdlugssuaq Fjord (Andrews et al., 2010; Andrews, 2011). Similar to the HSG results, the quartz data showed an overall increasing trend towards AD 1990 (Figure 6.10c and Figure 6.10e), possibly associated with the increased calving of tidewater glaciers that followed the local and regional Little Ice Age (Geirsdóttir et al., 2000; Reeh et al., 2001; Hall et al., 2008).

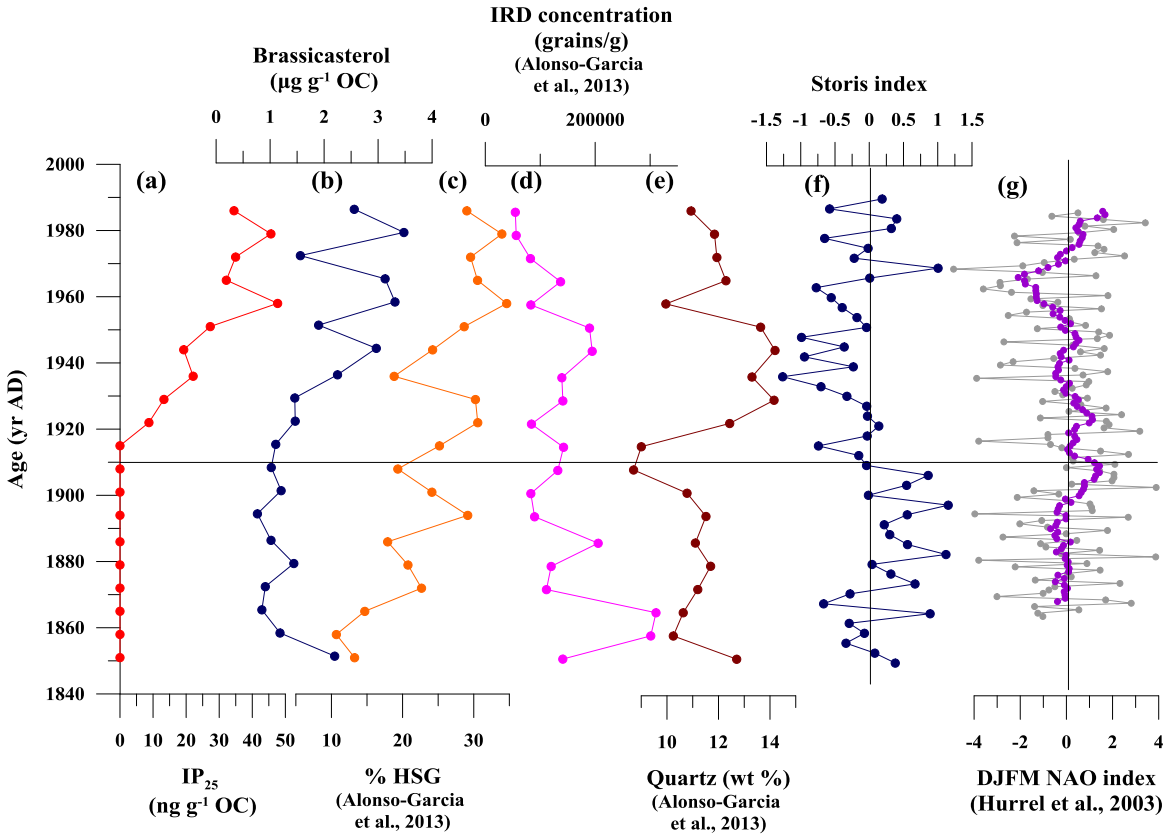

Figure 6.10: Temporal palaeoclimate profiles for the GKC#9 core (20 sampling points) for the last ca. 150 yr: (a) IP_{25} concentrations (TOC normalised); (b) brassicasterol concentrations (TOC normalised); (c) Percentage of hematite stained grains (HSG); (d) Total ice-rafted debris (IRD) concentration; (e) Quartz data; (f) Storis index; (g) winter NAO.

Source identifications were carried out based on Fe-oxide measurements (Darby, 2003; Darby et al., 2012), showing that the dominant sources are east and south Greenland, with average inputs of 28% and 27%, respectively (Alonso-Garcia et al., 2013) (Figure 6.2 and Figure 6.11). Other significant sources are from the Canadian Arctic Archipelago, especially Banks and Victoria Islands, and also southeast Ellesmere Island, all with an average of 6%. Franz Josef Land and the Yermak Plateau near Svalbard also contribute about 4% (Figure 6.11). These observations indicated that 'dirty' sea ice, or sediment entrained ice from the Arctic Ocean, survives through Denmark Strait (Alonso-Garcia et al., 2013) (Figure 6.11) carried by the clockwise Beaufort Gyre (BG) north of Alaska and Canada, and the TPD in the Eurasian Arctic (Russian Siberia) (Figure 6.2). The combination of the BG and TPD constitute the

major drift system that removes North American sea ice from the Arctic down to the east coast of Greenland. The TPD also carries sea ice from the Eurasian part of the Arctic down to the east coast of Greenland. Further, the comparison of Fe grains from BG sources in GKC#9 with the NAO records shows an overall weak correlation, indicating that the mechanisms that deliver Fe oxides from the Canadian Islands to the study area might be more complicated (Alonso-Garcia et al., 2013) (Figure 6.11).

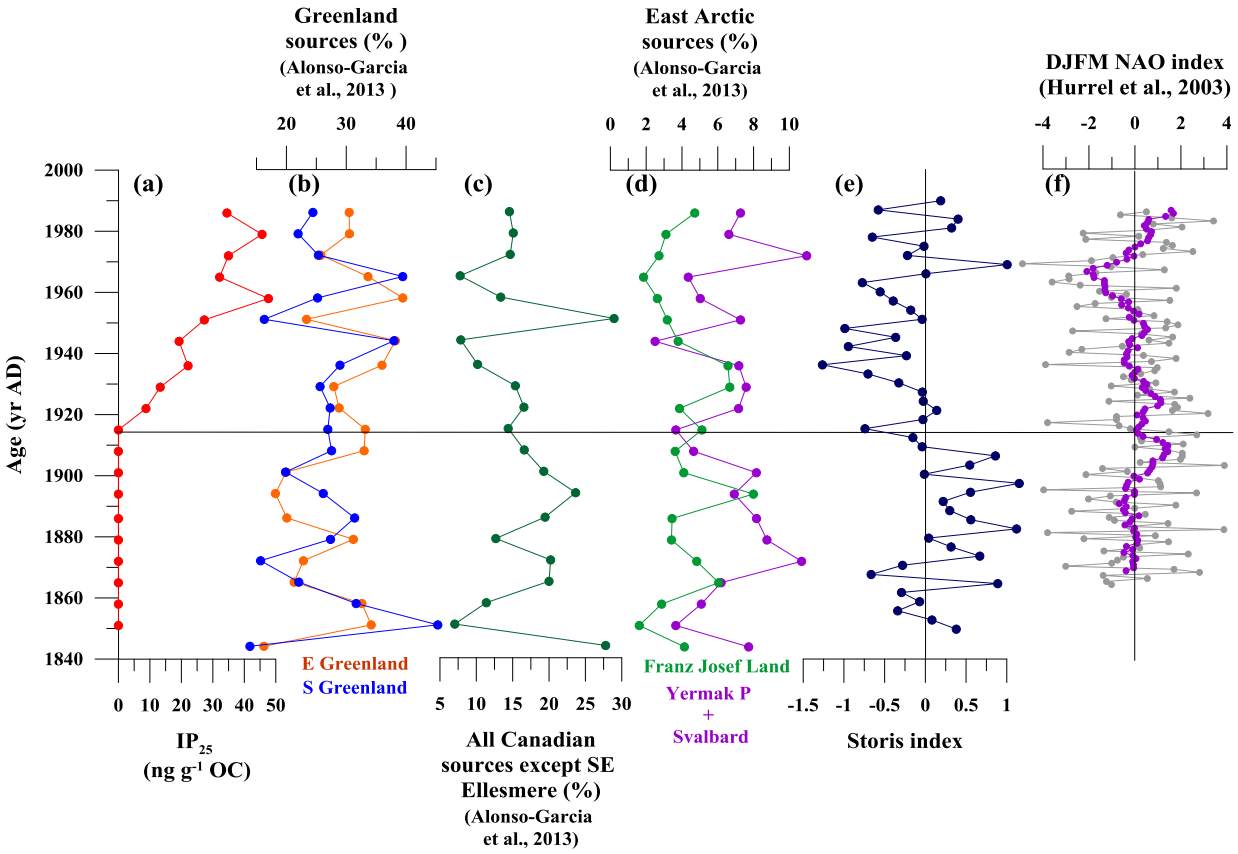

Figure 6.11: Temporal palaeoclimate profiles for the GKC#9 core (20 sampling points) for the last ca. 150 yr: (a) IP_{25} concentrations (TOC normalised); (b), (c) and (d) Fe-oxide sediment source analysis; (e) Storis index; (f) winter NAO.

6.4.3.3 Sea ice and environmental conditions during the last ca. 150 yr

The comparison of the biomarker data obtained for the GKC#9 core with these other mineralogical proxy data together with historical records indicates the occurrence of two distinct periods, distinguished by different sea ice and environmental conditions.

6.4.3.3.1 ca. AD 1850 – 1910

Between ca. 1850 – 1910 AD, IP_{25} and diene II concentrations for both GKC#8 and GKC#9 cores were very low or not detectable (Figure 6.7a and Figure 6.7b). Similarly, brassicasterol and TOC data were also low (Figure 6.7c and Figure 6.7d), indicating that primary productivity was inhibited, probably due to severe sea ice conditions. Alternating periods of higher and lower ice rafting in the area occurred especially during this interval, as inferred by the total IRD concentration (Figure 6.10d). It has previously been shown that ice streams may accumulate mass at times when perennial sea ice conditions prevail, and that when the sea ice breaks up, usually as a consequence of ocean temperature changes, an abrupt and strong iceberg calving occurs (Reeh et al., 2001; Alvarez-Solas et al., 2010). Therefore, periodic positive departures in IRD probably resulted from sea ice break-up resulting in strong iceberg calving in glaciers from Kangerdlugssuaq and Geikie Plateau (Alonso-Garcia et al., 2013). The strong ice-rafting events recorded at ca. AD 1860 and ca. AD 1885 (high IRD; Figure 6.10a) occurred slightly after MAT increases in Stykkisholmur (north-west Iceland) (Figure 6.10d and Figure 6.5a) supporting the hypothesis that ice break-up occurred as a result of oceanic warming (Alonso-Garcia et al., 2013). The increased ice cover from the strong calving probably prevented biological productivity during those events as shown by low brassicasterol concentrations (Figure 6.7c). When comparing the IP_{25} data with the Storis record, positive fluxes in the Storix index were mainly observed before AD

1910 (Figure 6.7e), suggesting that high fluxes of multi-year ice were exported from the Arctic Ocean. However, low or absent IP_{25} concentrations (Figure 6.7a) suggested that even if higher concentrations of sea ice were being exported from the Arctic Ocean along the east coast of Greenland, little or no sea ice reached the study area, due to the prevalence of severe local sea ice conditions. Historical records also suggest colder conditions and higher sea ice presence before AD 1920 (e.g. Gray, 1881; Ogilvie and Jónsson, 2001). Interestingly, a drift ice signal (inferred from IP_{25} concentrations) from a sediment core from north-west Iceland (MD99-2263; Figure 6.1) (Andrews et al., 2009) shows a downward trend from AD 1850 to more recent times, and follows the storis, showing an opposite trend to the GKC cores. This suggests that, even if sea ice flux from the Arctic was stronger before AD 1910, it was not recorded in the GKC sites, but was observed in north-west Iceland. Enhanced Arctic ice has been related to the conditions during the NAO positive phase (Kwok and Rothrock, 1999), whereas conditions during the negative phase of the NAO have been related to an increased influence of the IC in Denmark Strait and north of Iceland (Blindheim and Malmberg, 2005; Jennings et al., 2011). However, the NAO record does not show any clear pattern with the drift ice proxies (IP_{25}, HSG and Fe oxides; Figure 6.7, Figure 6.10 and Figure 6.11) before AD 1910, as the study site was covered by perennial ice. This likely illustrates the more generic nature of the NAO in contrast to specific local measurements such as the drift ice proxies studied in the GKC area.

6.4.3.3.2 ca. AD 1910 – 1986

After ca. AD 1910, IP_{25} and diene II concentrations increased towards the present (Figure 6.7a and Figure 6.7b) suggesting that more drift ice reached the study area. Brassicasterol concentrations also showed a general increasing trend (Figure 6.7c), although the values for the GKC cores are amongst the lowest reported from cores from the same area (Table 6.1). These observations suggest that sea ice conditions during this period were less severe than during before ca. 1910, although still only short periods of open water likely occurred, similar to those observed today, as shown by the summer sea ice distribution during August AD 2000 (Figure 6.3). Lower total IRD concentrations (Figure 6.10d), higher percentages of HSG (Figure 6.10c) and lower storis (Figure 6.10f) compared to those from before AD 1910, suggests that although less drift ice was carried out through the EGC, a greater amount of it reached the core site. Alonso-Garcia et al. (2013) also observed a larger influence in the input of sediment from distant sources after AD 1910, as inferred by the comparison of mineralogical data with the AO index, indicating that more drift ice (as icebergs containing sediments together with sea ice) was transported to the core site from the Arctic Ocean (Figure 6.11). Increased quartz and HSG after AD 1910 have also been related to a possible increase in calving of tidewater glaciers (e.g. Reeh et al., 2001; Hall et al., 2008) following the local and regional Little Ice Age (Alonso-Garcia et al., 2013). Overall, the main sediment sources, as given by Fe oxide data, are east and south Greenland and, to a minor extent, the Canadian Arctic, Franz Josef Land, Yermak Plateau and Svalbard areas (Figure 6.11). This observation confirmed that Arctic sea ice reached the GKC sites (Alonso-Garcia et al., 2013). It is known that IP_{25} is formed in sea ice from the Canadian Arctic (Vare et al., 2009; Belt et al., 2010; Brown et al., 2011) and northern Barents Sea (Stein et al., 2012). Hence, any IP_{25} formed there could have been transported as drift ice. However, the extent to which multi-year ice, carried

via the BG and TPD along the east coast of Greenland, can transport IP_{25} is unknown. Largest peak contributions of Fe oxides in the Canadian Islands were observed at ca. AD 1865, 1895 and 1960 (Figure 6.11). However, IP_{25} was absent in core GKC#9 before AD 1910, showing an overall weak correlation to the Fe oxide data (Figure 6.11). The generic nature of Fe oxide measurements for source identification and the specificity of IP_{25} to sea ice prevented any further comparison. The alternation of high and low total IRD concentration (Figure 6.10d) together with the presence of IP_{25} throughout this period, also suggested that alternating periods of "mixed" conditions between iceberg discharge from Kangerdlugssuaq/Nansen Fjords (high IRD) and drift ice from the Arctic (present IP_{25}, high HSG) could have prevailed during this period.

6.4.4 Conclusions

Two distinct periods with different environmental and drift ice conditions have been identified on the east Greenland shelf (ca. 66˚N) during the last ca. 150 yr based on a comparison of biomarker data measured in the current study with other proxy and observational data obtained from other researchers.

During the first interval (ca. AD 1850 – 1910; Figure 6.12a), it is proposed that perennial sea ice conditions prevailed in the south-east Greenland coast and very low biomarker abundances indicate that biological productivity was very low or absent. Further, even if high fluxes of Arctic sea ice were being exported along the east coast of Greenland as drift ice (high Storis), the presence of local severe sea ice conditions prevented any drift ice from reaching the study area (low biomarker data and low HSG), and was limited mainly to north-west Iceland. Some abrupt and strong iceberg calving events in the glaciers in Kangerdlugssuaq Fjord and Geikie Plateau were also recorded

in this area during this period (high IRD). Nevertheless, biological productivity during those strong calving events was also limited.

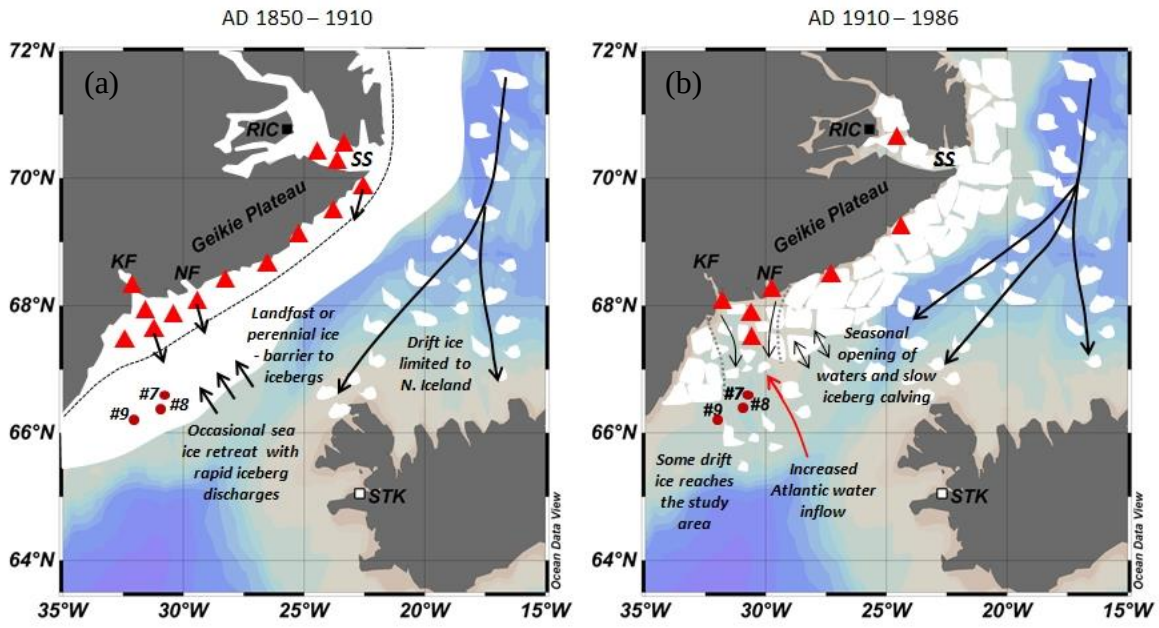

Figure 6.12: Schematic representations of sea ice conditions for the GKC study sites during the two intervals differentiated: (a) AD 1850-1910 and (b) AD 1910-1986.

During the second interval (ca. AD 1910 – 1986; Figure 6.12b), the biomarker and other proxy data suggest that sea ice conditions were less severe, coastal sea ice became more seasonal, and occasional open water conditions permitted limited biological productivity. Although lower fluxes of Arctic sea ice were exported from the Arctic Ocean compared to the first interval (low Storis), more of this drift ice reached the study area (higher IP_{25} and HSG). Interestingly, the proposed environmental and sea ice conditions during this interval more closely resemble those of present-day conditions as shown by satellite data (Figure 6.3).

A number of environmental factors need to be considered in the south-east Greenland area, such as the strength and temperature of the IC, atmospheric conditions, and sea ice conditions (landfast ice formation, iceberg calving from Greenland and drift ice

transported from the Arctic Ocean by the EGC). The complexity between these factors makes palaeoceanographic studies very challenging. Nevertheless, the complementary and individual information that all of the proxies used in this study provide, as well as historical records, have allowed some specific and variable oceanographic conditions to be deciphered.

6.5 Part B: Ancient sediments: ca. 16.3 – 10.9 cal. kyr BP

6.5.1 Introduction

During the Last Glacial Maximum (LGM; ca. 26.5 – 19 cal. kyr BP), ice sheets covered large areas in northern latitudes (e.g. Hughes et al., 1977; Clark et al., 2009; Clark et al., 2012). The Greenland Ice Sheet (GIS) represents the only remaining ice sheet that survived the climate warming after the LGM in the northern hemisphere (a review is given by Kelly and Long, 2009). The East Greenland continental margin, was probably covered by a continental ice sheet with a more or less closed sea ice cover during the LGM (Kellogg et al., 1978; Kellogg, 1980) and the same observations were inferred in a study from south west Greenland (ca. 65˚N) (Roberts et al., 2008). Previous studies based around southern Greenland have shown that such conditions lasted until ca. 15 cal. kyr BP (Funder and Hansen, 1996), at which time the break-up of the GIS probably began (Nam et al., 1995; Funder and Hansen, 1996; Wohlfarth et al., 2008).

The main aim of this investigation was to test the model proposed in part A of this chapter in the Kangerdlugssuaq area after the termination of the LGM. Thus, there are two considerations to take into account: can the model (previously proposed to explain the biomarker and proxy data for GKC cores) be used directly for longer timescales, or will it require some adaptation? With the aim of answering this question, a sediment core (JM96-1213; Figure 6.1), located close to the GKC cores, also in the Kangerdlugssuaq Trough, covering the mid-late Oldest Dryas – Bølling-Allerød – Younger Dryas periods was studied.

6.5.2 Material and methods

6.5.2.1 Field methods and chronology

The core JM96-1213 (67.17˚N, 30.57˚E; water depth 557 m; core length 540 cm; Figure 6.1), was recovered from the middle basin of the Kangerdlugssuaq Trough on board the R/V *Jan Mayen* in October 1996 and stored *in situ* (5˚C) until sampled for analysis. Individual sub-samples for biomarker analysis were taken at 5 cm intervals (15 – 115 cm) and at 5 – 40 cm intervals (120 – 493 cm), freeze-dried and stored at -20˚C prior to extraction. Samples were provided by Prof. John T. Andrews and Dr. Anne Jennings (University of Colorado).

A total of 6 AMS ^{14}C age determinations on foraminifers, molluscs and bryozoans were performed on JM96-1213 core previously by Jennings et al. (2002a), who also used tephrostratigraphy such as identification of the Vedde Ash tephra horizon identified at 99 – 101 cm (time marker corresponding to 11.980 ice-core yr; Grönvold et al., 1995). A final age model was then constructed by Jennings et al. (2006). A 400 yr marine reservoir correction was applied to all radiocarbon dates. The ^{14}C dates were calibrated to calendar years using Calib version 4.3 (Stuiver et al., 1998). A third-order polynomial fit was then applied to the calibrated ^{14}C dates (2 AMS ^{14}C dates were excluded from the age model) and tephra markers (Jennings et al., 2006) resulting in linear sedimentation rates of ca. 5 – 30 cm kyr^{-1}. Sampling and analysis was carried out at 5 – 40 cm intervals, corresponding to an effective age resolution of ca. 30 – 400 yr.

6.5.2.2 Experimental

Analysis of biomarkers (hydrocarbons and sterols) required extraction of lipids from the sediment samples and separation into individual fractions prior to GC-MS analysis. A complete description of the experimental procedure shown in Figure 6.13 is given in Chapter 2 (Methods).

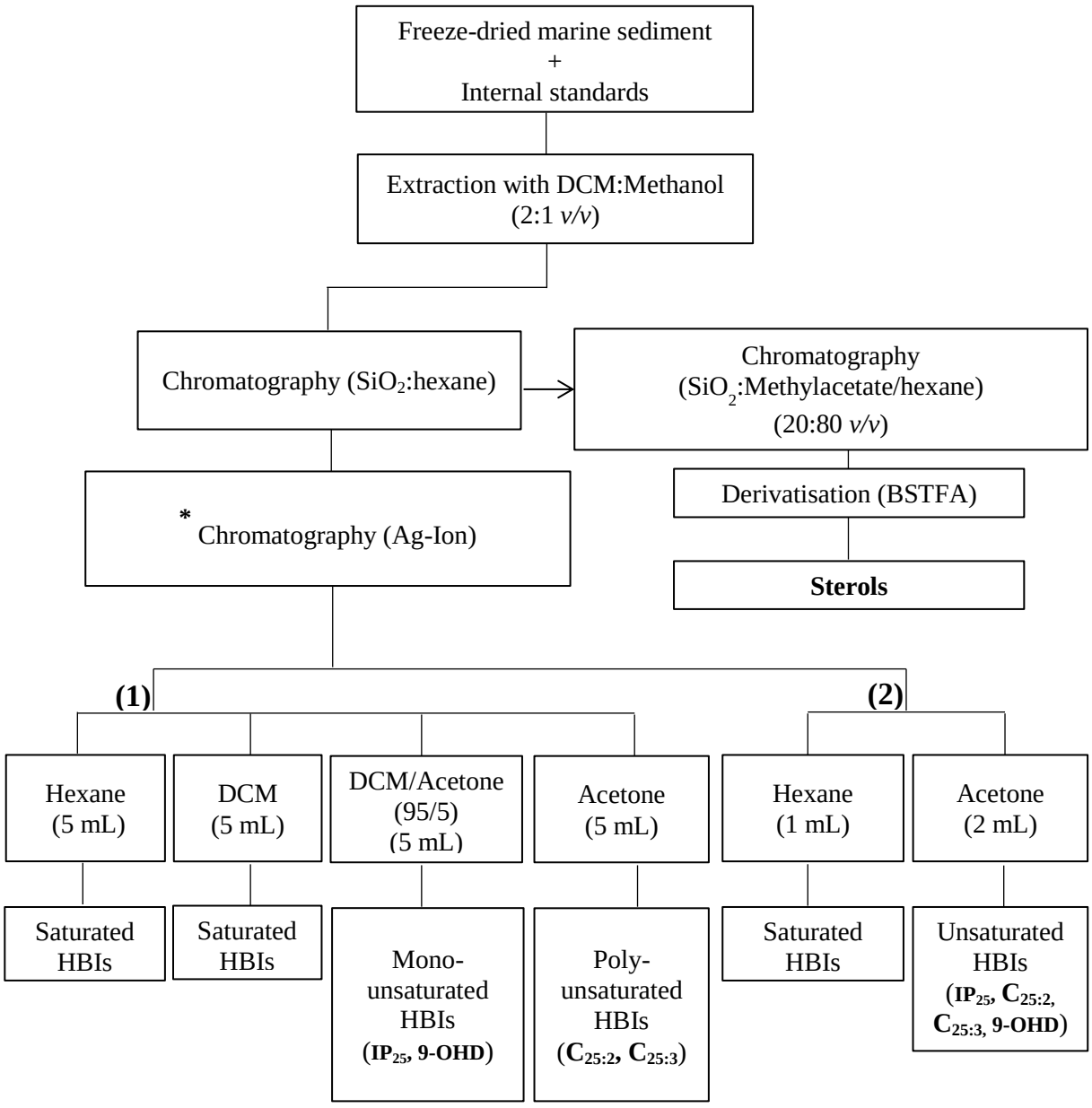

Figure 6.13: Sample extraction flow diagram for lipid biomarkers. * Two different approaches regarding Ag-Ion chromatography were adopted depending on level of purification and biomarkers required for GC-MS analysis. The use of approach (1) allowed the analysis of IP_{25} only. Approach (2) allowed the analysis of all HBIs under study using reduced amounts of Ag-Ion phase (more information is given in Chapter 2).

Briefly, following addition of the internal standards for quantification (7-hexylnonadecane; 10 μL; 10 μg mL^{-1} and 9-octylheptadec-8-ene; 10 μL; 10 μg mL^{-1}), the freeze dried sediments were extracted with DCM/Methanol (2:1 *v/v*; 3 x 3 mL) and then purified by open column silica chromatography with hexane (6 mL) used to yield apolar lipids. Methylacetate/hexane (20:80, 6mL) was then used to elute sterols. In some cases, the identification or quantification of some HBIs in these partially purified extracts was made difficult due to the low concentrations and the occurrence of other highly abundant co-eluting organic compounds that prevented further concentration of the extracts. Depending on which biomarkers were needed for analysis (Figure 6.13), two different approaches were adopted (detailed in Chapter 2, Section 2.5) using Ag-Ion chromatography material. All biomarker concentrations (μg g^{-1} dry sediment) were converted to fluxes (μg cm^{-2} kyr^{-1}) and normalised to TOC content (μg g^{-1} OC) (Chapter 2). TOC (wt. %) data were provided by Dr. Anne Jennings and Prof. John T. Andrews (University of Colorado).

6.5.3 Results

Overall, a total of 43 downcore sediment samples were analysed for the IP_{25} biomarker, the structurally related HBI diene II and two sterol biomarkers, 24-methylcholesta-5,22E-dien-3β-ol (brassicasterol) and 24-methylcholesta-5,24(28)-dien-3β-ol (24-methylenecholesterol) commonly found in marine algae (Volkman et al., 1998). IP_{25} was absent (or below the limit of detection: 0.54 ng g^{-1} dry sed) in 5 samples between ca. 16.3 – 15.2 cal. kyr BP (Figure 6.14a), after which IP_{25} was present, showing an increasing trend up to ca. 14.3 cal. kyr BP. Highest IP_{25} fluxes recorded for this record were observed between ca. 14.3 – 13.8 cal. kyr BP. After ca. 13.8 ca. kyr BP, a long-term decreasing trend in IP_{25} fluxes was observed, before disappearing at ca. 12.5 cal.

kyr BP. IP_{25} remained absent up to ca. 12.2 cal. kyr BP, after which, it was present again up to ca. 10.9 cal. kyr BP, although lower fluxes, compared to the rest of the record, were observed. A short-term (one data point only) increase in IP_{25} flux was also observed at ca. 11.7 cal. kyr BP (Figure 6.14a). The flux profile of the structurally related HBI diene II was similar to that of IP_{25} (Figure 6.14b), suggesting co-production of diene II and IP_{25} by sea ice diatoms, as suggested previously (Belt et al., 2007; Belt et al., 2008; Vare et al., 2009; Brown, 2011).

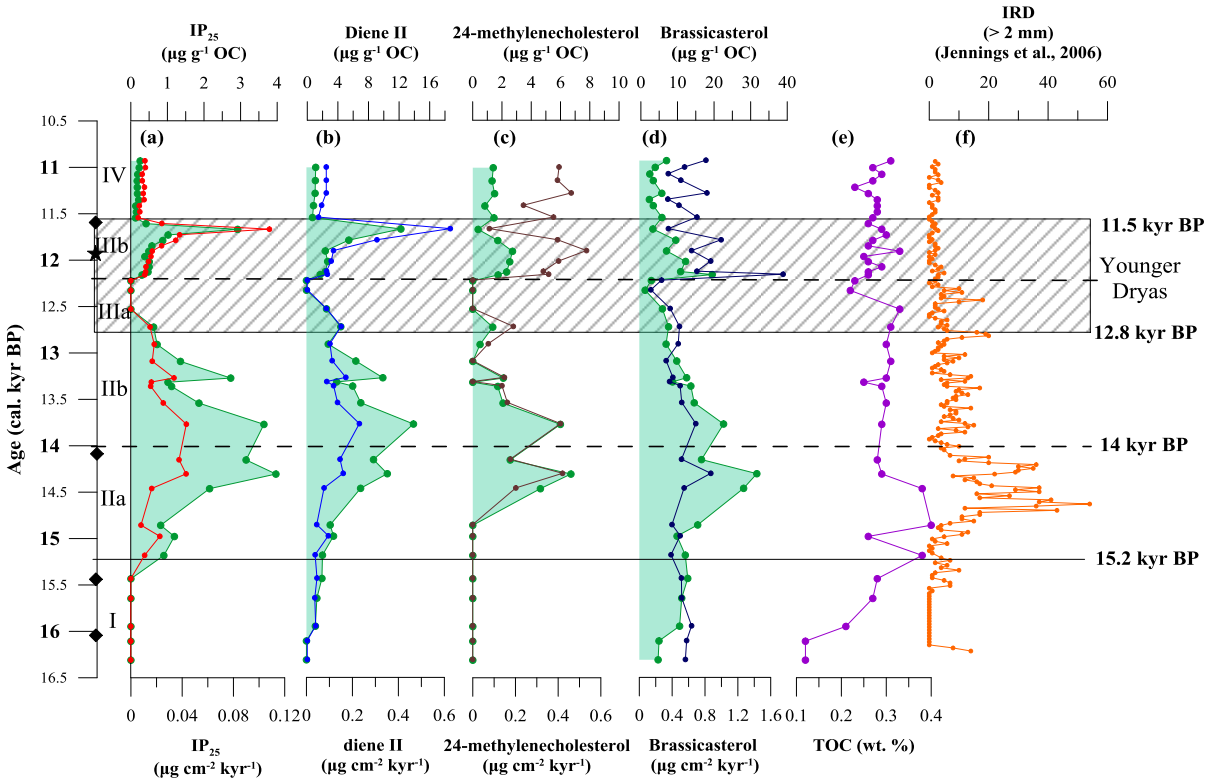

Figure 6.14: Individual temporal palaeoclimate profiles for the JM96-1213 core: (a) IP_{25} fluxes; (b) diene II fluxes; (c) 24-methylenecholesterol fluxes; (d) brassicasterol fluxes; (e) TOC (wt. %); (f) IRD (> 2mm). The horizontal solid and dashed lines at ca. 15.2 cal. kyr BP and ca. 14 cal. kyr BP, respectively, represent shifts in the sea ice conditions. The rectangle between ca. 12.8 – 11.5 cal. kyr BP represent the Younger Dryas cold stadial. The diamonds mark the AMS ^{14}C dates and the arterisk indicates the Vedde Ash tephra horizon used in the age model.

Regarding the two sterols analysed during this study (24-methylenecholesterol and brassicasterol), the brassicasterol flux profile was similar to those of IP_{25} and diene II (Figure 6.14d). This observation coincides with that seen in the previous study from Kangerdlugssuaq Trough during the last ca. 150 yr (GKC#8 and GKC#9; Figure 6.7). Unlike the previous study carried out on the GKC#8 and GKC#9 cores, however, where 24-methylenecholesterol was absent, this biomarker was present (Figure 6.14c), with a profile that also resembled somewhat those of brassicasterol, IP_{25} and diene II.

6.5.4 Discussion

Previously, a number of studies have focused on the Denmark Strait area over different timescales. These include, for example, reconstructions of palaeoclimate variability during the Late Quaternary (e.g. Kuijpers et al., 2003) and the Holocene (e.g. Jennings and Weiner, 1996; Jennings et al., 2002b; Andersen et al., 2004a; Andersen et al., 2004b; Solignac et al., 2006; Jennings et al., 2011; Andresen et al., 2013). Some other studies have also addressed the provenance of sediments deposited in this area, as inferred by mineralogical data such as IRD (e.g. Andrews et al., 1998; Andrews, 2000; Linthout et al., 2000; Andrews et al., 2010; Andrews and Eberl, 2012).

Further, the proxy-based study described in Part A of this chapter focused on the palaeoclimatic conditions in the Kangerdlugssuaq Trough (GKC cores), during the last ca. 150 yr. A model that explained variations in different proxy data and related this to different environmental settings was introduced. As such, two different scenarios with different environmental conditions were derived from this model (Figure 6.12). Nevertheless, this was reconstructed during a relatively short time period and needed to be further tested for longer term reconstructions. As such, a sediment core (JM96-1213;

Figure 6.1) located close to the GKC cores and that covered the period between ca. 16.3 – 10.9 cal. kyr BP was studied. This core, has previously been studied by Jennings et al. (2006), and was used to focus on the reconstruction of climatic conditions at the Kangerdlugssuaq Trough area after the termination of the LGM using benthic and planktic foraminifera, as well as oxygen stable isotopes ($\delta^{18}O$) and IRD data. In addition, Jennings et al. (2006) provided evidence for freshwater forcing from the GIS during the Younger Dryas.

6.5.4.1 Sea ice variability between ca. 16.3 – 10.9 cal. kyr BP in the Kangerdlugssuaq Trough

First of all, it is noted that TOC was low (ca. 0.1 – 0.4%) as well as low biomarker data for the JM96-1213 core during the whole studied period (ca. 16.3 – 10.9 cal. kyr BP; Figure 6.14). This indicates that primary productivity was very low in the Kangerdlugssuaq Trough. This observation suggests that this area experienced severe sea ice conditions, probably due to the close proximity of this core site to the Greenland margin which was still under the influence of the retreating GIS after the LGM (e.g. Jennings et al., 2006).

Based on the age model, biomarker data and comparisons with existing proxy data (e.g. IRD, stable isotopes), in addition to the model suggested in Part A of this chapter, it is proposed that the palaeoceanographic conditions at the JM96-1213 core location covering the period between ca. 16.3 – 10.9 cal. kyr BP can be divided into four main periods (Figure 6.14) (P-IV excluded from any interpretation; Section 6.5.4.1.4). A schematic representation of the sea ice conditions during the studied interval is shown in Figure 6.15. Thus, a description of the environmental conditions during each interval will be discussed here, alongside a comparison with the model proposed previously (Chapter 6, part A).

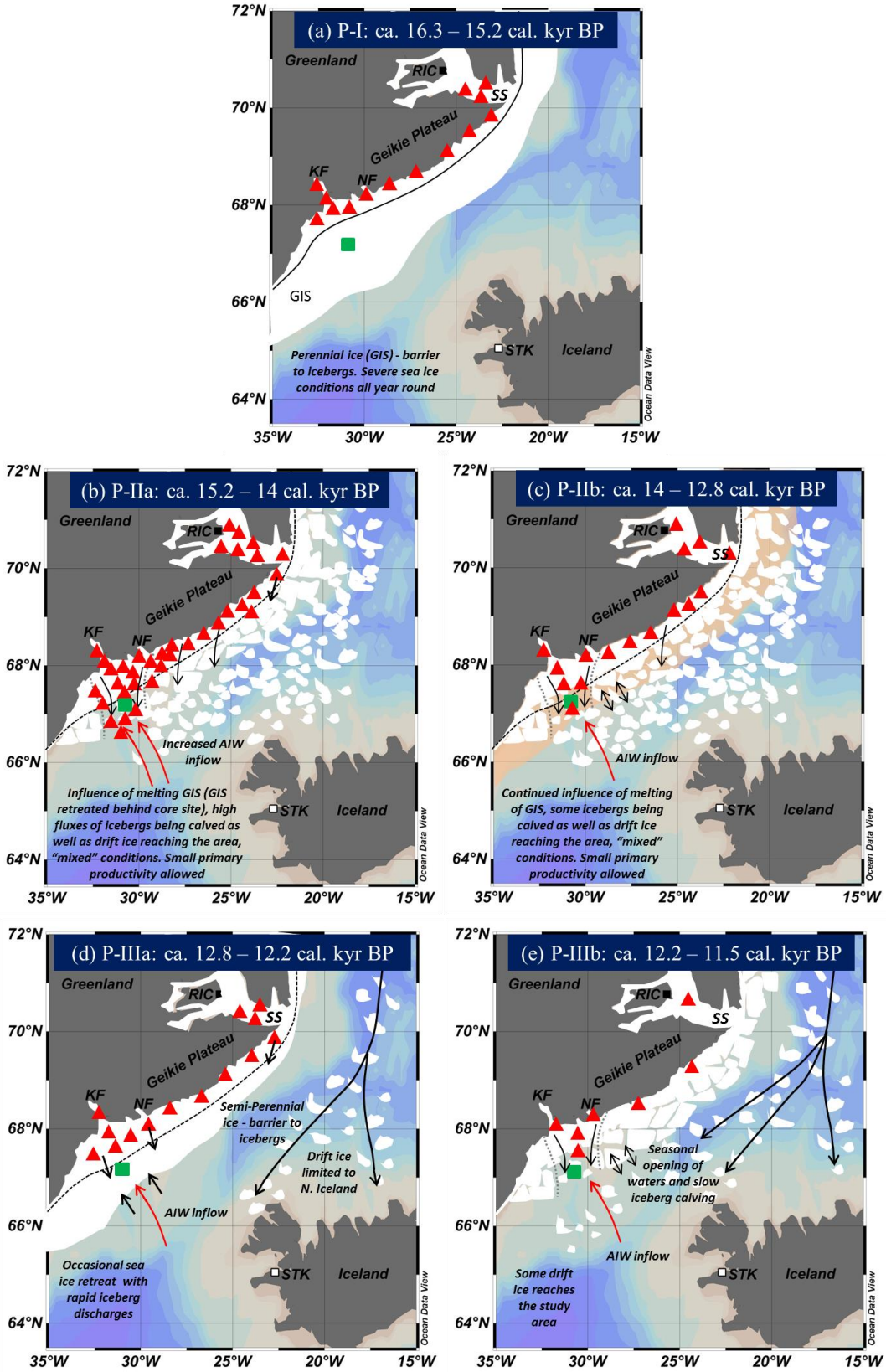

Figure 6.15: Schematic representations of sea ice conditions for the JM96-1213 study site (green square) during the five distinctive periods characterised: (a) P-I: ca. 16.3 – 15.2 cal. kyr BP; (b) P-IIa: ca. 15.2 – 14 cal. kyr BP; (c) P-IIb: ca. 14 – 12.8 cal. kyr BP. The shaded area indicates a possible cooling between ca. 13.4 – 13.2 cal. kyr BP ; (d) P-IIIa: ca. 12.8 – 12.2 cal. kyr BP; (e) P-IIIb: ca. 12.2 – 11.5 cal. kyr BP.

6.5.4.1.1 Period I: 16.3 – 15.2 cal. kyr BP (mid-late Oldest Dryas)

Period I (P-I) corresponds to the mid-late part of the Oldest Dryas (ca. 16.3 – 15.2 cal. kyr BP; Figure 6.14). During P-I, IP_{25} and 24-methylenecholesterol were absent (Figure 6.14a and Figure 6.14c), while diene II, brassicasterol and TOC (ca. 0.14 – 0.25%) were very low (Figure 6.14b, Figure 6.14d and Figure 6.14e). These data suggest that primary production was especially limited during this period, probably due to severe sea ice conditions. In addition, IRD was mainly absent (Figure 6.14f) and $\delta^{18}O$ (NPS) values of ca. 2.4% were recorded (Figure 6.16d), which further suggests that severe and cold conditions with a near-permanent to permanent ice cover existed in the area. This would have prevented drift ice from reaching the area (IP_{25} absent) as well as iceberg calving of nearby fjords (IRD absent) (e.g. Kangerdlugssuaq Fjord and Geikie Plateau). Previous studies based around this area have shown that the GIS extended offshore onto the continental shelf and that this continued until ca. 15 cal. kyr BP at least (Nam et al., 1995; Funder and Hansen, 1996; Kelly and Long, 2009). As such, the biomarker and proxy data also point to the presence of a (thick) permanent ice cover (as a result of the expanded GIS) in the Kangerdlugssuaq Trough during P-I (Figure 6.15a). These conditions would also have severely limited primary productivity (low TOC).

When comparing these results with the initial model (Part A of this chapter; Figure 6.12), the scenario of permanent or perennial ice cover with severe sea ice conditions (year round) observed during P-I was also suggested during AD 1850 – 1910 for the same region. However, it is worth pointing out that the environmental conditions surrounding the Kangerdlugssuaq Trough area were rather different between these periods. During P-I, this area was under the influence of the (thick) GIS, while between AD 1850 – 1910, this area was characterised by a less thick landfast sea ice cover. As such, no IRD was recorded during P-I, suggesting that the ice did not break-up and no

calving events occurred, unlike that seen in the initial model (AD 1850 – 1910). Therefore a further adaption to the model was required to consider this scenario (Figure 6.15a) in which all biomarkers were absent or very low in addition to absent IRD.

6.5.4.1.2 Period II: 15.2 – 12.8 cal. kyr BP (Bølling – Allerød)

P-II includes the Bølling – Allerød interstadials. This period is further divided into two sub-periods according to a pronounced change in IRD delivery (> 2 mm) recorded at ca. 14 cal. kyr BP (Figure 6.14f): P-IIa (ca. 15.2 – 14 cal. kyr BP) and P-IIb (ca. 14 – 12.8 cal. kyr BP). IP_{25} first appeared in the record at ca. 15.2 cal. kyr BP (Figure 6.14a). Previously, a study by Johnsen et al. (1992) pointed to the end of a long, cold period (LGM) at ca. 15 cal. kyr BP, as observed in the oxygen isotope data from the Renland ice core in Greenland, and a period when the break-up of the GIS probably began (e.g. Nam et al., 1995; Funder and Hansen, 1996; Wohlfarth et al., 2008). Jennings et al. (2002a) also observed that the GIS margin had retreated landward of Kangerdlugssuaq Trough and Grivel Basin by ca. 15 cal. kyr BP. These observations are consistent with the IP_{25} and diene II data, as the presence of these biomarkers after ca. 15.2 cal. kyr BP probably signified the beginning of less severe climatic conditions compared to P-I with delivery of some drift ice to the study area.

Overall, the presence of IP_{25} and diene II during the Bølling – Allerød (ca. 15.2 – 12.8 cal. kyr BP; P-II) with varying fluxes (Figure 6.14a and Figure 6.14b), suggests a period characterised by variability in the sea ice conditions and delivery of drift ice. Changes in the influence of Atlantic Intermediate Waters (AIW) were found to affect the variability of hydrographic and sea ice conditions in this area (e.g. Jennings et al 2006). For example, the presence of IP_{25} during ca. 15.2 – 14 cal. kyr BP (P-IIa) with highest IP_{25} fluxes for the entire record observed at ca. 14.3 cal. kyr BP coincides with very high

IRD (Figure 6.14a and Figure 6.14f). Jennings et al. (2006) attributed the enhanced IRD input in this core as derived by increasing influence of AIW, melting of the GIS and iceberg calving. The presence of IP_{25}, together with high IRD, suggests a period with "mixed" conditions, where sediments deposited in the seafloor were derived from icebergs produced locally (due to melting of the GIS) as well as icebergs and sea ice (containing IP_{25} and diene II) from the Arctic Ocean carried southwards by the EGC. In addition to high IP_{25}, higher fluxes were also observed for the sterol biomarkers (24-methylenecholesterol and brassicasterol, Figure 6.14c and Figure 6.14d). This observation may potentially indicate a marginal ice zone scenario, as high primary productivity has previously been related to sea ice edge conditions (Smith et al., 1985; Sakshaug, 1997). However, the observation of high IRD being released from the adjacent south-east Greenland fjords suggests this is not the case, as this scenario would prevent any icebergs from being released and low or absent IRD would be observed. In addition, overall TOC data values were very low (< 0.4%; Figure 6.14e), which is not consistent with a sea ice edge scenario. Instead, it is proposed that, during P-IIa, the increasing influence of the AIW, probably caused the retreat of the GIS (Jennings et al., 2006) which, in turn, triggered the release of high fluxes of icebergs (high IRD). Increasing IP_{25} and diene II fluxes also suggest increasing drift ice from the Arctic Ocean. At the same time, increasing sterol fluxes (but still low) are consistent with partial open water conditions during the summer although biological productivity was still limited (low TOC) due to the presence of icebergs and sea ice at the core site (Figure 6.15b).

Mixed conditions between iceberg calving and drift ice observed in the model described in Part A (Figure 6.12) were also recorded during P-IIa (presence of IP_{25}, diene II and IRD with varying fluxes). However, some further adaptions were required to account for different environmental conditions. For instance, during P-IIa, this site was greatly

influenced by the melting of the GIS after the LGM (Figure 6.15b), compared to modern conditions (ca. last 150 yr) and therefore a greater amount of icebergs calved from the south-east Greenland margin (high IRD) were observed, instead of the slow iceberg calving that was recorded between AD 1910 – 1986 (Figure 6.12).

Between ca. 14 – 12.8 cal. kyr BP (P-IIb), IP_{25} and diene II were still present showing a decreasing trend towards ca. 12. 8 cal. kyr BP (Figure 6.14a and Figure 6.14b). Unlike P-IIa, where IRD was very high, IRD was clearly lower (although still present) during P-IIb, (Figure 6.16c) which could indicate that fewer icebergs were being discharged from nearby locations. A pronounced light isotope event was recorded between ca. 13.4 – 13.2 cal. kyr BP (Figure 6.16d). It has previously been suggested that the increased melting of the retreating ice sheet resulted in reduced sea surface salinity, which would, in turn, have promoted the formation of sea ice by changing the freezing point of the ocean surface. The resulting brine rejection and subsequent increased salinity would lead to the sinking of surface water, resulting in a depletion of $\delta^{18}O$ (Dokken and Jansen, 1999; Jennings et al., 2006; Knudsen et al., 2008). Interestingly, this light isotope spike (Figure 6.16d), coincides with a small decrease in all the biomarker data during this interval (ca. 13.4 – 13.2 cal. kyr BP; Figure 6.14). Indeed, the presence of locally produced sea ice would have limited drift ice from reaching the area, as observed from current environmental conditions (Figure 6.4) and therefore, a reduction of IP_{25}, diene II and sterol fluxes.

Overall, P-IIb was still characterised by the influence of the GIS retreat, as recorded between ca. 13.4 – 13.2 cal. kyr BP (Jennings et al., 2006), which caused an increased freshwater influence and sea ice cover that limited IRD and biomarkers. For the rest of the interval this phenomenon could also be occurring but to a lesser extent. Therefore some drift ice reached the area (IP_{25} and diene II present) as well as some IRD being

deposited, although less than during P-IIa. Primary productivity was still rather limited (low sterols, low TOC).

Further, the environmental conditions inferred during P-IIb (Figure 6.15c) were to some extent different from those reported previously by the model described in Part A, as the Kangerdlugssuaq Trough area was still under the influence of the melting GIS. Iceberg calving from nearby locations and drift ice reached the core site, although to a lesser extent compared to P-IIa. A short-term cooling period was observed between ca. 13.4 – 13.2 cal. kyr BP (shaded area in Figure 6.15c).

6.5.4.1.3 Period III: 12.8 – 11.5 cal. kyr BP (Younger Dryas)

P-III corresponds to the Younger Dryas cold stadial (ca. 12.8 – 11.5 cal. kyr BP). Overall, the IP_{25} profile in JM96-1213 is clearly different to those previously observed during the Younger Dryas in two sediment records from north-western Norway (Chapter 4, Figure 4.4) and western Barents Sea (Chapter 5, Figure 5.7). This is potentially because the IP_{25} signal in the Denmark Strait area represents mainly advected drift ice from the north rather than locally produced sea ice, as was likely in the other studies. At the onset of the Younger Dryas (ca. 12.8 cal. kyr BP) both IP_{25} and diene II were present (only one data point), yet low fluxes were observed (Figure 6.14a). The onset of the Younger Dryas coincided with a spike of relatively high IRD (Figure 6.14f), suggesting that the AIW was rather strong during this period, producing rapid iceberg calving (Jennings et al., 2006) that would only have allowed little drift ice to reach the area (low IP_{25}) and low primary productivity (low TOC and low brassicasterol). Indeed, Jennings et al. (2006) provided evidence for freshwater forcing from the GIS during the last deglaciation, and linked this freshwater event to the Younger Dryas abrupt cooling. Between ca. 12.6 – 12.2 cal. kyr BP (P-IIIa) all

biomarkers were absent or extremely low (Figure 6.14), pointing to more severe sea ice conditions during this period. Interestingly, a further light isotope event occurred at this time (Figure 6.16d), coinciding with an increase in IRD (Figure 6.14f). This event was also thought to be derived by a glacial meltwater event onto the shelf during retreat of the GIS (Jennings et al 2006) similar to that recorded during P-IIb. Therefore, a pronounced meltwater event from the GIS (larger than the previous recorded meltwater event at ca. 13.4 – 13.2 cal. kyr BP) resulted in reduced surface salinity which in turn promoted the formation of sea ice. Primary productivity was mainly absent during this period (as evidenced by low brassicasterol and low TOC), all supporting a near-permanent sea ice scenario during this interval. Periodic positive departures in IRD probably resulted from eventual sea ice break-up resulting in strong iceberg calving in glaciers from Kangerdlugssuaq and Geikie Plateau (Alonso-Garcia et al., 2013). After ca. 12.2 cal. kyr BP and up to the end of the Younger Dryas (ca. 11.5 cal. kyr BP; P-IIIb) IP_{25} was present and increased (although with very low fluxes), suggesting that the seasonal opening of waters allowed some drift ice to reach the area. A rapid increase in IP_{25} and diene II was observed at ca. 11.6 cal. kyr BP, which could indicate a period with significantly increased drift ice in the area (or *in situ* production), although any attempt at interpretation cannot be considered reliable on the basis of one data point. Previous studies around the southern Greenland area have shown anomalously warm conditions during the Younger Dryas compared to other north Atlantic regions. For example, a study based on a lake from the southern tip of Greenland (ca. 59˚N) suggested cold and dry winters during the Younger Dryas (Björck et al., 2002). In contrast, summers were suggested to be warmer due to increased summer insolation. Further, the surrounding ocean was thought to be ice covered most of the year as shown by a minimum of the sea-spray-indicating diatom *Achnanthes conspicua* (Björck et al., 2002). Similarly, Kuijpers et al. (2003) carried out a study (ca. 62˚N) to the south of

Kangerdlugssuaq Trough and did not find evidence of a return to extreme glacial conditions during the Younger Dryas. A previous study of the JM96-1213 core, by Jennings et al. (2006) also revealed the influence of Atlantic bottom waters during this period. However, the strong dominance of the polar foraminifera species *Neogloboquadrina pachyderma* suggested the existence of cold surface waters. Therefore, low biomarker fluxes between ca. 12.8 – 12.2 cal. kyr BP (P-IIIa, Figure 6.15d) may indicate the existence of locally produced sea ice conditions (permanent or near-permanent sea ice cover) with occasional sea ice retreat and rapid iceberg discharges (Alonso-Garcia et al., 2013) and scarce or infrequent drift ice reaching the area. In contrast, during the second part of the Younger Dryas (ca. 12.2 – 11.5 cal. kyr BP, P-IIIb, Figure 6.15e), sea ice conditions were less severe compared to the early Younger Dryas, characterised by intrusion of drift ice, and seasonal opening of waters during summer. This is in agreement with warmer Younger Dryas conditions found in previous studies around southern Greenland (Björck et al., 2002; Kuijpers et al., 2003; Jennings et al., 2006). The differences in seasonality observed between different areas of southern Greenland studies however, can also be due to local weather conditions as previously stated by Björck et al. (2002).

Interestingly, during P-IIIa and P-IIIb (Figure 6.15) the outcomes were very similar to those obtained by the model proposed in Part A. In the first place, during P-IIIa, more perennial sea ice and occasional sea ice retreat with rapid iceberg discharges was suggested (Figure 6.15d), with similar environmental conditions to those observed between AD 1850 – 1910 in the GKC cores (Figure 6.12). Secondly, during P-IIIb, less severe sea ice conditions, with seasonal opening of waters and slow iceberg calving and more drift ice from the Arctic Ocean reaching the study area were observed (Figure 6.15e), similar to those recorded between AD 1910 – 1986 in the GKC cores (Figure 6.12).

6.5.4.1.4 Period IV: 11.5 – 10.9 cal. kyr BP (Early Holocene)

During the last part of the record (ca. 11.5 – 10.9 cal. kyr BP; Period IV) IP_{25} and diene II fluxes were generally low (Figure 6.14a and Figure 6.14b), and slightly lower than during the second part of the Younger Dryas (P-IIIb). Sterol fluxes showed intermediate/low values compared to the rest of the record (Figure 6.14c and Figure 6.14d) and IRD was very low (Figure 6.14f). However, due to the absence of a well dated chronology after ca. 11.5 cal. kyr BP, any attempt at interpretation of these data could potentially be misleading or inaccurate, especially as biomarker data are presented as fluxes and sedimentation rates following the Younger Dryas may have changed significantly. Nevertheless, Jennings et al. (2011) suggested that this was a cold period influenced by the melting of the GIS both locally and along the EGC. Similarly, high percentages of *N. pachyderma*, alongside light isotope data were recorded in a core further south from JM96-1213 during this interval (Jennings et al., 2006) and ascribed due to cold surface conditions.

6.5.4.1.5 Summary

Based on the model proposed by Alonso-Garcia et al. (2013), the outcomes obtained as part of this study further suggest that the IP_{25} signal in the Kangerdlugssuaq area is mainly derived from drifted sea ice from the Arctic Ocean. The first thing to note within the current study (JM96-1213) is the significant influence that the advance of the GIS during the LGM, and its subsequent retreat, had in the Denmark Strait area during the investigated interval (ca. 16.3 – 10.9 cal. kyr BP) (e.g. Jennings et al., 2006; Wohlfarth et al., 2008). This was not the case in the interval covered by the GKC cores (ca. last 150 yr) as the GIS had already receded from the shelf and into the fjords (e.g. Funder and Hansen, 1996).

The biomarker and proxy data available for the current study (JM96-1213) show that more sea ice scenarios with different environmental conditions can be found in this area at different time intervals (Figure 6.15) other than the two proposed initially by Alonso-Garcia et al. (2013). Nevertheless, this study has shown that the initial model can be used as a basis for elucidating different environmental conditions over longer timescales, at least in the Kangerdlugssuaq Trough area. This study has also shown that some adaptation of the previous model is required in order to take into account the greater variability of the biomarker and proxy data presented in the JM96-1213 compared to the GKC cores and differentiate between more environmental conditions.

To this point, what remains uncertain is whether this model can be applied in nearby locations within the Denmark Strait area (e.g. Grivel Basin, Nansen Fjord). So far this has only been tested in the Kangerdlugssuaq Trough area, and therefore the analysis of more sediment cores around Denmark Strait that cover different time periods is needed to improve confidence in the model suggested.

6.5.4.2 Application of the PIP_{25} index

For the JM96-1213 core, a PIP_{25} index profile that resulted from the combination of IP_{25} fluxes with those of brassicasterol (Müller et al., 2011) is shown in Figure 6.16e. Between ca. 16.3 – 15.2 cal. kyr BP (P-I), PIP_{25} values are zero due to the absence of IP_{25} (Figure 6.16a), which, with the presence of only low brassicasterol fluxes (Figure 6.16b) points towards possibly ice-free conditions. However, the comparison of the biomarker data (absent IP_{25} and low brassicasterol) with other proxy data such as IRD (absent IRD), points to the presence of permanent sea ice conditions during this time interval in the Kangerdlugssuaq Trough. Additionally, high fluxes of IP_{25} and brassicasterol between ca. 15.2 – 14 cal. kyr BP (P-IIa) would be interpreted in the

PIP_{25} index as a marginal ice zone (PIP_{25} values between ca. 0.5 – 0.75), which is ruled out given the presence of very high IRD recorded at this time interval (Figure 6.16c), which suggests a scenario characterised by mixed conditions between high fluxes of icebergs being discharged from Kangerdlugssuaq Fjord (and nearby locations) and drift ice from the Arctic Ocean reaching the area.

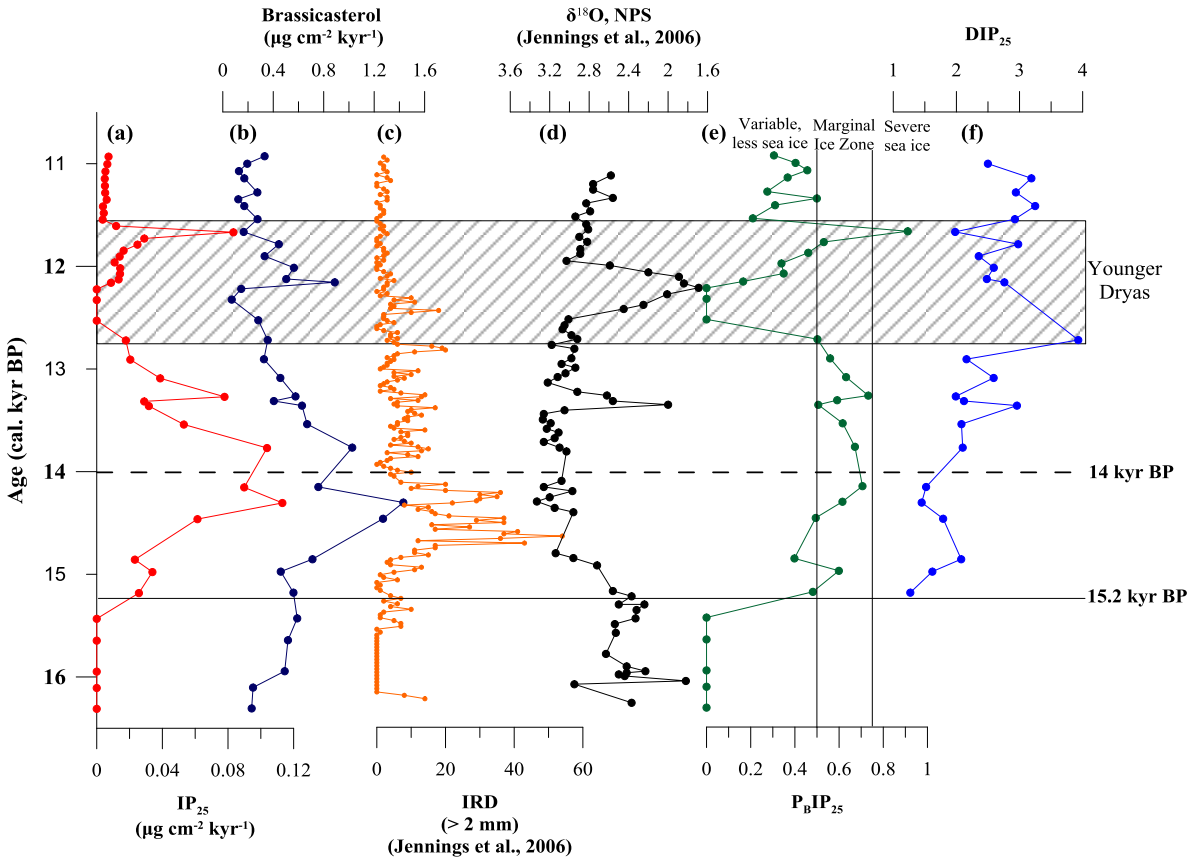

Figure 6.16: Individual temporal palaeclimate profiles for the JM96-1213 core: (a) IP_{25} fluxes; (b) brassicasterol fluxes; (c) IRD; (d) Planktic stable isotopes; (e) P_BIP_{25} index; (f) DIP_{25} ratio. The horizontal solid and dashed lines at ca. 15.2 cal. kyr BP and ca. 14 cal. kyr BP, respectively, represent shifts in the sea ice conditions. The rectangle between ca. 12.8 – 11.5 cal. kyr BP represents the Younger Dryas cold stadial.

Something to note at this point is the similarity of the brassicasterol and 24-methylenecholesterol profiles to those of IP_{25} and diene II (Figure 6.14). This feature is also mainly observed in the biomarker data (brassicasterol and IP_{25}) of the GKC cores (Figure 6.7). Brassicasterol fluxes were ca. 10 and 100 times higher than those of IP_{25} for the JM96-1213 core (Figure 6.14) and GKC cores, respectively (Figure 6.7). A

recent study by Belt et al. (2013b) observed the occurrence of brassicasterol and 24-methylenecholesterol in sea ice samples from Resolute Passage and the Amundsen Gulf. Individual sterol/IP_{25} ratios were determined in these sea ice samples. For example, mean brassicasterol/IP_{25} ratios of 11 and 35 were obtained for sea ice from Resolute Passage and the Amundsen Gulf, respectively. Similar ratios were obtained for 24-methylenecholesterol. In addition, these ratios were also obtained in surface sediments from the Canadian Arctic Archipelago with mean values of 9 and 1 for brassicasterol and 24-methyelencholesterol, respectively. These values were lower than those found in the sea ice samples. Belt et al. (2013b) postulated that the lower sterol/IP_{25} ratios observed in surface sediments compared to sea ice samples could indicate an important contribution of these sea ice derived sterols to the sedimentary sterol budget. Regarding the JM96-1213 core, values of 28 and 9 were obtained for brassicasterol/IP_{25} and 24-methylenecholesterol/IP_{25} ratios, respectively. These values were also quite low, consistent with the previous findings by Belt et al. (2013b). However, the lack of sea ice samples from this region prevented any further assessments. The lipid biomarker brassicasterol has previously been suggested as a suitable biomarker for representing open water conditions due to its phytoplanktonic origin (Müller et al., 2009; Müller et al., 2011). The similarity of the sterol profiles with those of IP_{25} and diene II in this study and the findings by Belt et al. (2013b), however, show that caution must be taken when interpreting the sterol biomarkers as their presence in the sediments could be due, in part to a contribution from sea ice.

A further caveat, or limitation of this approach, appears when the presence of IP_{25} is related to drift ice other than to locally produced sea ice, as noted here. In these cases, any attempt at calculating the PIP_{25} index would not give any indication of the presence of IP_{25} in the area as a result of ice being drifted from the Arctic Ocean, as this scenario is not contemplated in this approach.

Thus, the PIP_{25} index should be somehow modified to include these sea ice scenarios which given the complexity of the area, especially regarding the different sea ice conditions that need to be taken into account (landfast ice formation, iceberg calving from Greenland and drift ice transported from the Arctic Ocean by the EGC) would probably prove to be a very difficult task, if not incompatible with the principles of the PIP_{25} approach.

6.5.4.3 Application of the DIP_{25} ratio

Assessments regarding the relationship between IP_{25} and diene II as well as DIP_{25} ratios have been carried out previously (Chapter 4, section 4.5.3 and Chapter 5; section 5.5.3). Unlike these previous studies, however, where the presence of IP_{25} was attributed to locally produced sea ice (in the Denmark Strait area), the IP_{25} measured here most likely represents the signal of drift ice from the Arctic Ocean carried out by the EGC (Part A of this chapter). DIP_{25} ratios were calculated for the GKC cores and JM96-1213 (Note: when IP_{25} was absent, the DIP_{25} ratio could not be calculated; Figure 6.17). Comparison of DIP_{25} values between both studies (DIP_{25} values ranged between ca. 1.5 – 2.5 in the GKC cores (Figure 6.17a) and ca. 1 – 4 in the JM96-1213 core (Figure 6.17b)), showed that the ratio was relatively similar between both locations at different time scales.

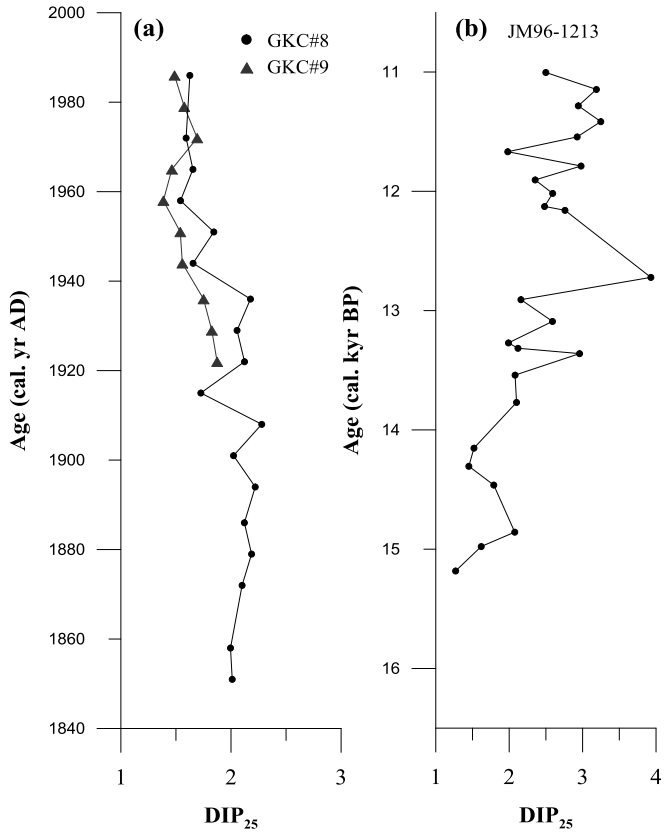

Figure 6.17: DIP_{25} index for (a) GKC cores and (b) JM96-1213 core.

In addition, linear correlations calculated for each core (Figure 6.18) showed a high degree of correlation between IP_{25} and diene II in both studies ($R^2 = 0.90 – 0.99$) further supporting the sea ice origin of diene II as suggested in previous studies (e.g. Belt et al., 2008; Vare et al., 2009; Massé et al., 2011). The gradient values of each linear correlation for both GKC cores were very similar (ca. 1.5), which is not surprising given that both cores are located close to each other and span the same time interval (last ca. 150 yr). Interestingly, the gradient value obtained for the correlation between IP_{25} and diene II in the JM96-1213 core, which is also located nearby to the GKC cores, but covers a different time period (ca. 16.3 – 10.9 cal. kyr BP), was also very similar (ca. 1.6) to those of the GKC cores (Figure 6.18).

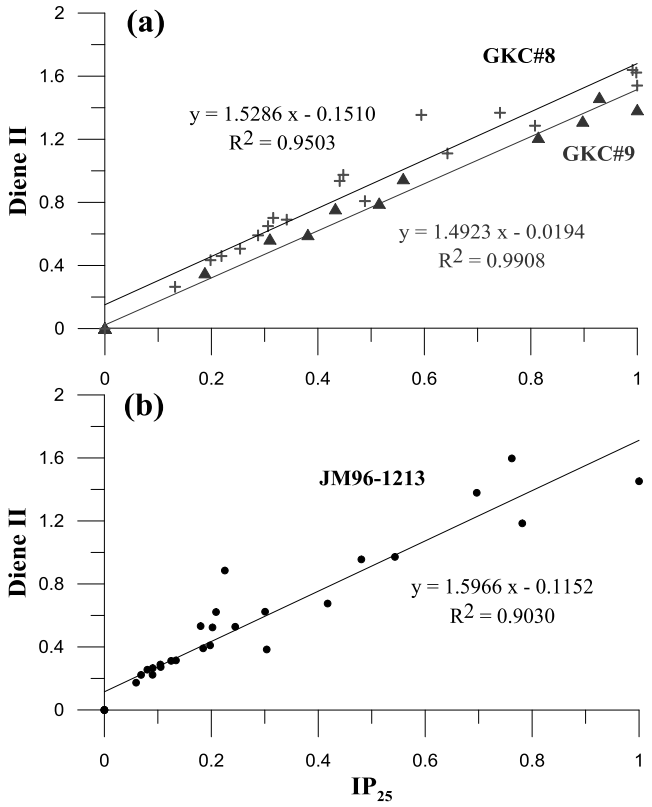

Figure 6.18: Relative abundances of Diene II *vs* IP_{25} for (a) GKC cores and (b) JM96-1213 core Relative abundances were normalised to the maximum values of IP_{25} observed for each dataset.

These outcomes suggest that there is possibly consistency in sea ice type, as in this case both studies (GKC cores and JM96-1213) are characterised by drift ice conditions. In contrast, the nature of sea ice bearing IP_{25} is probably different during different intervals for previously studied cores, where constant and fluctuating DIP_{25} values were suggested to indicate stable and variable sea ice conditions (locally produced sea ice), respectively (Chapter 4 and Chapter 5).

6.5.5 Conclusions

A reconstruction of the sea ice and oceanographic conditions from Kangerdlugssuaq Trough between ca. 16.3 – 10.9 cal. kyr BP, which included a multi-proxy study of biomarker data, in addition to mineralogical (IRD) and stable isotope ($\delta^{18}O$) data was carried out based on model proposed previously in Part A of this chapter.

The outcomes of this study showed that the principles behind the initial model provided the basis from which longer term palaeoclimatic reconstruction could be made. Additionally, this study showed that the model needed expanding to account for different environmental scenarios other than the two proposed initially during the last ca. 150 yr (Figure 6.12), especially due to the influence of the retreating GIS. As such, five distinct environmental scenarios were recreated within the studied interval. P-I (ca. 16.3 – 15.2 cal. kyr BP) was still under the influence of the expanded GIS and therefore severe sea ice conditions existed (permanent ice cover), which resulted in low or absent biomarker data and absent IRD with very low primary productivity (Figure 6.15a). During P-II (ca. 15.2 – 12.8 cal. kyr BP) all biomarker fluxes were relatively high, although this period was further subdivided in two sub-periods given by a shift in IRD counts at ca. 14 cal. kyr BP. During P-IIa (ca. 15.2 – 14 cal. kyr BP) the GIS had already retreated behind the core site. High fluxes of icebergs were being calved (high IRD) as a result of increased AIW and drift ice from the Arctic Ocean was also reaching the study area (high IP_{25} and diene II). Primary productivity was still limited due to the presence of abundant sea ice (Figure 6.15b). P-IIb (ca. 14 – 12.8 cal. kyr BP) was still influenced by the retreat of the GIS, some icebergs were released although to a lesser extent compared to P-IIa. Drift ice was still reaching the area and primary productivity was still rather limited (Figure 6.15c). The Younger Dryas, P-III (ca. 12.8 – 11.5 cal. kyr BP) was also further divided into two periods. During the first part, P-IIIa (ca. 12.8

– 12.2 cal. kyr BP) sea ice conditions were rather severe in this area, although occasional sea ice retreat with rapid iceberg discharges were recorded (Figure 6.15d), similar to those observed in the GKC cores during AD 1850 – 1910. During the late Younger Dryas, P-IIIb (ca. 12.2 – 11.5 cal. kyr BP), the environmental conditions were less severe, with seasonal opening of waters and some drift ice reaching the area together with some primary productivity allowed (Figure 6.15e), also similar to those observed in the GKC cores during AD 1910 – 1986. These findings were in line with milder conditions suggested from the same and nearby locations during the Younger Dryas (e.g. Björck et al., 2002; Kuijpers et al., 2003; Jennings et al., 2006).

In addition to this, the current study also enabled further discussion of the PIP_{25} approach, suggesting further limitations of this approach. For example, the most probable origin of IP_{25} from drifted ice from the Arctic Ocean in this region is not contemplated in the PIP_{25} approach and thus, the PIP_{25} index would not reveal any useful information regarding the sea ice conditions.

Further, the similarity between the IP_{25} and brassicasterol profiles in this study and in Part A of this chapter together with the recent findings by Belt et al. (2013b) suggested a possible common origin (sea ice) which could potentially result in misleading palaeoclimatic interpretations and therefore care must be taken when interpreting the biomarker brassicasterol.

Finally, regarding the DIP_{25} ratio, similar values were obtained for both cores spanning the last ca. 150 yr (GKC#8 and GKC#9 cores). Interestingly, similar values were also obtained for the JM96-1213 core which covers a very different time interval, further supporting the idea of consistency in sea ice type (drift ice) in both studies.

CHAPTER SEVEN

7 Conclusions and Future work

The main aim of this study was to reconstruct the sea ice conditions for a suite of sub-Arctic areas within the Greenland, Norwegian and Barents Seas, each of which represents contrasting oceanographic and environmental settings. In addition, the study focused mainly on the short-term cooling event (ca 12.9 – 11.5 cal. kyr BP), commonly referred to as the Younger Dryas, and the transition into the Holocene and onwards, which represented milder climate conditions. The reconstructions of the sea ice conditions described herein are based mainly on the occurrence and variable abundance of the organic geochemical biomarker IP_{25}, a proxy for seasonal sea ice in the Arctic.

In order to achieve this main aim, it was necessary to:

1. Isolate and confirm the structure of IP_{25} from Arctic marine sediments and obtain a GC-MS calibration of IP_{25} (and other HBIs), in order to permit accurate quantification in sediment extracts.

2. Use the IP_{25} sea ice proxy and other biomarkers to identify, unambiguously, sea ice occurrence during the Younger Dryas stadial from different sub-Arctic regions to better define the sea ice conditions.

3. Use a multi-proxy based approach, including the sea ice biomarker IP_{25}, to reconstruct the palaeo sea ice conditions in the western Barents Sea margin during the Holocene.

4. Carry out a multi-proxy based study to reconstruct the palaeo sea ice conditions in south-east Greenland during the last ca. 150 yr, to provide a model from which longer-term reconstructions could be made, and then test this model over longer time intervals.

5. Evaluate the usefulness of two new biomarker-based approaches to more detailed sea ice reconstruction (i.e. PIP_{25} and DIP_{25}) in different sub-Arctic areas covering different timescales.

In order to investigate these objectives, a number of Arctic marine sediment cores were analysed for IP_{25}, a related di-unsaturated HBI and various sterol biomarkers. In addition, these biomarker data were compared with other proxy data for the same cores, such as foraminiferal assemblages and IRD.

The **first aim** of this study was to confirm the chemical structure of IP_{25} from Arctic marine sediments and to obtain a GC-MS calibration of IP_{25} response in order to improve the accuracy of quantitative analytical measurements. Large amounts of sediment material (ca. 16.5 kg) were obtained from 3 locations within the Canadian Arctic Archipelago, extracted and purified using several chromatographic techniques and analysed by both NMR spectroscopy and GC-MS. This allowed the structure of IP_{25} in marine sediments to be confirmed as the same as that of a C_{25} monoene previously synthesised in the laboratory from a related C_{25} diene (Belt et al., 2007). In addition, the preparation of a series of standards of authentic IP_{25} (and internal standards) allowed the first thorough calibration of the GC-MS response factor between IP_{25} and the internal standard to be calculated and monitored on a routine basis. The fluctuation of the GC-

MS RF for IP_{25} (and other HBIs) showed that periodic calibration of the standards was needed (i.e. daily/weekly) for routine analysis of HBIs.

The **second aim** of this work was to identify and characterise the sea ice conditions during the Younger Dryas cold period within different sub-Arctic regions and compare the outcomes. Thus, the biomarker results provided some insights into the sea ice conditions during this period. In the first place, it is worth noting that the studied locations are characterised by different oceanographic and environmental settings. Regarding the present-day sea ice conditions, northern Norway is ice-free all year round, while the western Barents Sea lies close to the present day maximum sea ice extent with significant annual sea ice variability. A more contrasting setting is represented by the Greenland side of Denmark Strait, where more severe sea ice conditions exist. This region experiences 8 – 10 month sea ice cover in a year and is also influenced by large iceberg calving from east Greenland fjords and drift ice from the Arctic Ocean. Regional differences regarding climate conditions were also evident during the Younger Dryas from the biomarker data presented here. For example, the study from northern Norway (Chapter 4) provided unequivocal evidence for the occurrence of seasonal sea ice conditions during the Younger Dryas due to the occurrence of IP_{25} throughout this interval. The change in sea ice conditions at the onset and termination of the Younger Dryas in this location were especially clear (absent IP_{25} pre- and post-Younger Dryas), while in the study from western Barents Sea (Chapter 5) these transitions were less apparent, with IP_{25} being present both before and after (Figure 7.1). This difference was attributed to the presence of colder surface waters and the occurrence of seasonal sea ice before, during and after this stadial at higher latitudes. Previously, Rasmussen et al. (2007) also observed a less pronounced Younger Dryas

event at high latitudes (> 75˚ N) and attributed this to the presence of cold surface conditions leading up to and following this cold stadial. In Denmark Strait (Chapter 6, Part B) the onset and end of the Younger Dryas were also unclear, as this site also experienced sea ice conditions throughout the studied interval, consistent with modern observations.

Regarding the severity of the sea ice conditions during the Younger Dryas, some regional differences were observed, although an overall general picture is proposed with more severe sea ice conditions recorded during the early-mid Younger Dryas and less sea ice observed during the late Younger Dryas (Figure 7.1). However, the provenance of the IP_{25} sea ice signal was different amongst studies of different cores. For example, in northern Norway and the western Barents Sea, IP_{25} was probably of local origin, representing seasonal sea ice cover. Its absence in northern Norway pre- and post-Younger Dryas, therefore signified ice-free conditions. What remains unclear, at this point, is whether the sea ice started to form in more northern locations at the onset of the Younger Dryas and then extended southwards reaching northern Norway, or if regional conditions would have promoted the formation of localised land fast ice. Previous studies have shown that Norway was influenced by the Eurasian ice sheet prior to the Younger Dryas (e.g. Fahl and Stein, 2012), and this suggests that, most probably, the sea ice was locally produced. Future work related to the origin of the sea ice during the Younger Dryas would, therefore, be needed and could potentially be achieved by studying a number of cores, ideally those representing north-south and west-east transects.

Conversely, it is suggested that IP_{25} in sediments from Denmark Strait was derived mainly from drift ice, although local severe sea ice conditions prevail most of the year.

Hence, the absence of IP_{25} during the early Younger Dryas recorded in Denmark Strait (Figure 7.1) indicated a period characterised by (near) perennial sea ice cover.

In addition, the stability or consistency of the sea ice conditions during this cold stadial was also evaluated. For instance, in northern Norway, stable, then variable, seasonal sea ice conditions were predicted during the early-mid and late Younger Dryas, respectively, and this was supported by reconstructed SST for the same location and by a previous study in southern Norway (Bakke et al., 2009). The results from the western Barents Sea indicated more consistent seasonal sea ice conditions throughout the whole period and this suggested that the stability of the sea ice conditions during the Younger Dryas increased towards northern latitudes. This, in turn, could be attributed to a reduced influence of Atlantic waters or southward movement of the Polar Front.

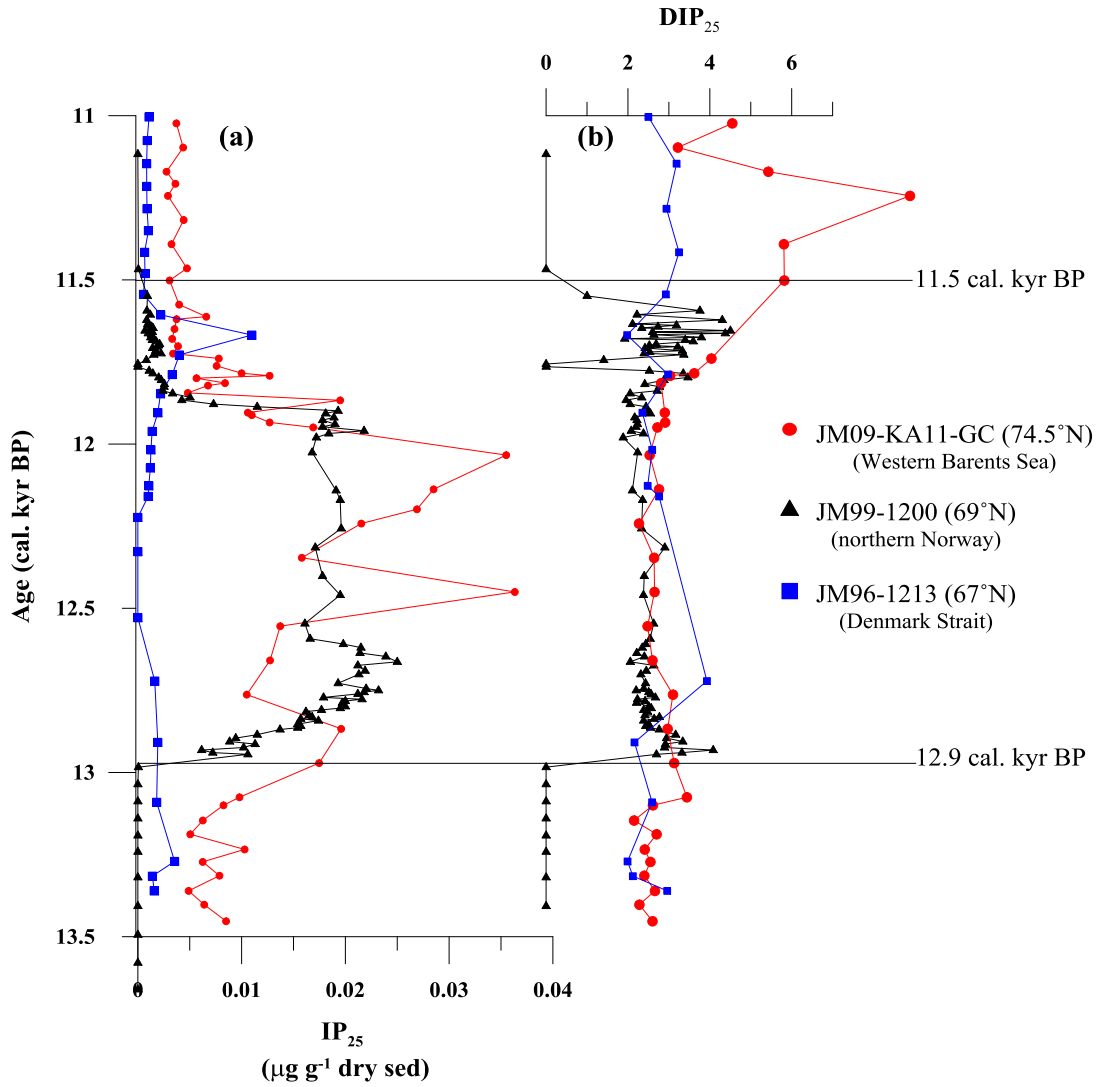

Figure 7.1: Temporal palaeoclimate profiles (a) IP_{25} concentrations; (b) DIP_{25} ratio from three different sub-Arctic regions.

The **third aim** of the study was to reconstruct the sea ice conditions from the western Barents Sea during the Holocene using a multi-proxy based approach. In order to do this, four researchers within the CASE network (including this study) analysed the same sediment core for different proxies such as biomarkers (IP_{25}, diene II and sterols), benthic and planktic foraminifera and dinocysts. A comparison of all proxy data showed a generally good agreement (Chapter 5) and it is proposed that the Holocene could be divided into three main climate periods. During the early Holocene (ca. 11.9 – 9.5 cal. kyr BP), the position of the ice edge was close to the study area resulting in high

productivity during summers. In the mid-late Holocene (ca. 9.5 – 1.6 cal. kyr BP), sea ice was mainly absent due to the increased influence of Atlantic waters and northward movement of the Polar Front. All proxy data pointed to a rather stable climate at this time. Finally, the last ca. 1.6 cal. kyr BP were characterised by sea ice conditions similar to those of the present day. Palaeoclimate studies are often limited by focusing on an individual proxy (e.g. foraminifera, IRD, dinocysts, GDGTs). However, the outcomes from this study show that the use of a multi-proxy approach provides a more complete picture of the climate conditions for a given period as it combines several aspects of the environment (e.g. water masses, sea ice, surface water conditions). Further, previous studies from the northern North Atlantic and close to the core site have recorded clear climate changes such as the Holocene Thermal Maximum warming, a cooling trend from the early to the mid-late Holocene, or the 8.2 kyr cooling event (e.g. Sarnthein et al., 2003b; Hald et al., 2007). These, however, were not clearly recorded within the JM09-KA11-GC core site and some explanations for this have been provided (Chapter 5).

The **fourth aim** of this work was to characterise the sea ice conditions from a very contrasting setting compared to the Norwegian-Barents Sea region, namely Denmark Strait which separates East Greenland and Iceland. Here, data from several proxies from 3 short cores covering the last ca. 150 yr from Kangerdlugssuaq Trough within Denmark Strait were compared with historical observations of climate conditions (e.g. temperature and sea ice) and this was used to develop a model of sea ice conditions which was then tested for longer time-scales. In the first place, it was suggested that the IP_{25} in sediments from this region was mainly derived from drift ice carried from the Arctic Ocean via the EGC. The model included two different environmental scenarios:

one where the sea ice conditions were more severe (ca. AD 1850 – 1910) with perennial sea ice conditions, and hence very low primary productivity, and a second, where the local sea ice conditions were less severe (ca. AD 1910 – 1986) with increased drift ice and enhanced primary productivity. This two-component model was subsequently tested through analysis of a sediment core from the same area, covering an older climatic period (ca. 16.3 – 10.9 cal. kyr BP). This core was studied for biomarkers and comparisons were made with existing data (e.g. IRD, stable oxygen isotopes). As a result, some adaptations to the initial model were required in order to account for different environmental scenarios, especially as the core site was influenced by the retreating GIS after the LGM. In the future, it will be interesting to see if this model can be used in different areas within the Denmark Strait (e.g. Scoresby Sund, Nansen Trough, Grivel Basin) or across Greenland and at different time intervals (e.g. Holocene). Therefore, this needs to be tested further by carrying out additional multi-proxy studies.

The investigation of IP_{25} in three different areas with different oceanographic and sea ice conditions has shown that IP_{25} can represent different sea ice settings, including locally produced landfast ice in addition to drift ice exported from elsewhere. Although IP_{25} found in the Denmark Strait area (Chapter 6) was suggested to be derived from drift ice this needs to be further confirmed, ideally through analysis and comparison of sea ice samples and underlying surface sediments.

The **fifth aim** of this work was to test two combined biomarker approaches (the PIP_{25} and DIP_{25} indices) for quantifying and/or refining definitions of sea ice conditions. Within this study, the PIP_{25} index was tested first in a sediment core from northern Norway during the Younger Dryas (Chapter 4). Firstly, IP_{25} and brassicasterol

concentrations showed opposite trends, consistent with their sea ice and phytoplankton origins, respectively. Secondly, the PIP_{25}-based estimated ranges in sea ice concentrations calculated according to the method of Müller et al. (2011) were consistent with the individual biomarker and other proxy data. For example, abrupt transitions such as the onset of the Younger Dryas were clearly recorded within the PIP_{25} profile. However, when this (PIP_{25}) approach was tested in other sub-Arctic locations, such as the western Barents Sea (Chapter 5) and Denmark Strait (Chapter 6, Part B) some anomalies with this approach were identified. It has previously been suggested by Belt and Müller (2013) that the use of a correction term ('c') in the PIP_{25} index to account for differences in biomarker concentrations could appear problematic in some palaeo sea ice reconstructions and this was shown to be the case for a surface calibration study in the Barents Sea (Navarro-Rodriguez et al., 2013). The sediment core from the western Barents Sea covered the last ca. 15.7 cal. kyr BP. Depending on the geological period studied, (i.e. Holocene, Younger Dryas, Bølling – Allerød) and on the distribution of these biomarkers (low, medium or high) within each period, different c factor values were obtained which, in turn, had an impact on sea ice concentration estimates. In addition, unlike in the study from northern Norway, IP_{25} and brassicasterol followed a rather similar trend. In some cases, in-phase fluctuations of both biomarkers (both low or both high) resulted in similar PIP_{25} values, even if they reflected known different sea ice scenarios (e.g. near-permanent sea ice and marginal ice zone, respectively) showing the need to consider the individual biomarker profiles in addition to the PIP_{25} index. Regarding the Denmark Strait area (Chapter 6), IP_{25} and brassicasterol profiles were also very similar. These observations further suggest that the previous assumption that brassicasterol represents open water (e.g. Müller et al., 2009) is not valid as it is also found in sea ice (Belt et al., 2013b). In addition, attempts to use the PIP_{25} index in the Denmark Strait resulted in misleading results, possibly as

the IP_{25} signal is thought to be derived from drift ice from the Arctic Ocean and this scenario is not considered in the PIP_{25} approach.

The outcomes from the current study show that the PIP_{25} index may be suitable when the brassicasterol signal is mainly derived from open-water phytoplankton (Chapter 4) but fails to provide a good interpretation in areas where there is co-production within different environments (e.g. sea ice). Thus, more research is needed to overcome potential caveats related to this approach and ultimately, improve or identify a better approach for making biomarker-based quantitative measures of sea ice reconstruction.

The relationship between IP_{25} and the HBI diene II (e.g. via the DIP_{25} ratio) within this study has provided some potential insight regarding further descriptions of sea ice conditions, such as variability (or otherwise) in sea ice occurrence. However, this approach, and the interpretation of the DIP_{25} ratio, in particular, needs to be tested much more rigorously, especially within areas with known sea ice conditions (i.e. variable *versus* stable). In addition, some issues regarding the chromatographic separation of diene II and other di-unsaturated HBIs encountered within this research (Chapter 5) need to be addressed in order that interpretations based on these biomarkers can be carried out with confidence.

Finally, regarding the preservation methods for sediment samples prior to biomarker analyses, some disparity in the results obtained for samples from the same core and same depths, but kept in different ways and sub-sampled at different times during this research (Chapter 4) was observed. The observations described here therefore suggest that a more systematic study is needed.

REFERENCES

Aagaard-Sørensen, S., Husum, K., Hald, M., Knies, J., 2010. Paleoceanographic development in the SW Barents Sea during the Late Weichselian–Early Holocene transition. Quaternary Science Reviews 29, 3442-3456.

Aagaard-Sørensen, S., Husum, K., Cabedo-Sanz, P., Belt, S.T., Forwick, M., Andreassen, K., Hald, M., *In prep*. Paleoceanographic reconstruction at the western Barents Sea Margin during the last deglaciation.

Aagaard, K., Coachman, L.K., 1968. The East Greenland Current north of Denmark Strait: Part I. Arctic 21, 181-200.

Aagaard, K., Carmack, E., 1989. The role of sea ice and other fresh water in the Arctic circulation. Journal of Geophysical Research 94, 485-414.

Allard, G., Belt, S.T., Massé, G., Naumann, R., Robert, J.-M., Rowland, S., 2001. Tetra-unsaturated sesterterpenoids (Haslenes) from *Haslea ostrearia* and related species. Phytochemistry 56, 795-800.

Alley, R.B., Meese, D., Shuman, C., Gow, A., Taylor, K., Grootes, P., White, J., Ram, M., Waddington, E., Mayewski, P., 1993. Abrupt increase in Greenland snow accumulation at the end of the Younger Dryas event. Nature 362, 527-529.

Alley, R.B., 2000. The Younger Dryas cold interval as viewed from central Greenland. Quaternary Science Reviews 19, 213-226.

Alley, R.B., Marotzke, J., Nordhaus, W., Overpeck, J., Peteet, D., Pielke Jr, R., Pierrehumbert, R., Rhines, P., Stocker, T., Talley, L., 2003. Abrupt climate change. Science 299, 2005-2010.

Alonso-Garcia, M., Andrews, J.T., Cabedo-Sanz, P., Darby, D.A., Jaeger, J., 2013. A comparison between multi-proxy and historical data (AD 1990-1840) of drift-ice conditions on the East Greenland shelf (~66°N). The Holocene 23, doi: 10.1177/0959683613505343.

Alvarez-Solas, J., Charbit, S., Ritz, C., Paillard, D., Ramstein, G., Dumas, C., 2010. Links between ocean temperature and iceberg discharge during Heinrich events. Nature Geoscience 3, 122-126.

Andersen, C., Koç, N., Jennings, A., Andrews, J.T., 2004a. Nonuniform response of the major surface currents in the Nordic Seas to insolation forcing: Implications for the Holocene climate variability. Paleoceanography 19, PA2003.

Andersen, C., Koç, N., Moros, M., 2004b. A highly unstable Holocene climate in the subpolar North Atlantic: evidence from diatoms. Quaternary Science Reviews 23, 2155-2166.

Andersson, C., Pausata, F., Jansen, E., Risebrobakken, B., Telford, R., 2010. Holocene trends in the foraminifer record from the Norwegian Sea and the North Atlantic Ocean. Climate of the Past 6, 179-193.

Andreassen, K., Laberg, J.S., Vorren, T.O., 2008. Seafloor geomorphology of the SW Barents Sea and its glaci-dynamic implications. Geomorphology 97, 157-177.

Andresen, C., Hansen, M., Seidenkrantz, M., Jennings, A., Knudsen, M., Nørgaard-Pedersen, N., Larsen, N., Kuijpers, A., Pearce, C., 2013. Mid-to late-Holocene oceanographic variability on the Southeast Greenland shelf. The Holocene 23, 167-178.

Andresen, C.S., Björck, S., 2005. Holocene Climate Variability in the Denmark Strait Region-a Land Sea Correlation of New and Existing Climate Proxy Records. Geografiska Annaler: Series A, Physical Geography 87, 159-174.

Andrews, J., Milliman, J., Jennings, A., Rynes, N., Dwyer, J., 1994. Sediment thicknesses and Holocene glacial marine sedimentation rates in three East Greenland fjords (ca. 68˚N). The Journal of Geology 102, 669-683.

Andrews, J., Cooper, T., Jennings, A., Stein, A., Erlenkeuser, H., 1998. Late Quaternary iceberg-rafted detritus events on the Denmark Strait-Southeast Greenland continental slope (65° N): related to North Atlantic Heinrich events? Marine Geology 149, 211-228.

Andrews, J., Belt, S., Olafsdottir, S., Massé, G., Vare, L., 2009. Sea ice and marine climate variability for NW Iceland/Denmark Strait over the last 2000 cal. yr BP. The Holocene 19, 775.

Andrews, J., 2011. Unraveling Sediment Transport Along Glaciated Margins (the Northwestern Nordic Seas) Using Quantitative X-Ray Diffraction of Bulk (< 2mm) sediment. In: Bhuiyan, A.F. (Ed), Sediment Transport. InTech, Rijeka, 225-248.

Andrews, J., Eberl, D., 2012. Determination of sediment provenance by unmixing the mineralogy of source-area sediments: The "SedUnMix" program. Marine Geology 291, 24-33.

Andrews, J.T., Smith, L.M., Preston, R., Cooper, T., Jennings, A.E., 1997. Spatial and temporal patterns of iceberg rafting (IRD) along the East Greenland margin, ca. 68˚N, over the last 14 cal. ka. Journal of Quaternary Science 12, 1-13.

Andrews, J.T., 2000. Icebergs and iceberg rafted detritus (IRD) in the North Atlantic: facts and assumptions. Oceanography 13, 100-108.

Andrews, J.T., Giraudeau, J., 2003. Multi-proxy records showing significant Holocene environmental variability: the inner N. Iceland shelf (Húnaflói). Quaternary Science Reviews 22, 175-193.

Andrews, J.T., Eberl, D.D., 2007. Quantitative mineralogy of surface sediments on the Iceland shelf, and application to down-core studies of Holocene ice-rafted sediments. Journal of Sedimentary Research 77, 469-479.

Andrews, J.T., Jennings, A.E., Coleman, G.C., Eberl, D.D., 2010. Holocene variations in mineral and grain-size composition along the East Greenland glaciated margin (ca 67°-70° N): Local versus long-distance sediment transport. Quaternary Science Reviews 29, 2619-2632.

Andrews, J.T., Jennings, A.E., 2013. Multi-decadal to-century NAO-like marine climate oscillations across the Denmark Strait (~66°N) over the last 2000 cal yr BP. Climate of the Past 9, 1-47, doi:10.5194/cpd-5199-5191-2013.

Antoniades, D., Francus, P., Pienitz, R., St-Onge, G., Vincent, W.F., 2011. Holocene dynamics of the Arctic's largest ice shelf. Proceedings of the National Academy of Sciences 108, 18899-18904.

Archer, D., Maier-Reimer, E., 1994. Effect of deep-sea sedimentary calcite preservation on atmospheric CO_2 concentration. Nature 367, 260-263.

Axford, Y., Andresen, C.S., Andrews, J.T., Belt, S.T., Geirsdóttir, Á., Massé, G., Miller, G.H., Ólafsdóttir, S., Vare, L.L., 2011. Do paleoclimate proxies agree? A test comparing 19 late Holocene climate and sea-ice reconstructions from Icelandic marine and lake sediments. Journal of Quaternary Science 26, 645-656.

Bakke, J., Lie, Ø., Heegaard, E., Dokken, T., Haug, G.H., Birks, H.H., Dulski, P., Nilsen, T., 2009. Rapid oceanic and atmospheric changes during the Younger Dryas cold period. Nature Geoscience 2, 202-205.

Baldini, J.U., McDermott, F., Fairchild, I.J., 2002. Structure of the 8200-year cold event revealed by a speleothem trace element record. Science 296, 2203-2206.

Bauch, H.A., Erlenkeuser, H., Spielhagen, R.F., Struck, U., Matthiessen, J., Thiede, J., Heinemeier, J., 2001. A multiproxy reconstruction of the evolution of deep and

surface waters in the subarctic Nordic seas over the last 30,000 yr. Quaternary Science Reviews 20, 659-678.

Baumann, K.H., Andruleit, H., Samtleben, C., 2000. Coccolithophores in the Nordic Seas: comparison of living communities with surface sediment assemblages. Deep Sea Research Part II: Topical Studies in Oceanography 47, 1743-1772.

Bé, A.W., Tolderlund, D.S., 1971. Distribution and ecology of living planktonic foraminifera in surface waters of the Atlantic and Indian Oceans. Cambridge University Press, London.

Beer, C.J., Schiebel, R., Wilson, P.A., 2010. Testing planktic foraminiferal shell weight as a surface water [CO_3^{2-}] proxy using plankton net samples. Geology 38, 103-106.

Belkin, I.M., Levitus, S., Antonov, J., Malmberg, S.-A., 1998. "Great salinity anomalies" in the North Atlantic. Progress in Oceanography 41, 1-68.

Belt, S.T., Allard, W.G., Massé, G., Robert, J.-M., Rowland, S.J., 2000a. Highly branched isoprenoids (HBIs): identification of the most common and abundant sedimentary isomers. Geochimica et Cosmochimica Acta 64, 3839-3851.

Belt, S.T., Allard, W.G., Rintatalo, J., Johns, L.A., van Duin, A.C.T., Rowland, S.J., 2000b. Clay and acid catalysed isomerisation and cyclisation reactions of highly branched isoprenoid (HBI) alkenes: implications for sedimentary reactions and distributions. Geochimica et Cosmochimica Acta 64, 3337-3345.

Belt, S.T., Allard, W.G., Massé, G., Robert, J.-M., Rowland, S.J., 2001a. Structural characterisation of C_{30} highly branched isoprenoid alkenes (*rhizenes*) in the marine diatom *Rhizosolenia setigera*. Tetrahedron Letters 42, 5583-5585.

Belt, S.T., Massé, G., Allard, W.G., Robert, J.-M., Rowland, S.J., 2001b. C_{25} highly branched isoprenoid alkenes in planktonic diatoms of the *Pleurosigma genus*. Organic Geochemistry 32, 1271-1275.

Belt, S.T., Massé, G., Allard, W.G., Robert, J.-M., Rowland, S.J., 2001c. Identification of a C_{25} highly branched isoprenoid triene in the freshwater diatom *Navicula sclesvicensis*. Organic Geochemistry 32, 1169-1172.

Belt, S.T., Massé, G., Rowland, S.J., Rohmer, M., 2006. Highly branched isoprenoid alcohols and epoxides in the diatom *Haslea ostrearia* Simonsen. Organic Geochemistry 37, 133-145.

Belt, S.T., Massé, G., Rowland, S.J., Poulin, M., Michel, C., LeBlanc, B., 2007. A novel chemical fossil of palaeo sea ice: IP_{25}. Organic Geochemistry 38, 16-27.

Belt, S.T., Massé, G., Vare, L.L., Rowland, S.J., Poulin, M., Sicre, M.-A., Sampei, M., Fortier, L., 2008. Distinctive ^{13}C isotopic signature distinguishes a novel sea ice biomarker in Arctic sediments and sediment traps. Marine Chemistry 112, 158-167.

Belt, S.T., Vare, L.L., Massé, G., Manners, H.R., Price, J.C., MacLachlan, S.E., Andrews, J.T., Schmidt, S., 2010. Striking similarities in temporal changes to spring sea ice occurrence across the central Canadian Arctic Archipelago over the last 7000 years. Quaternary Science Reviews 29, 3489-3504.

Belt, S.T., Brown, T.A., Cabedo-Sanz, P., Navarro-Rodriguez, A., 2012a. Structural confirmation of the sea ice biomarker IP_{25} found in Arctic marine sediments. Environmental Chemistry Letters 10, 189-192.

Belt, S.T., Brown, T.A., Navarro Rodriguez, A., Cabedo Sanz, P., Tonkin, A., Ingle, R., 2012b. A reproducible method for the extraction, identification and quantification of the Arctic sea ice proxy IP_{25} from marine sediments. Analytical Methods 4, 705-713.

Belt, S.T., Brown, T.A., Ampel, L., Cabedo-Sanz, P., Fahl, K., Kocis, J., Massé, G., Navarro-Rodriguez, A., Ruan, J., Xu, Y., 2013a. An inter-laboratory investigation

of the Arctic sea ice biomarker proxy IP_{25} in marine sediments: key outcomes and recommendations. Climate of the Past 9, 5263-5298, doi:5210.5194/cpd-5269-5263-2013.

Belt, S.T., Brown, T.A., Ringrose, A.E., Cabedo-Sanz, P., Mundy, C.J., Gosselin, M., Poulin, M., 2013b. Quantitative measurement of the sea ice diatom biomarker IP_{25} and sterols in Arctic sea ice and underlying sediments: Further considerations for palaeo sea ice reconstrucion. Organic Geochemistry 62, 33-45.

Belt, S.T., Müller, J., 2013. The Arctic sea ice biomarker IP_{25}: a review of current understanding, recommendations for future research and applications in palaeo sea ice reconstructions. Quaternary Science Reviews 79, 9-25.

Berben, S.M.P., Husum, K., Cabedo-Sanz, P., Belt, S.T., 2013. Holocene sub centennial evolution of Atlantic water inflow and sea ice distribution in the western Barents Sea. Climate of the Past 9, 4893-4938, doi:4810.5194/cpd-4899-4893-2013.

Bergami, C., Capotondi, L., Langone, L., Giglio, F., Ravaioli, M., 2009. Distribution of living planktonic foraminifera in the Ross Sea and the Pacific sector of the Southern Ocean (Antarctica). Marine Micropaleontology 73, 37-48.

Bigg, G.R., 1999. An estimate of the flux of iceberg calving from Greenland. Arctic, Antarctic and Alpine Research 31, 174-178.

Bischof, J.F., Darby, D.A., 2000. Quaternary ice transport in the Canadian Arctic and extent of Late Wisconsinan glaciation in the Queen Elizabeth Islands. Canadian Journal of Earth Sciences 36, 2007-2022.

Björck, S., Rundgren, M., Ingolfsson, O., Funder, S., 1997. The Preboreal oscillation around the Nordic Seas: terrestrial and lacustrine responses. Journal of Quaternary Science 12, 455-465.

Björck, S., Bennike, O., Rosén, P., Andresen, C.S., Bohncke, S., Kaas, E., Conley, D., 2002. Anomalously mild Younger Dryas summer conditions in southern Greenland. Geology 30, 427-430.

Björnsson, H., 1969. Sea ice conditions and the atmospheric circulation north of Iceland. Jokull 19, 11-28.

Blindheim, J., Malmberg, S., 2005. The mean sea level pressure gradient across the Denmark Strait as an indicator of conditions in the North Icelandic Irminger Current. Geophysical Monograph-American Geophysical Union 158, 65-71.

Boltovskoy, E., Boltovskoy, D., Brandini, F., 2000. Planktonic foraminífera from south-western Atlantic epipelagic waters: abundance, distribution and year-to-year variations. Journal of the Marine Biological Association of the UK 80, 203-213.

Bond, G., Kromer, B., Beer, J., Muscheler, R., Evans, M.N., Showers, W., Hoffmann, S., Lotti-Bond, R., Hajdas, I., Bonani, G., 2001. Persistent solar influence on North Atlantic climate during the Holocene. Science 294, 2130-2136.

Bond, G.C., Lotti, R., 1995. Iceberg Discharges into the North Atlantic on Millennial Time Scales During the Last Glaciation. Science 267, 1005-1010.

Bondevik, S., Birks, H.H., Gulliksen, S., Mangerud, J., 1999. Late Weichselian marine ^{14}C reservoir ages at the Western Coast of Norway. Quaternary Research 52, 104-114.

Bondevik, S., Mangerud, J., Birks, H.H., Gulliksen, S., Reimer, P.J., 2006. Changes in North Atlantic radiocarbon reservoir ages during the Allerød and Younger Dryas. Science 312, 1514-1517.

Brassell, S., Eglinton, G., Marlowe, I., Pflaumann, U., Sarnthein, M., 1986. Molecular stratigraphy: a new tool for climatic assessment. Nature 320, 129-133.

Brauer, A., Haug, G.H., Dulski, P., Sigman, D.M., Negendank, J.F.W., 2008. An abrupt wind shift in western Europe at the onset of the Younger Dryas cold period. Nature Geoscience 1, 520-523.

Broecker, W., Clark, E., 2001. An evaluation of Lohmann's foraminifera weight dissolution index. Paleoceanography 16, 531-534.
Broecker, W.S., 2003. Does the trigger for abrupt climate change reside in the ocean or in the atmosphere? Science 300, 1519-1522.
Brown, T.A., 2011. Production and preservation of the Arctic sea ice diatom biomarker IP_{25}, *PhD Thesis*, University of Plymouth.
Brown, T.A., Belt, S.T., Philippe, B., Mundy, C.J., Massé, G., Poulin, M., Gosselin, M., 2011. Temporal and vertical variations of lipid biomarkers during a bottom ice diatom bloom in the Canadian Beaufort Sea: further evidence for the use of the IP_{25} biomarker as a proxy for spring Arctic sea ice. Polar Biology 34, 1857-1868.
Cabedo-Sanz, P., Belt, S.T., Knies, J., Husum, K., 2013. Identification of contrasting seasonal sea ice conditions during the Younger Dryas. Quaternary Science Reviews 79, 74-86.
Carstens, J., Hebbeln, D., Wefer, G., 1997. Distribution of planktic foraminifera at the ice margin in the Arctic (Fram Strait). Marine Micropaleontology 29, 257-269.
Caseldine, C.J., Turney, C., Long, A.J., 2010. IPCC and palaeoclimate–an evolving story? Journal of Quaternary Science 25, 1-4.
Clark, P.U., Marshall, S.J., Clarke, G.K.C., Hostetler, S.W., Licciardi, J.M., Teller, J.T., 2001. Freshwater forcing of abrupt climate change during the last glaciation. Science 293, 283-287.
Clark, P.U., Dyke, A.S., Shakun, J.D., Carlson, A.E., Clark, J., Wohlfarth, B., Mitrovica, J.X., Hostetler, S.W., McCabe, A.M., 2009. The last glacial maximum. Science 325, 710-714.
Clark, P.U., Shakun, J.D., Baker, P.A., Bartlein, P.J., Brewer, S., Brook, E., Carlson, A.E., Cheng, H., Kaufman, D.S., Liu, Z., Marchitto, T.M., Mix, A.C., Morrill, C., Otto-Bliesner, B.L., Pahnke, K., Russell, J.M., Whitlock, C., Adkins, J.F., Blois, J.L., Clark, J., Colman, S.M., Curry, W.B., Flower, B.P., He, F., Johnson, T.C., Lynch-Stieglitz, J., Markgraf, V., McManus, J., Mitrovica, J.X., Moreno, P.I., Williams, J.W., 2012. Global climate evolution during the last deglaciation. Proceedings of the National Academy of Sciences 109, E1134-E1142.
Comiso, J.C., Parkinson, C.L., 2004. Satellite-Observed Changes in the Arctic. Physics Today 57, 38-44.
Condron, A., Winsor, P., 2012. Meltwater routing and the Younger Dryas. Proceedings of the National Academy of Sciences 109, 19928-19933.
Cooke, S., Rohling, E.J., 2001. Stable Isotopes in Foraminiferal Carbonate. Southampton Oceanography Centre Internal Document 72.
Cronin, T.M., Holtz, T.R., Whatley, R.C., 1994. Quaternary paleoceanography of the deep Arctic Ocean based on quantitative analysis of Ostracoda. Marine Geology 119, 305-332.
Cronin, T.M., Gemery, L., Briggs Jr, W.M., Jakobsson, M., Polyak, L., Brouwers, E.M., 2010. Quaternary Sea-ice history in the Arctic Ocean based on a new Ostracode sea-ice proxy. Quaternary Science Reviews 29, 3415-3429.
Cronin, T.M., Polyak, L., Reed, D., Kandiano, E.S., Marzen, R.E., Council, E.A., 2013. A 600-ka Arctic sea-ice record from Mendeleev Ridge based on ostracodes. Quaternary Science Reviews 79, 157-167.
Crosta, X., Koç, N., 2007. Chapter Eight Diatoms: From Micropaleontology to Isotope Geochemistry, In: Claude, H.-M., Anne De, V. (Eds.), Developments in Marine Geology. Elsevier, pp. 327-369.
Darby, D.A., 2003. Sources of sediment found in sea ice from the western Arctic Ocean, new insights into processes of entrainment and drift patterns. Journal of Geophysical Research 108, doi: 1111029/1112002JC1001350, 1112003.

Darby, D.A., Bischof, J.F., 2004. A Holocene record of changing Arctic Ocean ice drift analogous to the effects of the Arctic Oscillation. Paleoceanography 19, PA1027.

Darby, D.A., Ortiz, J.D., Grosch, C.E., Lund, S.P., 2012. 1,500-year cycle in the Arctic Oscillation identified in Holocene Arctic sea-ice drift. Nature Geoscience, doi: 10.1038/NGEO1629.

de Vernal, A., Hillaire-Marcel, C., Grafenstein, U., Barber, D., 1997. Researchers look for links among paleoclimate events. Eos, Transactions American Geophysical Union 78, 247-249.

de Vernal, A., Henry, M., Matthiessen, J., Mudie, P.J., Rochon, A., Boessenkool, K.P., Eynaud, F., Grøsfjeld, K., Guiot, J., Hamel, D., 2001. Dinoflagellate cyst assemblages as tracers of sea-surface conditions in the northern North Atlantic, Arctic and sub-Arctic seas: The new 'n= 677'data base and its application for quantitative palaeoceanographic reconstruction. Journal of Quaternary Science 16, 681-698.

de Vernal, A., Gersonde, R., Goosse, H., Seidenkrantz, M.-S., Wolff, E.W., 2013a. Sea ice in the paleoclimate system: the challenge of reconstructing sea ice from proxies – an introduction. Quaternary Science Reviews 79, 1-8.

de Vernal, A., Hillaire-Marcel, C., Rochon, A., Fréchette, B., Henry, M., Solignac, S., Bonnet, S., 2013b. Dinocyst-based reconstructions of sea ice cover concentration during the Holocene in the Arctic Ocean, the northern North Atlantic Ocean and its adjacent seas. Quaternary Science Reviews 79, 111-121.

Denton, G.H., Alley, R.B., Comer, G.C., Broecker, W.S., 2005. The role of seasonality in abrupt climate change. Quaternary Science Reviews 24, 1159-1182.

Dickson, R.R., Meincke, J., Malmberg, S.-A., Lee, A.J., 1988. The "great salinity anomaly" in the northern North Atlantic 1968–1982. Progress in Oceanography 20, 103-151.

Dieckmann, G.S., Hellmer, H.H., 2010. The importance of sea ice: an overview, in *Sea Ice*, ed. D. Thomas and G.S. Dieckmann, Blackwell Publishing Ltd.

Divine, D.V., Dick, C., 2006. Historical variability of sea ice edge position in the Nordic Seas. J. Geophys. Res 111, C01001.

Dokken, T.M., Jansen, E., 1999. Rapid changes in the mechanism of ocean convection during the last glacial period. Nature 401, 458-461.

Dowdeswell, J., Maslin, M., Andrews, J., McCave, I., 1995. Iceberg production, debris rafting, and the extent and thickness of Heinrich layers (H-1, H-2) in North Atlantic sediments. Geology 23, 301-304.

Duplessy, J.-C., Ivanova, E., Murdmaa, I., Paterne, M., Labeyrie, L., 2001. Holocene paleoceanography of the northern Barents Sea and variations of the northward heat transport by the Atlantic Ocean. Boreas 30, 2-16.

Dwyer, J.L., 1995. Mapping tide-water glacier dynamics in east Greenland using Landsat data. Journal of Glaciology 41, 584-595.

Dylmer, C.V., Giraudeau, J., Eynaud, F., Husum, K., de Vernal, A., 2013. Northward advection of Atlantic water in the eastern Nordic Seas over the last 3000 yr. Climate of the Past 9, 1505-1518.

Dylmer, C.V., submitted. Paléohydrologie de surface des Mers Nordiques à l'Holocène Terminal (derniers 3000 ans): le message du phytoplancton à squelette calcaire et organique, *PhD thesis*, Bordeaux University (EPOC).

Ebbesen, H., Hald, M., 2004. Unstable Younger Dryas climate in the northeast North Atlantic. Geology 32, 673-676.

Ebbesen, H., Hald, M., Eplet, T.H., 2007. Lateglacial and early Holocene climatic oscillations on the western Svalbard margin, European Arctic. Quaternary Science Reviews 26, 1999-2011.

Eglinton, G., Calvin, M., 1967. Chemical fossils. Scientific American 216, 32-43.
Eglinton, T.I., Eglinton, G., 2008. Molecular proxies for paleoclimatology. Earth and Planetary Science Letters 275, 1-16.
Eiríksson, J., Knudsen, K.L., Haflidason, H., Heinemeier, J., 2000. Chronology of late Holocene climatic events in the northern North Atlantic based on AMS ^{14}C dates and tephra markers from the volcano Hekla, Iceland. Journal of Quaternary Science 15, 573-580.
Elverhøi, A., Solheim, A., 1983. The Barents Sea ice sheet - a sedimentological discussion. Polar research 1, 23-42.
Elverhøi, A., Pfirman, S.L., Solheim, A., Larssen, B.B., 1989. Glaciomarine sedimentation in epicontinental seas exemplified by the northern Barents Sea. Marine Geology 85, 225-250.
Fahl, K., Stein, R., 2012. Modern seasonal variability and deglacial/Holocene change of central Arctic Ocean sea-ice cover: New insights from biomarker proxy records. Earth and Planetary Science Letters 351, 123-133.
Falk-Petersen, S., Mayzaud, P., Kattner, G., Sargent, J.R., 2009. Lipids and life strategy of Arctic Calanus. Marine Biology Research 5, 18-39.
Fimreite, S., Vorren, K.D., Vorren, T.O., 2001. Vegetation, climate and ice-front oscillations in the Tromsø area, northern Norway during the Allerød and Younger Dryas. Boreas 30, 89-100.
Funder, S., Hansen, L., 1996. The Greenland ice sheet—a model for its culmination and decay during and after the last glacial maximum. Bulletin of the Geological Society of Denmark 42, 137-152.
Gard, G., 1993. Late Quaternary coccoliths at the North Pole: Evidence of ice-free conditions and rapid sedimentation in the central Arctic Ocean. Geology 21, 227-230.
Gearing, P., Gearing, J.N., Lytle, T.F., Lytle, J.S., 1976. Hydrocarbons in 60 northeast Gulf of Mexico shelf sediments: a preliminary survey. Geochimica et Cosmochimica Acta 40, 1005-1017.
Geirsdóttir, Á., Hardardóttir, J., Andrews, J.T., 2000. Late-Holocene terrestrial glacial history of Miki and IC Jacobsen fjords, East Greenland. The Holocene 10, 123-134.
Gildor, H., Tziperman, E., 2000. Sea ice as the glacial cycles' climate switch: Role of seasonal and orbital forcing. Paleoceanography 15, 605-615.
Gildor, H., Tziperman, E., 2003. Sea-ice switches and abrupt climate change. Philosophical Transactions of the Royal Society of London. Series A: Mathematical, Physical and Engineering Sciences 361, 1935-1944.
Giraudeau, J., Grelaud, M., Solignac, S., Andrews, J.T., Moros, M., Jansen, E., 2010. Millennial-scale variability in Atlantic water advection to the Nordic Seas derived from Holocene coccolith concentration records. Quaternary Science Reviews 29, 1276-1287.
Goñi, M.A., O'Connor, A.E., Kuzyk, Z.Z., Yunker, M.B., Gobeil, C., Macdonald, R.W., 2013. Distribution and sources of organic matter in surface marine sediments across the North American Arctic margin. Journal of Geophysical Research: Oceans 118, 1-19.
Gooday, A.J., 2003. Benthic foraminifera (Protista) as tools in deep-water palaeoceanography: environmental influences on faunal characteristics. Advances in marine biology 46, 1-90.
Gray, D., 1881. The recent advance of the Polar ice in the Greenland and Spitzbergen Sea. Proceedings of the Royal Geographical Society and Monthly Record of Geography 3, 740-741.

Grimalt, J.O., Torras, E., Albaigés, J., 1988. Bacterial reworking of sedimentary lipids during sample storage. Organic Geochemistry 13, 741-746.

Grönvold, K., Óskarsson, N., Johnsen, S.J., Clausen, H.B., Hammer, C.U., Bond, G., Bard, E., 1995. Ash layers from Iceland in the Greenland GRIP ice core correlated with oceanic and land sediments. Earth and Planetary Science Letters 135, 149-155.

Groot, D.E., Aagaard-Sørensen, S., Husum, K., 2013. Reconstruction of Atlantic Water variability during the Holocene in the western Barents Sea. Climate of the Past 9, 4293-4322, doi:4210.5194/cpd-4299-4293-2013.

Gulliksen, S., Birks, H.H., Possnert, G., Mangerud, J., 1998. A calendar age estimate of the Younger Dryas-Holocene boundary at Kråkenes, western Norway. The Holocene 8, 249-259.

Hald, M., Vorren, T.O., 1984. Modern and Holocene foraminifera and sediments on the continental shelf off Tromsø, North Norway. Boreas 13, 133-154.

Hald, M., Aspeli, R., 1997. Rapid climatic shifts of the northern Norwegian Sea during the last deglaciation and the Holocene. Boreas 26, 15-28.

Hald, M., Hagen, S., 1998. Early Preboreal cooling in the Nordic seas region triggered by meltwater. Geology 26, 615-618.

Hald, M., Andersson, C., Ebbesen, H., Jansen, E., Klitgaard-Kristensen, D., Risebrobakken, B., Salomonsen, G.R., Sarnthein, M., Sejrup, H.P., Telford, R.J., 2007. Variations in temperature and extent of Atlantic Water in the northern North Atlantic during the Holocene. Quaternary Science Reviews 26, 3423-3440.

Hall, B.L., Baroni, C., Denton, G.H., 2008. The most extensive Holocene advance in the Stauning Alper, East Greenland, occurred in the Little Ice Age. Polar research 27, 128-134.

Hanna, E., Jónsson, T., Box, J.E., 2004. An analysis of Icelandic climate since the nineteenth century. International journal of Climatology 24, 1193-1210.

Hanna, E., Huybrechts, P., Steffen, K., Cappelen, J., Huff, R., Shuman, C., Irvine-Fynn, T., Wise, S., Griffiths, M., 2008. Increased runoff from melt from the Greenland Ice Sheet: a response to global warming. Journal of Climate 21, 331-341.

Harada, N., Ueno, T., Sagawa, Y., Taketomo, Y., Hashimoto, Y., Matsuura, Y., Sugiyama, K., 2012. Changes in physical and chemical properties of archived sediment. JAMSTEC Report of Research and Development 47-76.

Hassel, A., Skjoldal, H.R., Gjøsæter, H., Loeng, H., Omli, L., 1991. Impact of grazing from capelin (Mallotus villosus) on zooplankton: a case study in the northern Barents Sea in August 1985. Polar research 10, 371-388.

Heinrich, H., 1988. Origin and consequences of cyclic ice rafting in the Northeast Atlantic Ocean during the past 130,000 years. Quaternary Research 29, 142-152.

Hopkins, T.S., 1991. The GIN Sea - a synthesis of its physical oceanography and literature review 1972 - 1985. Earth Science Reviews 30, 175-318.

Hübschmann, H.-J., 2009. Handbook of GC/MS: Fundamentals and Applications, Second ed. Wiley-VCH, Weinheim.

Hughen, K.A., Baillie, M.G.L., Bard, E., Beck, J.W., Bertrand, C.J.H., Blackwell, P.G., Buck, C.E., Burr, G.S., Cutler, K.B., Damon, P.E., Edwards, R.L., Fairbanks, R.G., Friedrich, M., Guilderson, T.P., Kromer, B., McCormac, G., Manning, S., Ramsey, C.B., Reimer, P.J., Reimer, R.W., Remmele, S., Southon, J.R., Stuiver, M., Talamo, S., Taylor, F.W., van der Plitch, J., Weyhenmeyer, C.E., 2004. Marine04 marine radiocarbon age calibration, 0 - 26 cal kyr BP. Radiocarbon 46, 1059-1086.

Hughes, T., Denton, G., Grosswald, M., 1977. Was there a late-Würm Arctic ice sheet. Nature 266, 596-602.

Hurrell, J.W., Kushnir, Y., Ottersen, G., Visbeck, M., 2003. An overview of the North Atlantic oscillation. Geophysical Monograph-American Geophysical Union 134, 1-36.
Husum, K., Hald, M., 2002. Early Holocene cooling events in Malangenfjord and the adjoining shelf, north-east Norwegian Sea. Polar research 21, 267-274.
Husum, K., Hald, M., 2012. Arctic planktic foraminiferal assemblages: Implications for subsurface temperature reconstructions. Marine Micropaleontology 96-97, 38-47.
Ingólfsson, Ó., Landvik, J.Y., 2013. The Svalbard–Barents Sea ice-sheet – Historical, current and future perspectives. Quaternary Science Reviews 64, 33-60.
Isarin, R.F.B., Renssen, H., Vandenberghe, J., 1998. The impact of the North Atlantic Ocean on the Younger Dryas climate in northwestern and central Europe. Journal of Quaternary Science 13, 447-453.
Ishimura, T., Tsunogai, U., Hasegawa, S., Nakagawa, F., Oi, T., Kitazato, H., Suga, H., Toyofuku, T., 2012. Variation in stable carbon and oxygen isotopes of individual benthic foraminifera: tracers for quantifying the vital effect. Biogeosciences Discussions 9, 6191-6218.
Jennings, A., Andrews, J., Wilson, L., 2011. Holocene environmental evolution of the SE Greenland Shelf North and South of the Denmark Strait: Irminger and East Greenland current interactions. Quaternary Science Reviews 30, 980-998.
Jennings, A.E., Weiner, N.J., 1996. Environmental change in eastern Greenland during the last 1300 years: evidence from foraminifera and lithofacies in Nansen Fjord, 68 N. The Holocene 6, 179-191.
Jennings, A.E., Grönvold, K., Hilberman, R., Smith, M., Hald, M., 2002a. High-resolution study of Icelandic tephras in the Kangerlussuaq Trough, southeast Greenland, during the last deglaciation. Journal of Quaternary Science 17, 747-757.
Jennings, A.E., Knudsen, K.L., Hald, M., Hansen, C.V., Andrews, J.T., 2002b. A mid-Holocene shift in Arctic sea-ice variability on the East Greenland Shelf. The Holocene 12, 49-58.
Jennings, A.E., Weiner, N.J., Helgadottir, G., Andrews, J.T., 2004. Modern foraminiferal faunas of the southwestern to northern Iceland shelf: oceanographic and environmental controls. The Journal of Foraminiferal Research 34, 180-207.
Jennings, A.E., Hald, M., Smith, M., Andrews, J.T., 2006. Freshwater forcing from the Greenland Ice Sheet during the Younger Dryas: evidence from southeastern Greenland shelf cores. Quaternary Science Reviews 25, 282-298.
Jensen, S., Renberg, L., Reutergardh, L., 1977. Residue analysis of sediment and sewage sludge for organochlorines in the presence of elemental sulfur. Analytical Chemistry 49, 316-318.
Jernas, P., Klitgaard Kristensen, D., Husum, K., Wilson, L., Koç, N., 2013. Palaeoenvironmental changes of the last two millennia on the western and northern Svalbard shelf. Boreas 42, 236-255.
Johannessen, O.M., Bengtsson, L., Miles, M.W., Kuzmina, S.I., Semenov, V.A., Alekseev, G.V., Nagurnyi, A.P., Zakharov, V.F., Bobylev, L.P., Pettersson, L.H., 2004. Arctic climate change: observed and modelled temperature and sea ice variability. Tellus A 56, 328-341.
Johnsen, S., Clausen, H.B., Dansgaard, W., Fuhrer, K., Gundestrup, N., Hammer, C.U., Iversen, P., Jouzel, J., Stauffer, B., Steffensen, J.P., 1992. Irregular glacial interstadials recorded in a new Greenland ice core. Nature 359, 311-313.
Johnsen, S.J., Dahl-Jensen, D., Gundestrup, N., Steffensen, J.P., Clausen, H.B., Miller, H., Masson-Delmotte, V., Sveinbjörnsdottir, A.E., White, J., 2001. Oxygen isotope and palaeotemperature records from six Greenland ice-core stations:

Camp Century, Dye-3, GRIP, GISP2, Renland and NorthGRIP. Journal of Quaternary Science 16, 299-307.

Jones, R.L., Whatley, R.C., Cronin, T.M., Dowsett, H.J., 1999. Reconstructing late Quaternary deep-water masses in the eastern Arctic Ocean using benthonic Ostracoda. Marine Micropaleontology 37, 251-272.

Justwan, A., Koç, N., Jennings, A.E., 2008. Evolution of the Irminger and East Icelandic current systems through the Holocene, revealed by diatom-based sea surface temperature reconstructions. Quaternary Science Reviews 27, 1571-1582.

Karpuz, N.K., Jansen, E., 1992. A high-resolution diatom record of the last deglaciation from the SE Norwegian Sea: documentation of rapid climatic changes. Paleoceanography 7, 499-520.

Kaufman, D.S., Ager, T.A., Anderson, N.J., Anderson, P.M., Andrews, J.T., Bartlein, P.J., Brubaker, L.B., Coats, L.L., Cwynar, L.C., Duvall, M.L., Dyke, A.S., Edwards, M.E., Eisner, W.R., Gajewski, K., Geirsdottir, A., Hu, F.S., Jennings, A.E., Kaplan, M.R., Kerwin, M.W., Loshkin, A.V., MacDonald, G.M., Miller, G.H., Mock, C.J., Oswald, W.W., Otto-Bliesner, B.L., Porinchu, D.F., Rühland, K., Smol, J.P., Steig, E.J., Wolfe, B.B., 2004. Holocene thermal maximum in the western Arctic (0–180˚W). Quaternary Science Reviews 23, 529-560.

Kellogg, T.B., Duplessy, J.C., Shackleton, N.J., 1978. Planktonic foraminiferal and oxygen isotopic stratigraphy and paleoclimatology of Norwegian Sea deep‐sea cores. Boreas 7, 61-73.

Kellogg, T.B., 1980. Paleoclimatology and paleo-oceanography of the Norwegian and Greenland seas: glacial-interglacial contrasts. Boreas 9, 115-137.

Kelly, M.A., Long, A.J., 2009. The dimensions of the Greenland Ice Sheet since the Last Glacial Maximum. Past Global Changes Newsletter 17, 60-61.

Kim, J.-H., van der Meer, J., Schouten, S., Helmke, P., Willmott, V., Sangiorgi, F., Koç, N., Hopmans, E.C., Damsté, J.S.S., 2010. New indices and calibrations derived from the distribution of crenarchaeal isoprenoid tetraether lipids: Implications for past sea surface temperature reconstructions. Geochimica et Cosmochimica Acta 74, 4639-4654.

Kinnard, C., Zdanowicz, C.M., Fisher, D.A., Isaksson, E., de Vernal, A., Thompson, L.G., 2011. Reconstructed changes in Arctic sea ice over the past 1,450 years. Nature 479, 509-512.

Knies, J., Hald, M., Ebbesen, H., Mann, U., Vogt, C., 2003. A deglacial–middle Holocene record of biogenic sedimentation and paleoproductivity changes from the northern Norwegian continental shelf. Paleoceanography 18, 1096.

Knies, J., 2005. Climate-induced changes in sedimentary regimes for organic matter supply on the continental shelf off northern Norway. Geochimica et Cosmochimica Acta 69, 4631-4647.

Knudsen, K.L., Stabell, B., Seidenkrantz, M.-S., Eiriksson, J., Blake, W., 2008. Deglacial and Holocene conditions in northernmost Baffin Bay: sediments, foraminifera, diatoms and stable isotopes. Boreas 37, 346-376.

Knutti, R., Flückiger, J., Stocker, T., Timmermann, A., 2004. Strong hemispheric coupling of glacial climate through freshwater discharge and ocean circulation. Nature 430, 851-856.

Koç, N., Jansen, E., Haflidason, H., 1993. Paleoceanographic reconstructions of surface ocean conditions in the Greenland, Iceland and Norwegian seas through the last 14 ka based on diatoms. Quaternary Science Reviews 12, 115-140.

Koç, N., Klitgaard-Kristensen, D., Hasle, K., Forsberg, C.F., Solheim, A., 2002. Late glacial palaeoceanography of Hinlopen Strait, northern Svalbard. Polar research 21, 307-314.

Koch, L., 1945. The East Greenland Ice. Meddelelser om Gronland. 3, 346.
Kucera, M., Weinelt, M., Kiefer, T., Pflaumann, U., Hayes, A., Weinelt, M., Chen, M.-T., Mix, A.C., Barrows, T.T., Cortijo, E., 2005. Reconstruction of sea-surface temperatures from assemblages of planktonic foraminifera: multi-technique approach based on geographically constrained calibration data sets and its application to glacial Atlantic and Pacific Oceans. Quaternary Science Reviews 24, 951-998.
Kuijpers, A., Troelstra, S., Prins, M., Linthout, K., Akhmetzhanov, A., Bouryak, S., Bachmann, M., Lassen, S., Rasmussen, S., Jensen, J., 2003. Late Quaternary sedimentary processes and ocean circulation changes at the Southeast Greenland margin. Marine Geology 195, 109-129.
Kwok, R., Rothrock, D.A., 1999. Variability of Fram Strait ice flux and North Atlantic oscillation. Journal of Geophysical Research 104, 5177-5189.
Leorri, E., Cearreta, A., García-Artola, A., Irabien, M.J., Blake, W.H., 2013. Relative sea-level rise in the Basque coast (N Spain): Different environmental consequences on the coastal area. Ocean & Coastal Management 77, 3-13.
Leventhal, J.S., 1987. Carbon and sulfur relationships in Devonian shales from the Appalachian Basin as an indicator of environment of deposition. American Journal of Science 287, 33.
Leventhal, J.S., 1995. Carbon-sulfur plots to show diagenetic and epigenetic sulfidation in sediments. Geochimica et Cosmochimica Acta 59, 1207-1211.
Lie, Ř., Paasche, Ř., 2006. How extreme was northern hemisphere seasonality during the Younger Dryas? Quaternary Science Reviews 25, 404-407.
Linthout, K., Troelstra, S., Kuijpers, A., 2000. Provenance of coarse ice-rafted detritus near the SE Greenland margin. Netherlands Journal of Geosciences 79, 109-122.
Loeng, H., 1991. Features of the physical oceanographic conditions of the Barents Sea. Polar research 10, 5-18.
Loeng, H., Ozhigin, V., Ådlandsvik, B., 1997. Water fluxes through the Barents Sea. ICES Journal of Marine Science: Journal du Conseil 54, 310.
Loeng, H., Drinkwater, K., 2007. An overview of the ecosystems of the Barents and Norwegian Seas and their response to climate variability. Deep-Sea Research Part II: Topical Studies in Oceanography 54, 2478-2500.
Luckman, A., Murray, T., De Lange, R., Hanna, E., 2006. Rapid and synchronous ice-dynamic changes in East Greenland. Geophysical Research Letters 33, L03503, doi:03510.01029/02005GL025428.
Manabe, S., Stouffer, R.J., 2000. Study of abrupt climate change by a coupled ocean-atmosphere model. Quaternary Science Reviews 19, 285-299.
Mangerud, J., Dokken, T., Hebbeln, D., Heggen, B., Ingolfsson, O., Landvik, J.Y., Mejdahl, V., Svendsen, J.I., Vorren, T.O., 1998. Fluctuations of the Svalbard–Barents Sea Ice Sheet during the last 150 000 years. Quaternary Science Reviews 17, 11-42.
Marret, F., Zonneveld, K.A.F., 2003. Atlas of modern organic-walled dinoflagellate cyst distribution. Review of Palaeobotany and Palynology 125, 1-200.
Massé, G., Belt, S., Rowland, S., 2004. Biosynthesis of unusual monocyclic alkenes by the diatom *Rhizosolenia setigera* (Brightwell). Phytochemistry 65, 1101-1106.
Massé, G., Rowland, S.J., Sicre, M.-A., Jacob, J., Jansen, E., Belt, S.T., 2008. Abrupt climate changes for Iceland during the last millennium: Evidence from high resolution sea ice reconstructions. Earth and Planetary Science Letters 269, 565-569.

Massé, G., Belt, S.T., Crosta, X., Schmidt, S., Snape, I., Thomas, D.N., Rowland, S.J., 2011. Highly branched isoprenoids as proxies for variable sea ice conditions in the Southern Ocean. Antarctic Science 1, 1-12.

Mayewski, P.A., Meeker, L.D., Whitlow, S., Twickler, M.S., Morrison, M.C., Alley, R.B., Bloomfield, P., Taylor, K., 1993. The atmosphere during the Younger Dryas. Science 261, 195-197.

McManus, J., Francois, R., Gherardi, J.M., Keigwin, L., Brown-Leger, S., 2004. Collapse and rapid resumption of Atlantic meridional circulation linked to deglacial climate changes. Nature 428, 834-837.

Miller, G.H., Alley, R.B., Brigham-Grette, J., Fitzpatrick, J.J., Polyak, L., Serreze, M.C., White, J.W., 2010. Arctic amplification: can the past constrain the future? Quaternary Science Reviews 29, 1779-1790.

Miller, G.H., Geirsdóttir, Á., Zhong, Y., Larsen, D.J., Otto-Bliesner, B.L., Holland, M.M., Bailey, D.A., Refsnider, K.A., Lehman, S.J., Southon, J.R., 2012. Abrupt onset of the Little Ice Age triggered by volcanism and sustained by sea-ice/ocean feedbacks. Geophysical Research Letters 39, L02708.

Moritz, R.E., Bitz, C.M., Steig, E.J., 2002. Dynamics of recent climate change in the Arctic. Science 297, 1497.

Moros, M., Emeis, K., Risebrobakken, B., Snowball, I., Kuijpers, A., McManus, J., Jansen, E., 2004. Sea surface temperatures and ice rafting in the Holocene North Atlantic: climate influences on northern Europe and Greenland. Quaternary Science Reviews 23, 2113-2126.

Moros, M., Andrews, J.T., Eberl, D.D., Jansen, E., 2006. Holocene history of drift ice in the northern North Atlantic: Evidence for different spatial and temporal modes. Paleoceanography 21, PA2017.

Moseidjord, H., Svendsen, H., Slagstad, D., 1999. Sensitivity studies of circulation and ocean-shelf exchange off northern Norway. Sarsia 84, 191-198.

Mueller-Lupp, T., Bauch, H., Erlenkeuser, H., Hefter, J., Kassens, H., Thiede, J., 2000. Changes in the deposition of terrestrial organic matter on the Laptev Sea shelf during the Holocene: evidence from stable carbon isotopes. International Journal of Earth Sciences 89, 563-568.

Müller, J., Massé, G., Stein, R., Belt, S.T., 2009. Variability of sea-ice conditions in the Fram Strait over the past 30,000 years. Nature Geoscience 2, 772-776.

Müller, J., Wagner, A., Fahl, K., Stein, R., Prange, M., Lohmann, G., 2011. Towards quantitative sea ice reconstructions in the northern North Atlantic: A combined biomarker and numerical modelling approach. Earth and Planetary Science Letters 306, 137-148.

Murray, J.W., 2002. Introduction to benthic foraminifera. Quaternary environmental micropalaeontology. Haslett, S.K. Oxford, Arnold: 5-14.

Murton, J.B., Bateman, M.D., Dallimore, S.R., Teller, J.T., Yang, Z., 2010. Identification of Younger Dryas outburst flood path from Lake Agassiz to the Arctic Ocean. Nature 464, 740-743.

Myers, P.G., Kulan, N., Ribergaard, M.H., 2007. Irminger water variability in the West Greenland Current. Geophysical Research Letters 34, 1-6.

Nam, S.-I., Stein, R., Grobe, H., Hubberten, H., 1995. Late Quaternary glacial-interglacial changes in sediment composition at the East Greenland continental margin and their paleoceanographic implications. Marine Geology 122, 243-262.

Navarro-Rodriguez, A., Belt, S.T., Knies, J., Brown, T.A., 2013. Mapping recent sea ice conditions in the Barents Sea using the proxy biomarker IP_{25}: implications for palaeo sea ice reconstructions. Quaternary Science Reviews 79, 26-39.

Nesje, A., Dahl, S.O., Bakke, J., 2004. Were abrupt Lateglacial and early-Holocene climatic changes in northwest Europe linked to freshwater outbursts to the North Atlantic and Arctic Oceans? The Holocene 14, 299-310.

Nichols, D.S., Nichols, P.D., Sullivan, C.W., 1993. Fatty acid, sterol and hydrocarbon composition of Antarctic sea ice diatom communities during the spring bloom in McMurdo Sound. Antarctic Science 5, 271-278.

Nordby, E., Tande, K.S., Svendsen, H., Slagstad, D., 1999. Oceanography and fluorescence at the shelf break off the north Norwegian coast (69˚20'N-70˚30'N) during the main productive period in 1994. Sarsia 84, 175-189.

Nuttall, A.-M., 1993. Glaciological Investigations in East Greenland using Digital LANDSAT imagery. Cambridge, UK, 107 pp.

Ogilvie, A.E., Barlow, L.K., Jennings, A., 2000. North Atlantic climate c. AD 1000: Millennial reflections on the Viking discoveries of Iceland, Greenland and North America. Weather 55, 34-45.

Ogilvie, A.E., Jónsson, T., 2001. " Little Ice Age" research: a perspective from Iceland. Climatic Change 48, 9-52.

Ogilvie, A.E.J., Jónsdóttir, I., 2000. Sea ice, climate, and Icelandic fisheries in the eighteenth and nineteenth centuries. Arctic 53, 383-394.

Perovich, D.K., Richter-Menge, J.A., 2009. Loss of sea ice in the arctic*. Annual Review of Marine Science 1, 417-441.

Pflaumann, U., Duprat, J., Pujol, C., Labeyrie, L.D., 1996. SIMMAX: A modern analog technique to deduce Atlantic sea surface temperatures from planktonic foraminifera in deep-sea sediments. Paleoceanography 11, 15-35.

Pflaumann, U., Sarnthein, M., Chapman, M., d'Abreu, L., Funnell, B., Huels, M., Kiefer, T., Maslin, M., Schulz, H., Swallow, J., 2003. Glacial North Atlantic: sea-surface conditions reconstructed by GLAMAP 2000. Paleoceanography 18, 1065.

Poirier, R.K., Cronin, T.M., Briggs Jr, W.M., Lockwood, R., 2012. Central Arctic paleoceanography for the last 50kyr based on ostracode faunal assemblages. Marine Micropaleontology 88, 65-76.

Polyak, L., Alley, R.B., Andrews, J.T., Brigham-Grette, J., Cronin, T.M., Darby, D.A., Dyke, A.S., Fitzpatrick, J.J., Funder, S., Holland, M., Jennings, A.E., Miller, G.H., O'Regan, M., Savelle, J., Serreze, M., St. John, K., White, J.W.C., Wolff, E., 2010. History of sea ice in the Arctic. Quaternary Science Reviews 29, 1757-1778.

Polyakova, Y.I., Stein, R., 2004. Holocene paleoenvironmental implications of diatom and organic carbon records from the Southeastern Kara Sea (Siberian Margin). Quaternary Research 62, 256-266.

Rampen, S.W., Abbas, B.A., Schouten, S., Damsté, J.S.S., 2010. A comprehensive study of sterols in marine diatoms (Bacillariophyta): Implications for their use as tracers for diatom productivity. Limnology and Oceanography 55, 91.

Rasmussen, S., Andersen, K., Svensson, A., Steffensen, J., Vinther, B., Clausen, H., Siggaard-Andersen, M., Johnsen, S., Larsen, L., Dahl-Jensen, D., 2006. A new Greenland ice core chronology for the last glacial termination. Journal of Geophysical Research 111, D06102.

Rasmussen, T.L., Thomsen, E., Ślubowska, M.A., Jessen, S., Solheim, A., Koç, N., 2007. Paleoceanographic evolution of the SW Svalbard margin (76° N) since 20,000 ^{14}C yr BP. Quaternary Research 67, 100-114.

Rasmussen, T.L., Forwick, M., Mackensen, A., 2012. Reconstruction of inflow of Atlantic Water to Isfjorden, Svalbard during the Holocene: Correlation to climate and seasonality. Marine Micropaleontology 94-95, 80-90.

Ravelo, A.C., Hillaire-Marcel, C., 2007. Chapter Eighteen The Use of Oxygen and Carbon Isotopes of Foraminifera in Paleoceanography. Developments in Marine Geology 1, 735-764.

Reeh, N., Mayer, C., Miller, H., Thomsen, H.H., Weidick, A., 1999. Present and past climate control on fjord glaciations in Greenland: Implications for IRD-deposition in the sea. Geophysical Research Letters 26, 1039-1042.

Reeh, N., Thomsen, H.H., Higgins, A.K., Weidick, A., 2001. Sea ice and the stability of north and northeast Greenland floating glaciers. Annals of Glaciology 33, 474-480.

Reeh, N., 2004. Holocene climate and fjord glaciations in Northeast Greenland: implications for IRD deposition in the North Atlantic. Sedimentary Geology 165, 333-342.

Reimer, P.J., Baillie, M.G.L., Bard, E., Bayliss, A., Beck, J.W., Blackwell, P.G., Bronk Ramsey, C., Buck, C.E., Burr, G.S., Edwards, R.L., Friedrich, M., Grootes, P.M., Guilderson, T.P., Hajdas, I., Heaton, T.J., Hogg, A.G., Hughen, K.A., Kaiser, K.F., Kromer, B., McCormac, F.G., Manning, S.W., Reimer, R.W., Richards, D.A., Southon, J.R., Talamo, S., Turney, C.S.M., van der Plitch, J., Weyhenmeyer, C.E., 2009. IntCal09 and Marine09 radiocarbon age calibration curves, 0 - 50,000 years cal BP. Radiocarbon 51, 1111-1150.

Rignot, E., Box, J., Burgess, E., Hanna, E., 2008. Mass balance of the Greenland ice sheet from 1958 to 2007. Geophysical Research Letters 35, L20502, doi:20510.21029/22008GL035417.

Risebrobakken, B., Moros, M., Ivanova, E.V., Chistyakova, N., Rosenberg, R., 2010. Climate and oceanographic variability in the SW Barents Sea during the Holocene. The Holocene 20, 609-621.

Risebrobakken, B., Dokken, T., Smedsrud, L.H., Andersson, C., Jansen, E., Moros, M., Ivanova, E.V., 2011. Early Holocene temperature variability in the Nordic Seas: The role of oceanic heat advection versus changes in orbital forcing. Paleoceanography 26, 4206.

Roberts, D.H., Long, A.J., Schnabel, C., Freeman, S., Simpson, M.J.R., 2008. The deglacial history of southeast sector of the Greenland Ice Sheet during the Last Glacial Maximum. Quaternary Science Reviews 27, 1505-1516.

Robson, J., Rowland, S., 1986. Identification of novel widely distributed sedimentary acyclic sesterterpenoids. Nature 324, 561-563.

Rogers, J.C., Yang, L., Li, L., 2005. The role of Fram Strait winter cyclones on sea ice flux and on Spitsbergen air temperatures. Geophysical Research Letters 32, doi:10.1029/2004GL022262.

Rontani, J.-F., Belt, S.T., Vaultier, F., Brown, T.A., 2011. Visible light induced photo-oxidation of highly branched isoprenoid (HBI) alkenes: Significant dependence on the number and nature of double bonds. Organic Geochemistry 42, 812-822.

Rosell-Melé, A., 2001. Examination of the Use of Biomarker Proxies for the Reconstruction of Paleoceanographic Conditions in the Northern North Atlantic, In: Schäfer, P., Ritzrau, W., Schlüter, M., Thiede, J. (Eds.), The Northern North Atlantic. Springer Berlin Heidelberg, pp. 353-363.

Rowland, S.J., Robson, J.N., 1990. The widespread occurrence of highly branched acyclic C_{20}, C_{25} and C_{30} hydrocarbons in recent sediments and biota--A review. Marine Environmental Research 30, 191-216.

Rowland, S.J., Belt, S.T., Wraige, E.J., Massé, G., Roussakis, C., Robert, J.M., 2001. Effects of temperature on polyunsaturation in cytostatic lipids of *Haslea ostrearia*. Phytochemistry 56, 597-602.

Rudels, B., Fahrbach, E., Meincke, J., Budéus, G., Eriksson, P., 2002. The East Greenland Current and its contribution to the Denmark Strait overflow. ICES Journal of Marine Science: Journal du Conseil 59, 1133-1154.

Rüther, D.C., Bjarnadóttir, L.R., Junttila, J., Husum, K., Rasmussen, T.L., Lucchi, R.G., Andreassen, K., 2012. Pattern and timing of the northwestern Barents Sea Ice Sheet deglaciation and indications of episodic Holocene deposition. Boreas 41, 494-512.

Sakshaug, E., 1997. Biomass and productivity distributions and their variability in the Barents Sea. ICES Journal of Marine Science 54, 341-350.

Samtleben, C., Schröder, A., 1992. Living coccolithophore communities in the Norwegian-Greenland Sea and their record in sediments. Marine Micropaleontology 19, 333-354.

Sarnthein, M., Gersonde, R., Niebler, S., Pflaumann, U., Spielhagen, R., Thiede, J., Wefer, G., Weinelt, M., 2003a. Overview of glacial Atlantic Ocean mapping (GLAMAP 2000). Paleoceanography 18, 1030.

Sarnthein, M., Kreveld, S., Erlenkeuser, H., Grootes, P., Kucera, M., Pflaumann, U., Schulz, M., 2003b. Centennial-to-millennial-scale periodicities of Holocene climate and sediment injections off the western Barents shelf, 75˚N. Boreas 32, 447-461.

Sarnthein, M., Pflaumann, U., Weinelt, M., 2003c. Past extent of sea ice in the northern North Atlantic inferred from foraminiferal paleotemperature estimates. Paleoceanography 18, 25-21.

Schiermeier, Q., 2012. Ice loss shifts Arctic cycles. Nature 489, 185-186.

Schmith, T., Hansen, C., 2003. Fram Strait ice export during the nineteenth and twentieth centuries reconstructed from a multiyear sea ice index from southwestern Greenland. Journal of Climate 16, 2782-2791.

Schubert, C., Stein, R., 1996. Deposition of organic carbon in Arctic Ocean sediments: terrigenous supply vs marine productivity. Organic Geochemistry 24, 421-436.

Scott, D.B., Schell, T., St-Onge, G., Rochon, A., Blasco, S., 2009. Foraminiferal assemblage changes over the last 15,000 years on the Mackenzie - Beaufort Sea Slope and Amundsen Gulf, Canada: Implications for past sea ice conditions. Paleoceanography 24, PA2219. http://dx.doi.org/2210.1029/2007PA001575.

Seale, A., Christoffersen, P., Mugford, R.I., O'Leary, M., 2011. Ocean forcing of the Greenland Ice Sheet: Calving fronts and patterns of retreat identified by automatic satellite monitoring of eastern outlet glaciers. Journal of Geophysical Research: Earth Surface 116, F03013.

Seidenkrantz, M.-S., 2013. Benthic foraminifera as palaeo sea-ice indicators in the subarctic realm – examples from the Labrador Sea–Baffin Bay region. Quaternary Science Reviews 79, 135-144.

Sejrup, H.P., Birks, H.J.B., Klitgaard Kristensen, D., Madsen, H., 2004. Benthonic foraminiferal distributions and quantitative transfer functions for the northwest European continental margin. Marine Micropaleontology 53, 197-226.

Seppä, H., Birks, H.H., Birks, H.J.B., 2002. Rapid climatic changes during the Greenland stadial 1 (Younger Dryas) to early Holocene transition on the Norwegian Barents Sea coast. Boreas 31, 215-225.

Serreze, M.C., Barrett, A.P., Slater, A.G., Steele, M., Zhang, J., Trenberth, K.E., 2007. The large-scale energy budget of the Arctic. Journal of Geophysical Research 112, D11122.

Sinninghe-Damsté, J.S., Rijpstra, W.I.C., Schouten, S., Peletier, H., van der Maarel, M.J.E.C., Gieskes, W.W.C., 1999a. A C_{25} highly branched isoprenoid alkene and

C_{25} and C_{27} *n*-polyenes in the marine diatom *Rhizosolenia setigera*. Organic Geochemistry 30, 95-100.

Sinninghe-Damsté, J.S., Schouten, S., Rijpstra, W.I.C., Hopmans, E.C., Peletier, H., Gieskes, W.W.C., Geenevasen, J.A.J., 1999b. Structural identification of the C_{25} highly branched isoprenoid pentaene in the marine diatom *Rhizosolenia setigera*. Organic Geochemistry 30, 1581-1583.

Slagstad, D., Tande, K.S., Wassmann, P., 1999. Modelled carbon fluxes as validated by field data on the north Norwegian shelf during the productive period in 1994. Sarsia 84, 303-317.

Slagstad, D., McClimans, T.A., 2005. Modeling the ecosystem dynamics of the Barents sea including the marginal ice zone: I. Physical and chemical oceanography. Journal of Marine Systems 58, 1-18.

Ślubowska-Woldengen, M., Rasmussen, T.L., Koç, N., Klitgaard-Kristensen, D., Nilsen, F., Solheim, A., 2007. Advection of Atlantic Water to the western and northern Svalbard shelf since 17,500 calyr BP. Quaternary Science Reviews 26, 463-478.

Ślubowska, M.A., Koç, N., Rasmussen, T.L., Klitgaard-Kristensen, D., 2005. Changes in the flow of Atlantic water into the Arctic Ocean since the last deglaciation: evidence from the northern Svalbard continental margin, 80˚N. Paleoceanography 20, PA4014.

Smith, S.L., Smith, W.O., Codispoti, L.A., Wilson, D.L., 1985. Biological observations in the marginal ice zone of the East Greenland Sea. Journal of marine research 43, 693-717.

Solignac, S., Giraudeau, J., de Vernal, A., 2006. Holocene sea surface conditions in the western North Atlantic: Spatial and temporal heterogeneities. Paleoceanography 21, PA2004.

Sparkman, O.D., Penton, Z.E., G.Kitson, F., 2011. Gas Chromatography and Mass Spectrometry, Second ed. Elsevier, Oxford.

Spielhagen, R.F., Baumann, K.-H., Erlenkeuser, H., Nowaczyk, N.R., Nørgaard-Pedersen, N., Vogt, C., Weiel, D., 2004. Arctic Ocean deep-sea record of northern Eurasian ice sheet history. Quaternary Science Reviews 23, 1455-1483.

Stein, R., Dittmers, K., Fahl, K., Kraus, M., Matthiessen, J., Niessen, F., Pirrung, M., Polyakova, Y., Schoster, F., Steinke, T., 2004. Arctic (palaeo) river discharge and environmental change: evidence from the Holocene Kara Sea sedimentary record. Quaternary Science Reviews 23, 1485-1511.

Stein, R., 2008. Arctic Ocean Sediments: Processes, Proxies, and Paleoenvironment. Elsevier, Amsterdam.

Stein, R., Fahl, K., Müller, J., 2012. Proxy Reconstruction of Cenozoic Arctic Ocean Sea-Ice History–from IRD to IP_{25}–. Polarforschung 82, 37-71.

Stein, R., Fahl, K., 2013. Biomarker proxy shows potential for studying the entire Quaternary Arctic sea ice history. Organic Geochemistry 55, 98-102.

Stiansen, J.E., Filin, A.A., 2006. Joint PINRO/IMR report on the state of the Barents Sea ecosystem 2006, with expected situation and considerations for management, IMR/PINRO Joint Report Series No. 2/2007, p. 209 pp.

Stoynova, V., Shanahan, T.M., Hughen, K.A., de Vernal, A., 2013. Insights into Circum-Arctic sea ice variability from molecular geochemistry. Quaternary Science Reviews 79, 63-73.

Stuiver, M., Reimer, P.J., Bard, E., Beck, J.W., Burr, G.S., Hughen, K.A., Kromer, B., McCormac, G., Van Der Plicht, J., Spurk, M., 1998. INTCAL98 radiocarbon age calibration, 24,000-0 cal BP. Radiocarbon 40, 1041-1083.

Stuiver, M., Reimer, P.J., Reimer, R.W., 2005. CALIB 6.0 (Website Program and Documentation).

Syvitski, J.P.M., Andrews, J.T., Dowdeswell, J.A., 1996. Sediment deposition in an iceberg-dominated glacimarine environment, East Greenland: basin fill implications. Global and Planetary Change 12, 251-270.

Taldenkova, E., Bauch, H., Stepanova, A., Dem'yankov, S., Ovsepyan, A., 2005. Last postglacial environmental evolution of the Laptev Sea shelf as reflected in molluscan, ostracodal, and foraminiferal faunas. Global and Planetary Change 48, 223-251.

Tarasov, L., Peltier, W., 2005. Arctic freshwater forcing of the Younger Dryas cold reversal. Nature 435, 662-665.

Taylor, K., Lamorey, G., Doyle, G., Alley, R., Grootes, P., Mayewski, P.A., White, J., Barlow, L., 1993. The 'flickering switch'of late Pleistocene climate change. Nature 361, 432-436.

Taylor, K., Mayewski, P., Alley, R., Brook, E., Gow, A., Grootes, P., Meese, D., Saltzman, E., Severinghaus, J., Twickler, M., 1997. The Holocene-Younger Dryas transition recorded at Summit, Greenland. Science 278, 825-827.

Teller, J.T., Leverington, D.W., Mann, J.D., 2002. Freshwater outbursts to the oceans from glacial Lake Agassiz and their role in climate change during the last deglaciation. Quaternary Science Reviews 21, 879-887.

Teller, J.T., Boyd, M., Yang, Z., Kor, P.S.G., Mokhtari Fard, A., 2005. Alternative routing of Lake Agassiz overflow during the Younger Dryas: new dates, paleotopography, and a re-evaluation. Quaternary Science Reviews 24, 1890-1905.

Teller, J.T., Boyd, M., 2006. Two possible routings for overflow from Lake Agassiz during the Younger Dryas. Quaternary Science Reviews 25, 1142-1145.

Thomas, D.N., Dieckmann, G.S., 2010. Sea Ice, second ed. WIley Blackwell Publishing.

Thompson, D.W., Wallace, J.M., 1998. The Arctic Oscillation signature in the wintertime geopotential height and temperature fields. Geophysical Research Letters 25, 1297-1300.

Van de Wal, R., Boot, W., Van den Broeke, M., Smeets, C., Reijmer, C., Donker, J., Oerlemans, J., 2008. Large and rapid melt-induced velocity changes in the ablation zone of the Greenland ice sheet. Science 321, 111-113.

Vare, L.L., Massé, G., Gregory, T.R., Smart, C.W., Belt, S.T., 2009. Sea ice variations in the central Canadian Arctic Archipelago during the Holocene. Quaternary Science Reviews 28, 1354-1366.

Vare, L.L., Massé, G., Belt, S.T., 2010. A biomarker-based reconstruction of sea ice conditions for the Barents Sea in recent centuries. The Holocene 20, 637.

Verity, P.G., Wassmann, P., Ratkova, T.N., Andreassen, I.J., Nordby, E., 1999. Seasonal patterns in composition and biomass of autotrophic and heterotrophic nano-and microplankton communities on the north Norwegian shelf. Sarsia 84, 265-277.

Vinje, T., Kvambekk, Å.S., 1991. Barents Sea drift ice characteristics. Polar Research 10, 59-68.

Volkman, J.K., 1986. A review of sterol markers for marine and terrigenous organic matter. Organic Geochemistry 9, 83-99.

Volkman, J.K., Barrett, S.M., Dunstan, G.A., 1994. C_{25} and C_{30} highly branched isoprenoid alkenes in laboratory cultures of two marine diatoms. Organic Geochemistry 21, 407-414.

Volkman, J.K., Barrett, S.M., Blackburn, S.I., Mansour, M.P., Sikes, E.L., Gelin, F., 1998. Microalgal biomarkers: A review of recent research developments. Organic Geochemistry 29, 1163-1179.

Vorren, T.O., Plassen, L., 2002a. Deglaciation and palaeoclimate of the Andfjord Vågsfjord area, North Norway. Boreas 31, 97-125.

Vorren, T.O., Plassen, L.I.V., 2002b. Deglaciation and palaeoclimate of the Andfjord-Vågsfjord area, North Norway. Boreas 31, 97-125.

Wallevik, J.E., Sigurjonsson, H., 1998. The Koch Index. Formulation, Correction and Extension. Icelandic Meteorological Office Report.

Wang, J., Ikeda, M., 2000. Arctic oscillation and Arctic sea-ice oscillation. Geophysical Research Letters 27, 1287-1290.

Wang, L., Sarnthein, M., Erlenkeuser, H., Grootes, P.M., Grimalt, J.O., Pelejero, C., Linck, G., 1999. Holocene variations in Asian monsoon moisture: a bidecadal sediment record from the South China Sea. Geophysical Research Letters 26, 2889-2892.

Wassmann, P., Svendsen, H., Keck, A., Reigstad, M., 1996. Selected aspects of the physical oceanography and particle fluxes in fjords of northern Norway. Journal of Marine Systems 8, 53-71.

Wassmann, P., Andreassen, I.J., Rey, F., 1999. Seasonal variation of nutrients and suspended biomass on a transect across Nordvestbanken, north Norwegian shelf, in 1994. Sarsia 84, 199-212.

Winsborrow, M., Andreassen, K., Corner, G.D., Laberg, J.S., 2010. Deglaciation of a marine-based ice sheet: Late Weichselian palaeo-ice dynamics and retreat in the southern Barents Sea reconstructed from onshore and offshore glacial geomorphology. Quaternary Science Reviews 29, 424-442.

Wohlfarth, B., Lemdahl, G., Olsson, S., Persson, T., Snowball, I., Ising, J., Jones, V., 1995. Early Holocene environment on Bjørnøya (Svalbard) inferred from multidisciplinary lake sediment studies. Polar research 14, 253-275.

Wohlfarth, B., Bjorck, S., Funder, S., Houmark-Nielsen, M., Ingólfsson, Ó., Lunkka, J.-P., Mangerud, J., Saarnisto, M., Vorren, T., 2008. Quaternary of Norden. Episodes 31, 73-81.

Wollenburg, J., Kuhnt, W., 2000. The response of benthic foraminifers to carbon flux and primary production in the Arctic Ocean. Marine Micropaleontology 40, 189-231.

Wollenburg, J.E., Knies, J., Mackensen, A., 2004. High-resolution paleoproductivity fluctuations during the past 24 kyr as indicated by benthic foraminifera in the marginal Arctic Ocean. Palaeogeography, Palaeoclimatology, Palaeoecology 204, 209-238.

Wraige, E.J., T. Belt, S., A. Lewis, C., A. Cooke, D., Robert, J.M., Massé, G., Rowland, S.J., 1997. Variations in structures and distributions of C_{25} highly branched isoprenoid (HBI) alkenes in cultures of the diatom, *Haslea ostrearia* (Simonsen). Organic Geochemistry 27, 497-505.

Wraige, E.J., Belt, S.T., Massé, G., Robert, J.M., Rowland, S.J., 1998. Variations in distributions of C_{25} highly branched isoprenoid (HBI) alkenes in the diatom, *Haslea ostrearia*: influence of salinity. Organic Geochemistry 28, 855-859.

Xiao, X., Fahl, K., Stein, R., 2013. Biomarker distributions in surface sediments from the Kara and Laptev seas (Arctic Ocean): indicators for organic-carbon sources and sea-ice coverage. Quaternary Science Reviews 79, 40-52.